Sicong Liu

Research on the Key Technologies in Narrowband Interference and Impulsive Noise Mitigation and Cancellation

清华大学出版社
TSINGHUA UNIVERSITY PRESS

Springer

Springer Theses

Recognizing Outstanding Ph.D. Research

Aims and Scope

The series "Springer Theses" brings together a selection of the very best Ph.D. theses from around the world and across the physical sciences. Nominated and endorsed by two recognized specialists, each published volume has been selected for its scientific excellence and the high impact of its contents for the pertinent field of research. For greater accessibility to non-specialists, the published versions include an extended introduction, as well as a foreword by the student's supervisor explaining the special relevance of the work for the field. As a whole, the series will provide a valuable resource both for newcomers to the research fields described, and for other scientists seeking detailed background information on special questions. Finally, it provides an accredited documentation of the valuable contributions made by today's younger generation of scientists.

Theses are accepted into the series by invited nomination only and must fulfill all of the following criteria

- They must be written in good English.
- The topic should fall within the confines of Chemistry, Physics, Earth Sciences, Engineering and related interdisciplinary fields such as Materials, Nanoscience, Chemical Engineering, Complex Systems and Biophysics.
- The work reported in the thesis must represent a significant scientific advance.
- If the thesis includes previously published material, permission to reproduce this must be gained from the respective copyright holder.
- They must have been examined and passed during the 12 months prior to nomination.
- Each thesis should include a foreword by the supervisor outlining the significance of its content.
- The theses should have a clearly defined structure including an introduction accessible to scientists not expert in that particular field.

More information about this series at http://www.springer.com/series/8790

Sicong Liu

Research on the Key Technologies in Narrowband Interference and Impulsive Noise Mitigation and Cancellation

Doctoral Thesis accepted by
Tsinghua University, Beijing, China

清華大学出版社
TSINGHUA UNIVERSITY PRESS

Springer

Author
Dr. Sicong Liu
Department Information
and Communication Engineering
School of Informatics
Xiamen University
Xiamen, Fujian, China

Supervisor
Prof. Jian Song
Electronic Engineering, DTV Technology
R&D Center
Tsinghua University
Beijing, China

Supervisor's Foreword

With the commence of era of internet-of-things and the help from big data, the need for human-human, human-thing and thing-thing communications and interconnections is explosively increasing. To meet the requirements of "massive and intelligent interconnections" for those important scenarios such as intelligent lighting, smart grid, vehicular networks and the internet-of-lights, etc., the new communication technologies to support high rate, ultra-reliability, low latency, wide coverage and massive connections are emerging. However, the noise and interference in the communication systems have always been the bottleneck that limits the system performance. Especially the Narrowband Interference (NBI) and Impulsive Noise (IN) are special noise and interference that prevailingly exist in broadband transmission systems. They are quite different from the commonly perceived additive white Gaussian noise due to the characteristics of difficult to model, randomness, sparsity and high-intensity. Because of the passive nature, conventional methods couldn't effectively mitigate or accurately eliminate the noise and interference, leading to inevitable system performance loss. In order to support the effective transmission of broadband communication systems and improve both the throughput and QoS of the next-generation communication network, this critical issue needs to be well addressed.

Based on the classical digital communication theory and the emerging sparse recovery theory, Dr. Sicong Liu, the author of this book summarized his research results from his Ph.D. thesis, which investigates this issue from three strategies including anti-NBI synchronization, time-frequency interleaving against NBI and IN, and accurate NBI and IN recovery. The main contribution of this thesis is as follows. First, an efficient anti-NBI frame structure which can be applied for broadband power line communications was proposed, and an effective synchronization algorithm against NBI was therefore designed. Second, a time-frequency combined interleaver that is able to maximize the time-frequency diversity gain was devised, which can be applied in many broadband transmission scenarios such as digital terrestrial multimedia broadcasting. It provides a novel and effective interleaving scheme for the reliable transmission in the time-frequency doubly selective channel with both NBI and IN. Furthermore, a more important contribution in this

work is that, a sparse recovery and multi-dimensional compressed sensing-based framework of NBI and IN estimation was formulated, in which he designed several practical algorithms with superior performance for NBI and IN estimation and cancelation. The proposed schemes have provided novel research regimes and solutions with both theoretical and practical value for the area of NBI and IN mitigation.

I do hope that this book can be a good reference to researchers, undergraduate and graduate students in the area of communications and signal processing, and provide theoretical and technical support for the design and application of the next-generation communication systems.

Beijing, China   Prof. Jian Song
February 2020

Preface

With the rapid development of broadband digital communications, the requirements for transmission reliability, effectiveness and stability keep increasing. However, the ubiquitously existing Barrowband Interference (NBI) and Impulsive Noise (IN) have become a vital bottleneck constraining the system performance of broadband communications systems. Due to the complicated characteristics of the NBI and IN that are different from additive white Gaussian noise, such as randomness, sparseness and high intensity, the conventional methods cannot eliminate their impacts effectively. Aimed at this technological difficulty, this thesis is concentrated on the main topic of "key technologies in NBI and IN mitigation and cancelation" based on the theories of digital communications systems and sparse recovery. The research is taken on the four aspects including frame structure, interleaving, sparse recovery and noise elimination:

First, concerning about the severe impacts of NBI on the synchronization of orthogonal frequency division multiplexing systems, the optimized frame structure design that can effectively mitigate the NBI impacts on synchronization is studied. Optimized synchronization algorithm is proposed to mitigate NBI, which significantly improves the accuracy of frame and carrier synchronization in the presence of NBI. Thus, a new signal frame structure for broadband transmission, which takes both spectral efficiency and transmission robustness into consideration, is formed.

Second, considering about the drawback that conventional interleaving techniques cannot simultaneously mitigate NBI and IN effectively, the optimal time-frequency combined interleaving technology is studied. The techniques of the interleaving parameters optimization and the sub-matrix cyclic shifting for symbol interleaving are proposed to maximize both time and frequency diversity gains. The performance of both anti-NBI and anti-IN capability is significantly improved.

Moreover, to solve the crucial problem that conventional anti-NBI methods cannot exactly reconstruct the NBI, the technology of accurate NBI reconstruction based on the sparse recovery theory is researched on by exploiting the sparse property of NBI in the frequency domain. The Compressed Sensing (CS) and Structured CS (SCS)-based recovery algorithms are proposed. The spatially multi-dimensional SCS-based recovery algorithm for MIMO systems is proposed.

The research in sparse recovery theory-based NBI estimation is insufficient at present, so this thesis proffers cutting-edge and novel technology in this field to improve the performance of NBI estimation significantly, which can be widely applied to many different broadband transmission systems such as power line and wireless communications.

Finally, aimed at solving the drawbacks of the existing anti-IN methods such as high complexity, low spectral efficiency and inaccuracy, the technology of multi-dimensional CS-based IN cancelation is studied by exploiting the sparse property of IN in the time domain. The prior information aided CS-based method, along with the spatially multi-dimensional SCS-based method for IN cancelation, is proposed to effectively guarantee the reliable and efficient broadband transmission in the channel with severe noise and interference.

Through these researches, this thesis provides theoretical basis and technological essentials for the NBI and IN mitigation and cancelation in the next-generation broadband digital communications, and facilitates the application and standardization of the proposed technologies.

Xiamen, China   Dr. Sicong Liu
January 2020   Assistant Professor

Acknowledgements

Contents

Chapter 1
Introduction

Abstract As the introductory content of this thesis, this chapter firstly introduces the development process and key technologies of broadband digital communications systems and the main noise and interference in it, and describes the characteristics and detrimental effects of NBI and IN, raising the main research topic, i.e., NBI and IN in broadband communications systems; Secondly, a comprehensive survey on the current research on the technologies of NBI and IN mitigation is given, with the major problems and challenges that the current related researches are faced with; Later the key problems to be solved and the research aims are given, based on which the research routine, the main research contents, the technological roadmap, the research outcomes and contributions of this thesis are described; Finally, a brief introduction to the structure of the thesis contents is presented.

1.1 Research Background and Aims

Since the originator of information theory, Sir Claude E. Shannon, proposed information theory to lay the foundation of communications technologies in 1948 [1], modern communications theory, techniques and systems have gone through plenty of development and evolution. Through technological evolution and application practice, the communications system developed from the earliest analog communications system, to the digital communications system gradually. Since the 1990s, digital communications have been developing through a long-term process of over 30 years, with the bandwidth growing, the rate increasing, and tremendous changes have taken place till now. Broadband digital communications have a solid basis of technologies, covering most of the populations all over the world. The research and industrial applications on broadband digital communications technologies are developing very fast, pushing the modern communications technologies towards the prospects and aims of high-speed, low-latency, ultra-reliability, wide-coverage, ubiquitous-connection.

With the development of modern society, many strict requirements of the stability, robustness and reliability for broadband digital communications systems are challenging the people's ever-increasing communications needs and the demands

of big data as well as "everything interconnection" for Internet of Things (IoT). However, the noise and interference in communications systems are always a severe bottleneck that limits the communications system performance. Especially for the special noise and interference widely existing in broadband communications systems, such as narrowband interference (NBI) and impulsive noise (IN), due to the characteristics different from those of Gaussian white noise, such as complication, randomness, sparsity, and intensiveness, the state-of-the-art methods can only "passively" combat against them, resulting in lots of drawbacks. The unfavorable impacts cannot be effectively mitigated, and it is even harder to completely eliminate them accurately, leading to inevitable performance loss to broadband digital communications systems. In order to ensure the effective and correct transmission of broadband communications systems, to improve the network throughput and quality of service (QoS), and to meet the requirements of the next generation communications technologies including ultra-reliability and high-speed, this difficulty limiting the communications system performance should be overcome. Hence, it is in desperate need to study key technologies on NBI and IN mitigation and cancellation.

In this background, this thesis cuts in the research from the scientific problems of how to mitigate the impacts of NBI on synchronization, how to improve the time-frequency interleaving performance of communications systems in the presence of NBI and IN, and how to accurately recover and eliminate NBI and IN. The thesis follows the investigation routine of "scrambling for mitigation, diversity for avoidance, recovery for cancellation", and a series of specific researches on the key technologies are carried out. The thesis proposes the frame design method to effectively mitigate NBI, the optimal time-frequency joint interleaving scheme for maximizing time-frequency diversities, and accurate recovery and elimination algorithms based on the theory of sparse recovery. From multiple aspects, the capability of mitigating and eliminating NBI and IN for the next generation broadband communications systems is fully improved. Through the research in this thesis, it is expected to provide theoretical basis and technological support for the further research of the researchers in this area, and meanwhile, to endeavor to boost the standardization and industrial applications of the research technologies in this thesis.

As the introductory content of this thesis, this chapter firstly introduces the development process and key technologies of broadband digital communications systems and the main noise and interference in it, and describes the characteristics and detrimental effects of NBI and IN, raising the main research topic, i.e., NBI and IN in broadband communications systems; Secondly, a comprehensive survey on the current research on the technologies of NBI and IN mitigation is given, with the major problems and challenges that the current related researches are faced with; Later the key problems to be solved and the research aims are given, based on which the research routine, the main research contents, the technological roadmap, the research outcomes and contributions of this thesis are described; Finally, a brief introduction to the structure of the thesis contents is presented.

1.1.1   An Overview of Digital Communication Systems

There are various types of standards, formation and corresponding techniques of modern broadband communication systems. Among them, the basic components mainly include the signal source, the transmitter, the channel (with noise and interference), the receiver, and the signal sink [2]. The signal source is the component that generates the information of interest, which is commonly denoted by a binary bit stream. The bit stream is coded in the digital domain at the transmitter using channel coding, and then it is modulated using some kind of constellation mapping. Afterwards, the modulated symbols are converted from digital to analog signal by a digital-to-analog converter (DAC), and then pass the shaping filter. After frequency upshifting, the transmit signal is formulated by the analog front end, and sent to the channel. The signal passes through the fading channel and reaches the receiver, during which the signal suffers from the noise and interference in the channel. After receiving the signal coupled from the analog front end in the receiver, the received signal is down-converted in frequency and converted from analog to digital signal using an analog-to-digital converter (ADC), which generates the received digital baseband signal. After that, the processes of synchronization, noise and interference mitigation, channel estimation and equalization, demapping and decoding are carried out, and the binary bit stream conveying the information of interest is recovered. Finally, the recovered information is passed to the signal sink [3, 4]. Among these processes, the estimation, mitigation and elimination of noise and interference are an important part of broadband digital communication systems. Whether the noise and interference can be effectively mitigated, estimated and eliminated, has a significant impact on the performance of many other parts such as synchronization, channel estimation, demapping and decoding, etc. Thus, the mitigation and elimination of noise and interference is the core problem of this research.

In digital communication systems, all the components except the source and the sink, can be regarded as a kind of "digital interface", or "binary interface" [5]. The function of the binary interface is to provide a physical-layer digital interface of the exchange of binary information bit streams for the source and the sink. Meanwhile, it will provide a binary data transmission link for upper-layers and try to guarantee the reliability and accuracy of the transmission of the binary bit streams to improve the transmission rate, which is also the aims and functionality of digital communication systems. There are many advantages of applying binary interface (i.e. digitalization). For example, it is easy to design digital logic and circuits. Digital transmission algorithms have a better performance and a higher stability. According to Shannon's Theorem of source/channel separation [6], the source coding and channel coding can be independent of each other.

Recent years are witnessing a rapid growth of digital communication systems, and an enormous amount of technical and industrial applications and completed standards are brought into reality. In the evolution of digital communication technologies and standard architecture, the most representative one is the evolution of wireless communication technologies and standards. The first-generation wireless communication

(1G) is operating in an analog mode, supporting only voice telephone and a low speed. For example, the AMPS (Advanced Mobile Phone System) [7] is a representative 1G system. In the 1990s, the second-generation wireless communication system (2G) has developed digital communication mode, such as the IS-95 system [8] and the GSM (Global System for Mobile Communications) system [9, 10], which significantly improved the quality of voice telephone and even supported a low-rate data service, so it was rapidly applied in a wide range. With the ever-increasing demand of communication data rate, 2G standards were further evolved. The international standardization organization 3GPP (3rd Generation Partnership Project) proposed the WCDMA (Wideband CDMA) system [11], United States proposed cdma2000 [12], and China proposed TD-SCDMA standards [13]. These are the three dominant standards that formed the third-generation wireless communication (3G). In the beginning of the 21st century, 3GPP proposed the long term evolution (LTE) project, and put forward the LTE release-8 standards series, which opened up the fourth generation wireless communications (4G). The standards series of LTE release-10 put forward right after made the technological architecture of 4G more thorough, which is called LTE-Advanced (LTE-A) standards. The evolutionary key technological proposal in the 4G standards series is orthogonal frequency division multiplexing (OFDM) [14–17] and multiple-input multiple-output (MIMO) [2, 18–20]. The OFDM technique is capable of mitigating frequency-selective fading effectively, and improving the spectral efficiency significantly. The MIMO technique is able to fully exploit the spatial diversity to improve the system capacity, which further improves the data rate of the 4G system by a giant leap. Recently, in order to satisfy the desperate demands of many different and new scenarios including low power consumption, wide coverage, high rate, low latency, and ultra reliability, the 4G standards are evolving rapidly towards 5G in the project of the international telecommunications union (ITU) International Mobile Telecommunications-2020 (IMT-2020) [21–23]. The development of the new generation of wireless communication technologies calls for more advanced and pioneering communication techniques to guarantee the service quality in various different complicated scenarios. To this end, this thesis is dedicated to the study of the mitigation and elimination of the new and special noise and interference, which is aimed at providing a better and more advanced technology for the next generation wireless communications as well.

The development of broadband digital communication technologies also pushed forward the development of wireless digital terrestrial multimedia broadcasting techniques. After an evolution process of around 20 years, there are mainly four internationally adopted common standards for digital television terrestrial broadcasting (DTTB) systems. The first one is the ATSC standard based on single carrier modulation proposed by the Advanced Television Systems Committee (ATSC) of the United States [24]. The second one is the Digital Video Broadcasting-Terrestrial (DVB-T) standard based on coded OFDM technique proposed by the European Telecommunications Standards Institute (ETSI) [25]. The third one is the Integrated Service Digital Broadcasting-Terrestrial (ISDB-T) standard based on distinct sub-channel OFDM technique proposed by Japan [26]. The fourth one is the Digital Terrestrial Multimedia Broadcasting (DTMB) standard based on Time Domain Synchronous OFDM

(TDS-OFDM) technique proposed by China [27]. In recent years, with the development of coded modulation techniques, the DTTB system standards are also evolving continuously. Various more advanced systems, including the ATSC3.0 standards [28], the DVB-T2 standards [29], and the DTMB-A (DTMB-Advanced) systems [30], are developed based on the standards mentioned above. The high performance Low Density Parity Check (LDPC) code [31, 32] is introduced to the advanced standards. The advanced techniques such as the quadrature amplitude modulation (QAM) [33, 34] with high modulation order or amplitude phase shift keying (APSK) [35, 36], and bit-interleaved coded modulation (BICM) [36–38], are introduced as well, which facilitates a higher rate and better performance, approaching the channel capacity. There also exist many complicated noise and interference in terrestrial wireless multimedia broadcasting channels, such as narrowband interference and impulsive noise, which is still the major factor that constraints the performance of the DTTB systems [39–41].

Apart from these, the rapid development in many areas such as wireless local area networks, wireline communication networks, and the newly emerging internet of things, is also pushing forward wider industrial applications of digital communication technologies. The representative of wireless metropolitan access networks (WMAN) is IEEE 802.16 standards series, namely the WiMAX [42] standards series, covering outdoor cell areas, which is similar to the application scenarios of wireless cellular communications. The standards of wireless local area networks mainly refer to the broadband wireless local access networks (WLAN) systems specified by the IEEE 802.11 standards series, which is commonly called WiFi (Wireless Fidelity). WiFi adopted the 4G key technologies, such as OFDM and MIMO, so a high-quality indoor short range wireless access service is provided, and great commercial success has been achieved [43]. The wireless access in vehicular environments (WAVE) system specified by the IEEE 802.11p standards [44] is an extended application of wireless local area networks in the scenarios of vehicular communications. As far as wireline communication networks are concerned, the representative standards include the wireline broadband digital television system specified by DVB-C or DVB-C2 standards [45], the broadband power line communications (PLC) systems specified by the ITU-T G.9960 standards [46] and the IEEE P1901 [47], and the conventional fiber optics communications systems, etc. Among these wireline systems, broadband power line communication systems do not rely on dedicated communication cables, so it is very easy to deploy the PLC system in practice. The transmission rate can reach 500 Mbps [48], and even 1 Gbps based on the reported research in literature [49]. The coverage area is in the order of 100 m [50]. Thus, PLC systems have been widely applied in many areasd, such as smart home, smart city, etc. The representative of newly emerging internet of things is the narrowband internet of things system (NB-IoT) based on cellular networks proposed in 2016 [51–53], which is able to support the networking of an enormous amount of nodes with very low energy consumption and a very wide coverage. One thing that should be noted is that, no matter in the wireless local area networks or in the wireline systems, narrowband interference and impulsive noise widely and prevailingly exist, and they have a great

impact on the communication performance of the networks. Thus, it is necessary to study effective techniques to deal with this issue.

With the ever-increasing development of the theory and technologies of broadband digital communications and its wide applications in different scenarios, related advanced technologies are continuously being studied and proposed by both the academia and industry, which also facilitates the maturity of the new broadband digital communication technologies. Specifically, many researches on the key technologies of point-to-point transmission have set a solid theoretical and technological basis for the continuous increase of the performance of digital communications. Among them, some of the key techniques include: block transmission multi-carrier OFDM modulation, cyclic prefixed OFDM (CP-OFDM), zero padding OFDM (ZP-OFDM), and time-domain synchronous OFDM (TDS-OFDM) [14, 16, 54], which is able to improve the spectral efficiency of digital communication transmissions, and avoid inter-symbol interference and inter block interference. The accuracy of equalization can be improved, and a lower complexity of implementation can be achieved. Thus, it has been widely adopted by many different cutting-edge broadband digital communication systems. On the other hand as a contrary technique, the single carrier techniques such as the single carrier frequency division multiple access (SC-FDMA) [55] is proposed, but the performance of single carrier techniques is worse than that of OFDM techniques in the presence of multipath fading. Since OFDM systems have a strict requirement on accurate synchronization, the synchronization techniques such as frame synchronization, carrier recovery and synchronization, timing synchronization and sampling frequency recovery, are the key parts that guarantee the reliability of block transmission [56–59]. As far as the coded modulation techniques are concerned, the highly efficient channel coding and decoding techniques such as the Turbo code [60] adopted by LTE or LTE-A, the LDPC code adopted by the data link in the enhanced mobile broadband (eMBB) scenario of 5G [21], can approach the channel capacity. The high order constellation mapping and demapping techniques (such as QAM and APSK constellation mapping modulation) can significantly improve the spectral efficiency and data rate. Bit-interleaved coded modulation (BICM) and iterative decoding BICM (BICM-ID) techniques [61] are able to make full use of the signal space diversity (SSD) to improve the equivalent channel capacity between mapping and demapping [62]. The interleaving techniques can provide time, frequency, and coordinate diversity gains [63–65]. Multiple antennas techniques (such as MIMO-OFDM techniques, massive MIMO techniques) can provide space diversity gain and increase the degrees of freedom, which significantly increases the spectral efficiency [2].

Although the development of the technological standards evolution and industrial applications of broadband digital communication techniques is rapid and furious, the various kinds of noise and interference in modern broadband communication systems cannot be avoided. Furthermore, the complicated and time variant narrowband interference and impulsive noise in the communication systems will have a great and direct impact on the performance and functionality of the point to point transmission techniques mentioned above, which is a serious bottleneck that constraints the performance of communication systems. Therefore, in order to further improve

and overcome the performance limit of broadband digital communication systems, the issues of narrowband interference and impulsive noise cannot be neglected, and should be paid high attention to.

1.1.2   Noises and Interferences

There exist many kinds of noises and interferences in broadband digital communications systems. As is generally acknowledged, *noise* is a detrimental factor generated by some random noise source inside or outside the communications system, leading to impacts on the correct reception of the signal of interest, which is commonly represented by its random probability distribution; *interference* is a detrimental signal caused by some outside interfering source or inner derivative signal, leading to interference to the correct reception of the valuable signal, which can be represented by the deterministic frequency spectrum, the random power spectrum density, or the random probability distribution of the interference signal [66–68]. Viewed from the definition, interference is somewhat different from noise, but there are also some relations between them. The difference is that, the reason of generation and the source of noise and interference are different; the relation is that, both noise and interference have some random property and they are mixed up with the signal of interest, leading to unfavorable impacts on the correct transmission and reception of the signal of interest.

There are many different ways to classify noise and interference. According to their logical relation with the signal of interest, they can be classified into additive noise and multiplicative noise; According to their linearity, they can be classified into linear noise and nonlinear noise; According to the generation and source, they can be classified into system inner intrinsic noise (such as thermal noise inside amplifiers and electronic components, the shot noise of semiconductors, the intermodulation or harmonic interference caused by the device nonlinearity) and outside noise (such as cosmic background noise, atmospheric noise, electromagnetic radiation noise, impulsive noise generated by switching of electrical devices, interference from co-channel narrowband service); According to the cause and source, they can be classified into hostile interference (such as military electronic countermeasure interference, barrage jamming and frequency hopping interference) and unintentional interference (such as co-channel interference between different services on unlicensed public frequency bands); According to the probability distribution characteristics, they can be classified into white Gaussian noise (such as thermal noise and shot noise) and non-Gaussian noise (such as colored background noise, impulsive noise and narrowband interference), etc. [69–72].

No matter in the wireless channel or wired transmission environment, there always exist different kinds of noise and interference in communications systems. Some typical noises and interferences commonly seen in broadband digital communications systems are described as follows.

Noise: The noise from inside the system is called "system intrinsic noise", and the noise from outside is called "outside noise" or "external noise". The distribution of the system intrinsic noise is commonly random, which should be expressed in probability distribution functions. It is difficult to mitigate or suppress the system intrinsic noise due to its randomness. However, the intensity of system intrinsic noise is normally not strong, which is particularly harmful to analog circuits but is not so severe for digital circuits and digital communications systems whose electric levels have large variation [69]. On the other hand, external noise might be distributed randomly, but also likely to be from deterministic signals, whose intensity is usually far larger than that of system intrinsic noise, sometimes significantly higher than the amplitude of the signal of interest. Hence, external noise has severe impacts on digital communications systems [68]. Nevertheless, it is easier to find the rules of the distribution of external noise than intrinsic noise, so more effective methods of mitigation might be found. Some typical noises are listed as follows:

Additive white Gaussian noise (AWGN): The most typical, commonly seen and used model of background noise, which belongs to the category of system intrinsic noise. The cause of AWGN is the molecule thermal motion or the electric charge motion inside the electronic components that constitute the communications system. Because of the physical inherent characteristics of its cause of formation, AWGN cannot be eliminated. It is widely applied in the channel and noise modeling, analysis and practical simulation for communications systems. Typical AWGN includes the thermal noise caused by the intrinsic thermal motion of molecules or electrons, and the hot noise caused by the motion of discrete electric charges, etc [67]. Band-limited white noise is a special case of AWGN, which can be regarded as a kind of AWGN with a flat noise power spectrum density in the limited working bandwidth [70].

Colored background noise: Colored background noise should be classified into system intrinsic noise whose power spectrum density function is different from that of AWGN, since it is not "flat" in the frequency band of interest and thus not satisfied with the definition and condition of "white noise". Contrarily, its power spectrum density fluctuates with frequency, reflecting a characteristic of "color". The commonly seen colored background noise include the 1/f noise concentrated mainly in low frequency band caused by the direct current passing through discontinuous medium in electronic components (i.e., "flicker noise"), division noise mainly significant in high frequency in transistors, most audio noise whose spectrum is in mainly non-white low frequency band (such as pink noise, brown noise), and auto-regression noise [70].

Impulsive noise: Impulsive noise (IN), is defined as a bursting and impulsive outside noise in literature, whose pulse duration is sufficiently small with respect to the signal duration [68, 72]. As generally acknowledged in literature, quantitatively speaking, for block transmission systems, such as the orthogonal frequency division multiplexing (OFDM) system, IN can be regarded as a pulse noise signal whose nonzero pulse duration is no more than 5% of the OFDM symbol duration [73, 74]. Due to its time-domain bursting and impulsive characters, IN is

usually called "pulse noise". The cause of IN is various, commonly including the atmospheric noise produced in the atmosphere space, the spark noise produced by vehicles and electric devices, the runtime noise of industrial facilities, and the switching noise of household appliances, etc [50, 69].

Other types of noises: Apart from the typical noises mentioned above, there are some other noises in communications systems, such as the multiplicative noise having a multiplicative relation with the signal, the phase noise having an impact on the modulation phase of the signal, the nonlinear noise caused by nonlinear components or nonlinear signal processing operations like the clipping noise caused by the clipping operation to mitigate high peak-to-average-power-ratio (PAPR) in OFDM systems, and the quantization noise due to insufficient bit accuracy in the process of analog-to-digital conversion and other float-point or fixed-point quantization [70, 71].

Interference: Interference mainly comes from a certain interfering source outside the system, which is coupled into the communications system through a certain medium and mixed up with the signal of interest in time or frequency domain, resulting in detrimental effects on the correct reception, demodulation and decoding of the information signal. The interference signal can normally be represented by its deterministic spectrum or random power spectrum density [68]. Some kinds of interference signals might also come from inside the system itself. Some typical interferences in broadband digital communications systems are listed as follows:

Narrowband interference: In literature, narrowband interference (NBI) is commonly defined as a narrowband and spectrally-sparse interfering signal outside the system, whose effective bandwidth is sufficiently narrow with respect to the signal working bandwidth [68, 75]. As a duality of IN, it is generally acknowledged in literature that, the NBI in OFDM systems can be quantitatively defined as an interfering signal, where the ratio of the bandwidth occupied by its nonzero frequency components to the OFDM working bandwidth is no more than 5% [76, 77]. In some references, NBI is equivalently called "narrowband noise" [66], but in this thesis it is called NBI for consistency. NBI is prevailing existing in broadband digital communications systems with various causes, such as the NBI caused by the radio frequency leakage or wired coupling from the radiation of neighboring wireless devices or the interfering source in the same wired network topology [50, 67], and the interference to the broadband communication service from the co-channel narrowband licensed service or narrowband amateur radio service, etc [68, 69].

Electronic countermeasures interference: It belongs to intended malicious interferences, whose purpose is to disturb the normal transmission of the target communications system. The electronic countermeasures interference commonly seen include frequency-hopping interference (the frequency location of interference hops in a certain law or randomly), barrage jamming (jamming the whole working band), step disturbance (random or mixed frequency-sweeping interference to target signal); likewise, the NBI (such as single or multi-tone interference), and

impulsive interference (can be regarded as a kind of IN generated by intermittently transmitting high-power interfering signals), etc [68].

Other outside interferences: The other interferences coming from outside interfering sources still include the adjacent channel interference generated by other services in adjacent bands (such as the interference caused by the spectrum leakage of adjacent-band services), co-channel interference in the same band with the signal of interest (such as the interfering signal received by the UEs in the cell edge from the same frequency of the BS in the adjacent cell, as well as pilot contamination)[2], wireless coupling noise or crosstalk noise in wired communications, and electromagnetic interference (EMI) generated by the working circuits of electric and electronic devices, etc. [72].

System inherent interference: The interference signals produced inside the communications system, such as the cross-modulation interference (caused by high-order harmonics due to outside interfering signals or the nonlinear effects on the information signal at the receiver), intermodulation interference (the interference caused by the harmonics falling into the band of information signal because of the nonlinear operations on the different frequencies of the signal of interest), and image frequency interference (the image frequency components falling within the range of the intermediate frequency filter caused by frequency mixing and conversion), etc. [78].

1.1.3 Characteristics and Detrimental Effects of NBI and IN

NBI and IN exists widely in broadband digital communications systems and have significant detrimental effects on the system performance, which should be paid great attention to and the mitigation schemes need to be studied. In the following contents, the special distribution, the widely existing causes, and the detrimental effects on communications systems of NBI and IN are described.

(1) *Special Distribution of NBI and IN*

According to the Shannon information theory, noise and interference are the most essential and fundamental constraints to the communications system performance. If there is no noise or interference, theoretically, the channel capacity can be infinity [79, 80]. In the AWGN channel, the channel capacity has a closed-form solution [1], which has been studied comprehensively. AWGN is an additive stationary random process whose power spectrum density is flat (i.e. "white") and follows a multivariate Gaussian distribution [66]. However, NBI and IN are different from AWGN. No matter in characteristics and statistical distributions, or in the causes and detrimental effects, they are different in essence, so we cannot deal with them using conventional AWGN model, theory and method. Firstly, NBI does not belong to white noises, because its spectrum or power spectrum density is limited in a narrow band thus not reflecting a "white" character as in AWGN [75]. Secondly, the statistical distribution of IN is non-Gaussian [81], whose amplitude distribution usually follows

the *Middleton Class A* distribution [73, 74, 82, 83]; Meanwhile, the joint multivariate distribution of the signal samples of NBI or IN does not follow a multivariate Gaussian distribution, and the amplitude of each sample does not have the character of the covariance of multivariate Gaussian distribution [84, 85]. Besides, due to the impulsive, bursting and instantaneous characters of IN, its distribution can be regarded as a non-stationary (neither stationary nor wide-sense stationary) random process [86–88]. Although in some literature part of the characters of the statistical NBI or IN model is expressed by single-variable Gaussian distribution function, these references still insist that it is only a special extension of Gaussian variable within part of the features of NBI or IN: for example, for the band-limited Gaussian noise (BLGN) model of NBI, although the amplitude of each tone interferer is a single Gaussian variable, multiple tone interferers do not follow multivariate Gaussian distribution [84, 85, 89]; In the Gaussian mixture model of IN, the occurrence time of each nonzero pulse sample follows Poisson or Bernoulli distribution, so the model does not belong to conventional AWGN model despite the fact that the amplitude of its nonzero entries is a single Gaussian variable [90].

The time and frequency domain locations of NBI and IN have obvious irregular and random distributing characters [86, 91]. Usually, the intensity of the power spectrum density of NBI and IN is very high (typically 15–20 dB, sometimes 50 dB, over the background noise floor [88]), and they are mixed up with the signal of interest in both time and frequency domains completely, making it very difficult to distinguish between them [92]. Hence, it is hard to correctly analyze the theoretical performance bound of the channel in the presence of NBI and IN. It is difficult to mitigate and estimate NBI and IN, which will significantly impact the communications system performance.

(2) *NBI and IN Widely Exist in Broadband Communications*

NBI and IN widely exist in different channel environments and application scenarios of current broadband communications systems and standards, and have become an inevitably important aspect constraining the system performance of broadband communications systems.

Channels and systems with IN: firstly, in outdoor wireless communication channels, such as digital terrestrial television broadcasting channel and cellular wireless communication channel, there exists IN from ignition of transportation vehicles and weeding machines [93], and the IN generated by the switching of central air-conditioner, heater, lighting and household appliances [94]. Secondly, various wired communication channels, such as power line communication (PLC) networks, asymmetric digital subscriber line (ADSL), cabled TV lines, etc, suffer from the IN from the switching, plugging or topology changing of electric devices in the same power grid [88, 95, 96], and the coupling IN from the vehicle ignition, sparks, lightning and atmospheric noise [97], electric device leakage [50] and pulse radiation leakage [98]. In indoor wireless communications scenarios, there are also widely existing IN. For instance, it is shown by experimental tests that, there are IN in both the public Industrial Scientific and Medical (ISM) band and the 4 GHz high-frequency band, whose bandwidth can reach 40 MHz [99]. Besides, in the scenarios like internet of

vehicles (IoV), IN also prevails, such as the radio frequency coupling IN in wireless IoV IEEE 802.11p Wireless Access in Vehicular Environments (WAVE) system [44, 100]; In smart grid and wired Vehicle-to-Grid (V2G) networks, such as the smart IoV specified by HomePlug Green PHY standards, there also exists IN that impacts wired devices [101]. The operation of vehicle engines also introduces severe IN to IoV devices [102].

Channels and systems with NBI: on one hand, for wireless communications systems, the broadband wireless service networks working in the ISM unlicensed public band, such as the communication equipment in Wireless Local Area Networks (WLAN) [92], Wireless Metropolitan Area Networks (WMAN), wireless IoV [103], will suffer from interference from other unlicensed narrowband services (like bluetooth [104], cordless telephone, gate control, microwave oven, baby monitor, etc) [75, 105]; The narrowband signal produced by unlicensed amateur radio also has an impact on public unlicensed services, or spectrum leakage and abnormal usage of spectrum will also produce NBI to broadband communications in some licensed band [106]; Broadband multimedia wireless transmission systems and wireless digital terrestrial television broadcasting systems suffer from the co-channel NBI caused by analog broadcasting signals [39], and the NBI produced by the secondary users of cognitive radio who exploit the "white band" of digital television [40, 41]; Also, analog narrowband broadcasting signals will generate NBI to broadband communications systems like spread-spectrum and multi-carrier based systems [107]. On the other hand, wired communications systems like OFDM-based broadband PLC systems [108, 109] ADSL [106], ADSL [106] and cabled digital television broadcasting (such as digital video broadcasting-cable, DVB-C) suffer from NBI produced by the narrowband working harmonics from household appliances [50] (microwave oven [110], water heater, personal computers [111]). In addition, NBI exists in plenty of other scenarios, such as in the scenario of internet of things (IoT), the Narrowband Internet-of-Thing (NB-IoT) signal generates NBI to LTE (Long Term Evolution) or LTE-A (LTE-Advanced) cellular wireless communications systems working in the same in-band mode [51–53]; Ultra-Wideband (UWB) systems tend to suffer from NBI caused by many licensed or unlicensed wireless services with overlapping spectrum because of its very wide spectrum range [112, 113], and the malicious NBI aimed at UWB systems is also widely encountered in electronic countermeasure [114, 115]; The radio frequency nonlinearity due to the carrier ingress or carrier leakage at the transmitter will also introduce single-tone carrier remaining interference to the communications system itself, etc. [75].

(3) *Detrimental Effects of NBI and IN on Communications Systems*

NBI or IN has severe detrimental effects on the normal running of each module in the communications system, thus resulting in significant impacts on the performance of various broadband communications systems.

The major harmful effects of NBI: in the presence of NBI, it is easy for the dynamic range of the digital correlator or the front-end high-speed analog-to-digital-converter (ADC) at the receiver to be saturated. Likewise, analog receivers like rake do not have the inherent mechanism of eliminating the interference energy from decision

statistics, leading to significant performance degradation with NBI [113]; Also, NBI has significant detrimental effects on the synchronization performance (including frame synchronization, timing recovery and carrier estimation) of the receivers of broadband communications systems, especially multicarrier OFDM systems [116]; Furthermore, it is shown by theoretical analysis that, the bit error rate (BER) of the Fourier transform and wavelet transform based OFDM systems significantly increase in the presence of NBI [117]; It is proved by experiments that, when NBI is present, the BER performance of OFDM-based systems suffers from severe degradation [118]; It is validated that NBI might lead to complete loss of the data carried in sub-carriers, and significant increase of BER, symbol error rate (SER) as well as block error rate (BLER)[108]. For instance, UWB systems are very sensitive to NBI from many licensed or unlicensed services because of its mechanism of collecting the energy all over the frequency domain [113].

The major harmful effects of IN: it is shown in literature that, IN has severe impacts on the performance of digital communications receivers like decoding and demapping [119–122]; Due to the wide spectrum affected by IN, for multicarrier systems, almost all the OFDM sub-carriers are contaminated, especially when the intensity of IN is large enough to reach a certain threshold, leading to error reception of the whole OFDM block and performance degradation that channel coding cannot compensate [123]; The pulses of IN might occur in bursts in multiple continuous symbols, resulting in the failure of Viterbi decoding [124]; According to the analysis in literature, the currently widely applied broadband multicarrier systems like OFDM-based systems tend to be affected by IN more easily than single-carrier systems [125]; It is further shown by theoretical analysis and experimental tests that, IN brings significant performance degradation to the accuracy of demapping and decoding of multicarrier system receivers [96]; When the energy of IN exceeds some certain threshold, it is difficult to eliminate the impacts on all the sub-carriers using conventional signal processing methods [126], and inevitable bursting errors will appear in block transmission data [127]; It is shown by practical tests in wireless broadband multimedia transmission systems that, IN has severe impacts on the performance of the OFDM system receiver modulated in 64QAM [128].

Consequently, because of the special distribution, wide existence and severe detrimental effects of NBI and IN, it is in desperate need to research on the key technologies to effectively suppress, estimate and eliminate NBI and IN, which is utmost urgent for ensuring the performance of broadband communications systems.

1.2   Related Works and Challenges

1.2.1   Related Works and Problems on NBI Mitigation

As far as the problem of NBI mitigation, current existing researches in literature mainly include three basic categories, i.e., receiver-side frequency-domain estimation

and mitigation, transmitter-side time-domain filtering and receiver-side time-domain equalization, and transmitter-side orthogonal coding based mitigation.

(1) *Receiver-side frequency-domain estimation and mitigation*.

Nilsson proposed an NBI estimation method based on the rule of frequency-domain linear minimum mean square error (LMMSE) exploiting the values in null sub-carriers close to the real locations of NBI as measurement data [129]; Drawbacks: This method requires a large amount of reserved virtual sub-carriers, which is a great waste of spectrum resource, and it also requires the power spectrum density and central frequency location of the NBI to be known a priori, which is difficult to satisfy in practice, so the practical value of this method is relatively low.

Darsena proposed a successive interference cancelation method by sequentially doing symbol decision and error estimation for each sub-carrier in a recursive and iterative manner [76, 130]; Drawbacks: This method requires accurate channel estimation in the stage of sub-carrier symbol decision, and requires to know the accurate power spectrum density of NBI in the stage of error estimation, which is unpractical in realistic systems; Besides, the estimation error at some certain sub-carrier will accumulate and propagate to all the subsequent sub-carriers, leading to performance deterioration.

In addition, the receiver-side frequency-domain mitigation methods include the frequency threshold excision (FTE) method based on the decision according to the predefined threshold, which excludes the sub-carrier data with an amplitude larger than the given threshold [114, 131–133]; Drawbacks: The operation of directly excluding the sub-carrier will cause spectrum leakage and data loss, and it is easy to cause false alarm because of spectrum leakage or the peak power of OFDM signals in frequency-selective channels, leading to more loss of information data.

(2) *Transmitter-side time-domain filtering and receiver-side time-domain equalization*

Stamoulis designed an MMSE based NBI mitigation method using a nonlinear decision feedback equalizer [134]; Drawbacks: This method requires the accurate second-order statistics of the received signal to be known, otherwise the performance will be greatly degraded.

An optimized receiver with wide linear-zero forcing (WL-ZF) equalizer was designed based on the rule of constrained minimum mean output energy (CMMOE), and thus a related method to mitigate the impacts of NBI on receivers was proposed [135, 136]; Drawbacks: This method requires the prior statistical information of NBI to be known, and the receiver has to know the ideally accurate channel impulse response (CIR), which is, however, very difficult to accurately estimate in the presence of NBI in practice.

Coulson and Kelleci proposed an NBI suppression method by designing a time-domain suppression filter based on the linear prediction rule ahead of the discrete Fourier transform (DFT) at the transmitter, which is able to reduce spectrum leakage compared with the FTE method [132, 137]; Drawbacks: This method is effective only if the OFDM signal is under flat fading and the suppression filter has to be

designed in the frequency location of the NBI, which requires the precise location of NBI to be known in advance; Besides, this method is complicated to design and hard to implement efficiently.

(3) *Transmitter-side orthogonal coding based mitigation*

Gerakoulis and Wu proposed an interference suppressing OFDM (IS-OFDM) method for NBI mitigation, which spreads the transmitted signal power over all the sub-carriers using orthogonal spreading codes like orthogonal Walsh code at the transmitter [77, 138]; Drawbacks: The performance significantly degrades in high interference-to-signal ratio (ISR), making the method not working; And the required operation of orthogonal coding brings in additional high complexity.

On the basis of IS-OFDM systems, Popescu and Yaddanapudi proposed an NBI-avoidance method to mitigate the impacts of NBI and its spectrum leakage on related sub-carriers using the spectral shaping technique or the FTE method [139, 140]; Drawbacks: The spectral shaping operation and the FTE processing will introduce non-orthogonal property between sub-carriers; In addition, the performance of this method degrades when the number of nonzero entries of NBI is so large that many sub-carriers are forced to be set as zeros, so its applicability is relatively low.

It can be concluded from the above-mentioned existing conventional methods of NBI mitigation that, there are many drawbacks in the current research, such as the unstable performance of NBI mitigation, data loss, unrealistic assumptions, impractical for realistic systems, high implementation complexity, and difficulties in deployment, etc. The aims and strategies of most of the existing methods are "passively" mitigate the effects of NBI whereas they cannot effectively and accurately estimate the NBI signal, leading to the fact that they cannot completely eliminate the impacts of NBI in essence. Therefore, it is in great need to study a series of practice-oriented, realistic-system-applicable, stable and efficient methods of NBI mitigation and elimination. Designing the algorithms that are able to "actively" reconstruct the NBI accurately and eliminate NBI completely, is the key to solving this problem.

1.2.2 Related Works and Problems on IN Mitigation

Aimed at the problem of IN mitigation, the existing research literature works have addressed three basis categories, mainly including the receiver-side nonlinear operation method, the transmitter-side preprocessing method, and the receiver-side post-processing method.

(1) *Receiver-side nonlinear operation method*

The detrimental effects of too large amplitude of IN were constrained by clipping the time-domain samples that exceed a threshold [123]; Drawbacks: The clipping operation will introduce nonlinear distortion, leading to system performance loss; Because the clipping operation did not accurately estimate and eliminate the IN components, the impacts of IN cannot be completely excluded; In addition, it is

difficult to obtain the accurate locations of time-domain samples where IN occurs, so part of the samples affected by IN would be left out without processing when the intensity of IN did not exceed the predefined threshold.

The time-domain components of IN in the samples whose power exceeds the threshold can be eliminated by blanking these samples [141]; Drawbacks: When the PAPR of the OFDM signal is high, it is difficult to correctly estimate the precise locations of IN, so it is much probable to cause false alarm and mistakenly set the data not affected by IN to zeros, leading to additional performance loss; Besides, part of the samples affected by IN whose amplitude did not exceed the threshold would be left out.

Zhidkov tried to configure two thresholds for the clipping and blanking operations as a compromise of the two processing techniques [126]; Drawbacks: This combined scheme still has the drawback of either the clipping method or the blanking one; Because the locations of IN cannot be accurately obtained, part of the time-domain samples affected by IN is left out; When the PAPR of the OFDM signal is relatively high, it is much likely to cause false alarm and make the data set to zeros; When doing the clipping operation, the impacts of IN were not effectively mitigated and the detrimental effects remained; Nonlinear distortion might be introduced, etc.

(2) *Transmitter-side preprocessing method*

Matsuo and Haring studied the coding and decoding method using complex number for information data at the transmitter and receiver. Since IN was not encoded but only decoded by the complex number, it was equivalent to spreading its energy over all the sub-carriers by dispersive filtering processing, so the impacts of IN were suppressed; At the receiver, based on the Turbo recursive decoding mechanism and maximum a posterior (MAP) estimation, the significance of information signal with respect to IN was improved by multiple iterative decoding [142–144]; Drawbacks: The design of effective complex number codes is difficult and costs large complexity; Additional coding and decoding complexity should be included in the transmitter and receiver; large extra delay was introduced by iterative decoding with high implementation complexity; The performance of the iterative method of IN mitigation degraded significantly when the intensity of IN is large.

Another major transmitter-side preprocessing method is precoding frequency algebraic interpolation method: the frequency-domain OFDM symbols were pre-coded in the equivalent complex-valued Reed-Solomn (RS) codes [124, 145, 146], or precoded in the equivalent complex-valued or real-valued Bose-Chaudhuri-Hocquenghem (BCH) codes [147, 148], and the receiver exploited the received information at the known pilots with some certain distribution patterns, or continuous zero symbols [148, 149] for frequency-domain algebraic interpolation and decoding [150], thus mitigating the impacts of IN; Drawbacks: Extra complexity of precoding and decoding should be included to both the transmitter and receiver, and additional delay was produced; enough number of known pilots [124] or continuous zero symbols [147, 148] should be configured in the frequency domain. It was derived by theoretical analysis that, the distribution of the known pilots should satisfy a certain pattern in order to be the necessary and sufficient condition of successful

decoding [124], and the distribution of the successive zero symbols should appear in sequence [148, 149], but it is difficult for these two conditions to be satisfied in practical systems.

(3) *Receiver-side post-processing method*

Tulino made an assumption in research that, IN was independently identically distributed (i.i.d) and occurred with a certain probability. It was also assumed that, the accurate location of IN in the time-domain sample of the OFDM symbol was known to the receiver, and thus the sample contaminated by IN could be directly excluded [151]; Drawbacks: In practical systems, it is not possible for the receiver to directly obtain the accurate location of IN; the operation of excluding the sample will cause time-domain data loss and introduce non-orthogonality between OFDM sub-carriers and inter-carrier interference (ICI), which will lead to demodulation and decoding errors of OFDM symbols when the IN appears intensively (with a relatively large probability).

Rinne proposed a dynamic detection method using the predefined power or energy threshold, which online judges whether the OFDM data block was contaminated by IN. If so, this OFDM data block was deleted as a whole [152]; Drawbacks: This method causes too much loss of information, and significantly reduces the system throughput;

Apart from these, an important receiver-side post-processing method is the diversity combining method [153–155], which utilized the channel physical state diversity of different channels, and combined them in a certain manner, expecting to achieve diversity gain and improve the reliability of wireless communications systems in the presence of IN; Dubey provided a theoretical closed-form analysis of the BER of the system performance using selection combining method in the presence of IN [154]; Drawbacks: In practical communications systems, usually it is not easy to simultaneously get multiple physical channels with multiple different characteristics, so the physical channel diversity cannot be achieved in essence [155]; The combining of multiple sub-channels based on the same category of physical channel is lack of applicability, and the combining performance is also affected by the correlation between different channels; Besides, the method of diversity combining is still in the mode of "passively" combatting against IN, which is not capable of eliminating the impacts of IN completely.

It can be observed from these categories of conventional IN mitigation methods mentioned above that, there are plenty of drawbacks for the existing researches, such as the nonlinear distortion introduced by the operation of IN mitigation, the information data loss, the reduction of spectrum efficiency due to excessive time-frequency resources consumption, the false alarm and errors caused by inaccurate estimation, the high complexity of paradigm design, the unrealistic assumptions of the system and the available conditions of estimation, etc. The mechanism of most of the existing methods of IN mitigation is "passive" mitigation, which cannot accurately reconstruct and eliminate the IN signal. In all, it is necessary to study

highly efficient, robust and applicable algorithms of NBI and IN mitigation and elimination, in order to "actively" reconstruct and eliminate NBI and IN, which is also the main research aim of this thesis.

1.3   Key Research Problems and Research Aims

As far as the drawbacks of the above-mentioned conventional methods of NBI and IN mitigation are concerned, in order to overcome the many difficulties and challenges the current research is faced with, this thesis is concentrated on the center of "the key technologies of NBI and IN mitigation and cancelation", and is intended to focus on solving the following three key scientific problems:

Scientific Problem 1: How to overcome the severe impacts of NBI on the receiver synchronization performance. The existence of NBI severely impacts the performance of frame synchronization and carrier synchronization of the receiver, leading to great challenge to the synchronization-sensitive OFDM systems. Conventional design of synchronization frame structure and synchronization algorithms cannot mitigate NBI, thus causing the performance degradation in the presence of NBI, which is not capable of supporting the requirements of the improvement of the next-generation communications system performance and the accurate synchronization of OFDM systems. Hence, new synchronization frame structures and synchronization methods that can effectively mitigate NBI should be investigated.

Scientific Problem 2: How to improve the performance of the time-frequency interleaving scheme in the simultaneous presence of both IN and NBI. In the serious transmission environment where NBI and IN are simultaneously present, great impacts are imposed on the accuracy of demapping and decoding of the current broadband communications systems. However, conventional interleaving schemes were not jointly designed for aiming at the requirements of avoiding NBI and IN, and thus the optimal time and frequency diversities cannot be provided, resulting in limited interleaving performance gain. Hence, It is very urgent for guaranteeing the communications system performance in complicated serious channels to study novel time-frequency combined interleaving schemes.

Scientific Problem 3: How to break the bottleneck of conventional passive methods of mitigating NBI and IN to achieve accurate recovery and elimination. As is previously described, conventional methods of NBI and IN mitigation or estimation fall mostly in the category of "passively" combatting against the noise and interference, which is constrained by the limitation of conventional signal processing methods. The existing methods cannot accurately recover the precise time or frequency domain locations of NBI or IN, and cannot estimate their amplitude accurately, either. Thus, the unfavorable influences left by the noise and interference cannot be effectively eliminated, which has become a major bottleneck limiting the system performance improvement of existing communications systems. It is in desperate need to change the passive scheme to an active one, and introduce new signal processing theories and methods to establish the framework of highly efficient recovery. New algorithms

that can effectively reconstruct NBI and IN accurately should be devised, in order to break the bottleneck of conventional methods and the fundamental limitation of the system performance.

Through the study of these three scientific problems, this thesis is expecting to achieve the following related research aims:

Research Aim 1: Designing an optimized synchronization frame structure effectively improving the NBI mitigation performance and the highly efficient synchronization algorithm. The proposed frame structure outperforms the conventional frame design schemes in spectrum efficiency, and has significant gain in the same condition of frame synchronization accuracy and carrier recovery accuracy.
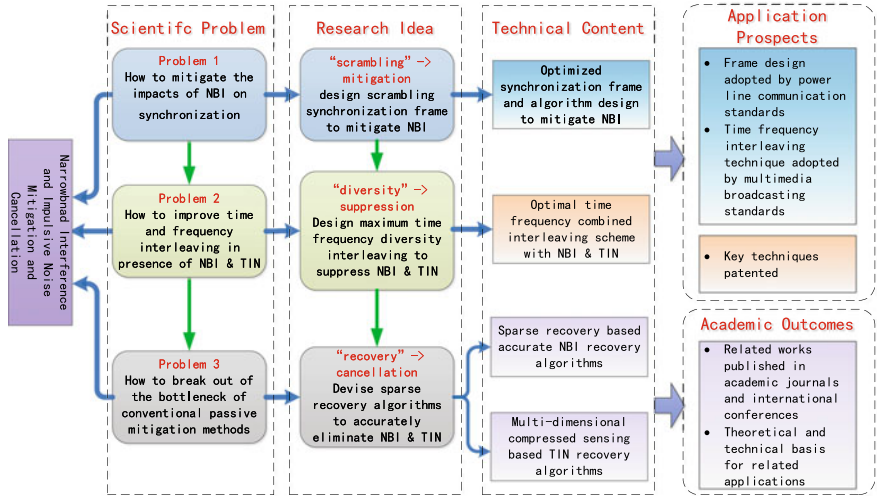
Research Aim 2: Investigating the optimal time-frequency combined interleaving scheme that can maximize time-frequency diversity gains in the presence of NBI and IN. Theoretically, the time-frequency interleaving scheme investigated can simultaneously achieve the target of the maximum time diversity gain and frequency diversity gain. Thus the capability of avoiding NBI and IN through interleaving for coded block transmission systems is improved to the most extent, and the system BER is significantly reduced.

Research Aim 3: Proposing the efficient and accurate sparse recovery framework and algorithms based on the new sparse recovery theory, realizing the accurate recovery and cancelation of NBI and IN. The estimation accuracy of recovering NBI and IN of the propose method is approaching the estimation theoretical bound; In the circumstance of the simultaneous existence of NBI and IN, the proposed method helps the performance of the system BER and the estimation accuracy of noise and interference outperform conventional mitigation methods significantly, which is able to approach the system performance where there is no NBI or IN present.

1.4   Main Works and Contributions

The research on key technologies of NBI and IN mitigation and cancelation is regarded as the kernel of this thesis. The relation framework of the scientific problems the works of this thesis are faced with, the main research idea adopted, and the major research contents and technical routine is illustrated in Fig. 1.1. The research framework of this thesis is elaborated mainly surrounding the following three major research routines.

Major Research Routine 1: Aimed at Scientific Problem 1, i.e., how to overcome the severe impacts of NBI on the receiver synchronization performance, this thesis cuts in from the perspective of smart mitigation of NBI and follows the research idea of designing the optimized "scrambling" synchronization frame structure that effectively mitigates NBI. Proposed in the research routine are the optimized design of synchronization frame structure mitigating NBI and the efficient and robust receiver synchronization algorithm, as well as designing novel high spectrum-efficient and robust synchronization frame structure to signiificantly improve the accuracy of frame synchronization and carrier recovery in the presence of NBI. The research

Fig. 1.1 The illustration of the research framework, scientific problems and the main research contents

outcomes have been published in one EI-indexed paper in the international conference IEEE International Symposium on Power Line Communications, and the core technique has achieved one national invention patent. The core technology of frame structure design has been adopted by the Chinese national standards for broadband power line communications—physical layer, and one standardization proposal has been submitted to the international telecommunications union. The technology studied is promisingly to be widely applied in various communications systems like power line communications and wireless communications severely contaminated by NBI, to achieve efficient and accurate synchronization.

Major Research Routine 2: Aimed at Scientific Problem 2, i.e., how to improve the performance of the time-frequency interleaving scheme in the simultaneous presence of both IN and NBI, this thesis follows the research idea of trying to provide the maximized time-frequency diversity gains and avoid NBI and IN. The optimal time-frequency combined interleaving scheme in the presence of NBI and IN is proposed. Proposed in the research routine are the optimized scheme for interleaving parameters to maximize the time-frequency diversity gains, and the block cyclic shifting technique for symbol interleaving to maximize the frequency diversity gain. The research aims of theoretically maximizing time-frequency diversity gains, effectively avoiding the impacts of NBI and IN on the demapping and decoding performance of coded block transmission systems, and significantly reducing the system BER in the condition of reducing the delay of conventional interleavers, are accomplished. The research outcomes have been published in one SCI-indexed journal paper in IEEE Transactions on Power Delivery, and in one EI-indexed paper in IEEE International Conference on Communications (ICC). The proposed technology of the optimal time-frequency combined interleaving has been adopted by the next-generation

national standard for digital wireless video broadcasting, i.e., Digital Terrestrial Multimedia Broadcasting-Advanced (DTMB-A), with the core techniques achieving one national invention patent. The interleaving technology studied is promisingly to be widely applied in the new generation broadband communications systems like the broadband wireless multimedia transmission and broadcasting, etc, and will improve the capability of jointly avoiding NBI and IN in severe transmission environments.

Major Research Routine 3: Aimed at Scientific Problem 3, i.e., how to break the bottleneck of conventional passive methods of mitigating NBI and IN to achieve accurate recovery and elimination, this thesis cuts in from the perspective of "actively reconstructing" NBI and IN and follows the research idea of the sparse recovery algorithms that can accurately recover the noise and interference. Based on the emerging sparse recovery theories such as the compressed sensing theory, the multi-dimensional structured compressed sensing theory, etc, the research routine is aimed at the sparse measuring of NBI and IN as well as the framework of recovering model. The algorithm of accurate NBI recovery based on sparse recovery theory and the algorithm of IN recovery based on multi-dimensional compressed sensing are proposed. The research aims of overcoming the drawback of conventional methods that "passively" combat against noise and interference, approaching the theoretical bound of the accuracy of NBI and IN estimation, significantly improving the BER performance of the system, and accurately recovering NBI and IN and eliminating the unfavorable effects of them, are accomplished. Until the time of writing this thesis, the related research on the sparse recovery theory based NBI and IN estimation has always been insufficient. The new technological outcomes from the research in this thesis have been published in three SCI-indexed long journal papers in IEEE Transactions on Vehicular Technology, one SCI-indexed long journal paper in IEEE Transactions on Broadcasting, IEEE Transactions on Communications, IEEE Transactions on Consumer Electronics, and IECIE Transactions on Fundamentals, respectively, and several conference papers in IEEE ICC and IEEE Global Communications Conference (Globecom), etc. The key techniques proposed have achieved six invention patents. The studied technology is widely applicable in many broadband communications systems and standards contaminated by NBI and IN, such as vehicular wireless communications, cellular communications, power line communications, and wireless local area networks, etc, which provides theoretical basis and technological support for effectively eliminating the detrimental effects of NBI and IN.

1.5 Structural Arrangements

All the contents of this thesis are arranged as follows:

This chapter firstly gives a brief introduction to the research background and purpose of this thesis, introduces the development history of broadband digital communications systems, and describes the major noise and interference in broadband digital communications, especially the characteristics and detrimental effects of NBI

and IN; Secondly, a literature survey is given concerning about the current status of related research, which concludes and analyzes the state-of-the-art techniques and methods as well as the existing problems and challenges they have; Later, the key scientific problems this thesis is intended to solve and the corresponding research aims are given, and the main works, research contents and contributions of this thesis are summarized; Finally a brief introduction to the content of each chapter is given.

Chapter 2 introduces the system model of this thesis and related fundamental knowledge. Firstly, the main blocks the broadband digital communications system is composed of and the key technologies are briefly introduced; Secondly, the existing frame structures commonly adopted in digital communications systems is introduced, mainly including the preamble structure of the frame header and the sub-frame structure of the OFDM data; Later, the NBI and IN models proposed and widely adopted in literature; Finally, the fundamental knowledge on sparse recovery theory is briefly presented, including compressed sensing theory, structured compressed sensing theory and sparse Bayesian learning theory.

Chapter 3 is in accordance with the scientific problem one this thesis is aimed at, i.e. "how to overcome the severe impacts of NBI on the receiver synchronization performance", and emphasizes on the description of the design of the synchronization frame structure to mitigate NBI. Firstly, the principles, models and conventional algorithms of frame synchronization and carrier recovery for broadband communication systems are introduced; Then the design of synchronization frame structure to mitigate NBI and the efficient receiver synchronization algorithms proposed in this thesis are focused on; Later, the method of signaling transmission robust to NBI is described; Finally, the performance analysis of the algorithms and the simulation results and discussions are given.

Chapter 4 is in accordance with the scientific problem two this thesis is aimed at, i.e. "how to improve the performance of the time-frequency interleaving scheme in the simultaneous presence of both IN and NBI", and emphasizes on the optimal time-frequency combined interleaving in the presence of NBI and IN. Firstly, the interleaving-deinterleaving system model of broadband coded block transmission in the circumstance of the existence of both NBI and IN is presented; Then the design of optimal time-frequency combined interleaving scheme is focused on. The optimized time interleaving scheme that maximizes the time diversity gain and the frequency interleaving scheme that maximizes the frequency diversity gain are given; Then the theoretical performance of the proposed interleaving algorithm in the multipath fading channel with NBI and IN is analyzed; Finally the simulation results as well as discussions are given.

Chapter 5 is in accordance with the first technological routine of the scientific problem three this thesis is aimed at, i.e. "how to break the bottleneck of conventional passive methods of mitigating NBI and IN to achieve accurate recovery and elimination", and emphasizes on the NBI recovery and elimination method based on sparse recovery theory. Firstly, the model of the frequency-domain sparse NBI as well as its time and space correlations is introduced; The NBI recovery algorithm based on compressed sensing and the NBI recovery algorithm based on structured compressed sensing in the multiple-input multiple output (MIMO) system are mainly

focused on, and the simulation results and discussions are given respectively; Finally, the complexity of the algorithms, the solution existence and the convergence of the algorithms, and the theoretical bound of the accuracy of sparse recovery, are all theoretically analyzed.

Chapter 6 is in accordance with the second technological routine of the scientific problem three this thesis is aimed at, and emphasizes on IN reconstruction and elimination based on sparse recovery theory. Firstly, the time-domain sparse IN model and its spatial correlation are introduced. The IN cancelation algorithm based on a priori aided compressed sensing and the IN elimination algorithm for MIMO systems based on structured compressed sensing are mainly focused on, along with the simulation results and discussions. Finally, the performance analysis and the theoretical proof of the convergence of the algorithms are given.

Chapter 7 comprehensively summarizes the innovative points of this thesis, and concludes on the scientific problems, proposed technical routines, research aims and contributions in accordance to each of the innovative points. Finally, based on the current work of this thesis, the possible extensions and future research insights are given.

Suggestions to Readers:

It is recommended that the readers who are interested to get a deep understanding of the overall content of this book start reading from the very beginning of this chapter, in order to get an idea of the impacts of special noise and interference on the 5G new air interface in modern digital communications, as well as the current research of related techniques, the key problems and scientific issues. Later, it is recommended to read Chap. 2 to know the related system models and get a brief review of associated basic knowledge, and prepare for understanding the technical content in subsequent chapters (surely, the readers who have a good knowledge of the related basic parts can feel free to skip this chapter, and directly read the following contents). After that, one can read the remaining chapters in sequence, or select some chapters corresponding to the scientific issue of interest to read. The sequence of reading Chap. 3 through Chap. 6 can be arranged freely as the readers like, since the sequence of them does not influence the understanding of any scientific issue or technological content. Finally, it is recommended that the readers who are interested in further research on the technological area and key problems of this book read Chap. 7, which might provide some inspirations to the problems of special noise and interference in the future 5G, B5G and 6G mobile communications and the possible research trends.

Notation Rules of Mathematical Formulas:

For all the notations in the mathematical formulas in this book, the following rules based on the commonly adopted common practice in scientific and academic literature, apply: Matrices are denoted by boldface upright uppercase letters; Vectors are denoted by boldface upright lowercase letters; Scalars are denoted by normal font slant letters; Variables in superscripts and subscripts also follow similar rules; The texts and descriptive words in superscripts and subscripts are denoted by normal font upright letters.

References

1. Shannon CE (2001) A mathematical theory of communication. ACM SIGMOBILE Mob Comput Commun Rev 5(1):3–55
2. Tse D, Viswanath P (2005) Fundamentals of wireless communication. Cambridge University Press, UK
3. Proakis JG (1995) Digital communications. McGraw-Hill, New York
4. Sklar B (2001) Digital communications, vol 2. Prentice Hall, Upper Saddle River (2001)
5. Gallager RG (2008) Principles of digital communication, vol 1. Cambridge University Press, Cambridge, UK
6. Cover TM, Thomas JA (2012) Elements of information theory. Wiley
7. Frenkiel R, Schwartz M (2010) Creating cellular: A history of the AMPS project (1971–1983) [History of Communications]. IEEE Commun Mag 48(9):14–24
8. EIA/TIA: Mobile station-base station compatibility standard for dual-mode wideband spread spectrum cellular system. EIA/TIA-95 Rev A (1995)
9. ETRI: Global system for mobile communications (GSM); Multiplexing and multiple access on the radio path. ETRI TS GSM 05.02 v5.1.0 (1996)
10. Rahnema M (1993) Overview of the GSM system and protocol architecture. IEEE Commun Mag 31(4):92–100
11. Holma H, Toskala A (2005) WCDMA for UMTS: radio access for third generation mobile communications. Wiley
12. Willenegger S (2000) cdma2000 physical layer: an overview. J Commun Netw 2(1):5–17
13. Li B, Xie D, Cheng S, Chen J, Zhang P, Zhu W, Li B (2005) Recent advances on TD-SCDMA in China. IEEE Commun Mag 43(1):30–37
14. Chiueh TD, Tsai PY (2008) OFDM baseband receiver design for wireless communications. Wiley
15. Cimini L (1985) Analysis and simulation of a digital mobile channel using orthogonal frequency division multiplexing. IEEE Trans Commun 33(7):665–675
16. Nee RV, Prasad R (2000) OFDM for wireless multimedia communications. Artech House, Inc
17. Weinstein S, Ebert P (1971) Data transmission by frequency-division multiplexing using the discrete fourier transform. IEEE Trans Commun 19(5):628–634
18. Alamouti SM (1998) A simple transmit diversity technique for wireless communications. IEEE J Sel Areas Commun 16(8):1451–1458
19. Goldsmith A, Jafar SA, Jindal N et al (2003) Capacity limits of MIMO channels. IEEE J Sel Areas Commun 21(5):648–702
20. Zheng L, Tse DNC (2003) Diversity and multiplexing: a fundamental tradeoff in multiple-antenna channels. IEEE Trans Inform Theory 49(5):1073–1096
21. 3GPP: Future mobile communication forum, 5G white paper (2015)
22. DOCOMO: 5G radio access: requirements, concept and technologies. Docomo 5G white paper (2014)
23. Ericsson: 5G radio access: research and vision. Ericsson 5G white paper (2013)
24. ATSC digital television standard. ATSC Standard A/53 (1995)
25. ETSI: Digital video broadcasting (DVB); Frame structure, channel coding and modulation for digital terrestrial television (DVB-T). ETSI EN 300 744 (1997)
26. Channel coding, frame structure and modulation scheme for terrestrial integrated service digital broadcasting (ISDB-T). ITU-R WP 11A/59, ARIB, Japan (1999)
27. Standard CN (2006) Frame structure, channel coding and modulation for digital television terrestrial broadcasting system. GB 20600-2006, Chinese National Standard
28. ATSC: ATSC candidate standard: Physical layer protocol, document ATSC S32-230r21, Advanced Television Systems Committee (ATSC), Washington, DC, USA (2015)
29. ETSI: Digital video broadcasting (DVB); Frame structure, channel coding and modulation for a second generation digital terrestrial television broadcasting system (DVB-T2). ETSI EN 302 755 v1.3.1 (2011)

30. Pan C, Wang J, Fang H, Song J (2013) Field trial of advanced DTMB system DTMB-A in Hong Kong. In: Proceedings of IEEE international symposium on broadband multimedia systems and broadcasting (BMSB'13), pp 1–4
31. ten Brink S, Kramer G, Ashikhmin A (2004) Design of low-density parity-check codes for modulation and detection. IEEE Trans Commun 52(4):670–678
32. Richardson TJ, Shokrollahi MA, Urbanke RL (2001) Design of capacity-approaching irregular low-density parity-check codes. IEEE Trans Inform Theory 47(2):619–637
33. Jablon NK (1992) Joint blind equalization, carrier recovery and timing recovery for high-order QAM signal constellations. IEEE Trans Signal Process 40(6):1383–1398
34. Rice F, Cowley B, Moran B, Rice M (2001) Cramér-rao lower bounds for QAM phase and frequency estimation. IEEE Transa Commun 49(9):1582–1591
35. Liu Z, Xie Q, Peng K, Yang Z (2011) APSK constellation with gray mapping. IEEE Commun Lett 15(12):1271–1273
36. Yang F, Yan K, Xie Q, Song J (2013) Non-equiprobable APSK constellation labeling design for BICM systems. IEEE Commun Lett 17(6):1276–1279
37. Chindapol A, Ritcey JA (2001) Design, analysis, and performance evaluation for BICM-ID with square QAM constellations in rayleigh fading channels. IEEE J Sel Areas Commun 19(5):944–957
38. Li X, Chindapol A, Ritcey JA (2002) Bit-interleaved coded modulation with iterative decoding and 8 PSK signaling. IEEE Trans Commun 50(8):1250–1257
39. Kang DH, Zhidkov SV, Choi HJ (2010) An adaptive detection and suppression of co-channel interference in DVB-T/H system. IEEE Trans Consum Electr 56(3):1320–1327
40. Kim H, Yoon H, Sunahara H, Kato A (2012) Study on coexistence of a narrow band system with terrestrial DTV system: focused on DTV white space utilization with TETRA release 1. In: 2012 world telecommunications congress (WTC'12), pp 1–5
41. Kim H, Sunahara H, Kato A (2012) Comparison on DTV affected range by difference of secondary user bandwidth in adjacent channel. In: 2012 international symposium on wireless communication systems (ISWCS'12), pp 96–100 (2012)
42. Ahmadi S (2009) An overview of next-generation mobile WiMAX technology. IEEE Commun Mag 47(6):84–98
43. IEEE: Wireless LAN medium access control (MAC) and physical layer (PHY) specifications (2009)
44. IEEE: IEEE standard for information technology—local and metropolitan area networks—specific requirements—part 11: Wireless LAN medium access control (MAC) and physical layer (PHY) specifications amendment 6: Wireless access in vehicular environments (2010)
45. Digital video broadcasting (DVB): Framing structure, channel coding and modulation for cable systems (DVB-C). ETSI EN 300 429 v1.2.1 (1998)
46. ITU-T: ITU G.9960, unified high-speed wire-line based home networking transceivers—system architecture and physical layer specification (2010)
47. IEEE: IEEE standard for broadband over power line networks: Medium access control and physical layer specifications (2010)
48. Rehman MU, Wang S, Liu Y, Chen S, Chen X, Parini CG (2012) Achieving high data rate in multiband-OFDM UWB over power-line communication system. IEEE Trans Power Deliv 27(3):1172–1177
49. Tonello AM, Siohan P, Zeddam A, Mongaboure X (2008) Challenges for 1 Gbps power line communications in home networks. In: 2008 IEEE 19th international symposium on personal, indoor and mobile radio communications, pp 1–6
50. Ferreira HC, Lampe L, Newbury J, Swart TG (2010) Power line communications–theory and applications for narrowband and broadband communications over power lines. Wiley, UK
51. Gozalvez J (2016) New 3GPP standard for IoT. IEEE Veh Technol Mag 11(1):14–20
52. Hoymann C, Astely D, Stattin M, Wikstrom G, Cheng JF, Hoglund A, Frenne M, Blasco R, Huschke J, Gunnarsson F (2016) LTE release 14 outlook. IEEE Commun Mag 54(6):44–49
53. Rico-Alvarino A, Vajapeyam M, Xu H, Wang X, Blankenship Y, Bergman J, Tirronen T, Yavuz E (2016) An overview of 3GPP enhancements on machine to machine communications. IEEE Commun Mag 54(6):14–21

54. Yang Z (2009) Digital terrestrial television transmission technologies and systems. People's Telecommunications Press, Beijing
55. Falconer D, Ariyavisitakul SL, Benyamin-Seeyar A, Eidson B (2002) Frequency domain equalization for single-carrier broadband wireless systems. IEEE Commun Mag 40(4):58–66
56. van de Beek JJ, Sandell M, Borjesson PO (1997) ML estimation of time and frequency offset in OFDM systems. IEEE Trans Signal Process 45(7):1800–1805
57. He L, Yang F, Zhang C, Wang Z (2010) Synchronization for TDS-OFDM over multipath fading channels. IEEE Trans Consum Electr 56(4):2141–2147
58. Minn H, Zeng M, Bhargava VK (2000) On timing offset estimation for OFDM systems. IEEE Commun Lett 4(7):242–244
59. Schmidl TM, Cox DC (1997) Robust frequency and timing synchronization for OFDM. IEEE Trans Commun 45(12):1613–1621
60. 3GPP: 3GPP TS 36.211 v10.3.0—evolved universal terrestrial radio access (E-UTRA); physical channels and modulation (release 8) (2011)
61. Tran NH, Nguyen HH, Le-Ngoc T (2007) Performance of BICM-ID with signal space diversity. IEEE Trans Wirel Commun 6(5):1732–1742
62. Xie Q, Song J, Peng K, Yang F, Wang Z (2011) Coded modulation with signal space diversity. IEEE Trans Wirel Commun 10(2):660–669
63. Basar E (2015) OFDM with index modulation using coordinate interleaving. IEEE Wirel Commun Lett 4(4):381–384
64. Ramseier S (2003) Shuffling bits in time and frequency: an optimum interleaver for OFDM. In: IEEE international conference on communications (ICC '03), vol 5, pp 3418–3422
65. Wang D, Kobayashi H (2000) On design of interleavers with practical size for turbo codes. In: 2000 IEEE international conference on communications (ICC'00), pp 618–622
66. Carlson AB, Crilly PB, Ruttledge J (1986) Communnication system. An introduction to signals and noise in electrical engineering. McGraw-Hill, New York
67. Pierce JR (2012) An introduction to information theory: symbols, signals and noise. Courier Corporation
68. Poisel, R.: Modern Communications Jamming Principles and Techniques. Artech House (2011)
69. Gao J (2016) Electronics noises and low-noise design. Tsinghua University Press, Beijing
70. Vaseghi SV (2008) Advanced digital signal processing and noise reduction. Wiley
71. Yi S (1984) Noises in electronics systems and low-noise design methods. Jilin People's Press, Jilin
72. Ziemer R, Tranter WH (2006) Principles of communications: system modulation and noise. Wiley
73. Middleton D (1979) Procedures for determining the parameters of the first-order canonical models of class A and class B electromagnetic interference. IEEE Trans Electromagn Compatib EMC-21(3):190–208
74. Schober R, Lampe L (2004) Sequence detection and adaptive channel estimation for ISI channels under class-A impulsive noise. IEEE Trans Commun 52(9):1523–1531
75. Coulson A (2004) Narrowband interference in pilot symbol assisted OFDM systems. IEEE Trans Wirel Commun 3(6):2277–2287
76. Darsena D (2007) Successive narrowband interference cancellation for OFDM systems. IEEE Commun Lett 11(1)
77. Wu Z, Nassar CR (2005) Narrowband interference rejection in OFDM via carrier interferometry spreading codes. IEEE Trans Wirel Commun 4(4):1491–1505
78. Dong Z (2002) Principles of communication circuits. Higher Education Press, Beijing
79. Shannon CE (1949) Communication in the presence of noise. Proc IRE 37(1):10–21
80. Zhu X (2001) Fundamentals of applied information theory. Tsinghua University Press, Beijing
81. Primak SL, Lyandres VZ (1998) On the generation of the baseband and narrowband non-Gaussian processes. IEEE Trans Signal Process. 46(5):1229–1237
82. Middleton D (1977) Statistical-physical models of electromagnetic interference. IEEE Trans Electromagn Compatib 3:106–127

83. Umehara D, Yamaguchi H, Morihiro Y (2004) Turbo decoding in impulsive noise environment. In: IEEE global communications conference (GLOBECOM'04), vol 1, pp 194–198
84. Tonello AM, Pecile F (2009) Efficient architectures for multiuser FMT systems and application to power line communications. IEEE Trans Commun 57(5)
85. Umehara D, Nishiyori H, Morihiro Y (2006) Performance evaluation of CMFB transmultiplexer for broadband power line communications under narrowband interference. In: 2006 IEEE international symposium on power line communications and its applications (ISPLC'06), pp 50–55
86. Andreadou N, Pavlidou F (2010) Modeling the noise on the OFDM power-line communications system. IEEE Trans Power Deliv 25(1):150–157
87. Lampe L (2011) Bursty impulse noise detection by compressed sensing. In: 2011 IEEE international symposium on power line communications and its applications (ISPLC), pp 29–34
88. Zimmermann M, Dostert K (2002) Analysis and modeling of impulsive noise in broad-band powerline communications. IEEE Trans Electromagn Compatib 44(1):249–258
89. Kawaguchi A, Okada H, Yamazato T, Katayama M (2006) Correlations of noise waveforms at different outlets in a power-line network. In: 2006 IEEE international symposium on power line communications and its applications (ISPLC'06), pp 92–97 (2006)
90. Nassar M, Gulati K, Mortazavi Y, Evans BL (2011) Statistical modeling of asynchronous impulsive noise in powerline communication networks. In: 2011 IEEE global communications conference (GLOBECOM'11), pp 1–6
91. Hooijen OG (1998) On the channel capacity of the residential power circuit used as a digital communications medium. IEEE Commun Lett 2(10):267–268
92. Chi DW, Das P (2008) Effects of nonlinear amplifiers and narrowband interference in MIMO-OFDM with application to 802.11 n WLAN. In: 2nd international conference on signal processing and communication systems (ICSPCS'08), pp 1–7
93. Shepherd RA, Gaddie JC, Nielson DL (1976) New techniques for suppression of automobile ignition noise. IEEE Trans Vehic Technol 25(1):2–12
94. Lago-Fernández J, Salter J (2004) Modelling impulsive interference in DVB-T: Statistical analysis, test waveforms and receiver performance. BBC R&D White Paper WHP 80
95. Chaudhuri A, Bhatnagar MR (2014) Optimised resource allocation under impulsive noise in power line communications. IET Commun 8(7):1104–1108
96. Ghosh M (1996) Analysis of the effect of impulse noise on multicarrier and single carrier QAM systems. IEEE Trans Commun 44(2):145–147
97. Darsena D, Gelli G, Melito F, Verde F, Vitiello A (2013) Impulse noise mitigation for MIMO-OFDM wireless networks with linear equalization. In: 2013 IEEE international workshop on measurements and networking proceedings (M&N), pp 94–99
98. Suraweera H, Armstrong J (2004) Noise bucket effect for impulse noise in OFDM. Electr Lett 40(18):1156–1157
99. Blackard KL, Rappaport TS, Bostian CW (1993) Measurements and models of radio frequency impulsive noise for indoor wireless communications. IEEE J Sel Areas Commun 11(7):991–1001
100. Thompson D, Dixon J (2004) Vehicle noise. Advanced applications in acoustics, noise and vibration, pp 236–291
101. HomePlugAlliance: Home plug green PHY the standard for in-home smart grid powerline communications (2010)
102. Vallejo-Mora AB, Sánchez-Martínez JJ, Canete FJ, Cortés JA, Diez L (2010) Characterization and evaluation of in-vehicle power line channels. In: 2010 IEEE global communications conference (GLOBECOM 2010), pp 1–5
103. Liu S, Yang F, Ding W, Song J (2016) Double kill: compressive-sensing-based narrow-band interference and impulsive noise mitigation for vehicular communications. IEEE Trans Vehic Technol 65(7):5099–5109
104. Park J, Kim D, Kang C, Hong D (2003) Effect of bluetooth interference on OFDM-based WLAN. In: 2003 IEEE 58th vehicular technology conference (VTC'03-Fall), vol 2, pp 786–789

105. Harjula I, Pinola J, Prokkola J (2011) Performance of IEEE 802.11 based WLAN devices under various jamming signals. In: Military communications conference (MILCOM'11), pp 2129–2135
106. Odling P, Borjesson O, Magesacher T, Nordstrom T (2002) An approach to analog mitigation of RFI. IEEE J Sel Areas Commun 20(5):974–986
107. Van Welden D, Steendam H (2007) Interference cancellation of AM narrowband interference signals. In: IEEE 65th vehicular technology conference (VTC'07-Spring), pp 1617–1621
108. Meng J (2007) Noise analysis of power-line communications using spread-spectrum modulation. IEEE Trans Power Deliv 22(3):1470–1476
109. Zhang J, Meng J (2010) Noise resistant OFDM for power-line communication systems. IEEE Trans Power Deliv 25(2):693–701
110. Matsumoto Y, Takeuchi M, Fujii K, Sugiura A, Yamanaka Y (2005) Performance analysis of interference problems involving DS-SS WLAN systems and microwave ovens. IEEE Trans Electromagn Compatib 47(1):45–53
111. Matsumoto Y, Shimizu T, Murakami T, Fujii K, Sugiura A (2007) Impact of frequency-modulated harmonic noises from PCs on OFDM-based WLAN systems. IEEE Trans Electromagn Compatib 49(2):455–462
112. Giorgetti A, Chiani M, Win MZ (2005) The effect of narrowband interference on wideband wireless communication systems. IEEE Trans Commun 53(12):2139–2149
113. Oka A, Lampe L (2009) Compressed sensing reception of bursty UWB impulse radio is robust to narrow-band interference. In: IEEE global communications conference (GLOBECOM'09), pp 1–7
114. Shi K, Zhou Y, Kelleci B, Fischer TW, Serpedin E, lker Karsilayan A (2007) Impacts of narrowband interference on OFDM-UWB receivers: analysis and mitigation. IEEE Trans Signal Process 55(3):1118–1128
115. Ye Z, Duan C, Orlik PV, Zhang J, Abouzeid AA (2010) A synchronization design for UWB-based wireless multimedia systems. IEEE Trans Broadcast 56(2):211–225
116. Marey M, Steendam H (2007) Analysis of the narrowband interference effect on OFDM timing synchronization. IEEE Trans Signal Process 55(9):4558–4566
117. Nadarajah S (2007) Explicit expressions for the bit error probabilities of OFDM. IEEE Trans Broadcast 53(1):138
118. Esli C, Deliç H (2006) Coded OFDM with transmitter diversity for digital television terrestrial broadcasting (corrected). IEEE Trans Broadcast 52(4):586–596
119. Al-Dharrab S, Uysal M (2009) Cooperative diversity in the presence of impulsive noise. IEEE Trans Wirel Commun 8(9):4730–4739
120. Gao P, Tepedelenlioglu C (2007) Space-time coding over fading channels with impulsive noise. IEEE Trans Wirel Commun 6(1):220–229
121. Savoia R, Verde F (2013) Performance analysis of distributed space-time block coding schemes in Middleton Class-A noise. IEEE Trans Vehic Technol 62(6):2579–2595
122. Tepedelenlioglu C, Gao P (2005) On diversity reception over fading channels with impulsive noise. IEEE Trans Vehic Technol 54(6):2037–2047
123. Juwono FH, Guo Q, Huang D, Wong KP (2014) Deep clipping for impulsive noise mitigation in OFDM-based power-line communications. IEEE Trans Power Deliv 29(3):1335–1343
124. Abdelkefi F, Duhamel P, Alberge F (2005) Impulsive noise cancellation in multicarrier transmission. IEEE Trans Commun 53(1):94–106
125. Zhidkov SV (2003) Impulsive noise suppression in OFDM-based communication systems. IEEE Trans Consum Electr 49(4):944–948
126. Zhidkov SV (2008) Analysis and comparison of several simple impulsive noise mitigation schemes for OFDM receivers. IEEE Trans Commun 56(1):5–9
127. Ma Y, So P, Gunawan E (2005) Performance analysis of OFDM systems for broadband power line communications under impulsive noise and multipath effects. IEEE Trans Power Deliv 20(2):674–682
128. Wu Y (1999) Performance comparison of ATSC 8-VSB and DVB-T COFDM transmission systems for digital television terrestrial broadcasting. IEEE Trans Consum Electr 45(3):916–924

129. Nilsson R, Sjoberg F, LeBlanc JP (2003) A rank-reduced LMMSE canceller for narrowband interference suppression in OFDM-based systems. IEEE Trans Commun 51(12):2126–2140
130. Darsena D, Verde F (2008) Successive NBI cancellation using soft decisions for OFDM systems. IEEE Signal Process Lett 15:873–876
131. Hsiao HF, Hsieh MH, Wei CH (1998) Narrow-band interference rejection in OFDM-CDMA transmission system. In: Proceedings of the 1998 IEEE international symposium on circuits and systems (ISCAS'98), vol 4, pp 437–440
132. Kelleci B, Fischer TW, Shi K, Zhou Y, Karsilayan AI, Serpedin E (2006) Narrowband interference suppression in multi-band OFDM ultra wideband communication systems: a mixed-mode approach. In: 12th-signal processing education workshop, pp 55–59
133. Yonggang Z, Ze Z (2007) A method of FFT-based spectral analysis for narrowband interference suppression. In: 8th international conference on electronic measurement and instruments (ICEMI'07), pp 3–787
134. Stamoulis A, Giannakis GB, Scaglione A (2001) Block FIR decision-feedback equalizers for filterbank precoded transmissions with blind channel estimation capabilities. IEEE Trans Commun 49(1):69–83
135. Darsena D, Gelli G, Paura L, Verde F (2005) Widely linear equalization and blind channel identification for interference-contaminated multicarrier systems. IEEE Transa Signal Process 53(3):1163–1177
136. Darsena D, Gelli G, Paura L, Verde F (2007) A constrained maximum-SINR NBI-resistant receiver for OFDM systems. IEEE Trans Signal Process 55(6):3032–3047
137. Coulson AJ (2006) Bit error rate performance of OFDM in narrowband interference with excision filtering. IEEE Trans Wirel Commun 5(9):2484–2492
138. Gerakoulis D, Salmi P (2002) An interference suppressing OFDM system for ultra wide bandwidth radio channels. In: 2002 IEEE conference on ultra wideband systems and technologies, pp 259–264 (2002)
139. Popescu DC, Yaddanapudi P (2007) Narrowband interference avoidance in OFDM-based UWB communication systems. IEEE Trans Commun 55(9):1667–1673
140. Yaddanapudi P, Popescu DC (2005) Narrowband interference avoidance in ultra wideband communication systems. In: IEEE global communications conference (GLOBECOM'05), vol 6
141. Cowley N, Payne A, Dawkins M (2002) COFDM tuner with impulse noise reduction. European Patent: EP1180851 (2002)
142. Häring J, Vinck AH (2000) OFDM transmission corrupted by impulsive noise. In: IEEE international symposium on powerline communications (ISPLC'00), pp 9–14
143. Haring J, Vinck AH (2003) Iterative decoding of codes over complex numbers for impulsive noise channels. IEEE Transa Inform Theory 49(5):1251–1260
144. Matsuo H, Umehara D, Kawai M, Morihim Y (2002) An iterative detection scheme for OFDM over impulsive noise channels. In: IEEE international symposium on powerline communications (ISPLC'02)
145. Abdelkefi F, Duhamel P, Alberge F (2007) A necessary condition on the location of pilot tones for maximizing the correction capacity in OFDM systems. IEEE Trans Commun 55(2):356–366
146. Kumaresan R (1985) Rank reduction techniques and burst error-correction decoding in real/complex fields. In: 19th Asilomar conference on circuits, systems and computers, pp 457–461
147. Marvasti F, Hasan M, Echhart M, Talebi S (1999) Efficient algorithms for burst error recovery using FFT and other transform kernels. IEEE Trans Signal Process 47(4):1065–1075
148. Wolf J (1983) Redundancy, the discrete Fourier transform, and impulse noise cancellation. IEEE Trans Commun 31(3):458–461
149. Redinbo GR (2000) Decoding real block codes: activity detection wiener estimation. IEEE Trans Inform Theory 46(2):609–623
150. Gabay A, Duhamel P, Rioul O (2000) Spectral interpolation coder for impulse noise cancellation over a binary symetric channel. In: 2000 10th European signal processing conference, pp 1–4

151. Tulino A, Verdú S, Caire G, Shamai S (2007) The Gaussian erasure channel. In: IEEE international symposium on information theory (ISIT'07), pp 1721–1725
152. Rinne J, Hazmi A, Renfors M (2003) Impulse burst position detection and channel estimation schemes for OFDM systems. IEEE Trans Consum Electr 49(3):539–545
153. Brennan D (2003) Linear diversity combining techniques. Proc IEEE 91(2):331–356
154. Dubey A, Mallik RK, Schober R (2014) Performance analysis of a power line communication system employing selection combining in correlated log-normal channels and impulsive noise. IET Commun 8(7):1072–1082
155. Lai SW, Messier GG (2010) The wireless/power-line diversity channel. In: 2010 IEEE international conference on communications (ICC'10), pp 1–5

Chapter 2
System Model and Fundamental Knowledge
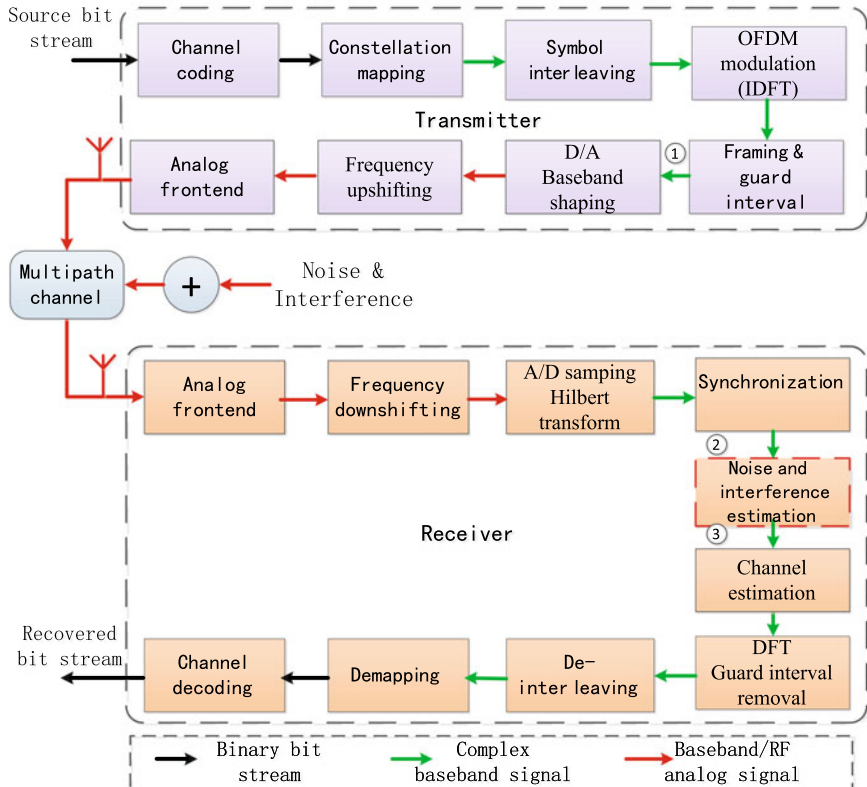
Abstract This chapter mainly introduces the background models and fundamental knowledge related with the research work of this thesis. Firstly, the main modules and the related key techniques of the broadband digital communication systems based on the technique of block transmission OFDM are briefly described. Secondly, the preamble structure in the frame header and the structure of data sub-frames commonly seen in many kinds of broadband digital communication systems and standards are introduced. Then, the theoretical models of the research objective of this thesis, i.e. narrowband interference and impulsive noise, which was proposed and widely adopted in literature, are described in detail, providing the model basis for the research contents of this thesis. Finally, the theory of sparse recovery is briefly introduced, including compressed sensing, structured compressed sensing, sparse Bayesian learning, etc, which provides theoretical basis and guidance for the research on sparse recovery in this thesis.

2.1 An Overview of Broadband Digital Communication Systems

2.1.1 OFDM-Based Block Transmission

The OFDM technique has the advantages of high spectral efficiency and strong capability of combatting against frequency selectivity, etc. The broadband block transmission technique based on the OFDM technique is able to effectively mitigate the inter-block interference (IBI) and inter-symbol interference (ISI), which makes it very convenient to implement accurate channel estimation [13, 42]. Thus, it is widely applied in many kinds of broadband communication systems and standards, including power line communications [30, 33], cellular wireless communications [1, 2], wireless local area networks [29], wireless vehicular networks [31], etc. This thesis is mainly focused on the broadband block transmission system based on the OFDM technique as a system background, and studies the key technologies on narrowband interference and impulsive noise mitigation and elimination.

Fig. 2.1 The illustration of the architecture and main modules of the broadband block transmission system based on the OFDM technique

The illustration of the system architecture of a typical point to point broadband block transmission system based on the OFDM technique is shown in Fig. 2.1, which contains three main logical components including the transmitter, the channel, and the receiver [23, 63]. The transmitter finishes the task of converting the binary bit stream in the source to the radio frequency signal and sending it to the channel through the antenna. The transmitted signal passes through the multi-path fading channel and suffers from the additive noise and interference. Then it is coupled into the antenna at the receiver and received by the receiver. The main modules of the receiver can be classified into two categories, namely "inner receiver" and "outer receiver", according to the functionality of the receiver. The modules of synchronization and noise and interference elimination can be regarded as the inner receiver, while the modules of deinterleaving and channel decoding can be regarded as the outer receiver. It can be observed from Fig. 2.1 that, the signals flowing through the transmission system can be classified into mainly three types, namely the binary bit stream, the complex

baseband signal, and the analog signal, which is denoted by black arrows, green arrows, and red arrows, respectively.

Specifically, the transmitter mainly consists of the following modules [23, 55]: bit stream sent from source $\longrightarrow$ channel coding (implementing forward error check coding on the signal source bit stream) $\longrightarrow$ constellation mapping (mapping the coded bit stream to the complex symbol domain according to a certain constellation mapping rule) $\longrightarrow$ symbol interleaving (implementing interleaving on the mapped symbols in order to combat against time selective and frequency selective fading, the time and frequency combined interleaving scheme investigated in Chap. 4 of this thesis is mainly focused on this module) $\longrightarrow$ OFDM modulation (mapping the complex symbols to the OFDM sub-carriers, and generating the time-domain OFDM symbols by exploiting the IDFT transform) $\longrightarrow$ frame formulation (adding the guard interval to generate the signal sub-frames, and generating superframes along with the preamble and control fields) $\longrightarrow$ digital to analog converting and baseband waveform shaping (the complex baseband signal is converted from digital to analog, and passes through the baseband shaping filter to generate the baseband analog signal) $\longrightarrow$ orthogonal frequency up-conversion $\longrightarrow$ sending signal from the analog front end. Among these, the signal after the frame formulation at the transmitter (the location denoted by the mark of ① in Fig. 2.1) can be denoted by $[\mathbf{p}_i^T, \mathbf{x}_i^T]^T$, which represents the ith signal frame in the time domain, including the length-M frame header (guard interval) of the ith signal frame $\mathbf{p}_i = [p_{i,0}, p_{i,1}, \ldots p_{i,M-1}]^T$, the length-$N$ frame payload of the ith signal frame (the time-domain OFDM symbol) $\mathbf{x}_i = [x_{i,0}, x_{i,1}, \ldots x_{i,N-1}]^T$.

The receiver mainly consists of the following modules [48, 63]: coupling received signal from the radio frequency analog front end $\longrightarrow$ frequency down-conversion $\longrightarrow$ analog to digital sampling and Hilbert transform (the complex baseband digital signal is obtained by analog to digital conversion and sampling, and Hilbert transform) $\longrightarrow$ synchronization (implementing receiver side frame synchronization and carrier recovery by exploiting the preamble, frame header, and time/frequency domain training sequences in the frame structure. The design of synchronization frame structure and the synchronization algorithms investigated in this thesis are mainly focused on this module) $\longrightarrow$ reconstruction and elimination of the noise and interference (implementing elimination of noise and interference in the baseband equivalent complex signal. The algorithms of narrowband interference and impulsive noise recovery and elimination based on sparse recovery investigated in this thesis are mainly focused on this process. The state-of-the-art conventional systems do not have this module that is able to eliminate the noise and interference) $\longrightarrow$ removing the guard interval and taking DFT transform (removing the guard interval between the data sub-frame and the OFDM symbol, and implementing the DFT transform, which is equivalent to implementing the "serial to parallel conversion", converting the serial complex baseband signal to the parallel OFDM sub-carrier data by using the DFT transform) $\longrightarrow$ deinterleaving (the deinterleaver is corresponding to the interleaver at the transmitter, which obtains the sequence of the complex baseband symbols before interleaving according to the deinterleaving rules) $\longrightarrow$ demapping (demapping the constellation mapped symbols to a binary bit stream according to a

certain soft or hard decision or iterative decision algorithm) $\longrightarrow$ channel decoding (decoding the coded codeword by exploiting the decoding algorithm corresponding to the forward error check code, meanwhile detecting and correcting the possible bit errors) $\longrightarrow$ the recovered data bit stream after decoding is obtained. Among these steps, in the signal after the synchronization at the receiver and before the estimation and elimination of the noise and interference (in the location as denoted by the mark of ② in Fig. 2.1), the frame payload of the ith received signal frame (the ith received OFDM symbol in the time domain) can be denoted by $\mathbf{y}_i = [y_{i,0}, y_{i,1}, \ldots y_{i,N-1}]^T$, which is given in detail by the following equation:

$$\mathbf{y}_i = \mathbf{h}_i \odot \mathbf{x}_i + \mathbf{e}_i + \mathbf{z}_i + \mathbf{w}_i \tag{2.1}$$

where $\mathbf{h}_i = [h_{i,0}, h_{i,1}, \ldots h_{i,L-1}]^T$ denotes the channel impulse response (CIR) of the multi-path channel with the maximum multi-path delay spread of L, $\odot$ denotes the convolution operation, $\mathbf{e}_i = [e_{i,0}, e_{i,1}, \ldots e_{i,N-1}]^T$ denotes the narrow-band interference signal corresponding to the ith received time-domain OFDM symbol, $\mathbf{z}_i = [z_{i,0}, z_{i,1}, \ldots z_{i,N-1}]^T$ denotes the impulsive noise corresponding to the ith received time-domain OFDM symbol, $\mathbf{w}_i = [w_{i,0}, w_{i,1}, \ldots w_{i,N-1}]^T$ denotes the corresponding background AWGN vector. After the estimation and elimination of the noise and interference (as denoted by the location of the mark of ③ in Fig. 2.1), the components of narrowband interference and impulsive noise in the received signal have been recovered and eliminated, and the received signal of interest can be used for the successive processing.

2.1.2 Key Techniques of OFDM-Based Block Transmission

The formulation and implementation of the main modules of the point to point broadband digital block transmission system based on OFDM are supported by the key techniques of point to point transmission in both theory and technology. The fundamental concepts, principles, and functionalities of some of the key techniques therein are listed as follows[1]:

- *OFDM Block Transmission Technique* [13, 42]:
  The OFDM technique is one kind of highly spectrally efficient multi-carrier block transmission technique, whose main principle is based on IDFT and DFT transforms. The IDFT transform maps the frequency domain data at the N sub-carriers with identical sub-carrier spacing to the time domain, which generates a time-domain OFDM data block (also known as an OFDM symbol in some literature). The generated OFDM block guarantees the sub-carriers are orthogonal to each

---

[1]Although the other modules, functions and related techniques in the broadband digital communication system are also very important to the overall system, due to the limit of the pages, only the modules and related fundamental techniques that are closely related to the research work in this thesis are briefly described in this chapter, while the other modules and techniques are omitted.

other and thus there is no inter-carrier interference (ICI). Since the sub-carrier spacing is identical, the orthogonality between different sub-carriers is ensured, which not only prevents from the ICI but also significantly improves the spectral efficiency. Since the bandwidth occupied by one single sub-carrier (also known as one OFDM sub-channel in some literature) is usually much smaller than the coherent bandwidth which is corresponding to the maximum multi-path delay, the data at the sub-carriers can be regarded as having passed a flat fading channel instead of a frequency-selective fading channel. Thus it is effective for the OFDM symbol to combat against the inter-symbol interference (ISI) and the frequency-selective fading (multi-path fading). The OFDM modulation can be simply and efficiently implemented by using the fast Fourier transform (FFT) algorithm in realistic systems, which is able to significantly reduce the implementation complexity and the computational resource costs. The guard intervals inserted in between the sub-frames of block transmission can avoid the inter-block interference (IBI), thus it can further combat against the multi-path fading, especially the difficulty of long delay channels can be better solved. The performance of transmission of different transmitted blocks can be independent of each other. When the cyclic prefixing is adopted as the guard interval, a better orthogonality between different sub-carriers can be ensured, which better facilitates the implementation of frequency domain equalization.

- *Synchronization Techniques* [37, 40, 52, 70]:
  The OFDM system is very sensitive to the performance of synchronization. Both the carrier synchronization error and the frame synchronization error will lead to the serious loss of the decoding performance of the OFDM systems. The requirements of synchronization in OFDM systems mainly include frame synchronization, carrier synchronization, and sampling synchronization. Frame synchronization is also called timing synchronization, which is implementing the synchronization of the accurate location of the transmitted OFDM sub-frames. The FFT window is adjusted to be accurately corresponding to the OFDM data block, which makes it easier to implement frequency-domain equalization, demapping, and decoding. The state of the art main methods of frame synchronization are implemented by exploiting the preamble in the physical layer super-frame. The specific patterns of the time or frequency known training sequences in the preamble are made use of, and the optimal synchronization peak is found based on the methods of auto-correlation and cross correlation, which obtains the accurate synchronization location of frame synchronization. Carrier synchronization is also called carrier recovery, which is acquiring the accurate carrier of the transmitted signal at the receiver. The recovered carrier is exploited for frequency down-conversion and carrier frequency offset (CFO) compensation. The state of the art techniques of carrier recovery are based on digital signal processing techniques, exploiting the phase of the synchronization frame structure to deal with and achieve the recovery of the digital carrier. Sampling synchronization is to obtain the synchronization of the clock of the analog to digital conversion sampling, which requires to be synchronous to the clock of the transmitter. The sampling frequency offset (SFO)

compensation can be implemented by the methods of algebraic interpolation and
feedback compensation, etc.

- *Coding and Modulation Techniques* [5, 9, 12, 51, 60]:
  The coding and modulation techniques are the fundamental theory of broadband
  OFDM systems, which will have a significant influence on the system performance
  to a great extent. Whether the coding and modulation schemes are efficient is also
  the key to approaching the channel capacity for the system, and it is also an indicator
  to classify different generations of communication technologies in essence.

  In the area of error correction coding, at present, the channel coding commonly
  adopted in broadband communications that is capable of approaching the Shannon
  coding channel capacity limit in theory mainly includes the low density parity
  check (LDPC) code and Turbo code, etc. The LDPC code was designed by Robert
  G. Gallager in 1960 and proposed in his doctoral thesis, which should be classified
  into a kind of linear error correction code. The coding theory shows that in the
  condition of constrained noise power, the Shannon limit can be approached by
  designing appropriate LDPC codes. The LDPC code can be efficiently decoded
  in a linear time scale proportional to the code length based on the iterative belief
  propagation method. Moreover, LDPC codes can support parallel decoding very
  well, thus improving the decoding efficiency and reducing the decoding delay,
  which has a significant advantage in the condition of limited spectrum and limited
  feedback transmission link. The LDPC code has already been adopted by the 5G
  working group as the data channel coding scheme of long code and short code in the
  enhanced mobile broadband (eMBB) scenarios. Turbo code was proposed in 1990.
  It is the first capacity approaching forward error correction code ever developed.
  Turbo code has become the channel coding scheme adopted by the 3G and 4G
  cellular mobile communication standards because of its superior performance and
  relatively low complexity of coding and decoding, which has been widely applied
  in realistic system implementation. In the recent years, the emerging polar code is
  the only code discovered till now that is theoretically proven to be able to achieve
  the Shannon limit, which has been adopted by the control channel of the 5G eMBB
  scenario.

  In the area of modulation and constellation mapping, currently the modulation
  and constellation mapping methods commonly applied in the broadband digital
  communication systems mainly include quadrature amplitude modulation (QAM),
  amplitude phase shift keying (APSK), etc. Both QAM and APSK can better sup-
  port high order mapping and modulation, such as 256QAM, 256APSK, etc, which
  is specified in many existing standards. High order modulations can improve the
  spectral efficiency. According to the Euclidean distance and Hamming distance
  between different bits of constellation mapped symbols, and due to the character-
  istics of them in the corresponding error correction code, the bits have different
  protection levels, so the constellation mapping scheme and the bit mapping mode
  can be further optimized based on the unequal bit protection levels. Furthermore,
  exploiting the techniques of bit loading and bit permutation can further improve
  the performance and coding and modulation. Besides, by making full use of the
  signal space diversity (SSD) gain and the iterative soft demapping and decoding

techniques, the advanced techniques of bit interleaved coded modulation (BICM), BICM-iterative decoding (BICM-ID), BICM-ID-SSD, etc, can be exploited to further improve the performance of decoding and demapping.

- *Interleaving Techniques* [7, 50, 66]:
  The performance and the transmission rate of point to point transmission suffer from the detrimental impacts of frequency selective and time selective fading, noises and interferences. By exploiting the interleaving techniques, the time diversity and frequency diversity can be made use of to achieve gain. The interleaving schemes in the coded block transmission OFDM systems mainly include bit interleaving and symbol interleaving. The interleaving schemes can be classified into time interleaving and frequency interleaving from the interleaving purpose perspective of view. For the coded block transmission systems, the interleaving schemes can be classified, from the interleaving pattern perspective of view, into intra block interleaving, inter block interleaving, intra codeword bit interleaving, and inter codeword bit interleaving, etc. The commonly used interleaving schemes include block interleaving, convolutional interleaving, row and column interleaving, etc. These different interleaving schemes are all applicable for bit interleaving and symbol interleaving. Bit interleaving is mainly aimed at the memory channel characteristics in the presence of impulsive noise. The impulsive errors and the statistical correlation among successive codewords are dispersed in the time scale, and thus the capability against impulsive errors and the time selective fading channel will be improved for most of the group codes and convolutional codes, which is usually designed for the independent and random errors instead of impulsive errors. By optimizing the bit interleaving technique inside the codeword or between codewords, and in accompany with bit loading, bit permutation, constellation bit mapping patterns, and the unequal bit protection schemes, the performance of the error correction decoder in the noisy memory channel can be improved. Symbol interleaving can include time interleaving schemes and frequency interleaving schemes. In coded block transmission systems, symbol interleaving can be implemented within the blocks, or in between different blocks. For the long codeword coding schemes, implementing symbol level time interleaving between different blocks is helpful for avoiding the unfavorable channel condition of successive impulsive errors, and can improve the time diversity gain. The delay of the interleaver is related with the number of block symbols that participate in the interleaving process. Frequency interleaving can be implemented inside one block or between different blocks, too. By exploiting a specific interleaving pattern, the frequency selective fading and spectral notches can be dispersed, and thus the frequency diversity gain can be improved.
- *MIMO Multiple Antenna Techniques* [3, 26, 36, 44, 72]:
  The multiple antenna techniques can make good use of the spatial diversity to achieve gains and compensate for the channel loss of the transmitter and receiver systems, thus significantly improving the transmission efficiency and system performance of point to point transmission. The MIMO spatial multiplexing techniques, the beamforming and precoding techniques can enhance the effective signal to noise ratio of the received signal, and significantly improve the system through-

put by transmitting in multiple links. The techniques of multiple antenna transmit diversity and space time coding can provide spatial and temporal combined diversity gain. Multiple antenna receive diversity and the optimized combining schemes can provide receiver side spatial diversity gain, and combat against channel fading and errors, which reduces the transmission bit error rate in complicated channel conditions. Therefore, the MIMO techniques have been deeply investigated and widely applied in the current broadband communication systems. In the future 5G mobile communication scenarios, the MIMO techniques have been developing rapidly. The massive MIMO techniques, which make use of the enhanced great amount of antenna arrays, can support a much higher spectral efficiency. Based on the advanced new beamforming techniques, the multi-user MIMO techniques, the non-orthogonal multiple access (NOMA) MIMO techniques, the efficient space time coding, and the precoding techniques, an even greater scale of multi-user diversity and multiplexing can be achieved, which will play a more important role in further improving the multi-user channel capacity and the system throughput.

2.2 Frame Structure of Broadband Digital Communication Systems

The physical layer frame structure of the commonly seen broadband communication system based on OFDM block transmission is as shown in Fig. 2.2. No matter for the burst transmission or for the continuous transmission and broadcasting transmission, the physical layer transmitted signal is all composed of several super-frames. Each super-frame contains a preamble (or usually also called "first frame of super-frame" in some continuous transmission systems), the control field (also called the control signalling or control information), the data field (also called the payload data). The preamble is usually composed of some known specific time and frequency domain training sequences, which can be used to implement the functionalities of frame detection, automatic gain control (AGC), synchronization, and channel estimation, etc. Some may also contain and convey some signalling information. The control field may contain several specific fields (or control bits), which can convey some important information such as the physical layer frame transmission mode, the coding and modulation mode, the physical layer parameters, and the physical layer frame type, etc. They can be used to control the operations of decoding and demodulation in the receiver, and support the implementation of the physical layer communication protocols. The data field contains several data sub-frames (also called information frames), and each data sub-frame contains a complete OFDM data block (also called OFDM symbol or frame body) and its guard interval (also called the frame header). The frame header guard interval therein can be padded by zeros to formulate the zero padding OFDM (ZP-OFDM) frame structure. When the frame header guard interval is padded by the cyclic prefix of the OFDM data block, the cyclic prefix OFDM (CP-OFDM) frame structure is formulated. When the frame header guard
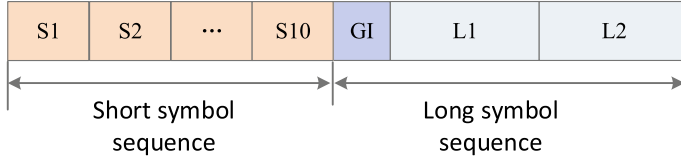
Fig. 2.2 Illustration of the physical layer frame structure of the broadband communication system based on OFDM block transmission

interval is filled with the specific known pseudo noise (PN) training sequences, the time-domain synchronous OFDM (TDS-OFDM) frame structure can be formulated.
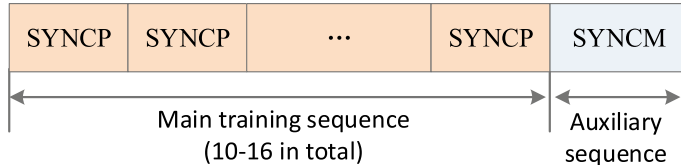
2.2.1   Structure of Preamble in Frame Header

In the physical layer frame structure, in order to facilitate the objectives of signal detection, synchronization, and channel estimation, usually a preamble is devised and included. In the burst transmission mode such as the wireless local area networks (WLAN) and the power line communication (PLC) systems, the preamble is transmitted in front of the information frames in the data field. Through the high speed processing on the training sequences of the preamble, the objectives of fast detection and synchronization for the physical layer data packets of burst transmission can be implemented. The receiver is enabled to enter the process of demodulation and decoding as fast as possible. In the continuous transmission scenario, the synchronization correction and channel estimation correction can be implemented dynamically in real time by making use of the preamble located at the beginning of the super-frame. The preamble is usually composed of several repeated and known training sequences. Similar preamble frame structures have been specified in many different communication standards, such as the WLAN systems specified by the IEEE 802.11n standard [29], the PLC systems specified by the IEEE P1901 standard [30] and the ITU-T G.9960 standard [33].

The preamble frame structure of the physical layer signal frame specified by the wireless local area networks IEEE 802.11 standards [29] is illustrated in Fig. 2.3. The preamble is composed of 10 *identical* short training sequences S1 to S10 and two *identical* long training sequences L1 and L2 and their guard intervals (cyclic prefixing) GI. The purpose of including the short training sequences is mainly to implement signal detection, automatic gain control, diversity selection, coarse estimation of carrier offset, and frame synchronization. The main purpose of the long

S1	S2	⋯	S10	GI	L1	L2

Short symbol
sequence

Long symbol
sequence

Fig. 2.3 Physical layer preamble frame structure specified by WLAN IEEE 802.11 standard

SYNCP	SYNCP	⋯	SYNCP	SYNCM

Main training sequence
(10-16 in total)

Auxiliary
sequence
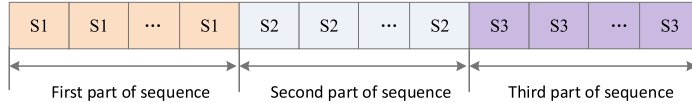
Fig. 2.4 Physical layer preamble frame structure specified by the PLC systems IEEE P1901 standard

training sequences is to implement channel estimation and the refined estimation of the carrier offset, etc. The time interval occupied by both one short training sequence and one long training sequence is $8.0\,\mu s$.

The physical layer preamble frame structure specified by the PLC systems IEEE P1901 standard [30] is illustrated in Fig. 2.4. The preamble is composed of 10–16 *identical* main sequences SYNCP and one auxiliary sequence SYNCM. Each main sequence SYNCP has a length of 512 time domain samples, which is generated by modulating the "+1" at several sub-carriers in the frequency domain. The auxiliary sequence SYNCM is defined by the opposite of the main sequence SYNCP, namely multiplying by -1. The main purpose of the main sequence includes automatic gain control, frame synchronization, and channel estimation, etc. The functionality of the auxiliary sequence is to help locating the synchronization location, and indicating the end of the preamble.

The physical layer preamble structure of the indoor broadband wireline interconnection systems specified by the international telecommunications union (ITU) G.9960 standard [33] is illustrated in Fig. 2.5. The preamble is composed of three groups of sequences, i.e. S1, S2, and S3. The number of frequency domain sub-carriers of the ith group of sequences and the number of the OFDM sub-carriers in the data payload are the same. The frequency domain training data are modulated on the sub-carriers with the step of k_i sub-carriers in between, where the value of k_i can be chosen as 1, 2, 4, and 8. The distance between the modulated data sub-carriers in the second group of sequences is the same to that of the first group of sequences, namely, $k_1 = k_2$. The number of the sequences in the ith group is N_i, whose values can be different for each group. The symbols in the second group of sequences are the inverse of those in the first group of sequences, namely, $S_2 = -S_1$. The parameters of the preamble, such as the length, can be configured according to different realistic channel conditions and the actual requirements of the system. These three groups of sequences can be adopted to implement the functions of analog or digital automatic

| S1 | S1 | ··· | S1 | S2 | S2 | ··· | S2 | S3 | S3 | ··· | S3 |

First part of sequence   Second part of sequence   Third part of sequence

Fig. 2.5 Physical layer preamble structure of the indoor broadband wireline interconnection specified by ITU-T G.9960 standard

gain control, coarse synchronization and accurate synchronization, carrier recovery, and channel estimation, etc.
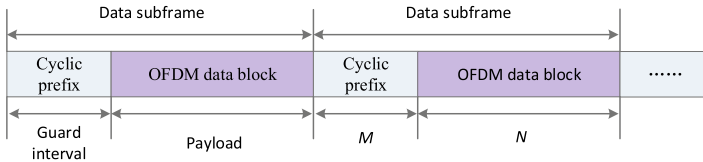
2.2.2   Structure of Data Sub-Frame

(1) *Structure of the CP-OFDM Data Sub-Frame*
In the frame structure of the data payload information frames, the CP-OFDM frame structure using the cyclic prefix of the OFDM data block as the padding frame header guard interval is widely adopted and applied as the frame structure of the data payload information frames, by the wireless cellular communication standards LTE/LTE-A, the wireless local area networks standards IEEE 802.11a/g/n, the European wireline/terrestrial digital television broadcasting standards DVB-C/DVB-T2, and the power line communication standards IEEE P1901/ITU-T G.9960, etc. The frame structure of CP-OFDM is illustrated in Fig. 2.6. The length of the cyclic prefix (the guard interval in the frame header) is V, and the length of the OFDM data block (the frame body) is N. The cyclic prefix is composed of the last V data samples of the OFDM data block. By exploiting the frame structure of cyclic prefixing, it is convenient for the receiver to convert the linear convolution between the signal and the channel impulse response into cyclic convolution, and thus it can facilitate the processing of DFT transform, frequency domain equalization, and demapping. The guard interval of cyclic prefixing can even ensure the OFDM sub-carriers are orthogonal to each other in the environment of multi-path fading, thus reducing the inter-channel interference between sub-carriers. The existence of the guard intervals is helpful for mitigating the inter-block interference between adjacent information frames in the block transmission system, which makes it easier to decode and demodulate the OFDM data block independently and avoid the mutual influences, finally improving the transmission efficiency.

(2) *Structure of the TDS-OFDM Data Sub-Frame*
In the structure of TDS-OFDM frames, the guard interval in the frame header of the information frames are padded by the known training sequences, which is specified by the terrestrial multimedia broadcasting standard and its evolved DTMB/DTMB-A standards [46, 56], and the ITU-R digital television broadcasting standards [32]. The structure of the TDS-OFDM signal frames is illustrated in Fig. 2.7. The guard interval in the frame header of the TDS-OFDM frames is filled with the pseudo

Fig. 2.6 CP-OFDM frame structure of the physical layer data payload information frames in the ITU-T G.9960 system

Fig. 2.7 TDS-OFDM frame structure

random (PN) sequences. The PN sequence is usually a frequency domain or time domain pseudo random training sequence, which can be generated by a group of linear shifting registers or m-sequence generators. The selected PN sequence should meet the requirements of spectrum compatibility, such as the spectrum mask and spectral notching, and the out of band spectrum leakage should be reduced. The PN sequence should be optimized and designed well to take a lower peak to average power ratio (PAPR) into account. Adopting the PN sequence as the padding guard interval has a lot of advantages such as fine spectrum characteristics and high spectral efficiency. It can be used for a lot of functions, including coarse channel estimation and accurate channel estimation, auxiliary accurate synchronization, and signalling transmission. Besides, in the multipath fading channel, the receiver can make use of the PN sequence and the subsequent OFDM data block that have passed the multipath fading channel and implement the overlap and add (OLA) operation, so as to achieve the cyclic convolution between the OFDM data block that is free from the impacts of the PN sequence and the CIR of the multipath channel. Then it can be utilized for equalization, demodulation, and decoding.

2.3 Narrowband Interference Model and Impulsive Noise Model

2.3.1 Narrowband Interference Model

As mentioned in Chap. 1, the intuitive definition of narrowband interference is the interfering signal outside the system with narrowband property and frequency domain sparsity, whose effective bandwidth occupied in the frequency domain is sufficiently

narrow and small compared with the working bandwidth of the information signal [14, 47]. The quantitative definition of narrowband interference is the interfering signal whose bandwidth occupied by the frequency domain nonzero entries is no more than 5% of the OFDM working bandwidth in the OFDM system [16, 69]. According the the definition of narrowband interference, the models of the narrowband interference usually adopted in literature for theoretical analysis and simulation experiments mainly contain the following:

(1) Single/multi-tone sinusoidal interferer model. It can be classified into classical deterministic spectrum models, which is composed of single or multiple asynchronous and mutually independent sinusoidal wave components with the frequency tones randomly distributed. It can be represented as a time domain real sinusoidal signal, or an equivalent complex baseband exponential signal [24, 25, 49].

(2) Frequency sparse multiple band-limited Gaussian noise interferers model. This model can be called as compound BLGN interferers model, which belongs to a kind of statistical narrowband interference model. This model is defined by the superposition of multiple BLGN interferers whose central frequencies lie in arbitrary locations, where each BLGN interferer is generated by a Gaussian noise source passing through a narrowband limited bandpass filter and upcoverted to a certain central frequency. In the OFDM system, the bandwidth of each BLGN interferer of the narrowband interference in the frequency domain is usually 0.5– 1.5 OFDM sub-carrier spacing. The distribution of the locations of the central frequencies of each BLGN is random and arbitrary. The total bandwidth occupied by the nonzero parts (the BLGN interferers) of the narrowband interference in the frequency domain is sufficiently small compared with the bandwidth of the OFDM signal, making this narrowband interference model a *sparse* model [27, 59, 64].

(3) Narrow bandlimited random power spectrum density model. This is also a kind of statistical narrowband interference model, which is a statistical model aimed at the narrowband interference generated by the randomly distributed interfering sources. The effective bandwidth of the power spectrum density function of the narrowband interference in the receiver is limited in a sufficiently small range compared with the signal bandwidth. This model is quantitatively expressed by the parameters of the narrowband interference source, such as the equivalent omni-radiation power, the average amplitude of the symbols, the symbol power, the effective bandwidth of the interference signal, the channel fading from the interferers to the receiver, etc. [45]. This model is better applicable for the analysis of the physical mechanism and power of the narrowband interference, rather than for the modeling requirements of the digital signal processing of interference estimation and elimination.

(4) Spatially randomly distributed narrowband interference generators fading model. This model can be classified into a kind of statistical narrowband interference model. Multiple different narrowband interferers located at the same frequency point follow a Poisson random distribution in the spatial domain. This model

is mainly expressed by the following parameters: the homogeneous Poisson process model of the narrowband interference and the related parameters which occurs in the spatial domain, the distribution of the signal of the interferer source, the transfer function, amplitude fading, delay and phase offset of the channel from the interferer source to the receiver, etc. As a typical example, in the uplink cellular wireless networks, the model from multiple narrowband interferer sources of the user equipment (UE) to the base station (BS) is formulated, which mainly includes the parameters of the radius of the BS and the UEs, the density of the UEs that generate the narrowband interference, the amplitude and phase fading of the channel that the interference passes through, etc. [4, 49].

Among the narrowband interference models mentioned above, the compound BLGN interferers model expresses the frequency domain characteristics of the narrowband interference correctly, which is consistent with the probabilistic statistics and characteristics of the narrowband interference commonly seen in the practical broadband communication systems. It is more applicable to represent the broadband systems and channel environment conditions in different OFDM-based systems [59, 64]. Hence, this model is mostly adopted in literature. In this thesis, this model is thus adopted in the research and simulations to conduct analysis and experiments. Specifically, in the OFDM block transmission system model described in Sect. 2.1.1 in this chapter, the ith OFDM symbol in the baseband signal received by the receiver is given by (2.1), where the narrowband interference component is $\mathbf{e}_i = [e_{i,0}, e_{i,1}, \ldots e_{i,N-1}]^T$. As adopted in most of the literature and in this thesis as well, the modeling of the narrowband interference is conducted in the complex baseband modules, which is regarded as the equivalent complex baseband model. In order to make it convenient for the analysis and research of digital signal processing, the receiver only has to consider the baseband processing in the digital domain, and there is no need for the analog signal in front of the analog-to-digital converter to be taken into consideration. The related digital baseband algorithms are aimed at the baseband digital signals, which is aimed at the target of eliminating the noises and interferences and facilitating the succeeding modules of digital demodulation and decoding. After the DFT transform, the time domain narrowband interference signal corresponding to the frequency domain narrowband interference signal can be denoted by $\tilde{\mathbf{e}}_i = \left[\tilde{e}_{i,0}, \tilde{e}_{i,1}, \cdots, \tilde{e}_{i,N-1}\right]^T$. This frequency domain narrowband interference signal can be modeled as the superposition of multiple narrowband tone interferers in the OFDM sub-carriers that are independent of each other [59, 64], where each narrowband tone interferer is modeled by a bandlimited Gaussian noise (BLGN) whose central frequency lies randomly and arbitrarily in the N OFDM subcarriers. The power spectrum density (PSD) of the signal is $N_{0,\text{NB}} = \sigma_e^2$. Thus, the amplitude of the spectrum of each narrowband tone interferer is a random Gaussian variable whose variance is also equal to σ_e^2. The relationship between the time domain and the frequency domain narrowband interference signals is given by

$$\mathbf{e}_i = \mathbf{F}_N \tilde{\mathbf{e}}_i \tag{2.2}$$

where the elements of the IDFT transform matrix $\mathbf{F}_N \in \mathbb{C}^{N \times N}$ are defined as
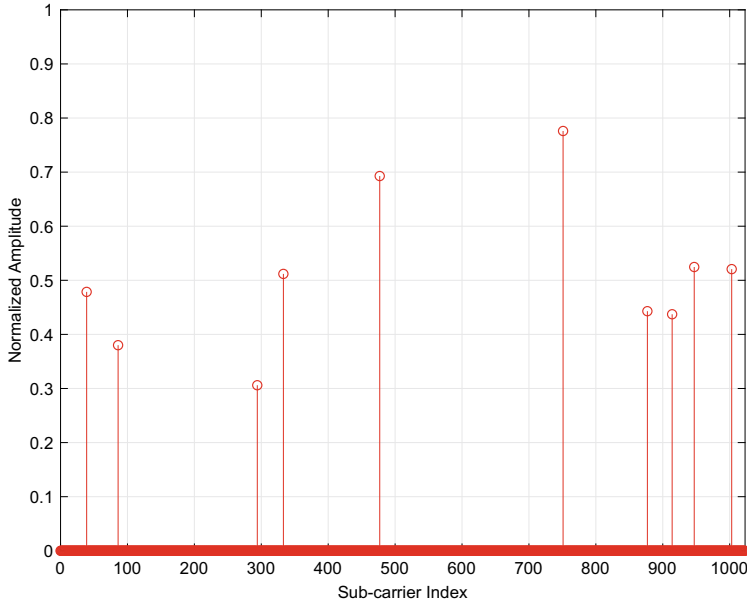
$$(\mathbf{F}_N)_{m,n} = \frac{1}{\sqrt{N}} \exp\left(\frac{\mathrm{j}2\pi mn}{N}\right) \tag{2.3}$$

The *sparsity level* of the narrowband interference is denoted by K, which is defined as the number of the nonzero elements of the frequency domain narrowband interference signal. The sparsity level is much smaller than the dimension of the signal, i.e. $K \ll N$. As described in Chap. 1, since in many broadband communication systems, the bandwidth of the narrowband interference is much smaller than that of the signal of interest, thus the sparsity level of the frequency domain narrowband interference is sufficiently small compared with the dimension of the signal, which also satisfies the definition and requirements of the sparse signal in the theory of compressed sensing [18]. The *support* of the narrowband interference $\tilde{\mathbf{e}}_i$ is denoted by $\Omega_i = \left\{k \,\middle|\, \tilde{e}_{i,k} \neq 0 \,, \; k = 0, 1, \ldots, N-1\right\}$, which is defined by the set of the locations (i.e. the subscripts) of all the nonzero elements of the narrowband interference. Then it can be derived that $K = |\Omega_i|$. Usually, the *interference-to-noise ratio (INR)* is adopted to indicate the intensity of the narrowband interference with respect to the background noise, which is denoted by $K = |\Omega_i|$ and defined as

$$\gamma_{\mathrm{NB}} = \frac{1}{\sigma_w^2}\mathbb{E}\left\{ \sum_{k \in \Omega_i} |\tilde{e}_{i,k}|^2 / K \right\} \tag{2.4}$$

where $\mathbb{E}\{\cdot\}$ denotes the expectation operator and the variance of the background AWGN is σ_w^2. The average power of the narrowband interference can be denoted by $P_{\mathrm{NB}} = \sum_{k \in \Omega_i} |\tilde{e}_{i,k}|^2 / K$. Based on the frequency domain distribution, it can be derived that $\mathbb{E}\{P_{\mathrm{NB}}\} = \sigma_e^2$, so the INR can also be represented as $\gamma_{\mathrm{NB}} = \sigma_e^2 / \sigma_w^2$. The locations of the nonzero elements of the narrowband interference signal can be arbitrarily and randomly distributed in all the N OFDM sub-carriers, and the sparsity level is also arbitrarily chosen. Thus, the support of the narrowband interference is random. For example, it can be a uniform distribution, but not necessarily a uniform distribution. In the compound BLGN interferer model, the amplitudes of the tone interferers with different frequencies are random variables following Gaussian distribution, and the amplitudes of the tone interferers are mutually independent of each other. Without loss of generality, the randomly distributing characteristic of the support of the narrowband interference signal makes it well suited for being applied in many practical broadband communication systems.

The power spectrum density of the narrowband interference was tested in a practical OFDM systems [64], where the power spectrum density of the background noise is $N_0 = -140$ dBm/Hz, and the power spectrum density of the narrowband interference is $N_{0,\mathrm{NB}} = -110$ dBm/Hz. Thus, the INR of the narrowband interference is $\gamma_{\mathrm{NB}} = 30$ dB. It can be noted from the experimental data that, the narrowband interference signal is mainly concentrated on some certain individual and randomly distributed tone interferers. The theoretical model of the narrowband interference mentioned above, which is also adopted as the model for simulation evaluations, is

Fig. 2.8 The theoretical and simulation model of the narrowband interference in the OFDM system

illustrated in Fig. 2.8, where the horizontal axis denotes the sub-carrier index. There are $N = 1024$ sub-carriers in total. The vertical axis denotes the frequency domain normalized amplitude of the narrowband interference. It can be observed that the sparsity level of the narrowband interference is $K = 10$, which means that there are 10 mutually independent narrowband interferers distributed randomly in 1024 sub-carriers locations.

2.3.2 Impulsive Noise Model

The definition of the impulsive noise is the noise outside the system with the characteristics of bursting and time domain sparsity, which occupies a time interval sufficiently short compared with the duration of the block transmission symbol [47, 73]. The quantitative definition of the impulsive noise is the impulsive signal, whose temporal duration is no more than 5% that of the block transmission OFDM symbol [39, 53]. Based on the definition of impulsive noise, the models proposed in literature for common theoretical analysis and adopted in simulation experiments mainly include the following categories:

(1) Gaussian mixture model, including the Gaussian-Bernoulli mixture model [41] and the Gaussian-Poisson mixture model [65]: in the Gaussian mixture model, the probability density function (PDF) of the instantaneous amplitude of the time

domain asynchronous impulsive noise is given by

$$p_Z(z) = \sum_{j=0}^{J_m} \beta_j \cdot g_j(z) \tag{2.5}$$

where $g_j(z)$ is the probability density function of a zero mean Gaussian distribution with the variance of σ_j^2. The parameter β_j is the mixture coefficient corresponding to the PDF of the Gaussian distribution. J_m is the number of the Gaussian components that formulate this model. As far as the Gaussian-Poisson mixture model [65] is concerned, the arrival rate (i.e. the number of impulses that arrive per second) of the impulses of the impulsive noise follows a Poisson process distribution, whose probability is given by

$$P(\Lambda) = \lambda^\Lambda e^{-\lambda} / \Lambda! \tag{2.6}$$

As far as the Gaussian-Bernoulli mixture model is concerned [41], the locations of the sampling points where the impulsive noise occurs follow a Bernoulli distribution.

(2) Middleton's Class A-Poisson model [38, 39]: The Middleton's Class A model is a commonly used statistical model of impulsive noise, whose main parameters include the overlapping factor A and the background-to-impulsive-noise power ratio ω. When the related parameters satisfy the following conditions:

$$\begin{aligned} \beta_j &= \frac{e^{-A} A^j}{j!} \\ \sigma_j^2 &= \frac{j/A + \omega}{1 + \omega}, J_m \to \infty, \end{aligned} \tag{2.7}$$

the Middleton's Class A distribution can be derived from the Gaussian mixture model. In the Middleton's Class A-Poisson model, the arrival rate and the occurrence locations of the impulsive noise follow the Poisson distribution described by Eq. (2.6).

(3) Bursty block-sparse model [35]: The impulsive noise in practical systems might be occurring in clusters or in blocks in the form of bursty clusters at some concentrated locations, which can be modeled by a bursty block-sparse model. Assuming that only a small portion of the received OFDM symbol is influenced by the impulsive noise, and they will be gathering in groups at some impulse blocks. Therefore, the occurrence frequency of the impulses in the bursty block-sparse model is in between two extreme cases, namely, the impulsive noise with independent and identical distribution and the long duration impulsive noise affecting the whole OFDM symbol. The bursty block-sparse model can be represented as

$$\mathbf{z} = [\overbrace{z_0, \dots, z_{D-1}}^{\mathbf{z}^T[1]}, \dots, \overbrace{z_{N-D}, \dots, z_{N-1}}^{\mathbf{z}^T[p]}]^T \tag{2.8}$$
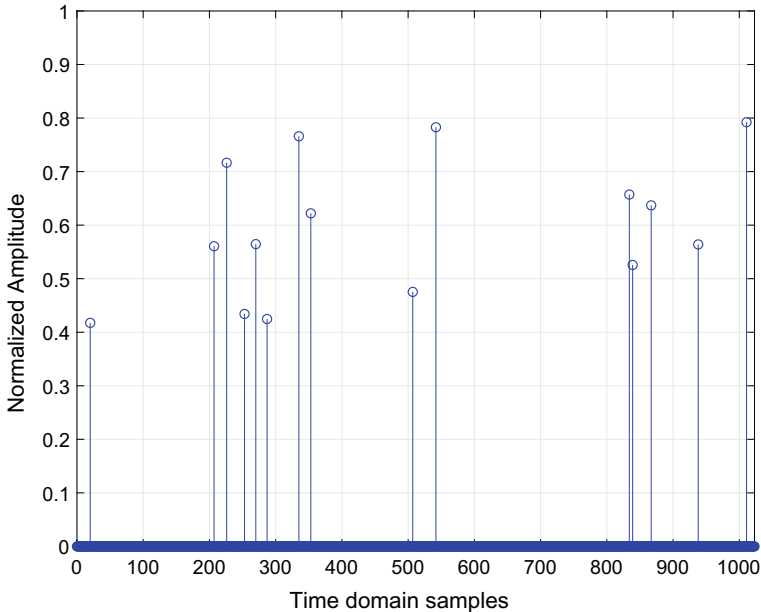
where the length of the impulse block is D, and within the sub-vector groups $\mathbf{z}[j]$ formed by each impulse block, only $q \ll p$ sub-vectors have nonzero Euclidean norm (i.e. ℓ_2 norm).

The Middleton's Class A-Poisson model among the impulsive noise models mentioned above accurately expresses the time domain bursting and sparse characteristics of the impulsive noise, which is relatively better consistent with the probabilistic and statistical characteristics of the impulsive noise commonly seen in practical broadband communication systems. It is also more applicable for different systems and different channel conditions [39, 53]. In literature, this model is mostly adopted for analysis, research and experiments, so it is also adopted in this thesis. Specifically, in the OFDM block transmission system model described in Sect. 2.1.1 in this chapter, the impulsive noise component in the ith OFDM symbol (2.1) can be represented by a length-N vector $\mathbf{z}_i = [z_{i,0}, z_{i,1}, \ldots z_{i,N-1}]^T$. In most literature and also in this thesis, the modeling of the impulsive noise is conducted in the complex baseband modules, namely using the equivalent complex baseband model. In order to make it more convenient for the analysis and research of digital signal processing, the receiver only needs to consider the baseband digital domain processing and does not need to consider the analog signal in front of the analog-to-digital converter. The related digital baseband algorithms are conducted for the baseband digital signal, which is targeting at eliminating the impulsive noise and facilitating the succeeding digital demodulation and decoding. The most fundamental characteristic of the impulsive noise is the sparsity. The support is defined as $\Pi_i = \{ j \,|\, z_{i,j} \neq 0 \,,\; j = 0, 1, \ldots, N-1 \}$, and the sparsity level is defined as $K = |\Pi_i|$. The INR of the impulsive noise is denoted by γ_{IN}, which is given in detail by

$$\gamma_{\text{IN}} = \mathbb{E} \left\{ \sum\nolimits_{j \in \Pi_i} |z_{i,j}|^2 / K \right\} / \sigma_w^2 \tag{2.9}$$

where $P_{\text{IN}} = \sum_{j \in \Pi_i} |z_{i,j}|^2 / K$ is the average power of the impulsive noise, and σ_w^2 is the power of the background AWGN. In the Middleton's Class A-Poisson model, the characteristics of the instantaneous amplitude and the random occurrence of the impulsive noise can be empirically modeled in literature. As described previously, the distribution of the instantaneous amplitude is given by (2.7), and the probability distribution of the occurrence is given by (2.6).

The time domain signal data of the impulsive noise that is tested in practical experiment fields was provided in the report [34]. In this report, the measurement data of the impulsive noise generated by the central air conditioner formed a randomly sparse model. Thus, it can be observed that the nonzero elements of the impulsive noise are randomly distributed in different time samples. The measurement data of the impulsive noise generated by the dishes washing machine formed a block-sparse model. It can be observed that the impulses occur in groups and clusters at random locations. The theoretical and simulation model of the impulsive noise mentioned above is illustrated in Fig. 2.9, where the horizontal axis is the time domain OFDM samples with each OFDM symbol having $N = 1024$ time domain samples. The vertical axis denotes the time domain normalized amplitude of the impulsive noise.

Fig. 2.9 Theoretical and simulation model of the impulsive noise in the OFDM system

It can be observed from the figure that the sparsity level of the impulsive noise is $K = 15$, which implies that there are 15 impulses randomly occurring in this OFDM symbol.

2.4 Fundamentals of Sparse Recovery Theory

The theory of sparse recovery is one of the recently emerging signal processing theories, which is aimed at the processing of the signals with some specific sparse properties in a certain domain, and the detection, estimation and reconstruction of the sparse signals are of interest. The efficiency of the conventional signal processing methods is limited by the Shannon-Nyquist sampling theorem [54]. The accuracy of signal estimation is also limited when the available sampling data are insufficient [28]. The limitation of the conventional signal processing methods is overcome by the emerging theory and technology of sparse signal processing. The problem of sparse signal reconstruction can be modeled based on the sparse recovery theory. Making use of the highly efficient and robust algorithms of sparse recovery, the target of significantly improving the accuracy of sparse signal recovery can be achieved in the condition of the sampling data amount far less than conventional requirements. Therefore, the theory and technology of sparse recovery have drawn plenty of attention from many areas in both academia and industry, including digital image

processing, radar signal detection, and communication and information systems, etc. The theory of sparse recovery mainly includes the compressed sensing theory, the structured compressed sensing theory, and the sparse Bayesian learning theory, etc. The fundamentals of the theories will be briefly discussed on in this section.

2.4.1 Compressed Sensing and Sparse Recovery

The compressed sensing (CS) theory was proposed by D. Donoho, E. Candes and J. Romberg et al., in 2006, which was applied in the area of digital image processing at first to conduct image compression, sampling and sparse recovery [10, 18]. The motivation and aims of compressed sensing is to make use of the inherent sparse structure of the signal to reduce the required sampling rate or data amount for accurate signal recovery. After the compressed sensing theory was proposed, it has drawn great attention from the academia, and extended to the areas of communication signal processing, medical signal processing, radar signal processing, etc. In the area of signal processing, the essence of the compressed sensing theory is the accurate solution of the under-determined linear inverse problem. The model of linear inverse problems include three categories, i.e. under-determined, over-determined and regular linear inverse problems [57], which is represented as follows

$$\mathbf{y} = \Phi\mathbf{x} \tag{2.10}$$

where $\mathbf{y} \in \mathbb{C}^M$ is a measurement vector or a known vector that can be obtained in some certain manner, $\mathbf{x} \in \mathbb{C}^N$ is the unknown vector to be estimated, $\Phi \in \mathbb{C}^{M \times N}$ is a certain known observation matrix or representation matrix. When $M > N$, Eq. (2.10) forms a "over-determined" linear inverse problem, which can be regarded as a linear equations set with the number of unknown variables greater than that of the equations. When the equations are independent of each other, there does not exist any solution that satisfies the linear equations set accurately (i.e. making all the equations consistent). However, there exists an approximate solution in the perspective of least squares (LS) [57]. When $M = N$, Eq. (2.10) forms a regular linear inverse problem, which can be regarded as a linear equations set with the number of unknown variables equal to that of the equations. When the coefficients matrix Φ is row full ranked (nontrivial), there exists and only exists one solution for $\mathbf{x}$. When $M < N$, Eq. (2.10) forms an "under-determined" linear inverse problem, which can be regarded as an equations set with the number of unknown variables smaller than that of the equations. Usually in conventional theories of signal processing and linear algebra, this kind of under-determined linear inverse problem has no accurate solution, because there exist infinite number of different solutions that can satisfy Eq. (2.10).

Different from the conventional signal processing theory, the compressed sensing theory shows that the under-determined linear inverse problem is invertible, i.e. the unknown vector $\mathbf{x}$ with the sparsity level of K (which can be denoted by a K-*sparse* vector) can be accurately and stably recovered, when the following conditions are

satisfied [10, 18, 19]: (i) the unknown vector is K-*sparse*. (ii) the observation matrix is diverse (the correlation between the columns of the observation matrix is low), which satisfies the (K, δ)-*restricted isometry property (RIP)* condition. (iii) the number of the measurement data M satisfies:

$$M = \mathcal{O}(K \log(N/K)) \tag{2.11}$$

where the sparsity is defined as:

Definition 2.1 (*sparsity*) Vector $\mathbf{x} \in \mathbb{C}^N$ is called K-*sparse*, $K \ll N$, if $\exists$ a certain set of indices $\Omega \subset \{1, \ldots, N\}$ such that $|\Omega| \leq K$ and $\mathbf{x}_\Omega \neq \mathbf{0}$, $\mathbf{x}_{\{1,\ldots,N\}-\Omega} = \mathbf{0}$. The *sparsity* of the vector $\mathbf{x}$ is K. The *support* (the set of the indices of the nonzero elements) is denoted by supp $(\mathbf{x})$, and supp $(\mathbf{x}) = \Omega$.

The RIP condition is defined as:

Definition 2.2 (*RIP*) The matrix $\Psi \in \mathbb{C}^{m \times N}$ is recognized to be satisfying the (K, δ_K)-*RIP condition* with the parameter of (K, δ_K) ($K \leq m, 0 \leq \delta_K \leq 1$), if for all the sets of indices $\Omega \subset \{1, \ldots, N\}, |\Omega| \leq K$, and for all the $\mathbf{q} \in \mathbb{C}^{|\Omega|}$, it holds that

$$(1 - \delta_K) \|\mathbf{q}\|_2^2 \leq \|\Psi_\Omega \mathbf{q}\|_2^2 \leq (1 + \delta_K) \|\mathbf{q}\|_2^2 \tag{2.12}$$

When the three conditions above are satisfied, it can also be implied that the unknown vector $\mathbf{x}$ can be linearly represented by the K vectors (also known as the "sparse atoms") from the vectors group (dictionary) formed by the column vectors of the observation matrix Φ. If the three conditions above are satisfied, to reconstruct the unknown sparse vector is equivalent to finding the sparse linear representation of the measurement vector using the given dictionary (the columns of the observation matrix), whose method is to solve the following ℓ_0 *norm minimization* problem:

$$(\mathrm{P}_0) : \min_{\mathbf{x} \in \mathbb{C}^N} \|\mathbf{x}\|_0, \quad \text{s.t.} \quad \mathbf{y} = \Phi \mathbf{x} \tag{2.13}$$

where ℓ_0 norm $\|\mathbf{x}\|_0$ is the number of nonzero elements in the vector $\mathbf{x}$. In order to solve this problem, intuitively the most sparse vector of $\mathbf{x}$ should be found, such that the compressed sensing relation $\mathbf{y} = \Phi \mathbf{x}$ is satisfied. Since this problem has a solution space of combinatorial scale to search from, it is an NP-hard problem which is difficult to track the solution of. However, by making use of convex relaxation, the original problem can be relaxed to the ℓ_1 *norm minimization problem*:

$$(\mathrm{P}_1) : \min_{\mathbf{x} \in \mathbb{C}^N} \|\mathbf{x}\|_1, \quad \text{s.t.} \quad \mathbf{y} = \Phi \mathbf{x} \tag{2.14}$$

where ℓ_0 norm $\|\mathbf{x}\|_0$ refers to the summation of all the elements in the vector of $\mathbf{x}$. The ℓ_1 norm minimization problem can be solved by convex optimization methods. Basis pursuit (BP) is a commonly applied method, which turns the original ℓ_0 norm minimization problem into an ℓ_1 norm minimization problem by convex relaxation. The BP method can further convert it to a linear programming problem equivalently,

of which the accurate solution can be derived when the observation matrix satisfies the RIP condition. Moreover, in the presence of background noise, the accuracy of the solution of the BP method has been theoretically guaranteed [10].

Another commonly applied method is the compressed sensing based greedy algorithms. Based on the idea of solving the ℓ_0 norm minimization problem, the target of finding the unknown vector with the smallest number of nonzero elements can be achieved by greedy iterative approach. In each iteration, the greedy strategy is conducted to select one or more atoms from the remaining atoms that are most likely to be included in the ground-truth support, and add them to the final support. Through several iterations, the optimal solution can be derived. The accuracy of the solution of the compressed sensing based greedy algorithms is also theoretically guaranteed by theoretical bounds [62]. The commonly adopted compressed sensing based greedy algorithms include OMP (Orthogonal Matching Pursuit) [61], SP (Subspace Pursuit) [15], CoSaMP (Compressed Sampling Matching Pursuit) [43], and SAMP (Sparsity Adaptive Matching Pursuit) [17], etc.

2.4.2 Structured Compressed Sensing Theory

The theory of structured compressed sensing is an extended theory of the compressed sensing theory. The structured compressed sensing theory is focused on the structural property of the unknown vector, and improving the performance of the classical compressed sensing methods by making use of it.

Firstly, the structured compressed sensing theory studies the joint structural property of the unknown vectors in the scenario of multiple measurements, i.e. the multiple measurement vectors (MMV) problem. The MMV problem is widely applied in many areas, including medical brain MRI imaging analysis, array processing, sparse channel equalization, cognitive radio, and multiple channel communications, etc. The characteristic of the MMV problem is that the inherent structure of the unknown data is needed, such as the unknown jointly sparse matrix composed of multiple unknown sparse vectors, to conduct joint signal reconstruction, which is also a typical theoretical model and problem representation of structured compressed sensing [8, 20]. Different from the single measurement vector (SMV) problem as in the conventional compressed sensing framework, the target of solving the MMV problem is to simultaneously reconstruct a group of D vectors $\{\mathbf{x}_j\}_{j=1}^{D}$ that share the same support Ω, rather than only reconstruct a single sparse vector $\mathbf{x}$. Rearranging the vectors group $\{\mathbf{x}_j\}_{j=1}^{D}$ in column forms the jointly sparse matrix $\mathbf{X}$. Since each vector shares the same support, the number of nonzero rows in the unknown jointly sparse matrix is K when the number of nonzero elements of each unknown sparse vector is K. The MMV problem framework can be represented as:

$$\mathbf{Y} = \begin{bmatrix} \mathbf{y}_1 \mathbf{y}_2 \cdots \mathbf{y}_D \end{bmatrix} = \Phi \mathbf{X} \qquad (2.15)$$

where $\mathbf{Y}$ is the multi-dimensional measurement matrix composed of the multiple measurement vectors in column, and $\mathbf{X} = [\mathbf{x}_1 \mathbf{x}_2 \cdots \mathbf{x}_D]$ is the unknown multi-dimensional jointly sparse matrix.

It has been proved that, in order to reconstruct an unknown K-sparse vector, the requirement of the length of the measurement vector M can be reduced from $M = \mathcal{O}(K \log(N/K))$ (a typical value is $2K$) in the single-dimensional SMV case to $M \geq K + 1$ in the MMV framework [20]. In the framework of the MMV problem based on the structured compressed sensing theory, the amount of the measurement data required for recovering D jointly sparse unknown vectors (i.e. the unknown jointly sparse matrix) is MD. Hence, the total amount of the required measurement vectors, i.e. $(K + 1)D$, is significantly reduced compared with the amount of $2KD$ when solving the SMV problem vector-by-vector for the D unknown vectors in the conventional compressed sensing methods [20].

The solutions of the MMV problem in literature mainly include the following two approaches:

(1) Convex relaxation optimization methods: in the MMV framework, the compressed sensing problem (2.14) is extended to the mixed matrix norm minimization problem, i.e. the mixed $\ell_{p,q}$-norm minimization problem, as represented by:

$$(\mathrm{P}_{0,q}) : \min_{\mathbf{X} \in \mathbb{C}^{N \times D}} \|\mathbf{X}\|_{0,q}, \quad \text{s.t.} \quad \mathbf{Y} = \Phi \mathbf{X} \tag{2.16}$$

where the mixed $\ell_{p,q}$ norm of a matrix is defined as:

$$\|\mathbf{X}\|_{p,q} = \left(\sum_m \left\| (\mathbf{X}^T)_m \right\|_p^q \right)^{1/q} \tag{2.17}$$

where $(\mathbf{X}^T)_m$ denotes the m-th row of $\mathbf{X}$. Similarly, the mixed $\ell_{0,q}$ norm is a nonconvex function, so the problem (2.18) is an NP-hard one, which cannot be solved. By convex relaxing, it can be turned to a mixed $\ell_{p,q}$ norm minimization problem ($p, q \geq 1$), and then it can be solved using convex optimization methods as:

$$(\mathrm{P}_{p,q}) : \min_{\mathbf{X} \in \mathbb{C}^{N \times D}} \|\mathbf{X}\|_{p,q}, \quad \text{s.t.} \quad \mathbf{Y} = \Phi \mathbf{X} \tag{2.18}$$

where usually in the convex relaxation $p = 1$, $q = 2$ is preferably chosen as the mixed norm for efficient solution [11, 22].

(2) Structured compressed sensing greedy algorithms: similar to the classical compressed sensing algorithms, the structured compressed sensing algorithms are also based on the greedy idea in multiple iterations. In each itearation, the currently optimal common support of $\mathbf{X}$ is selected and appended into the test support, and the optimal solution is gradually converged to. What is different from the classical compressed sensing greedy algorithms is that, in each iteration of the structured compressed sensing algorithm, the criterion that decides the currently optimal support to be appended comes from the contribution of

the multi-dimensional projection of the multi-dimensional measurement matrix and the multi-dimensional residue matrix on the dictionary atoms, rather than the single dimensional measurement vector and residue error vector as in the classical compressed sensing algorithm. Thus the accuracy of the algorithm can be effectively improved, and the required amount of the measurement vector in each dimension can be reduced [62]. State of the art commonly applied structured compressed sensing algorithms include Simultaneous OMP (S-OMP) [62] and OMP-MMV [11], etc.

Furthermore, based on the structured compressed sensing theory, in the framework of finite union of subspaces (FUS), the corresponding structured reconstruction methods can be derived by making use of the additional constraints and structural property of the unknown vector. A typical additional structural property of the unknown vector is its *block sparse* property, which is defined as:

Definition 2.3 (*Block Sparsity*) A vector $\mathbf{x} \in \mathbb{C}^N$ is regarded as K-*block-sparse* on the block partition of $\Gamma = \{d_1, \ldots, d_{N_{\mathrm{B}}}\}$, if the sub-block $\mathbf{x}[i]$ is nonzero for at most K different indices i, where $N = \sum_{i=1}^{N_{\mathrm{B}}} d_i$, the number of sub-blocks is N_{B}, and the length of the ith sub-block $\mathbf{x}[i]$ is d_i. Then it can be derived that:

$$\mathbf{x} = [\underbrace{x_1 \ldots x_{d_1}}_{\mathbf{x}[1]^T}, \ldots, \underbrace{x_{N-d_{N_{\mathrm{B}}}+1} \ldots x_N}_{\mathbf{x}[N_{\mathrm{B}}]^T}]^T. \tag{2.19}$$

When the unknown vector satisfies the block sparse property, it can be solved by the block sparse recovery algorithms. Definition 2.3 implies that, when $d_i = 1, \forall i$, block sparsity will degrade to the common sparsity. Based on the definition of block sparsity, the *mixed ℓ_2/ℓ_1 norm* of the block sparse vector $\mathbf{x}$ on the block partition $\Gamma = \{d_1, \ldots, d_{N_{\mathrm{B}}}\}$ is given by the following equation:

$$\|\mathbf{x}\|_{2,\Gamma} = \sum_{i=1}^{N_{\mathrm{B}}} \|\mathbf{x}[i]\|_2. \tag{2.20}$$

where the term of $\|\mathbf{x}\|_{2,\Gamma}$ denotes the summation of the power of all the sub-blocks of the block sparse vector $\mathbf{x}$. When the unknown vector $\mathbf{x}$ is block sparse, the condition on which the problem of block sparse recovery $\mathbf{y} = \Phi\mathbf{x}$ can be solved is extended to the *block-RIP condition*, as defined by:

Definition 2.4 (*block-RIP*) A matrix $\Psi \in \mathbb{C}^{M \times N}$ is recognized to have the *block-RIP* property with the *block-RIP constant* of $0 \le \delta_K^{(\mathrm{B})} \le 1$ on the block partition of $\Gamma = \{d_1, \ldots, d_{N_{\mathrm{B}}}\}$, if $\forall K$-block-sparse vector $\mathbf{x} \in \mathbb{C}^N$ on the block partition Γ, it holds that

$$(1 - \delta_K^{(\mathrm{B})}) \|\mathbf{x}\|_2^2 \le \|\Psi\mathbf{x}\|_2^2 \le (1 + \delta_K^{(\mathrm{B})}) \|\mathbf{x}\|_2^2. \tag{2.21}$$

The major difference between block-RIP condition and common RIP condition (see Definition 2.2) is that the condition holds for any K-block-sparse vector $\mathbf{x} \in \mathbb{C}^N$ on the block partition Γ.

It is revealed by the structured compressed sensing theory that, when the observation matrix satisfies the block-RIP condition, similar to the solution to the MMV problem, the convex relaxation optimization methods and the block sparse greedy algorithms can be utilized to recover the block sparse vector [20]. To exploit the convex relaxation optimization method, the following mixed ℓ_2/ℓ_1 norm minimization problem should be solved [22]:

$$\arg \min_{\mathbf{x} \in \mathbb{C}^N} \|\mathbf{x}\|_{2, \Gamma}, \quad \text{s.t.} \quad \mathbf{y} = \Phi \mathbf{x} \qquad (2.22)$$

Utilizing the block sparse greedy algorithms, such as block-OMP (BOMP) and block-CoSaMP, etc. [6, 21], the unknown block sparse vector can be iteratively solved.

2.4.3   Sparse Bayesian Learning Theory

The sparse Bayesian learning (SBL) theory was first proposed by Tipping in 2001, which was applied in the area of machine learning at first, and then extended to the area of sparse signal processing [58]. Compared with the compressed sensing methods, the sparse Bayesian learning methods are more capable of achieving the globally most sparse solution, and the requirements on the correlation property of the columns of the observation matrix is relatively loose. Hence, it has drawn wide research attention [67, 68]. The sparse Bayesian learning theory is aimed at solving the linear inverse problem of the unknown sparse vector in the presence of background noise:

$$\mathbf{y} = \Phi \mathbf{x} + \mathbf{w} \qquad (2.23)$$

where $\mathbf{x} \in \mathbb{C}^N$ is the unknown sparse vector to be estimated. $\mathbf{y} \in \mathbb{C}^M$ is the measurement vector or known vector that can be obtained in some way. $\Phi \in \mathbb{C}^{M \times N}$ a known observation matrix or representation matrix. $\mathbf{w}$ is the background noise vector. In the framework of sparse Bayesian learning, assuming that the prior distribution of each element of the unknown vector $\mathbf{x}$ follows a zero-mean Gaussian distribution:

$$p(x_i; \gamma_i) \sim \mathcal{N}(0, \gamma_i), i = 1, \dots, N \qquad (2.24)$$

where γ_i is the variance of the Gaussian distribution. In the framework of sparse Bayesian learning, it is assumed that γ_i is unknown but deterministic parameter (rather than random variable), which is estimated through the sparse Bayesian learning based algorithms. The background noise is assumed to follow Gaussian distribution, i.e.

$$p(\mathbf{w}; \varepsilon) \sim \mathcal{N}(\mathbf{0}, \varepsilon \mathbf{I}) \qquad (2.25)$$

where $\varepsilon\mathbf{I}$ is the covariance matrix of the Gaussian variable. The sparse Bayesian learning theory is focused on estimating the unknown parameters γ_i and ε through the sparse Bayesian learning based iterative algorithms, which is the key of the sparse Bayesian learning methods:

In the process of iterative learning, most of the parameters γ_i will approach zero, and the sparse Bayesian learning algorithms will force them to be zero by threshold decision. Then, the elements x_i corresponding to these are also forced to be zero, and only a few γ_i are remained, which ensures that the sparse Bayesian learning iterations will converge to a sparse solution [58]. Through adopting the Type II Maximum Likelihood (ML) method in the iteration process, all the unknown parameters are estimated finally. Afterwards, the posterior distribution, which is also a Gaussian one, of x_i can be derived based on the Bayesian criterion. The expectation of this very distribution is the maximum a posterior (MAP) estimation of the unknown vector $\mathbf{x}$ based on the Bayesian rule [68].

Furthermore, exploiting the block sparse property of the unknown vectors, Zhang et al. extended the sparse Bayesian learning theory to the block sparse Bayesian learning (BSBL) theory [71]. In the framework of block sparse Bayesian learning, in order to solve the problem (2.23), the block sparse property of the unknown vector $\mathbf{x}$ can be exploited, i.e.

$$\mathbf{x} = [\underbrace{x_1, \ldots x_{d_1}}_{\mathbf{x}_1^T}, \ldots \underbrace{x_{d_{g-1}+1}, \ldots x_{d_g}}_{\mathbf{x}_g^T}]^T, \qquad (2.26)$$

where the size of each sub-block d_i is not necessarily identical. In all the g sub-blocks, only $K_b(K_b \ll g)$ ones are nonzero. Equation (2.26) is the block sparse representation of the unknown vector. In the framework of block sparse Bayesian learning, the prior distribution of each sub-block $\mathbf{x}_i \in \mathbb{C}^{d_i}$ is assumed to follow a parametric multi-dimensional joint Gaussian distribution:

$$p(\mathbf{x}_i; \gamma_i, \mathbf{B}_i) \sim \mathcal{N}(\mathbf{0}, \gamma_i\mathbf{B}_i), \quad i = 1, \ldots, g, \qquad (2.27)$$

where $\mathbf{B}_i$ and γ_i are unknown and deterministic parameters. The block sparse property of the vector $\mathbf{x}$ is determined by the non-negative parameter γ_i. If γ_i is nonzero, it means that the ith sub-block is nonzero.

In the learning process of block sparse Bayesian learning, similarly, based on the principle of automatic relevance, most of the parameters $\{\gamma_i\}_i$ will gradually approach zero, leading to the block sparse property of the solution [71].

Compared with sparse Bayesian learning, the key of the block sparse Bayesian learning theory is to make use of the intra block correlation of the sub-blocks, i.e. exploiting the intra block correlation (IBC) matrix $\mathbf{B}_i$, which can improve the performance of the recovery of block sparse unknown vectors. The IBC matrix is denoted by $\mathbf{B}_i \in \mathbb{C}^{d_i \times d_i}$, which is a positive definite matrix and represents the inherent correlation structure of the ith sub-block. Before the learning iterations of block sparse Bayesian learning, the IBC matrix $\mathbf{B}_i$ can be initialized by the covariance matrix, and then

updated and optimized through the block sparse Bayesian learning iteration process. With the assumption that each sub-block is uncorrelated with each other, the prior distribution of the unknown vector $\mathbf{x}$ can be represented as $p(\mathbf{x}; \{\gamma_i, \mathbf{B}_i\}_i) \sim \mathcal{N}(\mathbf{0}, \Sigma_0)$, where the prior covariance matrix of $\mathbf{x}$ is

$$\Sigma_0 = \mathrm{diag}\{\gamma_1 \mathbf{B}_1, \ldots, \gamma_g \mathbf{B}_g\}. \tag{2.28}$$

Assuming that the background noise also follows a Gaussian distribution (2.25), then the posterior distribution of $\mathbf{x}$ based on the Bayesian rule is given by

$$p\big(\mathbf{x}|\mathbf{y}; \varepsilon, \{\gamma_i, \mathbf{B}_i\}_{i=1}^g\big) = \mathcal{N}(\boldsymbol{\mu}_x, \Sigma_x), \tag{2.29}$$

where

$$\boldsymbol{\mu}_x = \Sigma_0 \Phi^T \big(\varepsilon \mathbf{I} + \Phi \Sigma_0 \Phi^T\big)^{-1} \mathbf{y}, \tag{2.30}$$

$$\Sigma_x = \left(\Sigma_0^{-1} + \frac{1}{\varepsilon} \Phi^T \Phi \right)^{-1}. \tag{2.31}$$

The unknown parameters $\varepsilon, \{\gamma_i, \mathbf{B}_i\}_{i=1}^g$ can be estimated based on the Type-II maximum likelihood criterion through the core of the BSBL framework, i.e. the algorithm of learning the unknown parameters. Afterwards, the MAP estimation of the unknown vector $\mathbf{x}$ is given by $\hat{\mathbf{x}} = \boldsymbol{\mu}_x$, which is given in detail by Eq. (2.30) [58, 71].

References

1. Marey M, Steendam H (2007) Analysis of the narrowband interference effect on OFDM timing synchronization. IEEE Trans Signal Process 55(9):4558–4566
2. Umehara D, Nishiyori H, Morihiro Y (2006) Performance evaluation of CMFB transmultiplexer for broadband power line communications under narrowband interference. In: 2006 IEEE international symposium on power line communications and its applications (ISPLC'06), pp 50–55
3. Pan C, Wang J, Fang H, Song J (2013) Field trial of advanced DTMB system DTMB-A in Hong Kong. In: Proceedings of IEEE international symposium on broadband multimedia systems and broadcasting (BMSB'13), pp 1–4
4. Coulson A (2004) Narrowband interference in pilot symbol assisted OFDM systems. IEEE Trans Wirel Commun 3(6):2277–2287
5. Chiueh TD, Tsai PY (2008) OFDM baseband receiver design for wireless communications. Wiley
6. Nee RV, Prasad R (2000) OFDM for wireless multimedia communications. Artech House, Inc
7. Zheng L, Tse DNC (2003) Diversity and multiplexing: a fundamental tradeoff in multiple-antenna channels. IEEE Trans Inform Theory 49(5):1073–1096
8. Standard CN (2006) Frame structure, channel coding and modulation for digital television terrestrial broadcasting system. GB 20600-2006, Chinese National Standard
9. Ramseier S (2003) Shuffling bits in time and frequency: an optimum interleaver for OFDM. In: IEEE international conference on communications (ICC'03), vol 5, pp 3418–3422

10. Do T, Lu G, Nguyen N, Tran T (2008) Sparsity adaptive matching pursuit algorithm for practical compressed sensing. In: Asilomar conference on signals, systems and computers, pp 581–587
11. Han Z, Li H, Yin W (2013) Compressive sensing for wireless networks. Cambridge University Press, UK
12. Schober R, Lampe L (2004) Sequence detection and adaptive channel estimation for ISI channels under class-A impulsive noise. IEEE Trans Commun 52(9):1523–1531
13. Giorgetti A, Chiani M, Win MZ (2005) The effect of narrowband interference on wideband wireless communication systems. IEEE Trans Commun 53(12):2139–2149
14. Gomaa A, Al-Dhahir N (2011) A sparsity-aware approach for NBI estimation in MIMO-OFDM. IEEE Trans Wirel Commun 10(6):1854–1862
15. Lampe L (2011) Bursty impulse noise detection by compressed sensing. In: IEEE international symposium on power line communications 2011 (ISPLC'11), pp 29–34
16. Tipping ME (2001) Sparse bayesian learning and the relevance vector machine. J Mach Learn Res 1:211–244
17. 3GPP: 3GPP TS 36.211 v10.3.0—evolved universal terrestrial radio access (E-UTRA); physical channels and modulation (release 8) (2011)
18. Gallager RG (2008) Principles of digital communication, vol 1. Cambridge University Press, Cambridge, UK
19. Proakis JG (1995) Digital communications. McGraw-Hill, New York
20. Middleton D (1977) Statistical-physical models of electromagnetic interference. IEEE Trans Electromagn Compatib 3:106–127
21. Tropp J, Gilbert A (2007) Signal recovery from random measurements via orthogonal matching pursuit. IEEE Trans Inform Theory 53(12):4655–4666
22. IEEE: Wireless LAN medium access control (MAC) and physical layer (PHY) specifications (2009)
23. Vaseghi SV (2008) Advanced digital signal processing and noise reduction. Wiley
24. Chen J, Huo X (2006) Theoretical results on sparse representations of multiple-measurement vectors. IEEE Transa Signal Process 54(12):4634–4643
25. IEEE: IEEE standard for broadband over power line networks: Medium access control and physical layer specifications (2010)
26. Goldsmith A, Jafar SA, Jindal N et al (2003) Capacity limits of MIMO channels. IEEE J Sel Areas Commun 21(5):648–702
27. Wu Z, Nassar CR (2005) Narrowband interference rejection in OFDM via carrier interferometry spreading codes. IEEE Trans Wirel Commun 4(4):1491–1505
28. Ali A, Masood M, Sohail MS, Al-Ghadhban SN, Al-Naffouri TY (2016) Narrowband interference mitigation in SC-FDMA using bayesian sparse recovery. IEEE Trans Signal Process 64(24):6471–6484
29. Wipf DP, Rao BD (2004) Sparse bayesian learning for basis selection. IEEE Trans Signal Process 52(8):2153–2164
30. Ziemer R, Tranter WH (2006) Principles of communications: system modulation and noise. Wiley
31. Candès E, Romberg J, Tao T (2006) Robust uncertainty principles: exact signal reconstruction from highly incomplete frequency information. IEEE Trans Inform Theory 52(2):489–509
32. ITU-R: Error-correction, data framing, modulation and emission methods for digital terrestrial television broadcasting. ITU-R BT. 1306-6. Recommendation (2011)
33. Minn H, Zeng M, Bhargava VK (2000) On timing offset estimation for OFDM systems. IEEE Commu Lett 4(7):242–244
34. Middleton D (1979) Procedures for determining the parameters of the first-order canonical models of class A and class B electromagnetic interference. IEEE Trans Electromagn Compatib EMC-21(3):190–208
35. Ye Z, Duan C, Orlik PV, Zhang J, Abouzeid AA (2010) A synchronization design for UWB-based wireless multimedia systems. IEEE Trans Broadcast 56(2):211–225
36. Eldar Y, Kuppinger P, Bolcskei H (2010) Block-sparse signals: uncertainty relations and efficient recovery. IEEE Trans Signal Process 58(6):3042–3054

37. Wang D, Kobayashi H (2000) On design of interleavers with practical size for turbo codes. In: 2000 IEEE international conference on communications (ICC'00), pp 618–622
38. Alamouti SM (1998) A simple transmit diversity technique for wireless communications. IEEE J Sel Areas Commun 16(8):1451–1458
39. Nassar M, Gulati K, Mortazavi Y, Evans BL (2011) Statistical modeling of asynchronous impulsive noise in powerline communication networks. In: 2011 IEEE global communications conference (GLOBECOM'11), pp 1–6
40. Larsson EG, Edfors O, Tufvesson F, Marzetta TL (2014) Massive MIMO for next generation wireless systems. IEEE Commun Mag 52(2):186–195
41. Tropp JA, Gilbert AC, Strauss MJ (2006) Algorithms for simultaneous sparse approximation. Part I: Greedy pursuit. Signal Process 86(3):572–588
42. Berg EVD, Friedlander M (2010) Theoretical and empirical results for recovery from multiple measurements. IEEE Transa Inform Theory 56(5):2516–2527
43. Donoho D (2006) Compressed sensing. IEEE Trans Inform Theory 52(4):1289–1306
44. ITU-T: ITU G.9960, unified high-speed wire-line based home networking transceivers—system architecture and physical layer specification (2010)
45. ten Brink S, Kramer G, Ashikhmin A (2004) Design of low-density parity-check codes for modulation and detection. IEEE Trans Commun 52(4):670–678
46. Zhang Z, Rao B (2013) Extension of SBL algorithms for the recovery of block sparse signals with intra-block correlation. IEEE Trans Signal Process 61(8):2009–2015
47. Rabbachin A, Quek TQS, Pinto PC, Oppermann I, Win MZ (2010) Non-coherent UWB communication in the presence of multiple narrowband interferers. IEEE Trans Wirel Commun 9(11):3365–3379
48. Lago-Fernández J, Salter J (2004) Modelling impulsive interference in DVB-T: statistical analysis, test waveforms and receiver performance. BBC R&D White Paper WHP 80
49. Tonello AM, Pecile F (2009) Efficient architectures for multiuser FMT systems and application to power line communications. IEEE Trans Commun 57(5)
50. Duarte M, Eldar Y (2011) Structured compressed sensing: From theory to applications. IEEE Trans Signal Process 59(9):4053–4085
51. Glover J (1977) Adaptive noise canceling applied to sinusoidal interferences. IEEE Trans Acoust Speech Signal Process 25(6):484–491
52. Darsena D (2007) Successive narrowband interference cancellation for OFDM systems. IEEE Commun Lett 11(1)
53. Poisel R (2011) Modern communications jamming principles and techniques. Artech House
54. Shannon CE (2001) A mathematical theory of communication. ACM SIGMOBILE Mob Comput Commun Re 5(1):3–55
55. Nikopour H, Yi E, Bayesteh A, Au K, Hawryluck M, Baligh H, Ma J (2014) SCMA for downlink multiple access of 5G wireless networks. In: 2014 IEEE global communications conference, pp 3940–3945
56. Tse D, Viswanath P (2005) Fundamentals of wireless communication. Cambridge University Press, UK
57. Steven MK (1993) Fundamentals of statistical signal processing. PTR Prentice-Hall, Englewood Cliffs, NJ
58. Chindapol A, Ritcey JA (2001) Design, analysis, and performance evaluation for BICM-ID with square QAM constellations in rayleigh fading channels. IEEE J Sel Areas Commun 19(5):944–957
59. Needell D, Tropp JA (2009) Cosamp: iterative signal recovery from incomplete and inaccurate samples. Appl Comput Harmonic Anal 26(3):301–321
60. Dai W, Milenkovic O (2009) Subspace pursuit for compressive sensing signal reconstruction. IEEE Trans Inform Theory 55(5):2230–2249
61. Schmidl TM, Cox DC (1997) Robust frequency and timing synchronization for OFDM. IEEE Trans Commun 45(12):1613–1621
62. Oka A, Lampe L (2009) Compressed sensing reception of bursty UWB impulse radio is robust to narrow-band interference. In: IEEE global communications conference (GLOBECOM'09), pp 1–7

63. Arikan E (2009) Channel polarization: a method for constructing capacity-achieving codes for symmetric binary-input memoryless channels. IEEE Trans Inform Theory 55(7):3051–3073
64. IEEE: IEEE standard for information technology—local and metropolitan area networks–specific requirements—part 11: Wireless LAN medium access control (MAC) and physical layer (PHY) specifications amendment 6: Wireless access in vehicular environments (2010)
65. Richardson TJ, Shokrollahi MA, Urbanke RL (2001) Design of capacity-approaching irregular low-density parity-check codes. IEEE Trans Inform Theory 47(2):619–637
66. Sklar B (2001) Digital communications, vol 2. Prentice Hall, Upper Saddle River
67. Basar E (2015) OFDM with index modulation using coordinate interleaving. IEEE Wirel Commun Lett 4(4):381–384
68. 3GPP: 3GPP TS 36.104 v11.4.0—evolved universal terrestrial radio access (E-UTRA); base station (BS) radio transmission and reception (release 11) (2013)
69. Tran NH, Nguyen HH, Le-Ngoc T (2007) Performance of BICM-ID with signal space diversity. IEEE Trans Wirel Commun 6(5):1732–1742
70. Donoho D, Elad M, Temlyakov V (2006) Stable recovery of sparse overcomplete representations in the presence of noise. IEEE Trans Inform Theory 52(1):6–18
71. Eldar YC, Mishali M (2009) Robust recovery of signals from a structured union of subspaces. IEEE Trans Inform Theory 55(11):5302–5316
72. Baraniuk RG, Cevher V, Duarte MF, Hegde C (2010) Model-based compressive sensing. IEEE Trans Inform Theory 56(4):1982–2001
73. Wipf DP (2011) Sparse estimation with structured dictionaries. In: Advances in neural information processing systems, pp 2016–2024

Chapter 3
Synchronization Frame Design for NBI Mitigation

Abstract Synchronization has an important impact on the system performance of broadband communication systems. In particular, OFDM systems are very sensitive to the accuracy of synchronization. In the presence of narrowband interference, the performance of frame synchronization and carrier synchronization is severely influenced. The conventional synchronization frame structure and synchronization algorithms are not designed for mitigating the narrowband interference, resulting in serious performance loss of synchronization in the presence of narrowband interference. Hence, the problem of accurate and efficient synchronization in the presence of narrowband interference is the first utmost important problem to be solved to improve the system performance of broadband communication systems. In this chapter, the design of the OFDM preamble synchronization frame structure for effective narrowband interference mitigation is devised. Efficient and robust algorithms of receiver side frame synchronization and carrier recovery are studied. Besides, the method of frame header signalling transmission robust to the narrowband interference is investigated. Through these studies, the disadvantage of the conventional synchronization methods is overcome, and the synchronization performance of the OFDM system in the presence of narrowband interference is guaranteed. This research will provide basis technical support for the improvement of the overall system performance of the broadband communication systems in the presence of narrowband interference, and provide performance guarantee in the perspective of synchronization for the research of this thesis.

3.1 Introduction

3.1.1 Problem Description and Related Research

Due to its high transmission efficiency, simple implementation and especially the good performance to overcome frequency selectivity, the OFDM technique has been adopted as an effective physical layer modulation technique in many different broad-

band communication systems and standards, including the power line communication system, wireless local area network (WLAN), and digital video broadcasting (DVB), etc. However, the propagation channel of the OFDM system, including wired and wireless channels, tend to suffer from severe channel condition, noise, interference, and high attenuation, such as the narrowband interference and impulsive noise, which brings great challenge to the performance of OFDM systems, including synchronization, decoding, and demapping, etc.

In OFDM systems, a reliable and efficient communication relies on good synchronization performance, which has been investigated for long [1, 3, 5, 6]. Several methods have been proposed for preamble design and synchronization for OFDM systems. In literature [1], the classical sliding auto-correlation (SAC) method was proposed based on the cyclic prefix (CP). In [6], Schmidl proposed a preamble structure having two identical parts by using only even carriers in the frequency domain, which has been adopted into WLAN-based standards IEEE 802.11g and WMAN-based standards IEEE 802.16e. However, the SAC of this preamble produces a broad plateau around the correct timing position, which would cause ambiguity when determining the best start sample point, especially when the timing offset is beyond the scope of the length of CP so that the following operation cannot recover the right timing position. To solve this problem, Minn proposed a time-domain structure like $[\mathbf{A} \, \mathbf{A} - \mathbf{A} - \mathbf{A}]$ to reduce the plateau and sharpen the correlation peak [5]. However, the correlation result in Minn's method also introduces several sub-peaks, which might cause high false detection probability when the signal-to-noise ratio (SNR) of the channel is relatively low.

Furthermore, there is usually severe NBI in OFDM system propagation channels, which has a serious impact on communication reliability and synchronization. However, the above three synchronization methods could be severely deteriorated by NBI environments [2, 4]. Current methods for synchronization under NBI are not applicable and not effective. For instance, in the field tested indoor power line channel, the detrimental impacts of the NBI on the synchronization performance have been given in literature [3]. To solve this problem, it is in desperate need to propose an effective preamble design and corresponding synchronization method, which is also the main content in this chapter.

Besides, OFDM systems usually support different symbol constellation types and channel coding rates in order to meet different quality-of-service (QoS) requirements. Therefore, the transmission parameter signaling (TPS) can facilitate the succeeding channel estimation, and is critical for the receiver to demodulate the received data correctly. In the existing commercialized systems such as IEEE 802.11g and IEEE 802.16e, the TPS is transmitted separately following the preamble. After the timing and frequency synchronization have been accomplished, the receiver could then move to decode the signaling part. If the TPS can be integrated into the sub-carriers corresponding to the preamble, the process to obtain the TPS can be independent of the timing synchronization. Since the TPS information carried by the preamble does not occupy resources, the spectral efficiency can be significantly improved.

3.1.2 Research Aims and Problems

Concerning about the problem background mentioned above and the disadvantages of the current research, this chapter will focus on the solution of the scientific problem 1 in this thesis, i.e. how to overcome the severe impacts of the NBI on the synchronization performance of the receiver. Through investigating the research content including the optimized design of the synchronization frame structure for NBI mitigation and the efficient and robust synchronization algorithms at the receiver, the research aim of designing an optimized synchronization frame structure that can effectively improve the NBI mitigation performance and the efficient synchronization algorithm will be reached. More specifically, the major contribution of this chapter is twofold as follows:

- An OFDM based preamble design with the improved time domain structure is proposed, which has the advantages of both Schmidl's and Minn's methods. More importantly, a novel scrambling operation is applied to the cyclic extension of the time domain preamble OFDM symbol to mitigate the impact of the NBI on synchronization.
- Two identical training sequences are designed, which is distributed alternately in the active sub-carriers to achieve diversity gain under the frequency-selective fading channels. The relative distance between the two training sequences could be varied in order to indicate several bits of signaling information for the receiver to acquire the basic transmission parameters quickly.

3.2 Signal Model

The OFDM symbol is generated by an N-point inverse fast Fourier transform (IFFT) of the modulated data symbols $\{X_k\}$, as given by
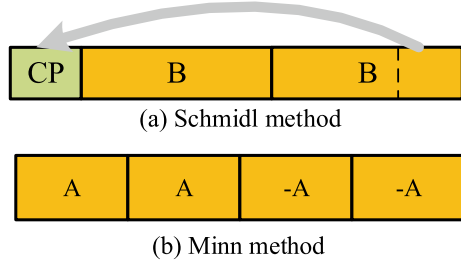
$$x_n = \frac{1}{\sqrt{N}} \sum_{k=0}^{N-1} X_k \cdot e^{j\frac{2\pi}{N}nk}. \tag{3.1}$$

Considering the channel delay spread, additive white Gaussian noise (AWGN), carrier frequency offset (CFO) and NBI, the received signal is modeled as

$$r_n = \sum_{l=0}^{L_h-1} h_l \cdot x_{n-n_0-l} \cdot e^{j2\pi n f_c} + I_0 \cdot e^{j2\pi n f_{\mathrm{NB}}} + \nu_n, \tag{3.2}$$

where n_0, f_c and ν_n are the unknown symbol arrival time (i.e. the accurate timing position to be estimated at the receiver), the CFO and AWGN, respectively. $\{h_l\}$ is the channel impulse response (CIR), which is modeled by L_h discrete weighted impulses. I_0 is the amplitude of the NBI at the frequency point f_{NB}. The CFO is

Fig. 3.1 Conventional
design of OFDM preamble

(a) Schmidl method

(b) Minn method

usually normalized by the sub-carrier spacing $1/N$, i.e., $f_c = k_0/N + f_{\text{frc}}$, where k_0 is an integer and f_{frc} is the residual fractional part of CFO.

The task of the synchronization process is to determine the timing position and estimate CFO without any knowledge of prior channel state information. To achieve this goal, Schmidl et al. [6] and Minn et al. [5] proposed some state of the art methods. Specifically, to this end, Schmidl proposed a preamble structure having two identical parts as illustrated in Fig. 3.1a by using only even carriers in the frequency domain [6]. The SAC operation for timing and frequency synchronization is based on the two cyclic parts '**B**', which could provide higher robustness than common CP-OFDM symbols. However, the SAC of such preamble will produce a broad plateau around the correct timing position due to the insertion of CP. The plateau would cause ambiguity when determining the best timing sample point.

To reduce the plateau, Minn proposed a novel time-domain structure like [**A A** $-$ **A** $-$ **A**], as illustrated in Fig. 3.1b [5]. With the deliberate design of two opposite parts, Minn's method could sharpen the correlation peak compared to Schmidl's method. However, the correlation in Minn's method introduces several sub-peaks, which might cause high false detection probability when the SNR is low.

Considering an NBI at the frequency point f_{NB}, the SAC result at the expected correct timing position of n_0' based on the conventional SAC operation on the two identical parts is given as (ignore the noise and channel terms for simplicity) is given by

$$
\begin{aligned}
R_{c,n_0'} &= \sum_{l=0}^{L_c-1} r_{n_0'+l} \cdot r_{n_0'+l+N_c}^* \\
&= \sum_{l=0}^{L_c-1} \left(x_l + I_0 e^{j2\pi f_{\text{NB}} l} \right) \cdot \left(x_l + I_0 e^{j2\pi f_{\text{NB}} (l+N_c)} \right)^* \\
&= \sum_{l=0}^{L_c-1} \left(|x_l|^2 + I_0 x_l e^{-j2\pi f_{\text{NB}} (l+N_c)} \right. \\
&\qquad\qquad \left. + I_0 x_l^* e^{j2\pi f_{\text{NB}} l} + I_0^2 e^{-j2\pi f_{\text{NB}} N_c} \right) \\
&\approx \sum_{l=0}^{L_c-1} |x_l|^2 + L_c \cdot I_0^2 e^{-j2\pi f_{\text{NB}} N_c}
\end{aligned}
\qquad (3.3)
$$

where L_c and N_c denote the length of the identical parts and the correlation lag, $(\cdot)^*$ denotes the complex conjugation. Since $\{x_l\}$ and $\{e^{j2\pi f_{\text{NB}} l}\}$ are non-coherent, the rest terms in (3.3) are eliminated after sum averaging, which can be neglected com-

pared with the SAC component of the preamble $|x_l|^2$ and the major NBI component $L_c I_0^2 e^{-j2\pi f_{\text{NB}} N_c}$. It is observed from (3.3) that the unpredictable NBI might deteriorate the correlation peak and thus degrade the detection performance. In order to solve the problems of the state of the art methods, this chapter designs an optimized preamble in particular, and propose the corresponding synchronization algorithm to improve the performance of synchronization against the NBI impact.

3.3 Synchronization Frame Structure Design for NBI Mitigation
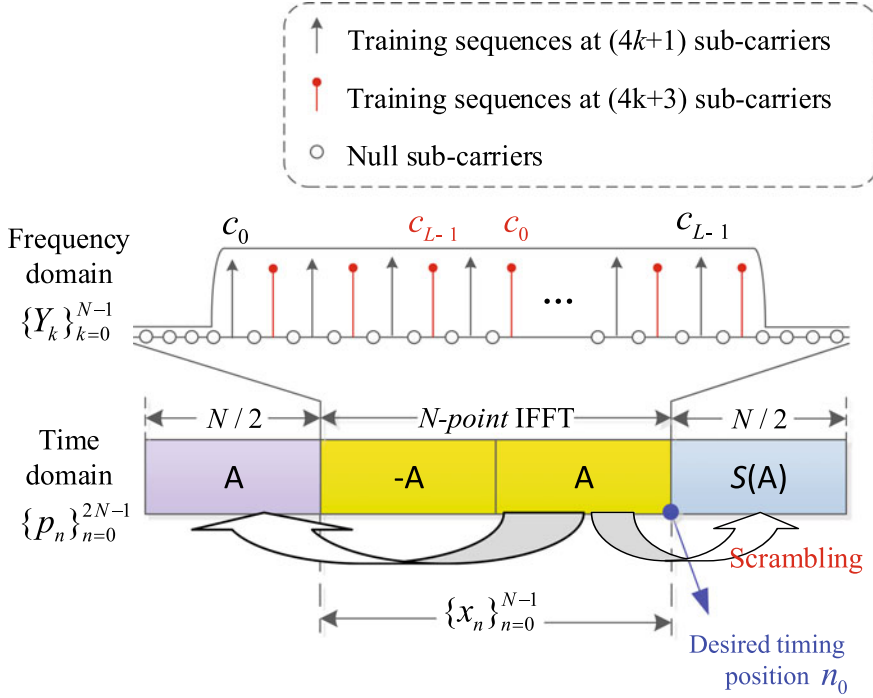
The proposed preamble is composed of a length-N OFDM symbol with its two cyclic extensions, as illustrated in Fig. 3.2. In the frequency domain, a pair of training sequences are alternatively inserted in the $\{4k + 1\}$ and $\{4k + 3\}$ indexed sub-carriers. The training sequence in the $\{4k + 1\}$ sub-carriers is located at the fixed position (i.e. it is configured as the reference initial phase for the pseudo random sequence), while the training sequence in the $\{4k + 3\}$ sub-carriers is cyclically right shifted by ΔL to form the frequency domain sequence of the preamble $\{Y_k\}_{k=0}^{N-1}$ as given by

$$\begin{cases} Y_{4k+1} = c_k, & k = 0, 1, \cdots, L - 1 \\ Y_{4k+3} = c_{(k-\Delta L) \bmod L}, & k = 0, 1, \cdots, L - 1 \\ Y_k = 0, \end{cases} \tag{3.4}$$

where c_k is the length-L ($L < N/4$) pseudo-random training sequence with good auto-correlation property. mod denotes the modular operation. The cyclical shift length ΔL could be varied in order to indicate different signaling information. There are L choices in total for the shift length corresponding to $\log_2 L$ bits of signaling. For the sake of fairness, all the preamble designs and the corresponding synchronization algorithms, including both the proposed algorithms and the state of the art ones engaged in this chapter, are compared in the same condition of identical preamble length.

Afterwards, the active sub-carriers in (3.4) are then differentially encoded and transformed to the time domain by N-point IFFT operation defined in (3.1). Since only odd sub-carriers are used, the time-domain OFDM symbol is divided into two opposite parts, denoted as '$-\mathbf{A}$' and '$\mathbf{A}$' in Fig. 3.2. The last half part '$\mathbf{A}$' is copied to the front as CP and also copied to the rear multiplying with a *scrambling sequence* $(-1)^n$ to form the '$\mathbf{S(A)}$' part. Then, the transmitted time-domain preamble signal $\{p_n\}_{n=0}^{2N-1}$ is thus represented as

$$p_n = \begin{cases} x_{n+N/2}, & 0 \le n < N/2 \\ x_{n-N/2}, & N/2 \le n < 3N/2 \\ (-1)^n \cdot x_{n-N}, & 3N/2 \le n < 2N \end{cases} \tag{3.5}$$

Fig. 3.2 Proposed OFDM preamble design
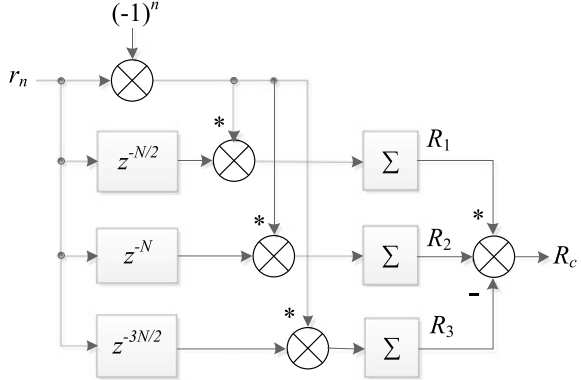
where $\{x_n\}_{n=0}^{N-1}$ denotes the time domain length-N OFDM symbol generated by the N-point IFFT operation, as illustrated by the part of $[-\mathbf{A}\ \mathbf{A}]$ in Fig. 3.2. The scrambling operation could effectively reduce the impact of the NBI. The superior performance of the proposed method in timing synchronization, carrier recovery and signalling detection compared with the conventional Schmidl's and Minn's methods will be further discussed in the following section.

3.4 Timing and Fractional CFO Synchronization

The timing algorithm adopts the cyclic properties of the proposed preamble, where three cyclic parts are observed and used for SACs:

$$R_{1,n} = \sum_{l=0}^{N/2-1} (-1)^{(n+l)} r_{n+l}^* \cdot r_{n+l-N/2}, \qquad (3.6)$$

Fig. 3.3 The process of the proposed time domain SAC based timing and carrier synchronization algorithm

$$R_{2,n} = \sum_{l=0}^{N/2-1} (-1)^{(n+l)} r_{n+l}^* \cdot r_{n+l-N}, \tag{3.7}$$

$$R_{3,n} = \sum_{l=0}^{N/2-1} (-1)^{(n+l)} r_{n+l}^* \cdot r_{n+l-3N/2}. \tag{3.8}$$

The multiplication with $(-1)^n$ in the summation of (3.6)–(3.8) is the *de-scrambling* operation between the three front parts and the last part '**S(A)**' of the preamble in Fig. 3.2. Finally, the above three correlation results are multiplied together to strengthen the correlation peak,
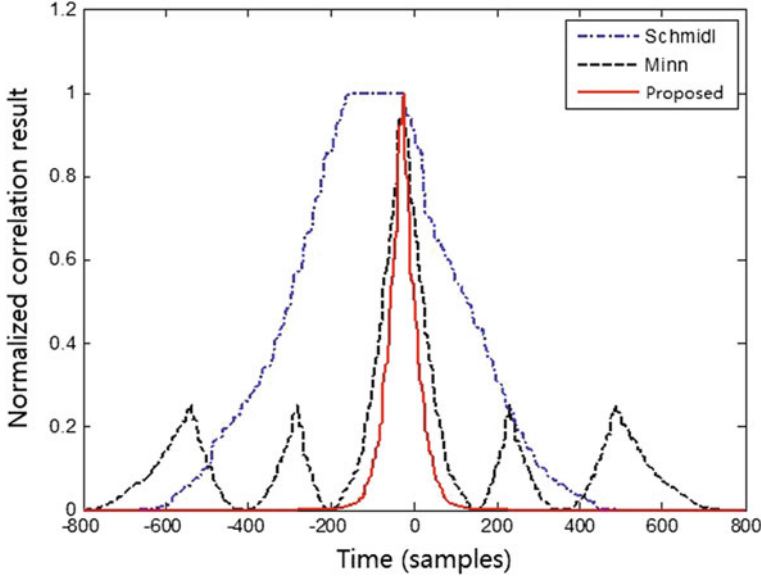
$$R_{c,n} = -R_{1,n}^* \cdot R_{2,n} \cdot R_{3,n}. \tag{3.9}$$

The process of the proposed time domain SAC based timing and carrier synchronization algorithm is illustrated in Fig. 3.3. According to the diagram and the SAC calculation methods given in (3.6)–(3.8), it can be observed that the theoretically desired timing position n_0 is the first sample of the '**S(A)**' part, as illustrated in Fig. 3.2.

Unlike the conventional SAC methods, a de-scrambling operation $(-1)^n$ is firstly applied to the received signal. Since the summations in (3.6)–(3.8) could be implemented with recursive method [6], the complexity of the proposed algorithm is low. Moreover, the correlation operations here are approximately 50% more than those in Minn's method with the same preamble length, since three pairs of correlation are calculated in the proposed method while only two pairs are needed in Minn's method.

The correlation peak of $R_{c,n}$ indicates the estimated timing position $\hat{n}_0$ in the preamble and the fractional CFO $\hat{f}_{\text{frc}}$ can also be obtained through the phase of the peak,

$$\hat{n}_0 = \arg \max_n \left\{ \left| R_{c,n} \right| \right\}, \tag{3.10}$$

Fig. 3.4 The comparison of the timing correlation peaks of the three synchronization methods

$$\hat{f}_{\mathrm{frc}} = \left. \frac{\arg\left(R_{c,n}\right)}{2\pi N} \right|_{n=\hat{n}_0}, \tag{3.11}$$

where arg max $\{\cdot\}$ denotes the set of variables that maximize the objective function, and arg $(\cdot)$ denotes the phase of a complex number.

Simulation examples of the SAC for Schmidl's, Minn's and the proposed methods without channel noise are illustrated in Fig. 3.4. A broad plateau with the duration of CP is observed in Schmidl's method, while four sub-peaks about one-fourth height of the main peak are introduced in Minn's method. It is noted that the proposed method could avoid either plateau or sub-peaks and obtain even sharper peak than Minn's method.

Considering an NBI at the frequency point f_{NB}, the auto-correlation result at the correct timing position n_0 derived by the branch R_1 in (3.6) after the de-scrambling operation is given as,

$$
\begin{aligned}
R_{1,n_0} &= \sum_{l=0}^{N/2-1} (-1)^l \left((-1)^l x_l + I_0 e^{j2\pi f_{\mathrm{NB}} l} \right)^* \\
&\quad \cdot \left(x_l + I_0 e^{j2\pi f_{\mathrm{NB}}(l-N/2)} \right) \\
&= \sum_{l=0}^{N/2-1} \left(|x_l|^2 + I_0 x_l^* e^{j2\pi f_{\mathrm{NB}}(l-N/2)} \right. \\
&\quad \left. + (-1)^l I_0 x_l e^{-j2\pi f_{\mathrm{NB}} l} + (-1)^l I_0^2 e^{-j2\pi f_{\mathrm{NB}} N/2} \right) \\
&\approx \sum_{l=0}^{N/2-1} |x_l|^2
\end{aligned}
\tag{3.12}
$$

where the cross terms are mitigated and eliminated after de-scrambling and sum averaging, since the NBI and the preamble are noncoherent signals. It is shown by Eq. (3.12) that, due to the de-scrambling operation, the NBI component $(-1)^l I_0^2 e^{-j2\pi f_{\mathrm{NB}} N/2}$ will be eliminated after sum averaging. Hence, the SAC result of $R_{1,n}$ reaches its maximum peak at the desired timing position n_0. Similarly, the SAC branch results of $R_{2,n}$ and $R_{3,n}$ in Eqs. (3.13) and (3.14) at the desired correct timing position are given respectively by

$$R_{2,n_0} \approx - \sum_{l=0}^{N/2-1} |x_l|^2, \qquad (3.13)$$

$$R_{3,n_0} \approx \sum_{l=0}^{N/2-1} |x_l|^2. \qquad (3.14)$$

Hence, $R_{2,n}$ and $R_{3,n}$ also reach their maximum peak value at the desired timing position n_0. Finally, the aggregated SAC result $R_{c,n}$ provided by Eq. (3.9) is free from the contamination of the NBI, and also reaches its maximum peak value at the desired timing position n_0. Therefore, the detected timing position $\hat{n}_0$ estimated by Eq. (3.10) at the receiver is the very accurate timing position n_0. The proposed timing synchronization method is robust to the NBI.
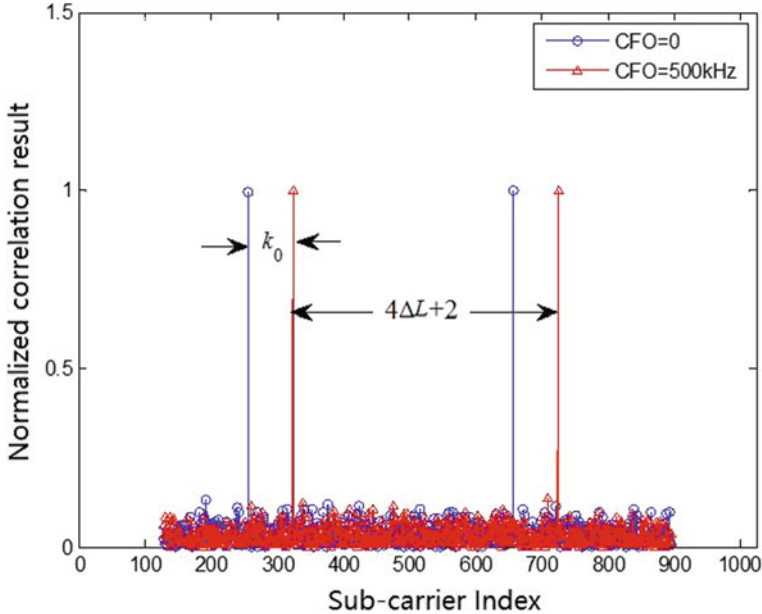
Besides, the proposed method can be easily extended to multipath fading channels, in which the mechanism of NBI mitigation given by Eqs. (3.12) and (3.3) still effectively holds. The detailed analysis is provided in Sect. 3.6.

3.5 Integer CFO Estimation and Signaling Detection with NBI

After the timing synchronization is accomplished, the received OFDM symbol is compensated with the estimated fractional CFO estimated by Eq. (3.11) and then transformed into frequency domain by N-point FFT operation. The received active carriers are denoted as

$$\hat{Y}_k^{(d)} = Y_{k-k_0}^{(d)} H_{k-k_0} e^{-j\frac{2\pi}{N} \Delta n \cdot k} + N \cdot I_0 \cdot \delta_{k-k_{\mathrm{NB}}} + V_k, \qquad (3.15)$$

where $Y_k^{(d)}$ is the transmitted active carrier after differential encoding operation, while H_k and V_k are the channel frequency response and the frequency domain noise term. δ_k is the Kronecker-delta function (the function value is 1 only if $k = 0$, and 0 otherwise). k_{NB} is the sub-carrier index at the frequency point f_{NB}. Δn is the timing error which causes a phase rotation of the active carriers. It is noted from (3.22) that the integer part of CFO k_0 leads to a shift of all carriers.

Fig. 3.5 Frequency-domain correlation results between the transmitted sequences with different CFOs and the local sequence

The NBI could be easily removed in the frequency domain by setting the carriers with excessively large power to zero. After that, a differential decoding operation is applied to the received active carries and yields

$$
\begin{aligned}
Z_k &= \hat{Y}_k^{(d)} \cdot \hat{Y}_{k-2}^{(d)*} \\
&= H_{k-k_0} H_{k-k_0-2}^* \cdot Y_{k-k_0} e^{j\frac{2\pi}{N}2\Delta n} + \tilde{V}_k \,, \\
&\approx \left| H_{k-k_0} \right|^2 Y_{k-k_0} e^{j\frac{2\pi}{N}2\Delta n} + \tilde{V}_k
\end{aligned}
\tag{3.16}
$$

where $\tilde{V}_k$ is the sum of residual noise terms. The approximation in (3.16) holds when the adjacent sub-carriers are closely similar in the frequency-selective fading channels.

Due to the differential decoding operation, the phase rotation caused by the timing error is canceled, leaving only a fixed phase offset. Therefore, the proposed method is also robust to timing errors.

The integer CFO and the signaling information could be simultaneously detected by the cross correlation between the received differentially decoded sub-carriers and the local training sequence, i.e.,

$$R_{d,k} = \frac{\sum_{l=0}^{L-1} Z_{(k+4l) \bmod 4L} \cdot c_l^*}{\sum_{l=0}^{L-1} \left| \hat{Y}_{(k+4l) \bmod 4L} \right|^2}, \quad 0 \le k < N. \tag{3.17}$$

The correlation in (3.17) is expected to generate two peaks, as illustrated in Fig. 3.5. The integer CFO could be estimated through the shift of the first peak from its reference position when CFO=0, while the signaling is inferred from the distance between those two peaks. Specifically, the signaling parameter ΔL can be derived by the distance between the two peaks generated by the correlation operation in (3.17) with the same CFO, as illustrated in Fig. 3.5, where the distance is $(4\Delta L + 2)$.

3.6   Performance Analysis of the Algorithms

Let us consider the computational complexity of the proposed synchronization method and compare it with that of the conventional Minn's method. Note that the comparison is done under the same preamble length for both methods, i.e. $2N$ according to Sect. 3.3. For both methods, the main consumption of computational complexity goes to the part of the calculation of SAC. Usually, the computational complexity can be evaluated by the quantity of additions and multiplications, given in detail as follows:

For the conventional Minn's method [5], there are two SAC windows for the positive preamble part and negative preamble part, respectively, with each being of N in length, as illustrated in Fig. 3.1b. The calculation begins when the first nonzero entry of the preamble falls into the previous positive SAC window, and ends when the last nonzero entry of the preamble leaves away from the latter negative SAC window. Hence, with the total preamble length being $2N$, the SAC operation during the synchronization of the Minn's method requires $T_{\text{mul}}^{(M)} = 2.5$ N times of multiplications and $T_{\text{add}}^{(M)} = 10$ N times of additions. Thus the total computational complexity of Minn's method is in the order of $\mathcal{O}(N)$.

For the proposed method, as described in Sect. 3.4, there are three SAC windows $R_{1,n}$, $R_{2,n}$, and $R_{3,n}$, with each being of length-N. The calculation of SAC begins when the first nonzero entry of the preamble falls into the $R_{3,n}$ SAC window, and ends when the last nonzero entry of the preamble leaves away from the $R_{1,n}$ SAC window. Hence, with the total preamble length also being $2N$, the SAC operation during the synchronization of the proposed method requires $T_{\text{mul}}^{(P)} = 9N$ times of multiplications and $T_{\text{add}}^{(P)} = 18N$ times of additions in total. Thus the total computational complexity of the proposed method is also in the order of $\mathcal{O}(N)$.

Although there is a moderate complexity increase to the proposed method due to more correlation and multiplication operations, both the proposed and conventional methods have a computational complexity in the order of $\mathcal{O}(N)$. Hence, the cost of

calculation resource is in the same order and the proposed method is applicable for practical system implementation.

Considering the effectiveness of the proposed synchronization algorithm in multipath fading channels, it can be proved that the proposed synchronization method is also applicable for multipath fading channels. The mechanism of NBI mitigation described by Eqs. (3.12) and (3.3) still holds. The proposition and the proof are provided in detail as follows.

Proposition 3.1 *The proposed synchronization method is effective for multipath fading channels, i.e., the mechanism of NBI mitigation described by Eqs.* (3.12) *and* (3.3) *still holds.*

Proof First, we look at the SAC window $R_{1,n}$ at the desired timing position n_0 as given by (3.12). Taking the multi-path fading channel condition into consideration, the SAC result is derived as

$$
\begin{aligned}
R_{1,n_0} &= \sum_{l=0}^{N/2-1} (-1)^l r^*_{n_0+l} \cdot r_{n_0+l-N/2} \\
&= \sum_{l=0}^{N/2-1} (-1)^l \left[\sum_{k=0}^{L_h-1} h_k \cdot (-1)^{l-k} x_{l-k} + I_0 \exp(j2\pi f_{\mathrm{NB}} l) \right]^* \cdot \\
&\qquad \left[\sum_{m=0}^{L_h-1} h_m \cdot x_{l-m} + I_0 \exp\left(j2\pi f_{\mathrm{NB}}(l - N/2)\right) \right] \\
&= \sum_{l=0}^{N/2-1} \Bigg[(-1)^l \left(\sum_{k=0}^{L_h-1} h_k \cdot (-1)^{l-k} x_{l-k} \right)^* \left(\sum_{m=0}^{L_h-1} h_m \cdot x_{l-m} \right) \\
&\qquad + (-1)^l \left(\sum_{k=0}^{L_h-1} h_k \cdot (-1)^{l-k} x_{l-k} \right)^* I_0 \exp\left(j2\pi f_{\mathrm{NB}}(l - N/2)\right) \\
&\qquad + (-1)^l \left(\sum_{m=0}^{L_h-1} h_m \cdot x_{l-m} \right) I_0 \exp(-j2\pi f_{\mathrm{NB}} l) \\
&\qquad + (-1)^l \underbrace{I_0^2 \exp(-j2\pi f_{\mathrm{NB}} N/2)}_{\text{NBI}} \Bigg] \\
&\approx \sum_{l=0}^{N/2-1} \sum_{k=0}^{L_h-1} \sum_{m=0}^{L_h-1} (-1)^k h_k^* h_m x^*_{l-k} x_{l-m},
\end{aligned}
\tag{3.18}
$$

where the cross terms between the NBI and the preamble sequence can still be eliminated by sum averaging and de-scrambling as they can be in the AWGN channel shown by (3.12), because they are incoherent signals. The NBI component as pointed

out in (3.18) above is also eliminated through de-scrambling and sum averaging as well. Hence, the SAC result of $R_{1,n}$ yields the peak value as given by (3.18) at the desired timing position n_0, which is free from the impacts of the NBI.

Similarly, we have

$$R_{2,n} \approx - \sum_{l=0}^{N/2-1} \sum_{k=0}^{L_h-1} \sum_{m=0}^{L_h-1} (-1)^k h_k^* h_m x_{l-k}^* x_{l-m} \tag{3.19}$$

$$R_{3,n} \approx \sum_{l=0}^{N/2-1} \sum_{k=0}^{L_h-1} \sum_{m=0}^{L_h-1} (-1)^k h_k^* h_m x_{l-k}^* x_{l-m} \tag{3.20}$$

Therefore, all the three SAC results are free from the impacts of the NBI, making the final peak value $R_{3,\hat{n}_0}$ immune to the NBI, so the estimated timing position $\hat{n}_0$ accurately matches the desired timing position n_0 in the presence of the NBI under the multi-path channel.

The analysis for the contamination of the NBI upon the conventional methods as given by (3.3) can be extended to multi-path channels through similar reasoning. Considering multi-path fading channel, the SAC result $R_{c,n}$ of the conventional methods at the desired timing position n_0' is given by

$$R_{c,n_0'} = \sum_{l=0}^{L_c-1} r_{n_0'+l} \cdot r_{n_0'+l-N_c}^*$$

$$= \sum_{l=0}^{L_c-1} \left[\sum_{m=0}^{L_h-1} h_m \cdot x_{l-m} + I_0 \exp(j2\pi f_{\mathrm{NB}} l) \right] \cdot \left[\sum_{k=0}^{L_h-1} h_k \cdot x_{l-k} + I_0 \exp\left(j2\pi f_{\mathrm{NB}}(l+N_c)\right) \right]^*$$

$$= \sum_{l=0}^{L_c-1} \left[\left(\sum_{k=0}^{L_h-1} h_k \cdot x_{l-k} \right)^* \left(\sum_{m=0}^{L_h-1} h_m \cdot x_{l-m} \right) + \left(\sum_{k=0}^{L_h-1} h_k \cdot x_{l-k} \right)^* I_0 \exp\left(j2\pi f_{\mathrm{NB}} l\right) \right.$$

$$\left. + \left(\sum_{m=0}^{L_h-1} h_m \cdot x_{l-m} \right) I_0 \exp\left(-j2\pi f_{\mathrm{NB}}(l+N_c)\right) + \underbrace{I_0^2 \exp(-j2\pi f_{\mathrm{NB}} N_c)}_{\mathrm{NBI}} \right]$$

$$\approx \sum_{l=0}^{N/2-1} \left(\sum_{k=0}^{L_h-1} \sum_{m=0}^{L_h-1} h_k^* h_m x_{l-k}^* x_{l-m} + \underbrace{I_0^2 \exp(-j2\pi f_{\mathrm{NB}} N_c)}_{\mathrm{NBI}} \right). \tag{3.21}$$

From (3.21), it can be noted that, although the cross terms between the NBI and the preamble sequences are eliminated through sum averaging, the NBI component as pointed out in (3.21) above is remained in the SAC result because there is no scrambling to eliminate it. Hence, under the multi-path fading channel, the remained NBI component will cause serious impacts on the peak value, so the conventional timing synchronization method will be seriously affected, which is similar to the result for the AWGN channel described by (3.3).

3.7   Simulation Results and Discussions

In this section, computer simulations are implemented to evaluate and compare the performance of the conventional and the proposed preamble and synchronization methods in the presence of the NBI under different channel conditions. As claimed in previous sections, note that all the methods are simulated with the same preamble length for fair comparison. The simulation setup is configured in a typical power line communications transmission system, and the simulation parameters are given in Table 3.1. The length of training sequences is chosen to be 192, and could be used to indicate at least 7-bit of signaling information. A multipath power line communications channel model [7] with NBI is adopted to evaluate the detection algorithm in power line transmission and reception scenarios. The parameter profile of the power line channel is listed in Table 3.2. An NBI with the power of -12 dB compared to the average signal power is also introduced in the simulations.
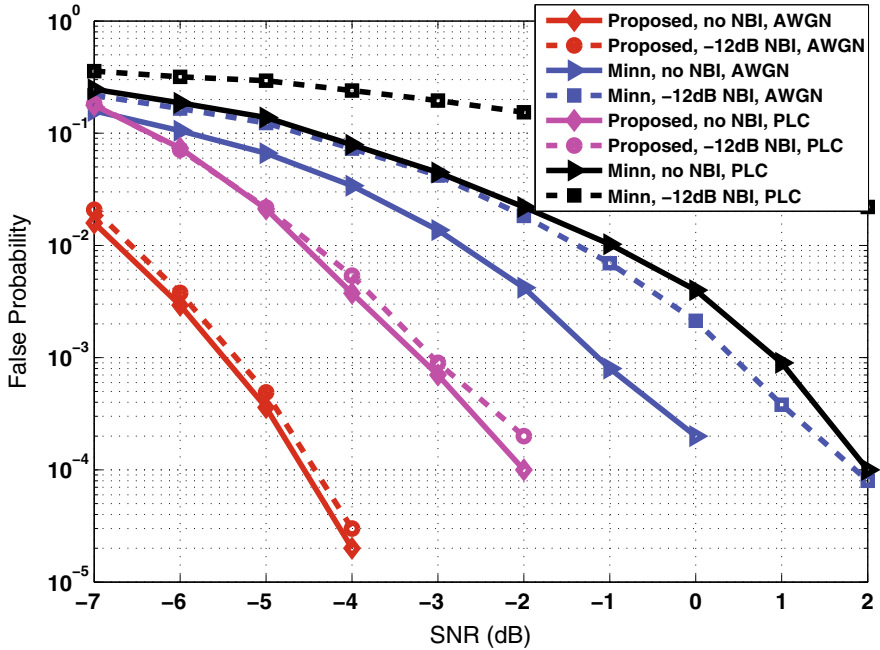
Firstly, the detection performance of the preamble is evaluated by the false probability and the missed probability of the SAC peak detection. The false probabilities of Minn's method and the proposed method are compared in Fig. 3.6 when the missed probability is required at a level of 10^{-3}. The false detection probability of the proposed preamble is improved by about 4dB compared to Minn's method in both AWGN and PLC channels when there is no NBI, with the cost of more correlation and multiplication operations than Minn's method. When the -12dB NBI is considered (marked with dashed lines in Fig. 3.6), it is noted that Minn's method degrades more than 1 dB in AWGN channel and more than 4 dB in the PLC channel, whereas the proposed method is much less affected by the NBI.

Table 3.1 Simulation parameter

Parameter	Value
Carrier frequency	6 6 MHz
Bandwidth	8 8 MHz
Symbol rate	7.56 M Symbol/s
FFT size	1024
Length of TS	192
Symbol duration	270.9 us
CFO	30 kHz
NBI power	-12 dB

Table 3.2 PLC channel parameter profile

Path Index	Distance $d_i(m)$	Gain g_i		
1	200	0.64	k	1.0
2	222.4	0.38	$a_0(s/m)$	0
3	244.8	-0.15	$a_1(s/m)$	7.8×10^{-10}
4	267.5	0.05		
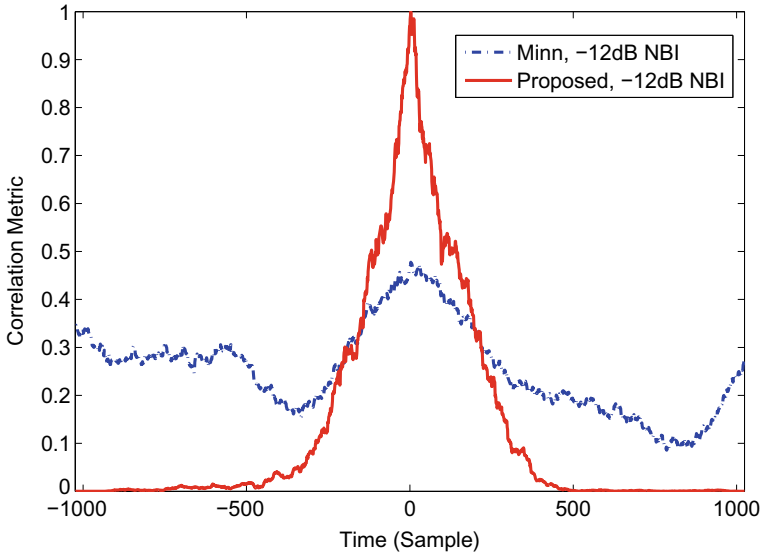
Fig. 3.6 False probability of preamble detection in AWGN and PLC channels when the missed probability is around 10^{-3}

Concerning the impact of the introduction of NBI on timing detection performance, simulation results of the SAC for Minn's and the proposed methods under the -12dB NBI in the power line channel are illustrated in Fig. 3.7 in comparison with those in Fig. 3.4. The timing correlation peak in Minn's method under the -12dB NBI is much smaller than that without NBI, as is illustrated in Fig. 3.4. Furthermore, the sub-peaks of Minn's method are higher and the central peak is not as sharp as that without NBI, which is much likely to cause timing detection errors. However, the peak is hardly affected by the -12dB NBI in the proposed method, thus achieving as good performance of timing detection as that without NBI.
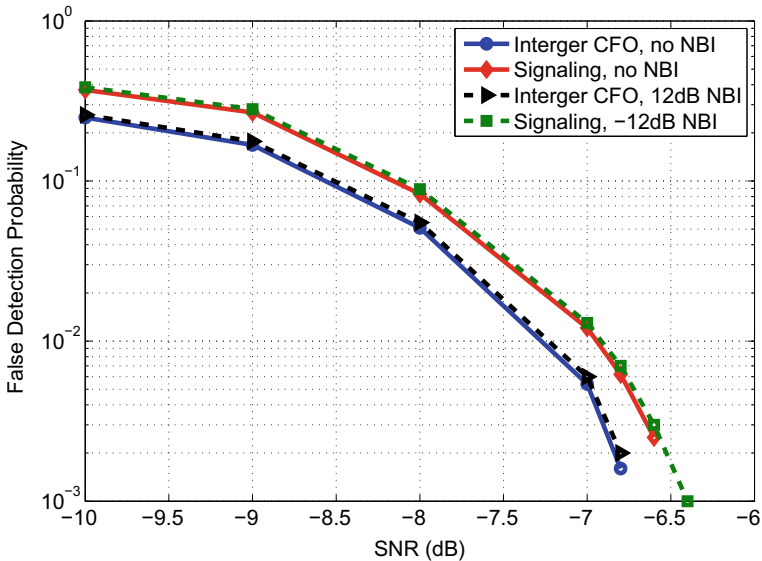
The false probabilities of the integer CFO estimation and signaling detection are depicted in Fig. 3.8. From Figs. 3.5 and 3.8, it's observed that both integer CFO and signaling could be well estimated if the preamble is detected. It should be pointed out that, only if both peaks are detected then the signaling could be decoded correctly. Therefore, the false probability of signaling detection $P_{f,\text{Sig}}$ and the false probability of integer CFO estimation $P_{f,\text{IntCFO}}$ approximate the following equation,

$$P_{f,\text{Sig}} = 1 - (1 - P_{f,\text{IntCFO}})^2. \tag{3.22}$$

The simulation results in Fig. 3.8 are aligned with the above analysis.

Fig. 3.7 Timing correlation peaks for two methods under NBI

Fig. 3.8 False probability of integer CFO estimation and signaling detection

3.8 Conclusion

In this chapter, an OFDM-based preamble has been designed for improving timing and frequency synchronization as well as robust signaling information transmission in OFDM systems contaminated by NBI. Compared to conventional Schmidl's and Minn's methods, the proposed preamble could achieve better timing synchronization performance with a moderate cost of complexity. With a simple scrambling operation, the proposed preamble could effectively combat against the narrowband interference, which is prevailing in wired and wireless channels. Furthermore, by using the proposed sub-carrier pattern, the preamble could simultaneously convey several bits of signaling for the receiver to acquire the basic transmission parameters quickly. The proposed preamble design can be further applied to various communication systems suffering from the NBI.

References

1. Beek van de JJ, Sandell M, Borjesson PO (1997) ML estimation of time and frequency offset in OFDM systems. IEEE Trans Signal Process 45(7):1800–1805
2. Coulson A (2004) Narrowband interference in pilot symbol assisted OFDM systems. IEEE Trans Wirel Commun 3(6):2277–2287
3. Godoy J, Canete FJ, Corts JA, Dez L (2012) A study on symbol timing recovery schemes for broadband in-home PLC. In: 2012 IEEE international symposium on power line communications and its applications (ISPLC'12), pp 188–193 (2012)
4. Marey M, Steendam H (2007) Analysis of the narrowband interference effect on OFDM timing synchronization. IEEE Trans Signal Process 55(9):4558–4566
5. Minn H, Zeng M, Bhargava VK (2000) On timing offset estimation for OFDM systems. IEEE Commun Lett 4(7):242–244
6. Schmidl TM, Cox DC (1997) Robust frequency and timing synchronization for OFDM. IEEE Trans Commun 45(12):1613–1621
7. Zimmermann M, Dostert K (2002) Analysis and modeling of impulsive noise in broad-band powerline communications. IEEE Trans Electromag Compatib 44(1):249–258

Chapter 4
Optimal Time Frequency Interleaving with NBI and TIN

Abstract As described in Chap. 2, in order to get rid of the time and frequency bursting errors or deep fading in communication systems, it is necessary to design interleavers and deinterleavers. The conventional interleaving methods have many disadvantages. For example, the design is complicated. It is required to re-design a corresponding interleaving scheme for each coding and modulation parameter, so the adaptability and flexibility are quite limited. The state of the art methods cannot take time and frequency interleaving into account simultaneously, so they cannot suppress the time domain and frequency domain bursting errors simultaneously. Conventional bit or symbol interleaving patterns have no theoretical guarantee for the optimal performance, so it cannot ensure that the optimal scheme is devised and the maximum time and frequency diversity gains are achieved. In order to overcome the disadvantages of the conventional methods, this chapter is focused on the research idea of providing time and frequency diversity gains to suppress the time and frequency bursting noise and interference. The optimal time and frequency combined interleaving scheme in the presence of narrowband interference and impulsive noise is proposed, for which the theoretical analysis and guarantee are provided. Firstly, the scheme to optimize the interleaving parameters that maximize time diversity gain is proposed. Then, the symbol interleaving block cyclic shifting technique is proposed to maximize the frequency diversity gain. In this way, the time and frequency diversity gains are maximized, and the time and frequency bursting errors are effectively suppressed. Meanwhile, the interleaving performance and the decoding performance are significantly improved in the presence of both narrowband interference and impulsive noise. The research in this chapter will provide theoretical basis and feasible technical routines for the interleaving schemes in broadband communication systems in the severe channel condition with complicated narrowband interference and impulsive noise.

4.1 Introduction

4.1.1 Problem Description and Related Research

Orthogonal frequency division multiplexing (OFDM) technique is widely adopted in various communication systems, including PLC systems, the digital television terrestrial broadcasting (DTTB) systems, and the cellular wireless communication systems, etc. The OFDM technique divides the entire bandwidth into many parallel narrow bands which can provide the higher-spectrum efficiency as well as better capability to handle the multi-path effect. Frequency-selectivity can be well mitigated using the OFDM technique, nevertheless the narrowband interference (NBI) and time-domain impulsive noise (TIN) prevailing the channel should be specially taken into consideration since they can both cause severe degradation on the system performance, which has drawn much research attention [3, 6, 13].

Interleaving is aimed at providing diversity in time, frequency and/or spatial domain, and has been adopted in the many various broadband transmission systems since the channel conditions are so poor that more diversity is beneficial to the system performance. Several interleaving schemes to improve the performance of different communication systems have been investigated [4, 9, 12]. Wang and Kobayashi proposed a method to design an interleaver with practical size for turbo codes [12]. Literature [9] investigated an adaptive interleaved beamforming approach for broadband MIMO/OFDM systems in which beamforming is adaptively interleaved in the spatial domain to achieve performance improvements over conventional adaptive antenna array based OFDM systems in wireless channels. In broadcasting systems, such as the prevailing second generation terrestrial digital video broadcasting standard (DVB-T2), interleaving is adopted to ensure better performance under the severe propagation environment [4]. However, these interleaving methods are not optimized for mitigating the performance degradation due to special impairments, such as TIN and NBI.

For the purpose of reducing the impact of impulse noise in OFDM systems, several methods have been proposed [1, 2]. An interleaving scheme performed post the inverse discrete Fourier transform (IDFT) can achieve better performance under TIN [1]. However, the method is very sensitive to the QAM order and will suffer from remarkable degradation in 64-QAM or higher-order QAM constellations. The performance of the coded OFDM system and the impact of the length of the adopted bit interleaver on coding performance are analyzed by Amirshahi in [2]. The aforementioned methods are not specifically designed or optimized for mitigating NBI impairments.

In order to deal with the impairments due to NBI, an OFDM system using convolutional coding with an interleaver designed for channels under narrowband and impulsive noise is described in [10] with bit interleaving rather than symbol interleaving proposed, and the interleaver is specially designed for systems using convolutional coding and BPSK modulation only. This constrains its application and performance

in other systems, and there is no experimental or simulation results provided in the paper to show the performance.

Consequently, the current research is not aimed at the severe propagation environment in the presence of both the narrowband interference and impulsive noise, and has not given an interleaving scheme that can provide the optimal time and frequency diversity gains. Hence, the complicated and severe noise and interference cannot be effectively suppressed, resulting in the limitation of the system performance. Moreover, the state of the art interleaving schemes are faced with a series of challenges such as the high design complexity, low applicability and low flexibility, and no theoretically optimal guarantee, etc. Thus, it is in desperate need to investigate and design a new, universally applicable and optimal time and frequency combined interleaving technique for the multi-mode coded modulation OFDM systems.

4.1.2 Research Aims and Problems

As far as the problem background and the disadvantages of the current research mentioned above are concerned, this chapter is devoted to solving the scientific problem 2 in this thesis, i.e. how to improve the performance of the time and frequency interleaving scheme in the environment in the presence of both impulsive noise and narrowband interference. The optimal time and frequency combined interleaving scheme in the presence of narrowband interference and impulsive noise, the strategy of interleaving parameter optimization that maximizes the time diversity gain, and the symbol interleaving block cyclic shifting technique that maximizes the frequency diversity gain, are investigated as the technical routines. Then, the theoretically maximum time and frequency diversity gains will be simultaneously achieved, and the capability of suppressing narrowband interference and impulsive noise for the coded block transmission systems will be improved. More specifically, the major contribution of this chapter is as follows:

- Based on the proposed two theoretical criteria, the optimal time and frequency interleaving schemes are proposed, in order to suppress the narrowband interference and impulsive noise in broadband communication systems. Based on the proposed two criteria, the design of the optimal interleaver is guided in theory, which is able to significantly improve the time and frequency diversity. One of the criteria is satisfied by optimizing the distribution of the OFDM data block in the forward error correction (FEC) codewords. The other criterion is satisfied by optimizing the distribution of the OFDM sub-carriers in the FEC codewords.
- Based on the theoretical optimization criteria, the block interleaver with the optimal interleaving size is investigated and proposed as the time interleaving scheme. A novel frequency interleaving scheme based on the technique of cyclic row shifting in sub-matrix is proposed. The proposed interleaving process in this thesis is at the data symbol level rather than the bit level, which makes it easier to achieve higher effectiveness with lower implementation complexity.
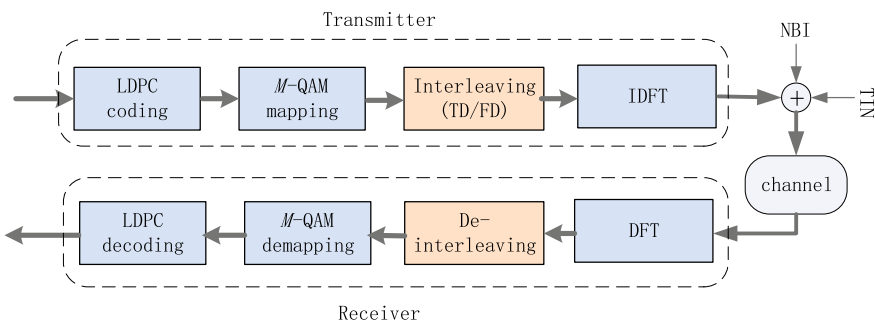
4.2   System Model

The OFDM system model used for the analysis in this chapter is depicted in Fig. 4.1.
This system diagram is consistent with the OFDM block transmission system archi-
tecture illustrated in Fig. 2.1 in Chap. 2, and it is simplified to be focused on the
major modules of interest in this chapter. The source bit stream $\{b_k\}$ is passing
through the encoder and generates forward error correction (FEC) codewords $\{e_l\}$
with the length of L_b, where the low density parity check (LDPC) code is adopted
as the FEC code. Bit-to-symbol mapping is performed by M-QAM constellation,
which produces complex data symbols $\{c_t\}$. The data symbols are then interleaved in
the block interleaver, which is adopted as a time and/or frequency interleaver, with
I_R rows and I_C columns. Afterwards, the pilots are inserted, and combined with the
interleaved data symbols to form the OFDM block in the frequency domain. The
number of data sub-carriers in an OFDM block is N. The frequency interleaving is
performed before the OFDM block data is processed by the IDFT module to obtain
the time-domain OFDM symbol $\mathbf{x}_i$. The OFDM symbols are then transmitted over
the multipath fading channel deteriorated by both NBI and TIN. The received signal
$\mathbf{y}_i$ at the receiver can be expressed as

$$\mathbf{y}_i = \mathbf{h}_i \odot \mathbf{x}_i + \mathbf{e}_i + \mathbf{z}_i + \mathbf{w}_i \tag{4.1}$$

where $\mathbf{e}_i = [e_{i,0}, e_{i,1}, \ldots e_{i,N-1}]^T$ denotes the NBI signal corresponding to the i-
th received time domain OFDM symbol, $\mathbf{z}_i = [z_{i,0}, z_{i,1}, \ldots z_{i,N-1}]^T$ denotes the
impulsive noise corresponding to the i-th received time domain OFDM symbol,
$\mathbf{h}_i = [h_{i,0}, h_{i,1}, \ldots h_{i,L-1}]^T$ denotes the channel impulse response (CIR) of the mul-
tipath channel with the maximum delay spread of L. $\odot$ denotes the convolution oper-
ation. $\mathbf{w}_i = [w_{i,0}, w_{i,1}, \ldots w_{i,N-1}]^T$ is the background noise in the channel, which
is usually modeled as additive white Gaussian noise (AWGN) with zero mean and
variance of σ_w^2.

Finally, the receiver performs the inverse operations of the transmitter in a reversed
order, and obtains the transmitted bits $\{b_k\}$.

Fig. 4.1   The coded OFDM system model with an interleaver

The compound BLGN interferer model described in detail in Chap. 2 is adopted as the narrowband interference model (refer to Sect. 2.3.1 for detail). The Middleton-Poisson model described in detail in Chap. 2 is adopted as the impulsive noise model (refer to Sect. 2.3.2 for detail). The notations and expressions are consistent with those defined in Chap. 2, so they are omitted in this chapter. The time and frequency interleaving method proposed in this thesis is nonparametric, but the transmission environment in the presence of both NBI and TIN can be simulated by the statistical model of noises and interferences, and the effectiveness of the proposed method can be verified.

4.3 Design of Optimal Time-Frequency Joint Interleaving Method

As for the conventional block interleaving scheme, data symbols are written row-wise into the block interleaver with I_R rows and I_C columns, and then read column-wise out to form the OFDM blocks. The conventional block interleaving is time interleaving, aiming at providing time diversity and the mitigation of TIN. Time-domain burst errors could be dispersed into several different FEC codewords to reduce the probability of decoding errors by block interleaving.

It is crucial to choose an appropriate block size for a block interleaver to achieve better anti-TIN capability for a certain system. The row number I_R is usually referred to as the interleaving depth, while the column number I_C is the interleaving width. If the block size is not specially designed for OFDM systems in the presence of TIN, the performance will degrade greatly. Meanwhile, in the presence of NBI, the conventional block interleaving scheme may have a serious drawback in sub-carrier allocation of LDPC codewords.

Another conventional interleaver, i.e. the random bit interleaver, distributes the bits among several codewords into different time slots and sub-carriers. The design of a bit interleaver is also aimed at providing larger time/frequency diversity, which is a fundamental idea of the proposed scheme in this chapter. However, in the presence of TIN and NBI, a good random bit interleaver is very difficult to design in practice, and one specific bit interleaver is not robust and is likely to degrade in different constellations, interleaving depths or transmission modes.

In order to solve the problem of the conventional interleaving schemes, in this chapter, we propose two theoretical criteria for improving and maximizing the time diversity and frequency diversity, respectively, and the optimized interleaver is designed to combat against both TIN and NBI according to the two criteria.

4.3.1 Interleaving with Maximizing Time Diversity

Firstly, for better anti-TIN capability, we propose *Criterion 1* as the criterion for choosing the optimized block size for the block interleaver as time interleaving. Under this criterion, the time diversity of the coded OFDM block transmission system is maximized.

Criterion 1. *The Maximum Independent OFDM Block (MIOB) Criterion*: to increase the number of different independent OFDM blocks for one FEC codeword.

Since the TIN bursts occur in groups and will ruin the data symbols of the OFDM block when they occur, the OFDM blocks should be average distributed in different codewords. If the allocation of OFDM blocks for one specific codeword is not average, e.g. the number of different OFDM blocks for a specific codeword is smaller and the number of data symbols of the TIN deteriorated OFDM block is larger on average, the impairments caused by TIN are more concentrated in this codeword, resulting in higher probability of decoding errors.

Therefore, the number of different OFDM blocks for one FEC codeword, i.e. the parameter of independent OFDM block (IOB) number N_{IOB}, should be increased to improve the anti-TIN capability. With the increase of IOBs mapped to each codeword, the possibility of unsuccessful decoding due to the concentration of TIN bursts is decreased. Moreover, we propose a time-domain merit factor ξ_T as a general indicator of N_{IOB} in one codeword to measure the anti-TIN capability of the interleaving schemes quantitatively as

$$\xi_T = \frac{1}{L_C} \sum_{n=0}^{L_C-1} \frac{N_{IOB}(n)}{\min\left\{\dfrac{I_R \cdot I_C}{N}, L_{sym}\right\}} \tag{4.2}$$

where L_{sym}, L_C and $N_{IOB}(n)$ denote the number of data symbols in each LDPC codeword, the number of LDPC codewords in the interleaver, and the number of IOBs in the nth LDPC codeword, respectively. Hence ξ_T is the average of the ratio of $N_{IOB}(n)$ to its theoretically maximum value $\min\left\{I_R \cdot I_C/N, L_{sym}\right\}$.

To satisfy **Criterion 1**, the design of the block size can be concluded as an optimization problem as

$$opt : \max_{I_R, I_C} \{\xi_T\} \tag{4.3}$$

To optimize (4.3), intuitively we should make sure that each LDPC codeword occupies as many IOBs as possible. After the optimization of the problem given in (4.3), we can obtain the optimized interleaving block size design as given by,

$$I_C = \frac{L_b}{p \cdot \log_2(M)} = L_{sym}/p \tag{4.4}$$

$$I_R = \delta \cdot \mathcal{L}\{N, L_{sym}\}/I_C \tag{4.5}$$

where $\mathcal{L}\{\cdot, \cdot\}$ is the least common multiple operator, and L_b denotes the number of bits in a codeword. The parameter p is optional and is usually set to a small prime number, such as 2, 3, 5, etc. Eq. (4.5) ensures that the proposed interleaver contains integer number of OFDM blocks and integer number of LDPC codes. The total interleaving delay is measured by the number of data symbols in the interleaver given by $I_R \cdot I_C = \delta \cdot \mathcal{L}\{N, L_{sym}\}$, where δ is an integer that can be adjusted according to the acceptable transmission delay.

Using the proposed block size in (4.4) and (4.5), the parameter of N_{IOB} and the anti-TIN capability of the block interleaver will be optimized. Equation (4.4) assures that each LDPC codeword occupies exactly p rows in the interleaver, which makes it possible for each codeword to be mapped to all the OFDM blocks without loss. Meanwhile, from (4.5) it can be deduced that each OFDM block occupies one column or more if $N \geq I_R$, which is equivalent to

$$\mathcal{G}\{L_{sym}, N\} \geq p \tag{4.6}$$

where $\mathcal{G}\{\cdot, \cdot\}$ is the greatest common divisor operator. Recall that we have set p as a small prime number. The reason is that when p is set as a small prime number, the parameter L_{sym} and N specified in G.hn or other OFDM systems are large enough to contain p as a common divisor. In this condition, it is easy to satisfy (4.6).

Hence each LDPC codeword will contain the components from all the OFDM blocks in the interleaver, which is the optimized status in the perspective of TIN mitigation and it is implemented based on ***Criterion 1***. On the contrary, with conventional block size, each LDPC codeword is much likely to occupy less than one row, or each OFDM block is much likely to occupy less than one column. This means N_{IOB} of the LDPC codewords are smaller, leading to poorer performance under TIN.

4.3.2 Interleaving with Maximum Frequency Diversity

Afterwards, ***Criterion 2*** is proposed as the criterion to design the optimized frequency interleaving scheme for better anti-NBI capability, with the constraint of ***Criterion 1*** to ensure the optimal anti-TIN capability. Hence based on both the two criteria, both the time and frequency diversity of the OFDM system can be maximized.

Criterion 2. *The Maximum Independent Sub-Carrier (MISC) Criterion*: to increase the number of different independent OFDM sub-carriers mapped to the data symbols in one FEC codeword.

The reason to set up ***Criterion 2*** is similar to that of ***Criterion 1***. If the allocation of sub-carriers of one codeword is uneven, e.g. the number of different sub-carriers for a specific codeword is smaller and the number of data symbols mapped to the NBI impacted sub-carrier is larger on average, the impairments caused by NBI are

more concentrated in this codeword, leading to the decoding errors even though the average signal-to-noise ratio is high enough to decode other codewords correctly.

Hence the number of different sub-carriers mapped to the data symbols of each codeword, i.e., the parameter of independent sub-carrier (ISC) number N_{ISC}, should be increased in order to distribute the NBI-contaminated sub-carriers in more codewords. Allocation of sub-carriers of the data symbols in one FEC codeword is better scattered and more average when N_{ISC} is larger, which would lead to more robust anti-NBI performance. To quantitatively evaluate the anti-NBI capability of different interleaving schemes and facilitate the frequency interleaving design based on *Criterion 2*, we propose another frequency-domain merit factor ξ_F as a general indicator of N_{ISC} in one codeword, which is given by

$$\xi_F = \frac{1}{L_C} \sum_{n=0}^{L_C-1} \frac{N_{ISC}(n)}{\min\{N, L_{sym}\}} \tag{4.7}$$

where $N_{ISC}(n)$ is the number of ISCs of the nth LDPC codeword. ξ_F can be regarded as the average of the ratio of $N_{ISC}(n)$ to its theoretical maximum value $\min\{N, L_{sym}\}$, which can be achieved under ideally average sub-carrier distribution.
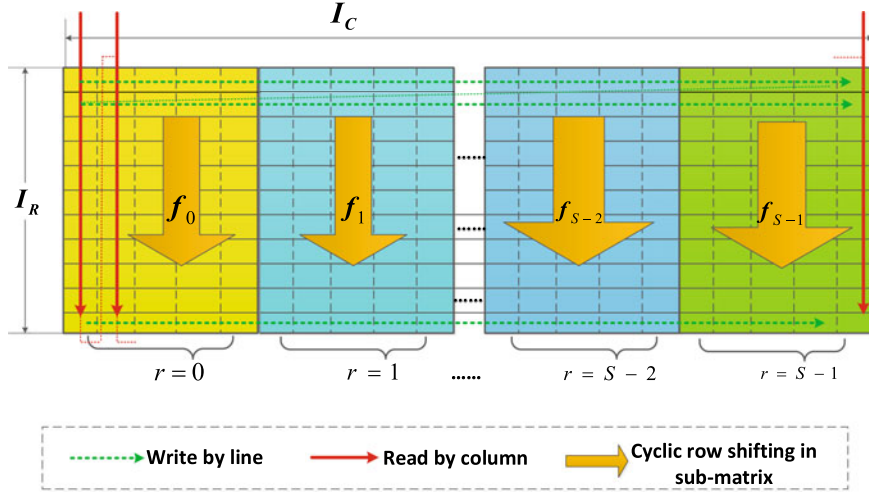
The design of the frequency interleaving scheme to meet *Criterion 2* can be also concluded as an optimization problem described by,

$$opt : \max \left\{ \xi_F \; \middle| \; I_C = \frac{L_{sym}}{p}, \; I_R = \frac{\delta \cdot \mathcal{L}\{N, L_{sym}\}}{I_C} \right\} \tag{4.8}$$

The constraints in (4.8) are set by (4.4) and (4.5) to ensure that the anti-TIN capability derived previously based on *Criterion 1* will not be affected during the optimization process of ξ_F. To solve the problem described in (4.8), from an intuitive perspective of view, we need to make sure that the data symbols of each LDPC codeword are mapped to as many ISCs as possible. Hence, we propose a novel frequency interleaving scheme using block interleaver as shown in Fig. 4.2. Firstly, data symbols are written row-wise into the block interleaver. The interleaving matrix is divided into several sub-matrices by column, each having the same number of columns. The number of sub-matrices S is optional and can be any divisor of I_C. The basic concept of the proposed interleaving scheme is to perform a novel row shifting in sub-matrix operation in the block interleaver. Assuming that $\boldsymbol{C}^{(r)}$ denotes the rth sub-matrix and $\boldsymbol{C} = [\boldsymbol{C}^{(0)}, \boldsymbol{C}^{(1)}, \ldots, \boldsymbol{C}^{(S-1)}]$ represents the whole block matrix, the row shifting in sub-matrix operation is to shift the rows of sub-matrix $\boldsymbol{C}^{(r)}$ ($r = 0, 1, \ldots, S-1$) cyclically down by f_r rows to produce the shifted new sub-matrix $\widetilde{\boldsymbol{C}}^{(r)}$, which is expressed by

$$\widetilde{\boldsymbol{c}}_i^{(r)} = \boldsymbol{c}_j^{(r)}, \; j = (i + I_R - f_r) \bmod I_R, \; 0 \le i, j < I_R \tag{4.9}$$

where $\boldsymbol{c}_j^{(r)}$ and $\widetilde{\boldsymbol{c}}_i^{(r)}$ denote the jth and ith rows of $\boldsymbol{C}^{(r)}$ and $\widetilde{\boldsymbol{C}}^{(r)}$, respectively. The cyclic shifting quantity (i.e. the numbers of rows to be shifted) for each sub-matrix

Fig. 4.2 The proposed combined time frequency interleaving scheme

can be any integer. To simplify the calculation, f_r can be given by

$$f_r = p \cdot r, 0 \leq r < S \tag{4.10}$$

where p is decided by (4.4). After the row shifting in sub-matrix operation, the derived new block matrix $\tilde{C}$ is read column-wise out to form the OFDM blocks that are processed by the sub-carrier mapping later.

Let us compare the anti-NBI capabilities between the conventional block interleaving scheme and the proposed frequency interleaving scheme. For the conventional scheme, we define every $\mathcal{L}\{I_R, N\}$ data symbols in the block interleaver as a "*cyclic unit*", which contains integer number of columns and OFDM blocks. Data symbols of each cyclic unit would be mapped to the sub-carriers with the same pattern repeatedly, since the mapping patterns of all cyclic units are the same. Hence the allocation of sub-carriers to a specific codeword in the other cyclic units is the same as in the first one, which provides no additional contribution to N_{ISC}.

Different from the conventional scheme, in the proposed scheme, since each cyclic unit can be treated as a sub-matrix, each sub-matrix is cyclically shifted down by different number of rows defined by (4.10) before forming OFDM blocks. Thus, the patterns of the sub-carriers mapped to the data symbols in a specific codeword within different sub-matrices are different and not repeated. From these analyses above and (4.10), it is obvious that the proposed scheme can achieve the optimized frequency merit factor ξ_F for (4.8). Therefore, N_{ISC} of a codeword in the proposed scheme is much larger than that in the conventional scheme, leading to a better anti-NBI capability. Since the row shifting in sub-matrix operation has the effect of scattering

the patterns of data symbols mapping to sub-carriers, the operation can be regarded as frequency interleaving. Consequently the proposed scheme is a combined time-frequency interleaving.

According to the two proposed criteria, the optimal time-frequency interleaver is designed with largest time and frequency diversity. This goal is achieved through the two optimization problems aimed at combatting against TIN and NBI, respectively. By utilizing both the time and frequency interleaving, we can significantly improve the anti-NBI and anti-TIN capabilities of broadband coded OFDM systems, such as G.hn system using LDPC coding studied in this work. Experimental simulations are carried out in different channel interference environments with the parameters specified in G.hn power line communications standard based on LDPC code and OFDM modulation to show the performance improvements of the proposed scheme in the next section.

4.4   Performance Analysis of the Algorithms

First of all, we investigate the time and frequency theoretical merit factors of different interleaving schemes to compare the theoretical anti-TIN and anti-NBI performance of different schemes. The computation of the merit factors of the proposed ***Criterion 1***, the proposed ***Criterion 1 & 2***, the conventional block interleaving and random bit interleaving schemes are listed in Table 4.1 with LDPC length $L_b = 8640$ and data sub-carrier number $N = 256$, which is specified in the PLC G.hn system [5]. The column and row numbers of the interleaver are also given in Table 4.1, which shows that the conventional block interleaving and random interleaving schemes have the same interleaving delay with that of the proposed scheme in both 16QAM and 64QAM modulations. The interleaving delay for the proposed scheme and the benchmarks for comparison are fixed to make an effective and fair comparison. It is noticed from the data listed in Table 4.1 that, ξ_T of the proposed ***Criterion 1*** scheme

Table 4.1 Evaluation with theoretical time and merit factors for different schemes

Schemes	QAM order	ξ_T	ξ_F	I_R	I_C	ITLV delay
S1. Criterion 1 & 2	16	1	1	240	432	103680
S2. Criterion 1	16	1	0.3125	240	432	103680
S3. Block ITLV	16	0.5500	0.3125	480	216	103680
S4. Random ITLV	16	0.7134	0.8269	–	–	103680
S1. Criterion 1 & 2	64	1	1	120	288	34560
S2. Criterion 1	64	1	0.6250	120	288	34560
S3. Block ITLV	64	0.5667	0.6250	480	72	34560
S4. Random ITLV	64	0.7268	0.8640	–	–	34560

is much larger than that of the conventional block and random interleaving schemes, and ξ_F of the proposed ***Criterion 1 & 2*** scheme is also significantly larger than those of the conventional block and random interleaving schemes in both QAM modes. It is quantitatively indicated from the data in Table 4.1 that, the anti-TIN and anti-NBI capabilities of the proposed schemes meeting ***Criterion 1*** and ***Criterion 2*** are remarkably better than those of its counterparts. According to the theoretical merit factors ξ_T and ξ_F, both the maximum time and frequency diversities can be achieved using the proposed ***Criterion 1 & 2*** interleaving scheme since both ξ_T and ξ_F reach their maximum theoretical value of one. Due to these analyzes, it is verified that the maximum time-frequency diversity can be achieved using the proposed scheme.

Furthermore, it can be verified the performance is guaranteed or improved under multi-path fading channels. The performance against multi-path fading can be quantitatively measured by the "duo-distance", which is commonly used in literature [12]. The definition of the duo-distance includes the interleaving duo-distance d_1 and the de-interleaving duo-distance d_2. The interleaving duo-distance d_1 of a pair of adjacent data symbols at the input of the interleaver is defined as the distance of these two data symbols at the output of the interleaver. Similarly, the de-interleaving duo-distance d_2 of a pair of adjacent data symbols at the output of the interleaver is defined as the distance of these two data symbols at the input of the interleaver. The duo-distances d_1 and d_2 should be made as large as possible in order to lower the correlation between the interleaver input sequence and the output sequence, and this will disperse the data symbols of one codeword into scattered frequencies and scattered time slots, leading to better performance under time-selective and frequency-selective fading channels.

The duo-distances d_1 and d_2 of the proposed ***Criterion 1 & 2*** interleaving scheme and the conventional block interleaving scheme are given in Table 4.2. It is noted from the results that the average duo-distances $\bar{d}_1$ and $\bar{d}_2$ of the proposed interleaving scheme are both significantly larger than those of the conventional block interleaving scheme, and the minimum duo-distances $d_{1,min}$ and $d_{2,min}$ are the same with those of the conventional scheme, which explicitly indicates that the data symbols of the proposed interleaving scheme are thoroughly dispersed in both the time and frequency dimensions. Hence the performance of the proposed interleaving scheme

Table 4.2 Duo-distances of the proposed and conventional interleaving schemes

I_R	I_C	QAM Order	Proposed ITLV	Block ITLV
240	432	16	$\bar{d}_1 = 477.89$	$\bar{d}_1 = 289.76$
			$d_{1,min} = 240$	$d_{1,min} = 240$
			$\bar{d}_2 = 859.74$	$\bar{d}_2 = 578.31$
			$d_{2,min} = 432$	$d_{2,min} = 432$
120	288	64	$\bar{d}_1 = 238.18$	$\bar{d}_1 = 127.92$
			$d_{1,min} = 120$	$d_{1,min} = 120$
			$\bar{d}_2 = 570.43$	$\bar{d}_2 = 351.66$
			$d_{1,min} = 288$	$d_{1,min} = 288$

can be guaranteed and is even better than the conventional block interleaving under multi-path fading channels.
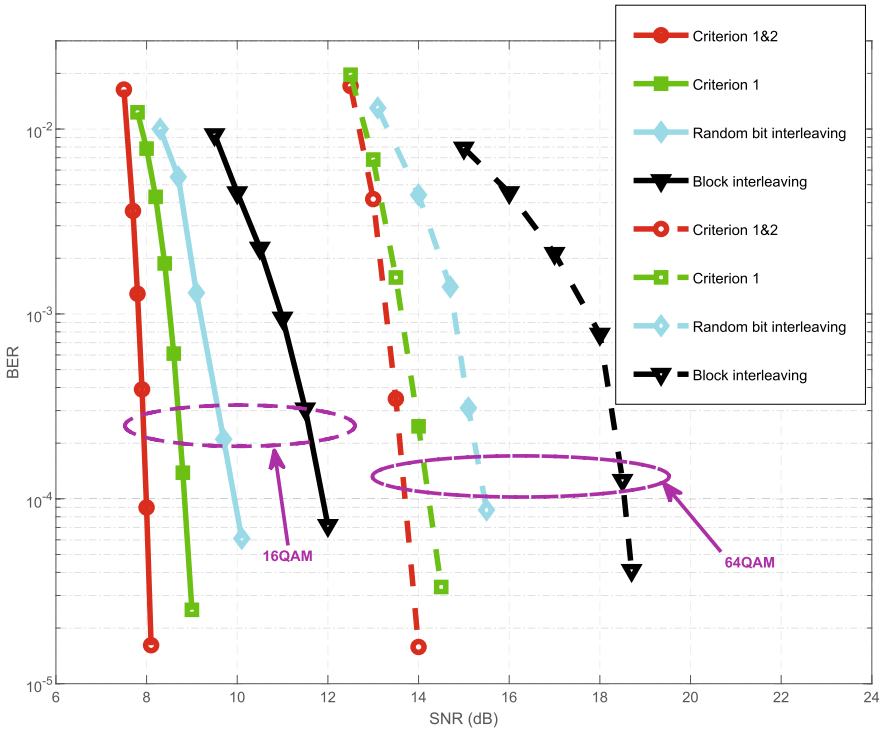
Based on the fact that the merit factors ξ_T and ξ_F are optimized and the large duo-distances d_1 and d_2 are guaranteed at the same time, it can be concluded theoretically that the proposed *Criterion 1 & 2* interleaving scheme is able to achieve the optimal anti-NBI and anti-TIN capabilities and the maximum time-frequency diversity under both AWGN and multi-path fading channels, with guaranteed interleaving performance under frequency-selective channels.

4.5 Simulation Results and Discussions

Simulations of the proposed *Criterion 1*, *Criterion 1 & 2* schemes and the conventional block interleaving and random bit interleaving schemes with the same interleaving delay are performed in the G.hn PLC system as a typical scenario. The LDPC code with code length of $L_b = 8640$ and code rate of 0.5 is adopted. The number of data sub-carriers is $N = 256$ [5]. The relevant simulation parameters are listed in Table 4.3. The signal-to-interference ratio (SIR) is defined as the power ratio between the signal of interest and the narrowband interference. The delay control parameter in Eq. (4.5) is configured as $\delta = 3$, and it is identical for the proposed scheme and the benchmarks to fix the interleaving delay for fair comparison. The AWGN channel and a multi-path PLC channel model [14] with NBI and TIN are adopted to evaluate the effectiveness of the schemes. The detailed parameters of the PLC multi-path channel are given in [14]. Non-ideal channel estimation is used at the receiver in the simulations. The SIR and the sparsity level K of the NBI for different different QAM orders are given in Table 4.3. All the N data sub-carriers are used to transmit data in simulations. As is described in Chap. 2, the occurrence of the impulsive noise has the bursting block-sparse property, and the arrival rate of the

Table 4.3 Simulation Parameters
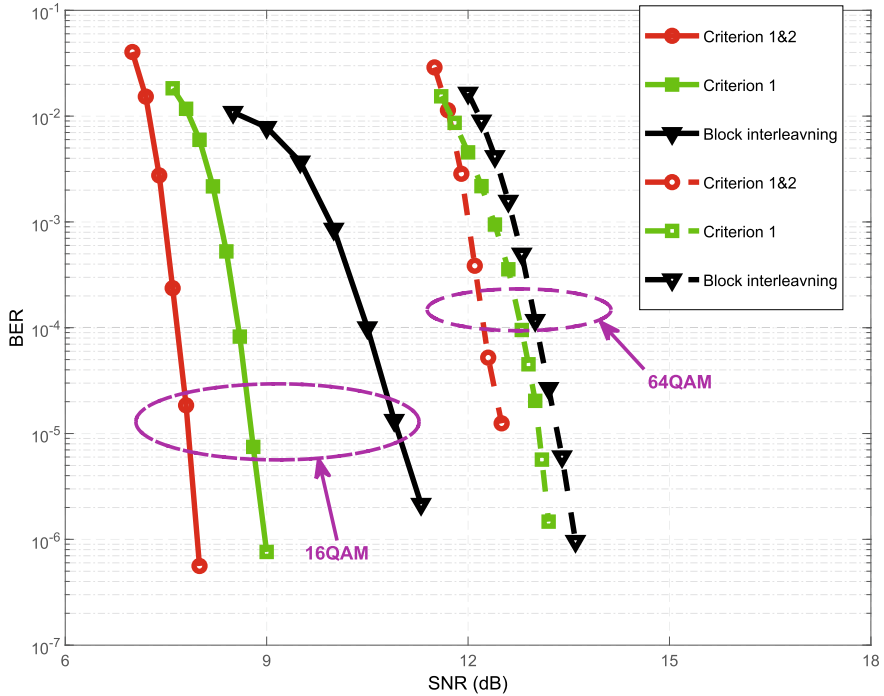
Schemes	I_R	I_C	QAM order	NBI parameters	TIN parameters
Proposed	240	432	16	$K = 5$	$A = 0.15$
Block ITLV	480	216		SIR$= -2.9$ dB	$\Omega = 0.02$
Random ITLV	–	–			
Proposed	120	288	64	$K = 4$	$A = 0.1$
Block ITLV	480	72		SIR$= -2.7$ dB	$\Omega = 0.01$
Random ITLV	–	–			

Fig. 4.3 BER performance of interleaving schemes under AWGN channel with both NBI and TIN

impulsive noise bursts is described by a Poisson point process (PPP) with a medium rate parameter of $\lambda = 50/s$ [11]. The instantaneous amplitude of the impulsive noise is modeled by the Middleton's Class A distribution [7] with the parameters of A and Ω that are also given in Table 4.3.

The simulation results of the BER performance of different interleaving schemes under the AWGN channel with different interferences are depicted in Figs. 4.3, 4.4 and 4.5, respectively. It can be noted from Fig. 4.3 that using the 16QAM and 64QAM modulations under the AWGN channel with both NBI and TIN, the proposed two schemes can achieve more than 2 dB and 1 dB gain compared to those of the conventional block interleaving and random interleaving schemes, respectively. Results in Fig. 4.3 indicate that the proposed two criteria and the optimized interleaver designed according to them have remarkable advantages over the counterparts.

Fig. 4.4 BER performance of interleaving schemes under AWGN channel with only NBI

In Fig. 4.4, it is shown by the simulation results that under the AWGN channel with only NBI, the proposed *Criterion 1 & 2* scheme is the best among the three schemes, with more than 1dB gain in 16QAM modulation and 0.7dB gain in 64QAM modulation. This verifies the effectiveness of *Criterion 2* and the row shifting in sub-matrix operation in improving the anti-NBI capability, since the other two schemes are not designed based on *Criterion 2*. From the previous theoretical analysis and the quantitative analysis in Table 4.1, the merit factor ξ_F of the proposed *Criterion 1 & 2* scheme is the best among all the three schemes, which indicates that it has the best anti-NBI capability, and it is also verified by the simulation results in Fig. 4.4.

The anti-TIN capability is also verified from Fig. 4.5, where it is shown by the simulation results that, both the proposed *Criterion 1* and the proposed *Criterion 1 & 2* schemes achieve more than 1dB gain at the BER of 10^{-5} in 64QAM, and 0.3dB gain in 16QAM compared with that of conventional block interleaving. Since the theoretical time merit factor ξ_T of the conventional block interleaving is the poorest in Table 4.1, it is proved by the simulation results that the anti-TIN capability can be greatly improved by designing the interleaver block size according to *Criterion 1*.

The simulation results of the system BER performance of different interleaving schemes under the PLC multi-path channel are also depicted in Figs. 4.6, 4.7 and 4.8, respectively. Similarly, it is observed from the simulation results in Fig. 4.6 that,
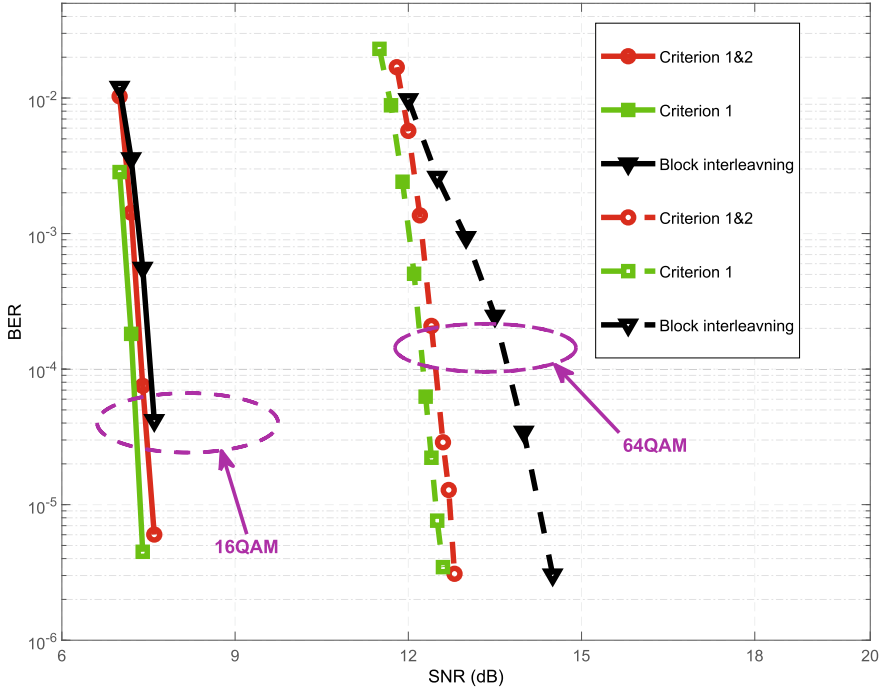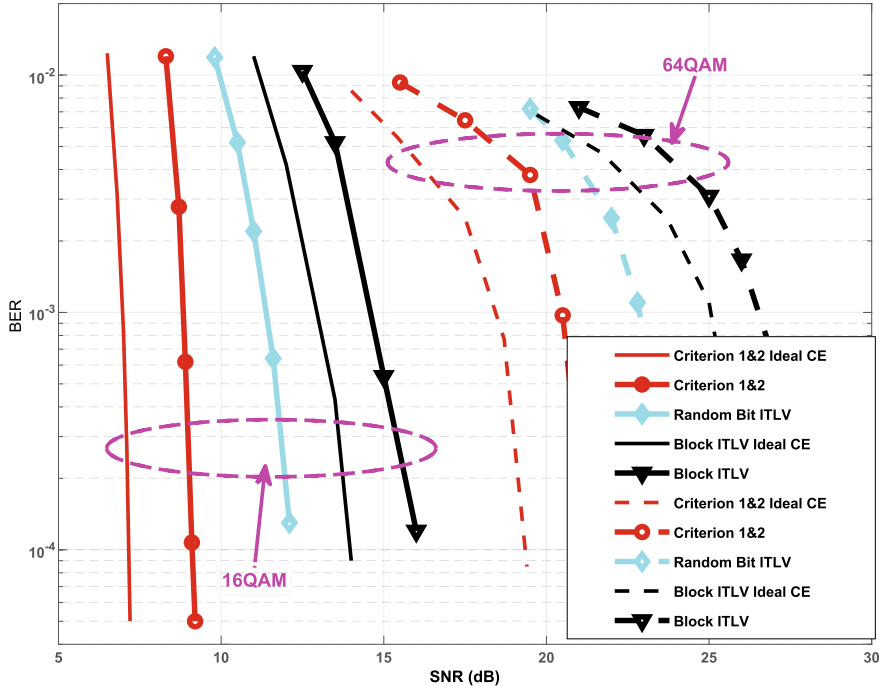
Fig. 4.5 BER performance of interleaving schemes under AWGN channel with only TIN

when considering non-ideal practical channel estimation, the proposed two schemes can achieve more than 4 dB and 2 dB gain over the block interleaving and random interleaving schemes, respectively, at the BER of 10^{-4} under the PLC multi-path fading channel with both NBI and TIN in 16QAM and 64QAM. It can be also noted from the simulation results that if the ideal channel knowledge is available at the receiver, the proposed interleaving scheme has a slightly larger gain over its counterparts compared to the case with non-ideal practical channel estimation at the receiver. However, if non-ideal channel estimation is adopted in practice, the proposed optimization criteria still work well and significantly outperforms its counterparts.

It can also be noted from the simulation results in Fig. 4.7 that, the proposed scheme outperforms the conventional block interleaving scheme by more than 3dB and 4dB, respectively, in 16QAM and 64QAM at the target BER of 10^{-4}, which indicates that the proposed scheme is capable of mitigating NBI impacts effectively under frequency-selective fading channels. The anti-TIN capability can be also verified through Fig. 4.8, where the BER performance of the proposed scheme outperforms the conventional block interleaving scheme by more than 2.4dB and 3.7dB, respectively, in 16QAM and 64QAM at the BER of 10^{-4}.

Fig. 4.6 BER performance of interleaving schemes under PLC channel with both NBI and TIN

The simulation results above are all consistent with the theoretical analysis described previously. The simulation results are also in accordance with the quantitative analysis of the merit factors ξ_T and ξ_F in Table 4.1 and the duo-distances d_1 and d_2 in Table 4.2, which proves not only the validity of the proposed two criteria but also the effectiveness and robustness of the optimal interleaving scheme designed based on them.

4.6   Conclusion

In this chapter, an optimized time-frequency interleaving scheme is proposed, which employs the block size optimization to improve the anti-TIN capability, and a simple row shifting in sub-matrix operation to optimize the performance in the presence of NBI. Two theoretical criteria to maximize the time and frequency diversity are set up to facilitate and guide the optimization process. Through both the quantitative analysis and the simulation results, it is derived that the proposed schemes can achieve better anti-NBI and anti-TIN capabilities compared with the conventional scheme with shorter interleaving delay and less complexity. The proposed scheme is expected
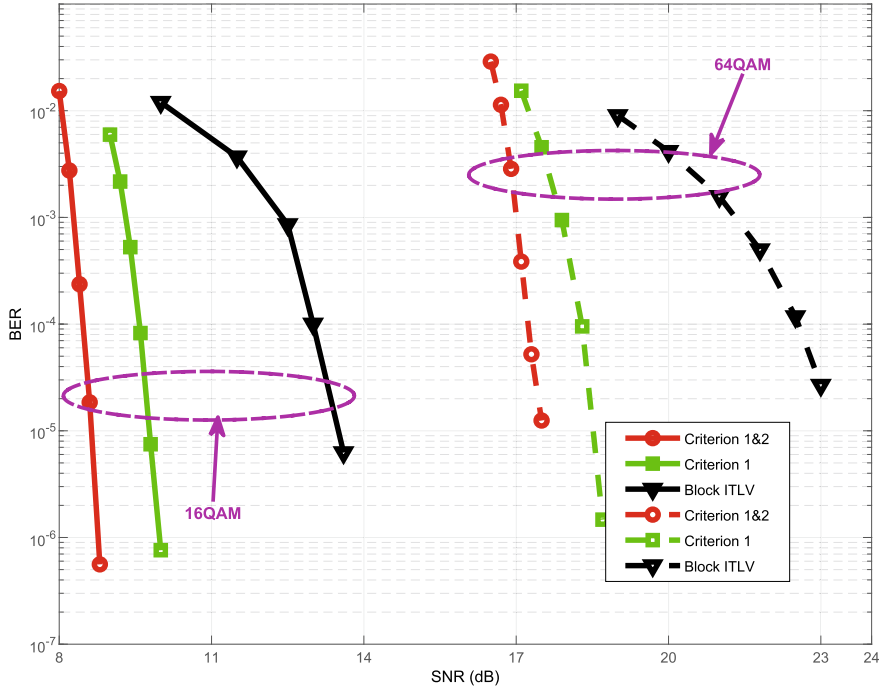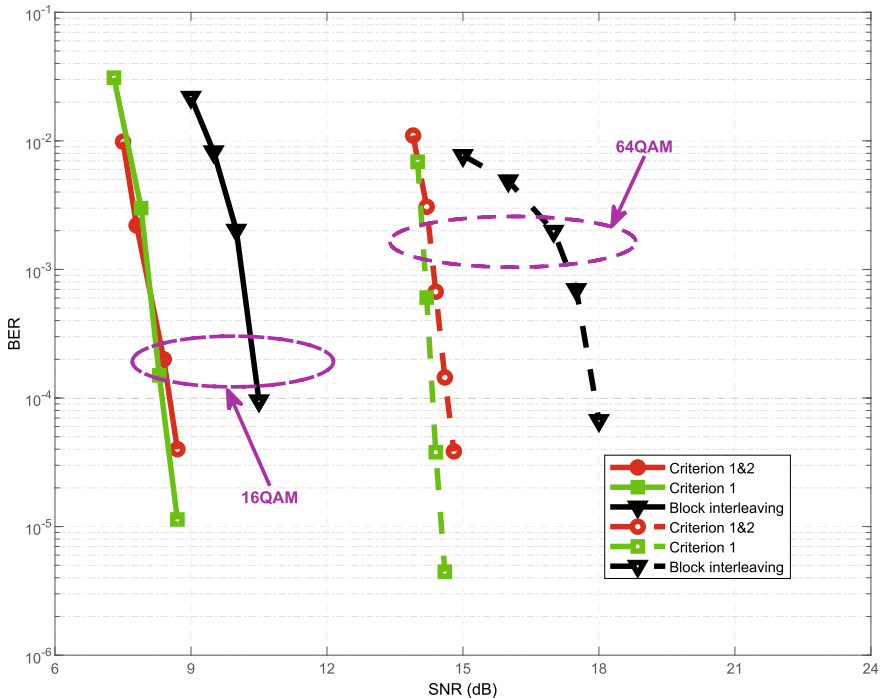
Fig. 4.7 BER performance of interleaving schemes under PLC channel with only NBI

to provide a simple, applicable, efficient and robust interleaving method for coded OFDM-based block transmission systems to combat against NBI and TIN in practice, which is theoretically applicable to other channel environments contaminated by NBI and/or TIN. The research outcomes are published in a journal paper in IEEE Transactions on Power Delivery and in a conference paper in IEEE International Conference on Communications. The proposed optimal time frequency combined interleaving technique has been adopted by the next generation digital terrestrial multimedia broadcasting advanced standards (DTMB-A) [8], and the core technology has been patented. The proposed theory and techniques can provide a technological support of the interleaving technique with anti-NBI and anti-TIN capability for the next generation broadband wireless multimedia transmission systems.

Fig. 4.8 BER performance of interleaving schemes under PLC channel with only TIN

References

1. Al-Dweik A, Hazmi A, Sharif B, Tsimenidis C (2010) Efficient interleaving technique for OFDM system over impulsive noise channels. In: 21st Annual IEEE international symposium on personal, indoor and mobile radio communications, pp 167–171
2. Amirshahi P, Navidpour SM, Kavehrad M (2006) Performance analysis of OFDM broadband communications system over low voltage powerline with impulsive noise. In: 2006 IEEE international conference on communications (ICC'06), vol 1, pp 367–372
3. Andreadou N, Pavlidou F (2010) Modeling the noise on the OFDM power-line communications system. IEEE Trans Power Deliv 25(1):150–157
4. ETSI: Digital video broadcasting (DVB); Frame structure, channel coding and modulation for a second generation digital terrestrial television broadcasting system (DVB-T2). ETSI EN 302 755 v1.3.1 (2011)
5. ITU-T: ITU G.9960, unified high-speed wire-line based home networking transceivers—system architecture and physical layer specification (2010)
6. Marey M, Steendam H (2007) Analysis of the narrowband interference effect on OFDM timing synchronization. IEEE Trans Signal Process 55(9):4558–4566
7. Middleton D (1979) Procedures for determining the parameters of the first-order canonical models of class A and class B electromagnetic interference. IEEE Trans Electromag Compatib EMC-21(3):190–208
8. Pan C, Wang J, Fang H, Song J (2013) Field trial of advanced DTMB system DTMB-A in Hong Kong. In: Proceedings of IEEE international symposium on broadband multimedia systems and broadcasting (BMSB'13), pp 1–4

9. Pan YH, Letaief KB, Cao Z (2004) MIMO/OFDM with adaptive interleaved beamforming and power allocation for high-capacity wireless access. In: 2004 IEEE 59th vehicular technology conference (VTC'04-Spring), pp 1906–1910
10. Ramseier S (2003) Shuffling bits in time and frequency: an optimum interleaver for OFDM. In: IEEE international conference on communications (ICC '03), vol 5, pp 3418–3422
11. Vaseghi SV (2008) Advanced digital signal processing and noise reduction. Wiley
12. Wang D, Kobayashi H (2000) On design of interleavers with practical size for turbo codes. In: 2000 IEEE international conference on communications (ICC'00), pp 618–622
13. Zhidkov SV (2003) Impulsive noise suppression in OFDM-based communication systems. IEEE Trans Consumer Electron 49(4):944–948
14. Zimmermann M, Dostert K (2002) Analysis and modeling of impulsive noise in broad-band powerline communications. IEEE Trans Electromag Compatib 44(1):249–258

Chapter 5
Sparse Recovery Based NBI Cancelation

Abstract As described in Chap. 1, the conventional methods of NBI mitigation in the state-of-the-art research cannot accurately estimate the NBI signal. The "passive" approach of suppressing the NBI makes it difficult to completely eliminate the impacts of the NBI on the system performance. Hence, it is necessary to find the theory and technology capable of accurately reconstructing the NBI. Making use of the naturally sparse property of the NBI signal in the frequency domain, and based on the newly emerged sparse recovery theory, this chapter will investigate and propose the compressed sensing based and structured compressed sensing based method of NBI differential measuring and sparse recovery, the efficient multi-dimensional compressed sensing based recovery algorithm, the sparse Bayesian learning based recovery algorithm, etc, in order to solve the scientific problem that the NBI is difficult to estimate and cannot be completely eliminated. The technical challenge of accurate sparse signal recovery in complicated and severe conditions, such as intensive background noise, insufficient measurement data, large sparsity level, low interference-to-noise ratio, etc, will be overcome. A new theoretical framework of sparse recovery for proactive NBI reconstruction is formulated in this chapter, which provides a new approach and theoretical and technical support for breaking the bottleneck of the system performance using the conventional methods and essentially improving the performance of the broadband communication system.

5.1 Introduction

5.1.1 Problem Description and Related Research

The state-of-the-art research on the conventional methods of NBI mitigation mainly include three basic aspects, i.e. receiver-side frequency domain estimation and mitigation, transmitter-side time domain filtering and receiver-side time domain equalization, and transmitter-side orthogonal coding and mitigation. There has been plenty of research on this problem, which is presented in detail in Chap. 1. The state-of-the-art conventional methods of NBI mitigation have a lot of drawbacks, such as

unstable performance of NBI mitigation, data loss, unrealistic assumptions, unapplicable to practical systems, high complexity, and complicated implementation, etc. The motivation and idea of most of the current methods are to "passively" mitigate or combat against the impact of the NBI, which has a fundamental limit and is unable to effectively and accurately estimate the NBI signal. Neither can the NBI signal be accurately estimated in practical system channel conditions, which makes it impossible to completely eliminate the impact of the NBI and avoid the limitation of the system performance subject to the NBI influence. Therefore, it is in desperate need that we should investigate a series of accurate, stable and efficient NBI mitigation and cancellation methods for practical system applications, and formulate a proactive and accurate theoretical and technical framework of NBI recovery. To eliminate the impact of the NBI on the system is the key to breaking out the bottleneck of the broadband communication system.

In order to overcome the constraint of the conventional methods, the recently emerged sparse signal processing theory, i.e. the compressed sensing theory, can be introduced to the problem of NBI estimation. As described in Chap. 2, it is revealed by the compressed sensing theory that, the high-dimensional unknown sparse vector can be accurately reconstructed from a low-dimensional measurement vector using sparse recovery methods and compressed sensing algorithms in the presence of background noise [1, 2]. The condition in which the compressed sensing theory can be applied is that the unknown high-dimensional vector should be of sparsity, and the measurement matrix should satisfy the uncorrelation, i.e. the restricted isometry property (RIP), and the measurement data amount should satisfy the quantitative condition given by Eq. (2.11). For the problem of NBI estimation, according to the definition of the NBI, the NBI has natural sparsity in the frequency domain, hence it satisfies the sparse requirement of the unknown vector. Therefore, we only need to try to obtain an NBI measurement vector satisfying a certain data amount condition by some means in a certain domain. Then through the mathematical and physical relations we can design a reasonable, efficient and uncorrelated measurement matrix to formulate the theoretical model of the NBI sparse measurement and recovery. In this way, the NBI can be accurately reconstructed by applying theoretically the compressed sensing and sparse recovery theory and technology. Upon this basis, we can further optimize the compressed sensing reconstruction algorithm to achieve a better recovery accuracy and algorithm efficiency.

However, the research of NBI mitigation is still mainly concentrated on conventional methods. The state of the art sparse recovery based NBI estimation methods are insufficient. The only related research mainly includes three aspects, i.e. the null space measuring method, the zero pilot measuring method, and the signal-interference combined sparse method. However, these methods have a series of drawbacks, as explained in detail below:

Null space measuring method: A. Gomma proposed the NBI estimation method based on null space measuring in 2011 for the ZP-OFDM system. Firstly the null space matrix of the known channel matrix is calculated. Then the received signal is multiplied by the null space matrix to eliminate the data signal component in the transmitted signal to obtain the NBI measurement data and formulate the measurement

model. Finally the NBI is estimated by the compressed sensing based algorithm [3, 4]. The drawback is that, this method requires the ideal channel matrix to be known at the receiver, which is difficult in practical systems and unable to be applied. Since the null space matrix with high correlation is inevitably introduced to the observation matrix, the RIP of the observation matrix is poor, so the recovery accuracy of the compressed sensing algorithm is low. In order to obtain the NBI measurement vector, the null space matrix is required to be calculated, so it requires to calculate the pseudo-inverse of a high-dimensional matrix, which costs very high algorithm complexity.

Zero pilot measuring method: This method is to transmit zero pilots in the time domain on purpose, which can become the measurement vector of the NBI at the receiver. S. Alawsh proposed an NBI sparse recovery method in the discrete cosine transform domain for ultra wide band systems in 2013, which makes use of the time domain zero pilots for measuring [5, 6]. A. Ali proposed a Bayesian sparse recovery method for SC-FDMA systems, which makes use of the time domain zero pilots for measuring [7]. These methods exploited the sparsity of the NBI in a certain domain, and regarded the time domain zero pilots (or also known as time domain null pilots) as the sparse measurement data for NBI estimation. The drawback of these methods is that, additional dedicated resources, i.e. the transmitted time domain zero pilots, are required to obtain the measurement data for NBI recovery, which costs a lot of time and frequency domain resources and makes the spectral efficiency and the system throughput degrade seriously. Thus it is not suitable for practical implementation.

Signal-interference combined sparse method: M. Duarte proposed a detection method of the chirp signal in the presence of NBI, which makes use of the sparse representation property of the signal of interest, i.e. the chirp signal, and formulate the sparse recovery model combining the signal of interest and the NBI to conduct combined signal and interference estimation [8]. J. Zhang proposed an echo signal detection method for ultra wide band targets in 2012, which exploited the sparsity of the echo signal of the UWB system target in the waveform matching dictionary, and conducted combined NBI sparse estimation [9]. The drawback is that, this method is only applicable for the communication system whose signal of interest has sparse property in a specific domain and can be jointly sparse represented with the NBI, such as the above mentioned chirp signal system and the UWB target echo system. It is not applicable for other common broadband signals such as the OFDM signal, so the applicable range is too narrow and not adaptive to the major broadband communication systems.

Consequently, the current research of the sparse recovery theory based NBI estimation is quite insufficient and in great need. The related current research has a series of drawbacks, including poor applicability, no theoretical guarantee, high cost of additional resources. Hence, we need to investigate efficient, applicable and well theoretically guaranteed NBI reconstruction techniques based on sparse recovery theory.

5.1.2 Research Aims and Problems

In order to break the limitation of the conventional NBI mitigation methods, such as "passive" mitigation, and overcome the problems of the current sparse recovery methods, such as the low applicability and high resource cost, this chapter studies proactive NBI reconstruction based on compressed sensing, multi-dimensional structured compressed sensing and sparse Bayesian learning theories. We will investigate spectrum-efficient and low-complexity sparse NBI measurement and reconstruction model, and propose accurate NBI reconstruction and cancellation algorithms based on sparse recovery theory. In this way, the bottleneck of the conventional methods can be broken through. The theoretical bound of the NBI estimation accuracy can be approached, and the performance of the broadband OFDM transmission system in the presence of the NBI can be significantly improved. Specifically, the contributions of this chapter are summarized as follows:

- A temporal differential measuring (TDM) method for NBI measurement is proposed, which does not rely on channel estimation. The pseudo-random (PN) sequences between signal frames or the repeated training sequences in the preamble are exploited to conduct the TDM operation with low complexity to obtain the NBI measurement vector. The partial Fourier transform matrix is adopted as the observation matrix to formulate the NBI reconstruction problem model based on compressed sensing. The algorithm of prior aided sparsity adaptive matching pursuit (PA-SAMP) is proposed, which effectively improves the NBI recovery efficiency and accuracy in severe conditions.
- Based on the temporal and spatial correlation of the NBI, the spatial multiple differential measuring (SMDM) method is proposed, which combines the differential measured data in multiple receive antennas, and formulate the NBI reconstruction problem framework in MIMO systems based on time-space domain two-dimensional structured compressed sensing. A structured compressed sensing based efficient greedy algorithm, i.e. structured SAMP (S-SAMP), is proposed to achieve higher recovery efficiency and robustness compared with classical compressed sensing algorithms.
- The block sparse Bayesian learning (BSBL) theory is introduced to the problem of NBI estimation. Aimed at the block sparse NBI signal with frequency offset in the extended case, and exploiting the CP-OFDM frame structure to obtain the differential measurement data of the NBI, the framework of the sparse Bayesian learning based NBI estimation problem is formulated. Based on the block partition estimation, the partition estimated block sparse Bayesian learning (PE-BSBL) algorithm is proposed. By fully utilizing the intra block correlation, the informative BSBL (I-BSBL) algorithm is proposed, which further optimizes the accuracy of Bayesian parametric learning and sparse recovery.

5.2 System Model

(1) *Frequency domain sparse NBI model*
According to the NBI definition given in literature, as described in Chap. 2, to see it quantitatively, the bandwidth occupied by the frequency domain nonzero entries of the NBI is no more than 5% that of the OFDM working bandwidth [10, 11]. Specifically in the OFDM system, the ratio between the number of the nonzero entries in the frequency domain NBI signal $\tilde{\mathbf{e}}_i = \left[\tilde{e}_{i,0}, \tilde{e}_{i,1}, \ldots, \tilde{e}_{i,N-1}\right]^T$ and the OFDM sub-carrier number N is no more than 5%. We continue to apply the notations of NBI models and parameters in Chap. 2, and the sparsity level is $K = |\Omega_i|$ where $K/N \leq 5\%$.

In the theoretical framework of sparse recovery, it is required that the unknown high-dimensional signal should satisfy sparse property. Thus it can be known that, the dimension of the frequency domain NBI signal is N, which belongs to a high-dimensional unknown signal, while the sparsity level is sufficiently small, so it satisfies the "sparse property" condition of the signal required by the compressed sensing and sparse recovery theory. We only need to design a compressed sensing observation matrix with good RIP property, and seek for efficient method to obtain NBI measurement data. Then, the theoretical and technical framework of NBI sparse recovery can be formulated, and the sparse recovery algorithm can be designed to conduct accurate NBI reconstruction.

The NBI model adopted in this chapter is the same as the compound band-limited Gaussian noise (BLGN) interferer model described in Chap. 2 [4, 12, 13], and the definitions of the related parameters are also adopted, such as the sparsity level K, the support Ω_i, and the interference-to-noise ratio γ_{NB}, etc.

(2) *Temporal and spatial correlation of the NBI*
It is shown by the related research literature, communication standards and realistic channel measurement data that, the NBI signal usually has two basic characteristics, i.e. temporal correlation and spatial correlation. The techniques proposed in this chapter will also make full use of the temporal and spatial correlation of the NBI to formulate the framework of NBI measurement and sparse recovery.

Firstly, the temporal correlation of the NBI is that, within the duration of the received adjacent OFDM symbols, the support (the set of the locations of the nonzero entries of the frequency domain NBI) of the NBI signal keeps invariant, and the amplitude of the frequency domain nonzero entries also keeps invariant (i.e. the magnitude of the complex nonzero entries keeps invariant, and phase offset is probable), which is given by

$$\Omega_i = \Omega_{i+1} \tag{5.1}$$

$$|\tilde{e}_{i,k}| = |\tilde{e}_{i+1,k}|, k = 0, 1, \ldots, N-1 \tag{5.2}$$

where Ω_i corresponds to the support of the NBI signal at the i-th frame OFDM symbol. $\tilde{e}_{i,k}$ is the amplitude of sub-carrier k corresponding to the i-th frame frequency

domain NBI signal. For the support of the NBI, as described in Chap. 1, the NBI signal in broadband communication systems usually comes from the services working at a relatively fixed frequency, such as the licensed broadcasting service (analog broadcasting and television broadcasting [14, 15]), narrowband wireless service (such as bluetooth [16]), unreasonable spectrum allocation [17], amateur wireless signal [18], narrowband radiation of electric devices (microwave oven, personal computers, etc) [19, 20], the narrowband internet-of-things (NB-IoT) signal occupying the LTE/LTE-A bands [21, 22], etc. The nonzero entries of these frequency domain NBI are usually located in some fixed frequencies, so it can be reasonably assumed that the NBI signal is located in the same OFDM sub-carriers within the duration of adjacent OFDM symbols in broadband communication systems.

As for the amplitude, it can be shown by standards and field tests that, the *coherence time* of the NBI signal is typically longer than that of the received broadband OFDM symbol, so that the amplitude of the NBI signal can be regarded as invariant over the OFDM symbol. Typically, according to the field tests and experimental observations in real house/apartments, the NBI interferer source signal has a bandwidth of around 50–5000 Hz, resulting in a coherence time of around 200 μs–20 ms [23]. The supportive data are provided in detail [23], where it is reported that in many cases, during the mains cycle of alternating current (20 ms), the NBI signal is stationary and its levels do not change based on the field test [23]. As another example, among the frequencies and bands of radio amateur signals in Italy, most of them have the bandwidth of 200, 500 and 2700 Hz, which implies that the NBI generated by radio amateur ingress will be static over 370 μs–5 ms [24]. Considering about the NBI generated by NB-IoT signals, the typical duration of one NB-IoT symbol is in the range of 90–350 μs (OFDM/SC-FDMA modulated, with sub-carrier spacing of 3.75kHz/15kHz, including the guard interval) according to the specifications of NB-IoT [21, 22].

Compared with the relatively long duration of the coherence time of the NBI, the existing broadband transmission systems specify transmission frames (OFDM symbols) with much shorter duration. For instance, the longest CP-OFDM symbol duration (including the guard interval and the IFFT period) of the WLAN and WAVE system specified in the IEEE 802.11n and IEEE 802.11p standards, is 3.2 μs for the channel spacing of 5 MHz (see Table 18-5 in [25, 26] for detail). For the LTE-A signal, the duration of one OFDM symbol (with sub-carrier spacing of 15kHz, including the cyclic prefix) is less than 72 μs according to the LTE-A standards [27, 28]. Therefore, it is shown that the coherence time of NBI is normally longer than that of the OFDM symbol, which implies that the amplitude of NBI can be considered static over the OFDM symbol.

Secondly, the spatial correlation of the NBI is that, the support of the frequency domain NBI signals at different receive antennas in MIMO systems is assumed to be identical, i.e. the frequency domain NBI signal shares the same sparse pattern, which is represented by

$$\Omega_{i,(1)} = \Omega_{i,(2)} = \cdots = \Omega_{i,(N_r)} = \Omega_i \qquad (5.3)$$
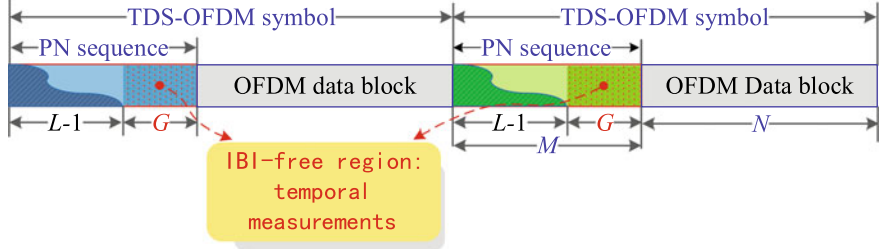
where N_r is the number of MIMO receive antennas, $\Omega_{i,(r)}, r = 1, \ldots N_r$ denotes the support of the frequency domain NBI signal corresponding to the i-th frame OFDM symbol at the r-th receive antenna. Due to the spatial correlation of the NBI, the locations of the nonzero entries of the frequency domain NBI signals at different receive antennas are identical, while the amplitude might be different. The reason why the NBI signal has the property of spatial correlation is that, the distance between different receive antennas in MIMO systems is sufficiently small, such that the frequency points the NBI is located in are closely related with each other. Specifically, the first reason why the support is identical is that, the distance between different receive antennas is much smaller than the distance between the NBI signal and the receive antenna array, which makes the NBI interferers affecting different receive antennas to be the same, i.e. there will not be an NBI interferer that only interferes with part of the receive antennas. Secondly, since the carrier frequency of the signal of interest is usually much higher than the bandwidth of the NBI, i.e. the radio frequency sampling interval of the signal of interest is much smaller than the coherence time of the NBI, so the time difference for the same NBI signal to reach different receive antennas is much smaller than the time needed for the baseband signal of the NBI interferer to change. Hence, as is commonly agreed, different receive antennas will all suffer from the NBI signal from the same source and frequency locations, with the number of the NBI interferers and their frequency locations to be the same. On the other hand, the reason why the amplitude might be different is that, the channel fading and the front end gain of the receive antenna of different receive antennas are usually different, so the amplitude of the received NBI signal might be different although their frequency locations are the same.

5.3 Compressed Sensing Based NBI Reconstruction

In this section, the proposed method of compressed sensing theory based NBI reconstruction will be introduced. Making use of the repeated training sequences in the preamble or the guard interval between frames to conduct temporal differential measuring of the NBI, the compressed sensing measurement model using the partial Fourier transform matrix as the observation matrix will be formulated. The optimized compressed sensing greedy algorithms are proposed to accurately reconstruct the NBI signal.

5.3.1 System Model of Frame Structure

In broadcasting systems and other various communication systems, repeated training sequences are utilized in the preamble or the prefix of each payload frame for constellation demapping, channel estimation, synchronization or as guard interval. For example, in broadcasting systems such as DTMB standard using the TDS-OFDM

Fig. 5.1 Repeated PN training sequences between TDS-OFDM frames in DTMB system

technology in multi-carrier mode as shown in Fig. 5.1, repeated training sequences
are used as guard intervals of OFDM data blocks.

We take TDS-OFDM in DTMB as shown in Fig. 5.1 as a typical example of multi-
carrier systems without loss of generality. The i-th symbol $\mathbf{s}_i = \begin{bmatrix} \mathbf{c}^T & \mathbf{x}_i^T \end{bmatrix}^T$ consists of
the constant training sequence $\mathbf{c} = \begin{bmatrix} c_0, c_1, \ldots, c_{M-1} \end{bmatrix}^T$ of length M and the follow-
ing OFDM data block $\mathbf{x}_i = \begin{bmatrix} x_{i,0}, x_{i,1}, \ldots, x_{i,N-1} \end{bmatrix}^T$ of length N, where the training
sequences for different symbols are identical [29]. Then the transmitted signal passes
through the multi-path fading channel with the CIR of $\mathbf{h}_i = \begin{bmatrix} h_{i,0}, h_{i,1}, \ldots, h_{i,L-1} \end{bmatrix}^T$
of length L in the presence of NBI $\tilde{\mathbf{e}}_i$ and AWGN $\mathbf{z}_i$, and the received time-domain
training sequences $\mathbf{y}_i = \begin{bmatrix} y_{i,0}, y_{i,1}, \ldots, y_{i,M-1} \end{bmatrix}^T$ at the receiver can be denoted by

$$\mathbf{y}_i = \Phi_M \mathbf{h}_i + \mathbf{F}_M \tilde{\mathbf{e}}_i + \mathbf{z}_i, \tag{5.4}$$

where the training sequence component at the receiver is denoted by $\Phi_M \mathbf{h}_i$, with the
matrix $\Phi_M \in \mathbb{C}^{M \times L}$ given by

$$\Phi_M = \begin{bmatrix}
c_0 & x_{i-1,N-1} & x_{i-1,N-2} & \cdots & x_{i-1,N-L+1} \\
c_1 & c_0 & x_{i-1,N-1} & \cdots & x_{i-1,N-L+2} \\
c_2 & c_1 & c_0 & \cdots & x_{i-1,N-L+3} \\
\vdots & \vdots & \vdots & \ddots & \vdots \\
c_{L-2} & c_{L-3} & c_{L-4} & \cdots & x_{i-1,N-1} \\
c_{L-1} & c_{L-2} & c_{L-3} & \cdots & c_0 \\
c_L & c_{L-1} & c_{L-2} & \cdots & c_1 \\
\vdots & \vdots & \vdots & \ddots & \vdots \\
c_{M-1} & c_{M-2} & c_{M-3} & \cdots & c_{M-L}
\end{bmatrix}, \tag{5.5}$$

where the partial inverse Fourier transform matrix $\mathbf{F}_M \in \mathbb{C}^{M \times N}$ is composed of the
first M rows of the complete $N \times N$ inverse Fourier transform matrix $\mathbf{F}_N$ which is
given by

$$\mathbf{F}_M = \frac{1}{\sqrt{N}} [\boldsymbol{\beta}_0 \ \boldsymbol{\beta}_1 \ \cdots \ \boldsymbol{\beta}_{N-1}], \tag{5.6}$$

where the n-th element of $\boldsymbol{\beta}_k$ is $\exp(j2\pi kn/N)$, $n = 0, 1, \ldots, M - 1$. The entries $\{x_{i-1,n}\}_{n=N-L+1}^{N-1}$ in Eq. (5.5) represent the last $L - 1$ samples of the $(i - 1)$-th OFDM data block $\mathbf{x}_{i-1}$, which causes inter-block interference (IBI) on the current i-th training sequence. Since the $(i - 1)$-th OFDM data block $\mathbf{x}_{i-1}$ only causes IBI on the first $L - 1$ samples of the i-th received training sequence $\mathbf{y}_i$, the last $G = M - L + 1$ samples of $\mathbf{y}_i$ will form the IBI-free region $\mathbf{q}_i = \left[y_{i,L-1}, y_{i,L}, \ldots, y_{i,M-1} \right]^T$.

The IBI-free region exists in practical systems because a common rule for system design is to configure the guard interval length M to be larger than the maximum channel delay spread L in the worst case to avoid IBI between OFDM data blocks, so L is usually smaller than M in practice, i.e., $L < M$. For instance, both the DTMB standard [29] based on TDS-OFDM and the DVB-T2 standard [30] based on cyclic prefixed OFDM (CP-OFDM) obey this rule. Moreover, the guard interval length M is much larger than the actual CIR length L in practical scenarios such as urban areas, because M should be configured to work well in the worst case such as in mountain areas where there are long channel delays [31]. Even in the extreme case where $L = M$, the training sequence length can be extended a little to provide the IBI-free region [29].

Hence, the two IBI-free regions at the end of the two adjacent received training sequences can be rewritten as

$$\mathbf{q}_i = \Phi_G \mathbf{h}_i + \mathbf{F}_G \tilde{\mathbf{e}}_i + \mathbf{w}_i, \tag{5.7}$$

$$\mathbf{q}_{i+1} = \Phi_G \mathbf{h}_{i+1} + \mathbf{F}_G \tilde{\mathbf{e}}_{i+1} + \mathbf{w}_{i+1}, \tag{5.8}$$

where $\mathbf{q}_i$ and $\mathbf{q}_{i+1}$ consist of the last G elements of $\mathbf{y}_i$ and $\mathbf{y}_{i+1}$, respectively, while $\mathbf{F}_G$ is the $G \times N$ observation matrix composed of the last G rows of $\mathbf{F}_M$. The AWGN vectors related to the two IBI-free regions are denoted by $\mathbf{w}_i$ and $\mathbf{w}_{i+1}$ with zero mean and the variance of σ^2.

Usually, when the channel is not varying so fast, the CIR for adjacent symbols keeps approximately invariant, i.e. $\mathbf{h}_i \approx \mathbf{h}_{i+1} = \mathbf{h}$, since the distance between the two symbols is sufficiently small so that the duration is within the channel coherence time. The linear convolution between the training sequence and the CIR is denoted by $\Phi_G \mathbf{h}$, in which Φ_G is a $G \times L$ Toeplitz matrix given by
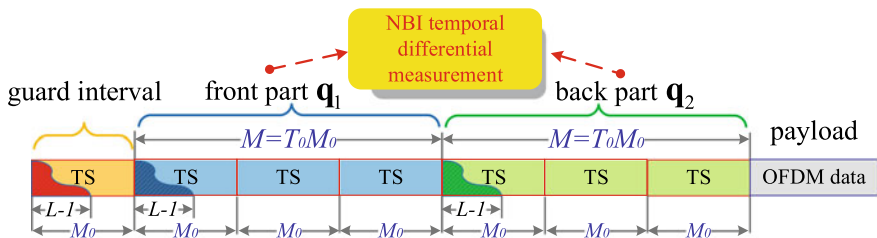
$$\Phi_G = \begin{bmatrix} c_{L-1} & c_{L-2} & c_{L-3} & \cdots & c_0 \\ c_L & c_{L-1} & c_{L-2} & \cdots & c_1 \\ \vdots & \vdots & \vdots & \ddots & \vdots \\ c_{M-1} & c_{M-2} & c_{M-3} & \cdots & c_{M-L} \end{bmatrix}. \tag{5.9}$$

The frequency-domain NBI vectors corresponding to the two IBI-free regions are denoted by $\tilde{\mathbf{e}}_i = \left[\tilde{e}_{i,0}, \tilde{e}_{i,1}, \ldots, \tilde{e}_{i,N-1} \right]^T$ and $\tilde{\mathbf{e}}_{i+1} = [\tilde{e}_{i+1,0}, \tilde{e}_{i+1,1}, \ldots, \tilde{e}_{i+1,N-1}]^T$, respectively. As describe before, the NBI has temporal correlation, i.e. the amplitude of the nonzero entries of the frequency domain NBI signal within the duration of adjacent OFDM symbols keeps invariant. It can be observed that the time-domain

NBI vector at the $(i + 1)$-th training sequence $\mathbf{e}_{i+1}$ equals the time-domain NBI vector at the i-th training sequence $\mathbf{e}_i$ delayed by Δl samples, where $\Delta l = M + N$ is the distance between the two training sequences. Hence, the frequency-domain NBI vector at the $(i + 1)$-th training sequence $\tilde{\mathbf{e}}_{i+1}$ should be $\tilde{\mathbf{e}}_i$ with a phase shift, i.e., $\tilde{e}_{i+1,k} = \tilde{e}_{i,k} \exp(j2\pi k \Delta l / N)$, $k = 0, 1, \ldots N - 1$. This relation of the frequency-domain NBI vectors at adjacent training sequences facilitates the differential measuring of the NBI, which will be explained shortly in the following sections.

Another typical case is applying the repeated training sequences in the preamble, such as the preamble in the power line communications (PLC) systems specified by the ITU-T G.hn standards [32]. In various PLC systems and many other communication systems, repeated training sequences are utilized in the preamble or the prefix of each payload frame for signaling transmission, channel estimation, synchronization or as guard interval. The following payload data is the OFDM data blocks. In the G.hn PLC system as shown in Fig. 5.2, the preamble consists of $T_1 = 2T_0 + 1$ known repeated training sequences, where T_0 is an integer not less than 3. Each training sequence is denoted by $\mathbf{c} = [c_0, c_1, \ldots, c_{M_0-1}]^T$ where $M_0 = N/8$. Therefore, the preamble is represented as $\mathbf{p} = [\mathbf{c}^T \mathbf{c}^T \ldots \mathbf{c}^T]^T$. Apart from the first training sequence, we divide the rest of the preamble into two parts: the 2nd to the $(T_0 + 1)$th training sequences are defined as the "front part" of the transmitted preamble denoted by $\mathbf{p}_1$, and the $(T_0 + 1)$th to the $(2T_0 + 1)$th training sequences are defined as the "end part" of the transmitted preamble denoted by $\mathbf{p}_2$. Thus both the front and the end parts are of length $M = T_0 M_0$. The reason for the definition of the two parts is to facilitate the differential measuring of the NBI signal, which will shortly be explained in the following section.

Then the transmitted signal passes through the multipath PLC channel [33] with the channel impulse response (CIR) of $\mathbf{h} = [h_0, h_1, \ldots, h_{L-1}]^T$ in the presence of NBI, and the time-domain preamble at the receiver contains the received $(2T_0 + 1)$ repeated training sequences. The first received training sequence can be treated as the guard interval to avoid inter-block-interference due to the channel delay spread. The CIR $\mathbf{h}$ for the front part and the end part keeps approximately invariant since the distance M between the two parts is sufficiently small so that no significant changes

Fig. 5.2 The received repeated training sequences in the preamble of the G.hn PLC system utilized for CS-based differential measuring NBI cancellation

for the CIR come about between them. Therefore, the received front part $\mathbf{q}_1$ and end part $\mathbf{q}_2$, are respectively denoted by

$$\mathbf{q}_1 = \Psi\mathbf{h} + \mathbf{F}_M\tilde{\mathbf{e}}_1 + \mathbf{w}_1 \tag{5.10}$$

$$\mathbf{q}_2 = \Psi\mathbf{h} + \mathbf{F}_M\tilde{\mathbf{e}}_2 + \mathbf{w}_2 \tag{5.11}$$

where the frequency-domain NBI vectors at the front part and the end part are denoted by $\tilde{\mathbf{e}}_1 = \left[\tilde{e}_0^1, \tilde{e}_1^1, \ldots, \tilde{e}_{N-1}^1\right]^T$ and $\tilde{\mathbf{e}}_2 = \left[\tilde{e}_0^2, \tilde{e}_1^2, \ldots, \tilde{e}_{N-1}^2\right]^T$, respectively. The partial inverse Fourier transform matrix is defined by Eq. (5.6). Similarly, due to the temporal correlation of the NBI, it can be observed that the time-domain NBI vector of the end part $\mathbf{e}_2$ equals the time-domain NBI vector of the front part $\mathbf{e}_1$ delayed by Δl samples, where $\Delta l = M$ is the distance between the front part and the end part. Hence the frequency-domain NBI vector of the end part $\tilde{\mathbf{e}}_2$ should be $\tilde{\mathbf{e}}_1$ with a phase shift, i.e., $\tilde{e}_k^2 = \tilde{e}_k^1 \exp(j2\pi k \Delta l/N), k = 0, 1, \ldots N - 1$. The additive white Gaussian noise (AWGN) is denoted by the vector $\mathbf{w}_1$ and $\mathbf{w}_2$ with each entry having zero mean and variance of σ_w^2. The linear convolution between the T_0 training sequences of the transmitted front/end part and the CIR is denoted by $\Psi\mathbf{h}$, in which Ψ is a $M \times L$ Toeplitz matrix given by

$$\Psi = \begin{bmatrix} c_0 & c_{M_0-1} & c_{M_0-2} & \cdots & c_{M_0-L+1} \\ c_1 & c_0 & c_{M_0-1} & \cdots & c_{M_0-L+2} \\ \vdots & \vdots & \vdots & \ddots & \vdots \\ c_{M_0-1} & c_{M_0-2} & c_{M_0-3} & \cdots & c_{M_0-L} \\ c_0 & c_{M_0-1} & c_{M_0-2} & \cdots & c_{M_0-L+1} \\ \vdots & \vdots & \vdots & \ddots & \vdots \\ c_{M_0-1} & c_{M_0-2} & c_{M_0-3} & \cdots & c_{M_0-L} \end{bmatrix}_{M \times L}. \tag{5.12}$$

5.3.2 Temporal Differential Measuring

In order to introduce the compressed sensing based methods, according to the compressed sensing based framework of solving the under-determined linear inverse problem described in Sect. 2.4.1 in Chap. 2, we should first of all formulate the compressed sensing problem model given in Eq. (2.10). Formulating the problem model in (2.10) requires two aspects: one is that the measurement vector of the NBI to be reconstructed should be obtained. The other is that the observation matrix satisfying the sparse measurement relationship should be designed. The problem in Eq. (2.10) describes a noiseless case. In practical systems, there is background noise, which is usually modeled by AWGN. Then the corresponding compressed sensing problem model is extended to

$$\mathbf{y} = \Phi\mathbf{x} + \mathbf{w} \tag{5.13}$$

where $\mathbf{y} \in \mathbb{C}^M$ is the measurement vector of the NBI that can be obtained in a certain manner. $\mathbf{x} \in \mathbb{C}^N$ is the unknown high-dimensional vector to be estimated. $\Phi \in \mathbb{C}^{M \times N}$ is a certain kind of known observation matrix or representation matrix. $\mathbf{w}$ is the background AWGN vector, where $M < N$. The compressed sensing theory has proved that, when the three conditions described in Sect. 2.4.1 are satisfied, i.e. when the unknown vector is sparse, the observation matrix satisfies the RIP condition, and the number of measurement data satisfies the requirement in Eq. (2.11), the underdetermined linear inverse problem in Eq. (5.13) can be solved by solving the ℓ_0-*norm minimization* problem with noise and its convex relaxed version. The unknown sparse signal $\mathbf{x}$ can be accurately recovered from the measurement vector $\mathbf{y}$, with the error constrained in the range of the variance $\mathbf{w}$ [1, 2, 34]. Using the notations of the NBI model given in Sect. 2.3.1, when $\mathbf{x}$ in Eq. (5.13) is the unknown high-dimensional NBI signal component $\tilde{\mathbf{e}}_i$, $\mathbf{y}$ is the NBI measurement vector that can be obtained in some manner at the receiver, and Φ is the observation matrix designed correspondingly, the compressed sensing based model of NBI measurement and reconstruction can be formulated and efficiently solved.

How to obtain the above mentioned measurement vector of the NBI and design the corresponding observation matrix to formulate the compressed sensing based model of NBI measurement, is one of the key problems to be solved in this chapter. It is noteworthy that, the NBI measurement vector in Eq. (5.13) can only contain the NBI component and the power constrained background noise component, but cannot contain the component of the training sequence or the signal of interest. This is because the intensity of the training sequence or the signal of interest is relatively high and they will have a severe impact on the accurate measuring of the NBI component, so they should be eliminated first.

Firstly, for the digital terrestrial multimedia broadcasting systems utilizing the TDS-OFDM frame structure, we can make use of the identical PN sequences in the guard interval between the signal frames to conduct the temporal differential measuring (TDM) operation to obtain the time domain differential measurement vector of the NBI for reconstructing the frequency domain high-dimensional unknown NBI vector. The model of the TDS-OFDM frame structure has been given in Sect. 5.3.1, as shown in Fig. 5.1.

It is noted from (5.7) and (5.8) that the training sequence component $\Phi_G \mathbf{h}$ is supposed to be nulled out in order to acquire the measurement vector, which contains the NBI component affected by AWGN only. Unlike the conventional null space method that utilizes the null space to acquire the measurement vector [4], a novel compressed sensing based differential measuring (CSDM) method is proposed to obtain the measurement vector of the NBI. The proposed CSDM method acquires the measurement vector $\Delta \mathbf{q}_i$ simply by subtracting (5.8) from (5.7), i.e. through the differential operation between the IBI-free regions of the adjacent received training sequences, which yields the compressed sensing measurement equation

$$\Delta \mathbf{q}_i = \mathbf{F}_G \Delta \tilde{\mathbf{e}}_i + \Delta \mathbf{w}_i, \tag{5.14}$$

where $\Delta\mathbf{q}_i = \mathbf{q}_i - \mathbf{q}_{i+1}$, $\Delta\mathbf{w}_i = \mathbf{w}_i - \mathbf{w}_{i+1}$ and the NBI differential vector $\Delta\tilde{\mathbf{e}}_i \in \mathbb{C}^N$ is denoted as

$$\Delta\tilde{\mathbf{e}}_i = \tilde{\mathbf{e}}_i - \tilde{\mathbf{e}}_{i+1} = \left[\Delta\tilde{e}_{i,0}, \Delta\tilde{e}_{i,1}, \ldots, \Delta\tilde{e}_{i,N-1}\right]^T, \tag{5.15}$$

where the entries of the NBI differential vector are given by

$$\Delta\tilde{e}_{i,k} = \tilde{e}_{i,k}(1 - \exp(j\frac{2\pi}{N}k \cdot \Delta l)), k = 0, 1, \ldots, N-1. \tag{5.16}$$

In the CS framework, with the measurement vector $\Delta\mathbf{q}_i$, the unknown sparse NBI differential vector $\Delta\tilde{\mathbf{e}}_i$ will be reconstructed after solving (5.14) using the compressed sensing algorithms [2], which will be discussed shortly in the following contents. Due to the time-domain correlation of the NBI, the duration of each symbol is sufficiently small so that the NBI is assumed to be quasi-static within adjacent symbols. Hence, the NBI estimation at the training sequence can be used to obtain the NBI of the subsequent OFDM data block in the same symbol without loss of accuracy, which will also be presented in the following sections.

Solving the under-determined compressed sensing measurement Eq. (5.14) acquired through the proposed CSDM approach is equivalent to solving the convex relaxed optimization problem given by

$$\min_{\Delta\tilde{\mathbf{e}}_i \in \mathbb{C}^N} \|\Delta\tilde{\mathbf{e}}_i\|_1, \text{s.t.} \|\Delta\mathbf{q}_i - \mathbf{F}_G\Delta\tilde{\mathbf{e}}_i\|_2 \leq \varepsilon \tag{5.17}$$

where ε is the bound of the ℓ_2 constraint due to the AWGN $\Delta\mathbf{w}_i$ in (5.14), and ε is set according to the AWGN distribution [34]. The problem (5.17) can be efficiently solved using classical compressed sensing greedy algorithms, such as the subspace pursuit (SP) [35] and SAMP [36]. Since the realistic NBI model is variable and unknown at the receiver, and the algorithms of SP and SAMP that require the information of the sparsity level to be known are no longer applicable, we adopt SAMP which does not require the sparsity level to be known. However, the performance of the classical algorithm of SAMP is constrained in severe conditions and needs improving. This chapter will improve the recovery accuracy and robustness of the classical SAMP algorithm in severe conditions by utilizing the prior information of the support of the NBI estimated from some consecutive received symbols as the auxiliary input information for the algorithm iterations. The proposed improved algorithms will be described in detail in the following contents.

Secondly, for the bursting transmission system utilizing repeated training sequences in the preamble such as the PLC system and WLAN system, the method described above can also be applied. The repeated training sequences in the preamble can be exploited to conduct the temporal differential measuring operation to obtain the measurement vector for compressed sensing based NBI recovery. We take the preamble structure of the PLC system specified by the ITU-T G.hn standards described in Sect. 5.3.1 as shown in Fig. 5.2.

In order to obtain the differential measurement vector of the NBI, it is noted from (5.10) and (5.11) that we should null out the training sequence component $\Psi\mathbf{h}$ in order to acquire the measurement vector including the NBI component affected by only AWGN. Similar to the description in the previous contents, the proposed CSDM method acquires the measurement vector $\varDelta\mathbf{q}$ simply by subtracting (5.11) from (5.10), i.e. through the differential operation between the front part and the end part of the received preamble, which generates the CS measurement equation

$$\varDelta\mathbf{q} = \mathbf{F}_M \varDelta\tilde{\mathbf{e}} + \varDelta\mathbf{w} \tag{5.18}$$

where $\varDelta\mathbf{q} = \mathbf{q}_1 - \mathbf{q}_2$, $\varDelta\mathbf{w} = \mathbf{w}_1 - \mathbf{w}_2$ and the NBI differential vector $\varDelta\tilde{\mathbf{e}} \in \mathbb{C}^N$ is denoted by

$$\varDelta\tilde{\mathbf{e}} = \tilde{\mathbf{e}}_1 - \tilde{\mathbf{e}}_2 = \left[\varDelta\tilde{e}_0, \varDelta\tilde{e}_1, \ldots, \varDelta\tilde{e}_{N-1}\right]^T \tag{5.19}$$

where the entries of the NBI differential vector are given by

$$\varDelta\tilde{e}_k = \tilde{e}_k^1 (1 - e^{\frac{j2\pi k \varDelta l}{N}}), k = 0, 1, \ldots, N-1. \tag{5.20}$$

With the measurement vector, the unknown NBI differential vector $\varDelta\tilde{\mathbf{e}}$ can be reconstructed after solving the CS Eq. (5.18). Due to the burst transmission in the PLC system, the duration of each transmission frame is sufficiently small so that the frequency and the amplitude of the NBI signal is assumed to be quasi-static during the current frame. Hence the NBI estimate at the preamble can be used to obtain the NBI signals at the subsequent OFDM data blocks without significant loss of accuracy.

Similarly, solving the under-determined compressed sensing measurement Eq. (5.18) acquired through the proposed CSDM approach is equivalent to solving the convex relaxed optimization problem given by

$$\min_{\varDelta\tilde{\mathbf{e}}\in\mathbb{C}^N} \|\varDelta\tilde{\mathbf{e}}\|_1, \text{s.t.} \|\varDelta\mathbf{q} - \mathbf{F}_M \varDelta\tilde{\mathbf{e}}\|_2 \leq \varepsilon \tag{5.21}$$

where ε is the bound of the ℓ_2 constraint due to the AWGN $\varDelta\mathbf{w}$, which is set according to the AWGN distribution. The problem (5.21) can also be efficiently solved by using classical compressed sensing greedy algorithms, such as the SP and SAMP algorithms. Since the realistic NBI model is variable and unknown at the receiver, we still adopt SAMP which does not require the sparsity level to be known.

5.3.3   Compressed Sensing Based Reconstruction Algorithm

As described in the previous section, the compressed sensing problems (5.17) and (5.21) can be efficiently solved using the greedy algorithms. The performance of NBI reconstruction relies on the accurate result of the compressed sensing algorithm. If

we can obtain the partial information of the support of the NBI in advance as the prior information, the iteration process of the compressed sensing based greedy algorithm can be facilitated and the performance of the classical compressed sensing based algorithms in severe conditions can be effectively improved.

Now we take the DTMB system as an example to introduce the method of acquiring the partial information of the support utilized in this work. According to the temporal correlation of the NBI, the NBI supports corresponding to D consecutive symbols share the same sparse pattern. Hence, the priori information of the partial NBI support Γ_0 at the i-th symbol can be jointly acquired through the superposition of the following D differential measured NBI vectors, which is given by

$$\Gamma_0 = \{k \left| \sum_{j=i}^{i+D-1} \left| \Delta \tilde{q}_{j,k} \right|^2 > \eta_{th} \, , k = 0, \ldots N-1 \}, \right. \tag{5.22}$$

where $\Delta \tilde{\mathbf{q}}_i = \left[\Delta \tilde{q}_{i,0}, \Delta \tilde{q}_{i,1}, \ldots, \Delta \tilde{q}_{i,N-1} \right]$ is the N-point DFT of $\Delta \mathbf{q}_i$, and the power threshold η_{th} used to determine the partial support of the NBI is given by

$$\eta_{th} = \frac{\alpha}{N} \sum_{k=0}^{N-1} \sum_{j=i}^{i+D-1} \left| \Delta \tilde{q}_{j,k} \right|^2, \tag{5.23}$$

where α is a coefficient that can be configured proportional to the INR in different scenarios.

The partial NBI support priori can be correctly obtained through (5.22), since the superposition of the NBI vectors of the consecutive symbols will increase the equivalent INR of the NBI significantly. The reason is that the powers of the NBI components at each nonzero entry are linearly accumulated and strengthened due to the joint time-domain correlation of the NBI support, while the superposition of the power of the background AWGN follows chi-square distribution, which results in significant increment of the power of NBI components compared with that of AWGN. Furthermore, through the joint acquisition of D consecutive NBI signals in the frequency domain, the spectral leakage due to the DFT operation of the differential measured signal $\Delta \mathbf{q}_i$ will be relieved, which improves the definition of the NBI components in the power spectrum.

With the aid of the partial NBI support priori, the prior aided SAMP (PA-SAMP) algorithm is proposed. The pseudo-code of the proposed PA-SAMP algorithm is summarized in Algorithm 1. The inputs of Algorithm 1 is the priori partial support Γ_0, the initial sparsity level $K_0 = |\Gamma_0|$, the measurement vector $\Delta \mathbf{q}_i$, the observation matrix $\mathbf{\Psi} = \mathbf{F}_G$, and the iteration step size δs that could be adjusted according to NBI strength and occurrence probability. During the iterations that may be composed of multiple *iteration stages*, the testing sparsity level for the current stage is T, which is increased by the step size δs with the switching of the stages. The output of Algorithm 1 is the final output support Γ_f and the recovered NBI differential vector $\Delta \hat{\mathbf{e}}_i$ s.t. $\Delta \hat{\mathbf{e}}_i |_{\Gamma_f} = \mathbf{\Psi}_{\Gamma_f}^{\dagger} \Delta \mathbf{q}_i$, $\Delta \hat{\mathbf{e}}_i |_{\Gamma_f^c} = \mathbf{0}$.

From Algorithm 1, one is able to observe that the prior information of partial NBI support is utilized at the beginning of the algorithm to reduce the complexity of the total compressed sensing iterations compared with that without the aid of the prior information. During the iteration process, the prior information is also made good use of to improve the accuracy of the temporary support estimation in each iteration, and to reduce the computational complexity. Due to the introduction of prior partial support, the proposed PA-SAMP algorithm outperforms classical compressed sensing algorithms and ensures robust and accurate NBI recovery, especially in severe conditions whereby the INR is too low or the IBI-free region is too short due to long channel delay.

As shown in Algorithm 1, PA-SAMP differs from SAMP mainly in the following three aspects:

- Complexity: With the aid of the prior partial support, the initialization of PA-SAMP is optimized to reduce computational complexity compared with SAMP. The initial support is set as Γ_0 in PA-SAMP instead of an empty set $\emptyset$ used in SAMP, while the initial NBI differential vector is approximated as $\Delta\hat{\mathbf{e}}_i^0\big|_{\Gamma_0} \leftarrow \mathbf{\Psi}_{\Gamma_0}^{\dagger}\Delta\mathbf{q}_i$ instead of a zero vector adopted in SAMP, and the initial residue vector $\mathbf{r}_0 \leftarrow \Delta\mathbf{q}_i - \mathbf{\Psi}\Delta\hat{\mathbf{e}}_i^0$ is utilized in PA-SAMP to replace its counterpart $\mathbf{r}_0 \leftarrow \mathbf{0}$ in SAMP. The testing sparsity level T is initialized as $T \leftarrow \delta s + K_0$ in PA-SAMP instead of $T \leftarrow \delta s$ in SAMP. With K_0 nonzero entries acquired from prior information, actually there are only $K - K_0$ remaining nonzero entries to be recovered. Hence, the average number of total iterations is reduced from K in SAMP to $K - K_0$ in PA-SAMP, which reduces computational and time complexity.
- Accuracy: The priori aided initialization in PA-SAMP is more accurate than the trivial initialization in SAMP. In each iteration of PA-SAMP, only $(T - K_0)$ new entries are necessarily identified in the preliminary test and merged with the previous temporary final list, while the K_0 initial entries acquired from prior information are remained in the candidate list in the first iteration. This makes the iterations of PA-SAMP more efficient than those of SAMP, whereby all the T entries are identified in each iteration. Moreover, during the stage switching, the testing sparsity level is changed to $T \leftarrow K_0 + j \times \delta s$ instead of $T \leftarrow j \times \delta s$ in SAMP. This makes it possible to adopt smaller step size δs in PA-SAMP, which leads to more accurate estimation of the actual sparsity level K than that in SAMP. Meanwhile, the convergence rate of the iterations is also improved since the testing sparsity level starts much closer to the actual one.
- Adaptivity: Since in different channel conditions the prior inputs of PA-SAMP vary accordingly, and the contributions of the prior information will significantly facilitate the accurate NBI recovery especially when the sparsity level becomes large, the proposed algorithm of PA-SAMP is very adaptive to the variant sparsity level K. It is also robust to the variation of INR, the length of the IBI-free region G, and the number of consecutive symbols D for prior information acquisition, etc.

Algorithm 1 Prior Aided Sparsity Adaptive Matching Pursuit (PA-SAMP) for NBI Recovery

---

Input:
    1) measurement vector $\Delta \mathbf{q}_i$
    2) observation matrix $\mathbf{\Psi} = \mathbf{F}_G$
    3) prior partial support Γ_0 initial sparsity level $K_0 = |\Gamma_0|$
    4) iteration step δs
    Initialization:
1: $\Delta \hat{\mathbf{e}}_i^0 \big|_{\Gamma_0} \leftarrow \mathbf{\Psi}_{\Gamma_0}^{\dagger} \Delta \mathbf{q}_i, \mathbf{r}_0 \leftarrow \Delta \mathbf{q}_i - \mathbf{\Psi} \Delta \hat{\mathbf{e}}_i^0,$
2: $T \leftarrow \delta s + K_0, k \leftarrow 1, j \leftarrow 1$
    Iterations:
3: **repeat**
4:    $S_k \leftarrow \max(\mathbf{\Psi}^H \mathbf{r}_{k-1}, T - K_0)$ {preliminary test}
5:    $C_k \leftarrow \Gamma_{k-1} \cup S_k$ {candidate list generation}
6:    $\Gamma_t \leftarrow \max(\mathbf{\Psi}_{C_k}^{\dagger} \Delta \mathbf{q}_i, T)$ {temporary final list}
7:    $\Delta \hat{\mathbf{e}}_i^k \big|_{\Gamma_t} \leftarrow \mathbf{\Psi}_{\Gamma_t}^{\dagger} \Delta \mathbf{q}_i, \Delta \hat{\mathbf{e}}_i^k \big|_{\Gamma_t^c} \leftarrow \mathbf{0}$
8:    $\mathbf{r} \leftarrow \Delta \mathbf{q}_i - \mathbf{\Psi}_{\Gamma_t} \mathbf{\Psi}_{\Gamma_t}^{\dagger} \Delta \mathbf{q}_i$ {residue calculation}
9:    **if** $\|\mathbf{r}\|_2 \geq \|\mathbf{r}_{k-1}\|_2$ **then**
10:      $j \leftarrow j + 1, T \leftarrow K_0 + j \times \delta s$ {stage switching}
11:   **else**
12:      $\Gamma_k \leftarrow \Gamma_t, \mathbf{r}_k \leftarrow \mathbf{r}$
13:      $k \leftarrow k + 1$ {same stage, next iteration}
14:   **end if**
15: **until** $\|\mathbf{r}\|_2 < \varepsilon$
Output:
    1) final output support Γ_f
    2) recovered NBI differential vector $\Delta \hat{\mathbf{e}}_i$ s.t. $\Delta \hat{\mathbf{e}}_i \big|_{\Gamma_f} = \mathbf{\Psi}_{\Gamma_f}^{\dagger} \Delta \mathbf{q}_i, \Delta \hat{\mathbf{e}}_i \big|_{\Gamma_f^c} = \mathbf{0}$

    In common cases, as described above, the prior partial NBI support is accurately acquired based on the time-domain support correlation of D consecutive symbols. Accurate prior partial support facilitates the CSDM process with PA-SAMP and improves the NBI recovery performance. On the other hand, even in the extreme case where the NBI support changes so fast that the partial support acquired from several consecutive symbols is not accurate enough, NBI reconstruction can be also implemented from only one measurement vector based on the proposed CSDM method using conventional SAMP algorithm without the aid of the prior information. In this chapter, the NBI reconstruction method based on SAMP without prior information is also given as a complementary approach, which will be compared with the PA-SAMP approach in the following simulations.

    After reconstructing the NBI signal using the PA-SAMP algorithm, the estimation accuracy can be further refined, and the elements estimated in error can be excluded. Since the sparsity level is variable and unknown, the final output support Γ_f of PA-SAMP described in Algorithm 1 might include some false positions whose amplitude is significantly lower than the NBI, which should be refined to achieve better performance. The threshold-based support adjustment method is proposed in

order to further improve the support estimation accuracy of PA-SAMP. The refined support Γ_{th} includes the entries whose norms are larger than the given threshold

$$\lambda_{th} = \beta \log\left(\frac{\hat{P}_e}{\sigma^2}\right) \cdot \hat{P}_e, \tag{5.24}$$

where $\hat{P}_e = (1/N) \sum_{k=0}^{N-1} \left|\Delta \hat{e}_{i,k}\right|^2$ is the estimated NBI average power with $\Delta \hat{e}_{i,k}$ being the k-th entry of $\Delta \hat{\mathbf{e}}_i$. $(\hat{P}_e/\sigma^2)$ is the estimated INR, and β is a coefficient which can be set properly according to different scenarios. The entries whose norms are larger than the threshold are much more likely to be the true NBI entries and should thus be retained. Therefore, the refined support is given by

$$\Gamma_{th} = \left\{ k \;\middle|\; \left|\Delta \hat{e}_{i,k}\right|^2 > \lambda_{th} \,, k = 0, 1, \ldots, N-1 \right\}. \tag{5.25}$$

Afterwards, the recovered NBI differential vector $\Delta \hat{\mathbf{e}}_i$ of PA-SAMP can be then updated at the refined support Γ_{th} such that $\Delta \hat{\mathbf{e}}_i \big|_{\Gamma_{th}} = \boldsymbol{\Psi}_{\Gamma_{th}}^{\dagger} \Delta \mathbf{q}_i$ and $\Delta \hat{\mathbf{e}}_i \big|_{\Gamma_{th}^c} = \mathbf{0}$.

Furthermore, the NBI values at the refined support can be more accurate through least squares (LS) estimation, which is implemented by solving

$$\min_{\Delta \hat{\mathbf{e}}_i \in \mathbb{C}^N} \left\| \Delta \mathbf{q}_i - \Pi \Delta \hat{\mathbf{e}}_i \right\|_2, \tag{5.26}$$

where $\Pi = \mathbf{F}_G \mathbf{B}$, and $\mathbf{B}$ is the $N \times N$ diagonal selection matrix whose elements $b_{k,k} = 1$ for $k \in \Gamma_{th}$ and zero otherwise. After solving the LS problem, the recovered NBI differential vector is given by

$$\Delta \hat{\mathbf{e}}_i = \mathbf{B} \Pi^{\dagger} \Delta \mathbf{q}_i. \tag{5.27}$$

The final step is to conduct the actual NBI signal cancellation at the location of the OFDM data block. As shown in Fig. 5.1, in TDS-OFDM systems, the original frequency-domain NBI vector $\tilde{\mathbf{e}}_i$ at the i-th PN training sequence can be reconstructed from the recovered NBI differential vector $\Delta \hat{\mathbf{e}}_i$ according to (5.16) by

$$\tilde{e}_{i,k} = \Delta \hat{e}_{i,k} / (1 - \exp(j \frac{2\pi k \Delta l}{N})), k = 0, 1, \ldots, N-1. \tag{5.28}$$

Then, the frequency-domain NBI vector corresponding to the i-th OFDM data block $\tilde{\mathbf{e}}_i^D = \left[\tilde{e}_{i,0}^D, \tilde{e}_{i,1}^D, \ldots, \tilde{e}_{i,N-1}^D\right]^T$ is similarly obtained by

$$\tilde{e}_{i,k}^D = \tilde{e}_{i,k} \cdot \exp(j 2\pi k \Delta d / N), k = 0, 1, \ldots, N-1, \tag{5.29}$$

where $\Delta d = M$ is the distance between the i-th PN training sequence and the i-th OFDM data block. Then the NBI can be eliminated from the received OFDM data block for the successive process.

The compressed sensing problem model (5.18) and (5.21) formulated by differential measurement of the preamble in the PLC system as shown in Fig. 5.2 can also be solved using the compressed sensing recovery algorithm PA-SAMP based on the differential measurement of the PN sequences similar to the DTMB system described above. By utilizing the multiple repeated training sequences in the preamble of the PLC system, the prior information of the NBI partial support can be obtained by the method similar to Eq. (5.22). With the aid of the prior information and based on the input of the measurement vector and the observation matrix, the NBI differential vector $\Delta\hat{\mathbf{e}}$ corresponding to the preamble in Eq. (5.18) can be accurately recovered using the PA-SAMP algorithm. Similarly, the recovered NBI differential vector can be further refined by the threshold detection based adjusting method and the LS method.

Afterwards, the original frequency-domain NBI vector $\tilde{\mathbf{e}}_1$ at the front part of the preamble as shown in Fig. 5.2 can be recovered according to (5.20) by

$$\tilde{e}_k^1 = \Delta\hat{e}_k / (1 - e^{j\frac{2\pi}{N}k\cdot\Delta l}), k = 0, 1, \ldots, N - 1. \tag{5.30}$$

Finally, the frequency-domain NBI vector corresponding to the OFDM data block $\tilde{\mathbf{e}}_i^D = \left[\tilde{e}_{i,0}^D, \tilde{e}_{i,1}^D, \ldots, \tilde{e}_{i,N-1}^D\right]^T$ of the payload is similarly obtained by

$$\tilde{e}_{i,k}^D = \tilde{e}_k^1 \cdot \exp(j2\pi k \Delta d_i/N), k = 0, 1, \ldots, N - 1, \tag{5.31}$$

where Δd_i is the distance between the i-th OFDM block and the front part of the preamble. Then the NBI signal can be eliminated from the received OFDM data block for better performance of the successive process.

5.3.4   Simulation Results and Discussions

In this section, the simulation results and discussions of the proposed compressed sensing based NBI recovery algorithms in the DTMB and PLC systems are reported. The major metrics for simulations include the process of NBI recovery, the mean square error (MSE) of the NBI estimation, the recovery probability of the NBI reconstruction, and the system bit error rate (BER) of different schemes, etc. According to the DTMB and ITU-T G.hn standards, the simulation parameters of the digital terrestrial multimedia broadcasting system and the broadband power line communication system are listed in Table 5.1 [29, 32, 37]. The channel parameters of the ITU-R Vehicular-B multipath channel are listed in Table 5.2 [38], and the channel parameters of the multipath PLC channel are listed in Table 3.2 [33]. The model of the NBI signal is consistent with that presented in Sect. 2.3.1, i.e. the compound BLGN interferer source model. In the DTMB system, the number of TDS-OFDM symbols utilized to acquire the prior information of the partial support is $D = 4$. In the PLC system, the number of the repeated training sequences included in the front part and latter part of the preamble is $T_0 = 3$.

Table 5.1 Simulation parameters of compressed sensing based NBI recovery

	OFDM sub-carrier number	Training sequence length	Constellation mapping	LDPC code length	Code rate	Channel
DTMB sytem [29]	$N = 3780$	$M = 595$	64QAM	7488	0.6	Vehicular-B channel [38]
PLC system [32]	$N = 1024$	$M_0 = 128$	64QAM	8640	0.5	PLC channel [33]
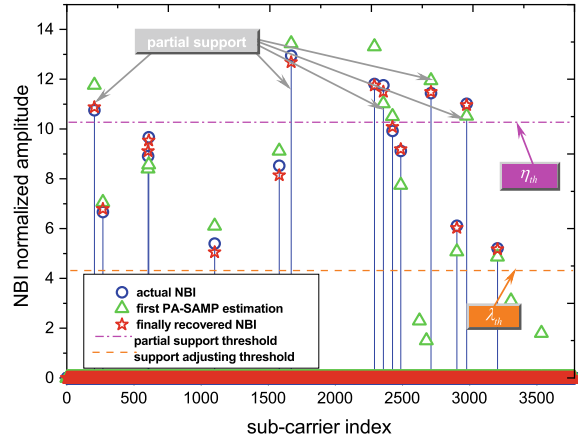
Table 5.2 ITU-R Vehicular-B multipath channel parameters [38]

Multipath index	Relative delay (ns)	Average power (dB)
1	0	−2.5
2	300	0
3	8 900	−12.8
4	12 900	−10.0
5	17 100	−25.2
6	20 000	−16.0
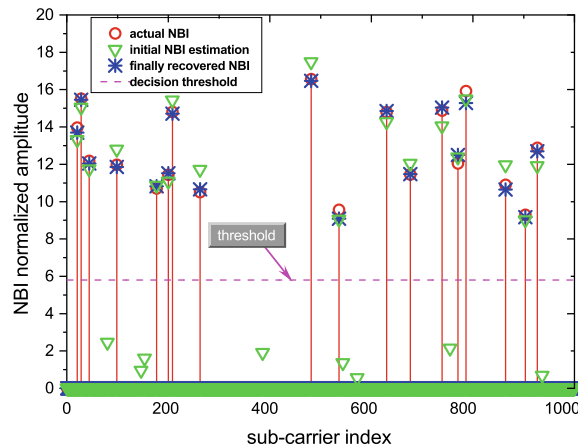
The simulation results of the overall process of the compressed sensing based NBI reconstruction in the DTMB system and PLC system are shown in Figs. 5.3 and 5.4, respectively. The parameters are configured as follows. The INR of the NBI is 30 dB. The sparsity level of the DTMB system is $K = 15$. The sparsity level of the PLC system is $K = 18$. During the process of recovery, firstly, the partial support is obtained based on the threshold η_{th} given by Eq. (5.23), where $\alpha = 8.0$ is adopted as the parameter. Then, the compressed sensing based NBI recovery model is formulated using the proposed temporal differential measuring method, and the NBI signal is recovered using the PA-SAMP algorithm. The obtained support is further refined by the threshold λ_{th} given by the Eq. (5.24), where $\beta = 3.0$ is adopted as the parameter. Consequently, the final recovered realistic NBI can be obtained. The simulation results have shown that, the finally estimated NBI is accurately matching the realistic NBI signal.

The MSE performance of the compressed sensing based NBI recovery algorithm in DTMB system and PLC system is reported in Figs. 5.5 and 5.6, respectively. The sparsity level in DTMB system is configured as $K = 10$ or $K = 20$, while the sparsity level in the PLC system is set as $K = 18, 24, 36$. The MSE performance of the PA-SAMP algorithm in the framework of the proposed temporal differential measuring and the classical SAMP algorithm in the DTMB system is compared, and the results are reported in Fig. 5.5. The Cramér-Rao lower bound (CRLB) of the estimation is $2\sigma_w^2 \cdot (K/G)$ [39], which is also depicted as a benchmark for comparison. The theoretical derivation of the CRLB is given in detail in the performance evaluation in Sect. 5.6. It is revealed by the simulation results in Fig. 5.5 that, the proposed PA-SAMP algorithm reaches the target MSE of 10^{-3} at INR = 26.8 and 33.7 dB with the

Fig. 5.3 Compressed
sensing based temporal
differential measuring and
PA-SAMP algorithm enabled
NBI recovery in DTMB
system
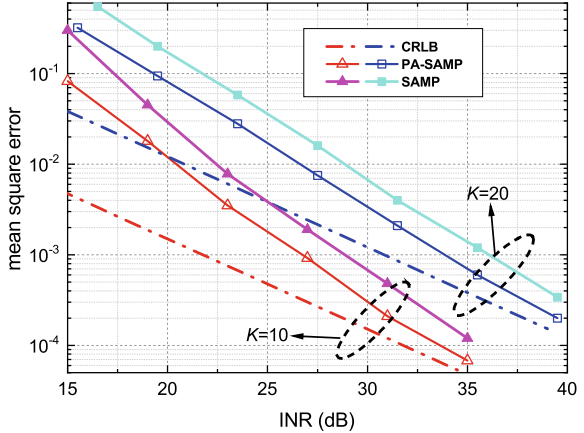
Fig. 5.4 Compressed
sensing based temporal
differential measuring and
PA-SAMP algorithm enabled
NBI recovery in PLC system
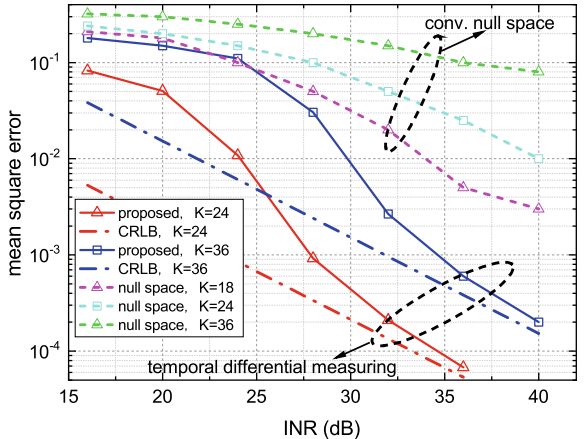
sparsity level of $K = 10$ and $K = 20$, respectively, which outperforms the classical SAMP algorithm by approximately 2.0 dB. Meanwhile, it is observed that with the increase of INR, the MSE performance of the proposed method is approaching the theoretical CRLB. Figure 5.6 shows the MSE performance of the proposed temporal differential measuring method along with the PA-SAMP algorithm, whose theoretical CRLB is $2\sigma_w^2 \cdot (K/M)$, and it is also depicted as a benchmark for comparison. Apart from these, the simulation results of the conventional compressed sensing estimation method based on null space measuring [4] is provided for comparison, too. It can be observed from the simulation results that, the proposed method reaches the target MSE of 10^{-3} at INR $= 27.5$ and 34.8 dB with the sparsity level of $K = 24$ and $K = 36$, respectively, and the MSE performance of the proposed method is also approaching the theoretical CRLB with the increase of INR. It is also verified by the simulation results that, the proposed method has a significant advantage over the conventional null space method in the accuracy of NBI recovery with different

Fig. 5.5 MSE performance of compressed sensing temporal differential measuring based PA-SAMP and SAMP algorithms for NBI recovery in DTMB system

Fig. 5.6 MSE performance of compressed sensing temporal differential measuring based PA-SAMP algorithm and conventional null space measuring method for NBI recovery in PLC system
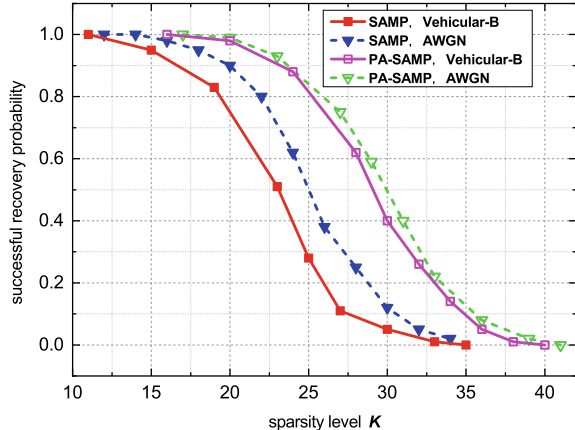
sparsity levels. The simulation results above have validated the high accuracy of the proposed compressed sensing based NBI recovery method.

The simulation results of the success probability of the compressed sensing based NBI recovery in the DTMB system and the PLC system are reported in Figs. 5.7 and 5.8, respectively. The INR of the NBI is 30 dB. The recovery probability of the proposed temporal differential measuring method along with the PA-SAMP and classical SAMP algorithms with different sparsity levels is illustrated in Fig. 5.7, which is evaluated in the AWGN channel and the ITU Vehicular-B multipath channel.

In the realistic simulations, the recovery probability is calculated over 10^3 number of simulations, in which the frequency of accurate NBI recovery is regarded as the success recovery probability [35]. It is shown by the simulation results that, the proposed PA-SAMP algorithm is able to reach a recovery probability of 0.90 at the sparsity level of 23 in both the AWGN and Vehicular-B channels. It has verified that, the proposed temporal differential measuring method along with the PA-SAMP

Fig. 5.7 Successful
recovery probability of
compressed sensing temporal
differential measuring based
PA-SAMP and SAMP
algorithms in DTMB system
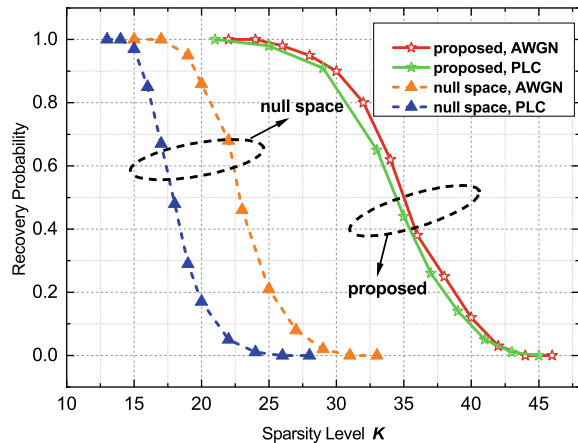
algorithm is able to make use of the only small number of measurement data obtained
from the IBI-free region, and accurately recover the NBI signal with a relatively large
sparsity level, with the aid of the prior information of the partial support. From the
gap between the curves of PA-SAMP and SAMP in the simulation results, it is shown
that the proposed compressed sensing greedy algorithm PA-SAMP is able to make
full use of the prior information and accurately reconstruct the NBI signal with a
relatively large sparsity level.

Apart from this, it is also shown by the simulation results that, the performance
of the conventional SAMP algorithm is significantly degraded in multipath chan-
nel compared with the AWGN channel because the IBI-free region available for
measurement data in multipath channels is shorter. On the other hand, the proposed
PA-SAMP algorithm is hardly affected by the multipath fading with the aid of the
prior information, so it is insensitive to the channel conditions.
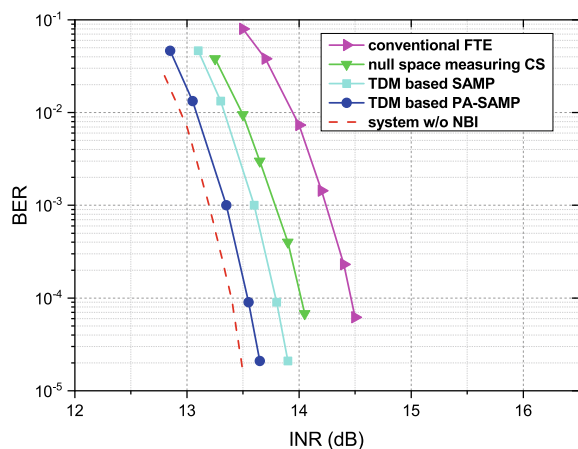
The recovery probability of the proposed temporal differential measuring method
and the conventional null space method [4] in the AWGN and PLC channels in the
PLC system is reported in Fig. 5.8. It is observed from the simulation results that, the
proposed temporal differential measuring based PA-SAMP algorithm is able to reach
a successful recovery probability of 0.98 at the sparsity level of up to 25 in both the
AWGN and PLC channels, and it has a significant advantage over the conventional
null space measuring method [4] in supporting to recover large sparsity levels.

Moreover, the simulation results show that the sparsity level successfully recov-
ered by the conventional method in the PLC multipath channel is significantly reduced
compared with that in the AWGN channel, but the sparsity level supported by the
proposed method is almost invariant in the two different channels. It is revealed by
the simulation results that, the proposed method is able to obtain a small number of
NBI measurement data from the preamble of the PLC system, and accurately recover
the NBI signal with a relatively large sparsity level, and it is meanwhile insensitive
to the channel fading.
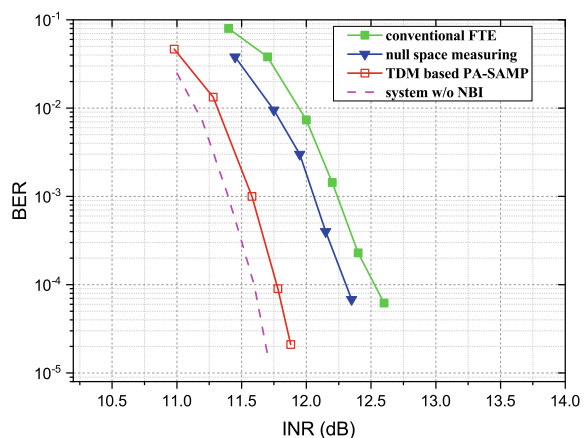
Fig. 5.8 Successful
recovery probability of
compressed sensing temporal
differential measuring based
PA-SAMP and SAMP
algorithms in PLC system

Fig. 5.9 System bit error
rate of different NBI
mitigation and cancelation
schemes in Vehicular-B
channel in DTMB system

Fig. 5.10 System bit error
rate of different NBI
mitigation and cancelation
schemes in Vehicular-B
channel in PLC system

The performance of the system bit error rate (BER) of various different NBI mitigation and cancelation schemes for the DTMB system and the PLC system is reported in Figs. 5.9 and 5.10, respectively. During the simulations of BER, the receiver adopted the algorithm of independent demapping max-log-MAP (maximum a posteriori) [40]. The sum-product algorithm (SPA) was adopted as the LDPC decoding method, where the maximum iteration number was set as 50. The INR of the NBI is 30 dB. The sparsity level for the DTMB system and the PLC system is $K = 20$ and $K = 24$, respectively.

The BER performance of the conventional method of frequency threshold excision (FTE) [41] and the conventional null space measuring based compressed sensing estimation method [4] is also evaluated for comparison. Besides, the BER of the system without the NBI is simulated as a benchmark. For the DTMB system, the simulation parameters are listed in Table 5.1.

The simulation results of the system BER using the proposed temporal measuring method along with the PA-SAMP or SAMP algorithm for NBI recovery and cancelation in the Vehicular-B multipath channel in the DTMB system are reported in Fig. 5.9. It is shown by the simulation results that, the proposed temporal differential measuring method along with the PA-SAMP algorithm has the SNR gain of 0.5 and 0.9 dB over the conventional null space measuring method and the conventional FTE method, respectively, at the target BER of 10^{-4}. The proposed method along with the classical SAMP algorithm has the SNR degradation of 0.25 dB compared with the proposed PA-SAMP algorithm, which is because the classical SAMP algorithm does not make use of the prior information of the partial support. However, it still has a significant gain over the conventional methods. Apart from this, the proposed method along with the PA-SAMP algorithm has a performance very close to the system BER without the NBI, with a gap of only 0.18 dB, which means that the proposed method has good effectiveness in recovering and canceling the NBI and it can significantly improve the system performance.

For the PLC system, the simulation parameters are also listed in Table 5.1. In the PLC multipath channel, the system BER performance of the proposed temporal differential measuring method along with the PA-SAMP algorithm for NBI recovery and cancelation is reported in Fig. 5.10. It is shown by the simulation results that, the proposed method has an SNR gain of 0.70–85 dB over the conventional null space measuring method and the conventional FTE method at the target BER of 10^{-4}. Besides, the gap between the proposed method and the system without NBI is only 0.20 dB, which also indicates the effectiveness of the proposed NBI recovery and cancelation method in the PLC system.

5.4   Structured Compressed Sensing Based NBI Recovery

The NBI recovery method based on classical compressed sensing theory does not make full use of the spatial correlation of the NBI between different antennas in the MIMO system, so the performance might be degraded in severe conditions such as

insufficient measurement data and intensive background noise, etc. To fully exploit the temporal and spatial correlation of the NBI, this section proposes the spatial multiple differential measuring (SMDM) method for NBI recovery in MIMO systems. Firstly, the NBI signal model in MIMO systems is presented. Then the framework of NBI recovery based on time-space domain two-dimensional structured compressed sensing is formulated. Furthermore, the improved greedy algorithm of S-SAMP based on structured compressed sensing is proposed to achieve a higher recovery accuracy and robustness than classical compressed sensing algorithms.
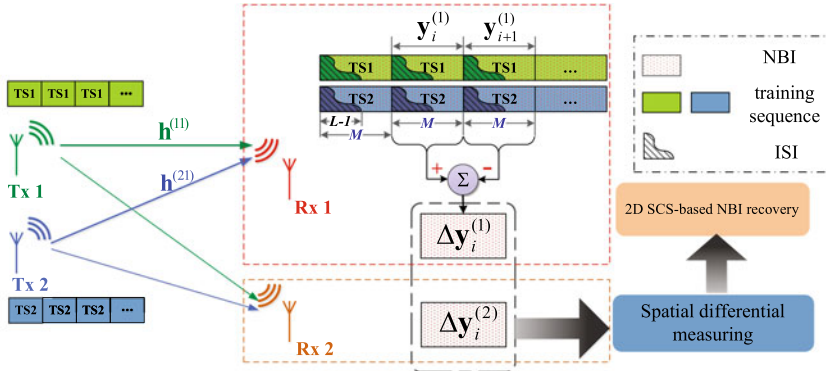
5.4.1 NBI and Signal Models in MIMO Systems

In MIMO systems, repeated training sequences are adopted for synchronization and channel estimation, such as in the preamble of the IEEE 802.11 series standards [25, 26]. Without loss of generality, the repeated training sequences specified by the IEEE 802.11p standard [26] is adopted as an instance to demonstrate the mechanism of the proposed method of spatial multiple differential measuring (SMDM), which is illustrated in Fig. 5.11. Typically, a 2×2 MIMO system configured in the IEEE 802.11p standard is investigated in this section, while the proposed scheme is also applicable in arbitrary $N_t \times N_r$ MIMO systems. At each transmit antenna, a group of D_T identical training sequences are sent continuously, with each denoted as $\mathbf{c}^{(t)} = [c_0^{(t)}, c_1^{(t)}, \ldots, c_{M-1}^{(t)}]^T$ for the t-th transmit antenna and having the identical length M. All the N_t groups of training sequences are sent simultaneously at N_t transmit antennas. After being transmitted over the $N_t \times N_r$ wireless MIMO channel [42] with the channel impulse response $\mathbf{h}^{(tr)} = [h_0^{(tr)}, h_1^{(tr)}, \ldots, h_{L-1}^{(tr)}]^T$ between the t-th transmit antenna and r-th receive antenna where $\mathbf{h}^{(tr)}$ is assumed to be invariant during temporally adjacent training sequences [38], the received i-th training sequence impacted by the NBI at the r-th receive antenna $\mathbf{y}_i^{(r)} = [y_{i,0}^{(r)}, y_{i,1}^{(r)}, \ldots, y_{i,M-1}^{(r)}]^T$, $i = 1, 2 \ldots, D_T$, is given by

$$\mathbf{y}_i^{(r)} = \mathbf{F}_M \tilde{\mathbf{e}}_i^{(r)} + \mathbf{w}_i^{(r)} + \sum_{t=1}^{N_t} \Phi^{(t)} \mathbf{h}^{(tr)}, \tag{5.32}$$

where $\tilde{\mathbf{e}}_i^{(r)}$ denotes the frequency-domain NBI vector for the i-th training sequence at the r-th receive antenna, and $\mathbf{w}_i$ is the AWGN vector with zero mean and variance of σ^2. At the r-th receive antenna, the received training sequence components from the N_t transmit antennas are denoted by $\sum_{t=1}^{N_t} \Phi^{(t)} \mathbf{h}^{(tr)}$ in (5.32), with the matrix $\Phi^{(t)} \in \mathbb{C}^{M \times L}$ given by

$$\Phi^{(t)} = \begin{bmatrix} c_0^{(t)} & c_{M-1}^{(t)} & c_{M-2}^{(t)} & \cdots & c_{M-L+1}^{(t)} \\ c_1^{(t)} & c_0^{(t)} & c_{M-1}^{(t)} & \cdots & c_{M-L+2}^{(t)} \\ \vdots & \vdots & \vdots & \ddots & \vdots \\ c_{M-1}^{(t)} & c_{M-2}^{(t)} & c_{M-3}^{(t)} & \cdots & c_{M-L}^{(t)} \end{bmatrix}_{M \times L}. \tag{5.33}$$

Fig. 5.11 The two-dimensional structured compressed sensing based NBI recovery through SMDM in MIMO systems

At each receive antenna, the received signal of the i-th training sequence is given in the form of (5.32), including the superposition of the received N_t i-th training sequences from N_t transmit antennas, the NBI signal, and the background AWGN. The proposed SMDM method will firstly acquire a one-dimensional differential measurement of the NBI exploiting the temporal correlation from each receive antenna, and then fully utilize the spatial correlation of the NBI at the N_r receive antennas and implement the multiple differential measuring of the NBI for the two-dimensional SCS based NBI recovery, and finally obtain the NBI at each receive antenna through the structured compressed sensing algorithm, which is described in detail in the following section.

5.4.2   Spatial Multi-dimensional Differential Measuring

How to acquire the measurement matrix of the NBI with two-dimensional correlations to build up the structured compressed sensing model is vital to NBI recovery. In this section, we first propose the spatial multiple differential measuring method to accomplish this task.

As has been described previously, according to the compressed sensing theory, obtaining the measurement vector of the NBI signal is crucial for the compressed sensing algorithms. It has been proved that using compressed sensing algorithms, a sparse vector will be exactly recovered from measurement data sampled by a rate lower than the Shannon-Nyquist sampling rate in the presence of power constrained background AWGN [34]. Nevertheless, the training sequences or data components with much higher power than AWGN should be excluded to ensure the effective recovery of the unknown sparse signal. This is a difficult task for conventional schemes since the NBI signal is messed up with data or training sequences in

both time and frequency domains and difficult to measure separately. To achieve this goal, a novel temporal differential measuring method has been proposed previously to obtain the measurement vector simply by the differential operation between adjacent received training sequences. For MIMO systems considered in this section, as illustrated in Fig. 5.11, the NBI differential measurement vector $\Delta\mathbf{y}_i^{(r)}$ for the r-th receive antenna can be similarly acquired by subtracting $\mathbf{y}_{i+1}^{(r)}$ from $\mathbf{y}_i^{(r)}$ given by (5.32) to exclude the common received training sequence components $\sum_{t=1}^{N_t} \Phi^{(t)} \mathbf{h}^{(tr)}$, which yields the compressed sensing measurement equation as follows

$$\Delta\mathbf{y}_i^{(r)} = \mathbf{F}_M \Delta\tilde{\mathbf{e}}_i^{(r)} + \Delta\mathbf{w}_i^{(r)}, \tag{5.34}$$

where $\Delta\mathbf{y}_i^{(r)} = \mathbf{y}_i^{(r)} - \mathbf{y}_{i+1}^{(r)}$, $\Delta\mathbf{w}_i^{(r)} = \mathbf{w}_i^{(r)} - \mathbf{w}_{i+1}^{(r)}$, the NBI differential vector at the r-th receive antenna $\Delta\tilde{\mathbf{e}}_i^{(r)} \in \mathbb{C}^N$ is denoted as

$$\Delta\tilde{\mathbf{e}}_i^{(r)} = \tilde{\mathbf{e}}_i^{(r)} - \tilde{\mathbf{e}}_{i+1}^{(r)} = \left[\Delta\tilde{e}_{i,0}^{(r)}, \Delta\tilde{e}_{i,1}^{(r)}, \ldots, \Delta\tilde{e}_{i,N-1}^{(r)} \right]^T. \tag{5.35}$$

It is noted that the differential AWGN $\Delta\mathbf{w}_i^{(r)}$ in (5.34) is the addition of two AWGN variables with identical and independent distribution, which results in a new AWGN variable with the power two times as the original background noise. However, it has hardly any impact on the effectiveness of the proposed method. It is proved in literature that it is highly probable to recover the sparse signal accurately in the presence of the power constraint background noise [2, 34]. Besides, the power of the practical NBI is much larger than that of AWGN in the frequency domain, which leads to high INR and facilitates the recovery of the NBI. The simulation results are also reported in the following content to show the effectiveness and accuracy of NBI recovery in the presence of the background AWGN.

Due to its temporal correlation, the frequency locations and the magnitude of the NBI signal keeps invariant during adjacent training sequences, and thus the time-domain NBI vector at the $(i + 1)$-th training sequence $\mathbf{e}_{i+1}^{(r)}$ equals the time-domain NBI vector at the i-th training sequence $\mathbf{e}_i^{(r)}$ delayed by Δl samples, where $\Delta l = M$ is the distance between the two adjacent training sequences. Hence, the frequency-domain NBI vector at the $(i + 1)$-th training sequence $\tilde{\mathbf{e}}_{i+1}^{(r)}$ should be $\tilde{\mathbf{e}}_i^{(r)}$ with a phase shift, i.e.,

$$\tilde{e}_{i+1,k}^{(r)} = \tilde{e}_{i,k}^{(r)} \exp\left(\frac{j2\pi k\Delta l}{N} \right), k = 0, 1, \ldots, N - 1. \tag{5.36}$$

Here, equation is the very temporal correlation of the NBI between adjacent training sequences that facilitates the temporal differential measuring of the NBI as well as the proposed SMDM framework. Consequently, the entries of the NBI differential vector in (5.35) are given by

$$\Delta \tilde{e}_{i,k}^{(r)} = \tilde{e}_{i,k}^{(r)} \left(1 - \exp\left(\frac{j2\pi k \Delta l}{N}\right)\right), k = 0, 1, \ldots, N-1. \tag{5.37}$$

The unknown sparse NBI differential vector is estimated from only a one-dimensional measurement vector by using compressed sensing algorithms in the previous section. However, this approach might suffer from large NBI sparsity levels, strong background noise, and insufficient measurement data in severe circumstances.

In the proposed framework of two-dimensional structured compressed sensing and SMDM, the spatial correlation as well as the temporal correlation of the NBI signal is taken full advantage of to improve the stability of NBI recovery for MIMO systems. Recall that one measurement vector at the i-th received training sequence given by (5.34) is acquired for each receive antenna using the previously proposed temporal differential measuring method. Now in the proposed SMDM framework, considering the N_r measurement vectors at the i-th received training sequence from the N_r receive antennas, with each having the form of the compressed sensing sparse measurement model given by (5.34), we obtain the structured compressed sensing measurement equation, i.e. the multiple measurement vectors (MMV) problem formulation, by stacking all the measurement vectors into one matrix by column, as given by

$$\Delta \mathbf{Y} = \left[\Delta \mathbf{y}_i^{(1)}, \Delta \mathbf{y}_i^{(2)}, \ldots, \Delta \mathbf{y}_i^{(N_r)}\right]_{M \times N_r} = \mathbf{F}_M \Delta \tilde{\mathbf{E}} + \Delta \mathbf{W}, \tag{5.38}$$

where $\Delta \tilde{\mathbf{E}} = [\Delta \tilde{\mathbf{e}}_i^{(1)}, \Delta \tilde{\mathbf{e}}_i^{(2)}, \ldots, \Delta \tilde{\mathbf{e}}_i^{(N_r)}]$ are the spatially jointly sparse matrix of the NBI whose columns share the same support Ω (i.e., NBI supports at the N_r receive antennas are the same), while the values of the nonzero entries in the same row of the matrix might be different from each other. $\Delta \mathbf{W} = [\Delta \mathbf{w}_i^{(1)}, \Delta \mathbf{w}_i^{(2)}, \ldots, \Delta \mathbf{w}_i^{(N_r)}]$ is the corresponding AWGN matrix. Consequently, the mathematical model (5.38) formulated by the proposed SMDM method complies with the newly developed theory of structured compressed sensing [43, 44].

According to the structured compressed sensing theory, it is proved that the jointly sparse vectors within $\Delta \tilde{\mathbf{E}}$ (the columns of $\Delta \tilde{\mathbf{E}}$) will be simultaneously recovered accurately by solving the convex optimization problem (mixed $\ell_{p,q}$-norm minimization problem), which is deduced from the structured compressed sensing MMV problem (5.38), as follows

$$\Delta \hat{\mathbf{E}} = \arg \min_{\Delta \tilde{\mathbf{E}} \in \mathbb{C}^{N \times N_r}} \left\|\Delta \tilde{\mathbf{E}}\right\|_{p,q}, \text{s.t.} \left\|\Delta \mathbf{Y} - \mathbf{F}_M \Delta \tilde{\mathbf{E}}\right\|_{q,q} \leq \epsilon, \tag{5.39}$$

where ϵ^2 denotes the power constraint of the background AWGN $\Delta \mathbf{W}$, and the $\ell_{p,q}$-norm of the matrix $\Delta \tilde{\mathbf{E}}$ is defined by

$$\left\|\Delta \tilde{\mathbf{E}}\right\|_{p,q} = \left(\sum_m \left\|\Delta \tilde{\mathbf{E}}_m\right\|_p^q\right)^{1/q}, \tag{5.40}$$

with $\Delta\tilde{\mathbf{E}}_m$ being the m-th row of the matrix $\Delta\tilde{\mathbf{E}}$. Usually $\ell_{1,2}$ norm is adopted as the convex relaxation norm, which turns the original problem (5.39) into a convex optimization problem to solve [44]. In this way, the problem (5.40) is turned into

$$\Delta\hat{\mathbf{E}} = \arg\min_{\Delta\tilde{\mathbf{E}}\in\mathbb{C}^{N\times N_r}} \left\|\Delta\tilde{\mathbf{E}}\right\|_{1,2}, \text{ s.t.} \left\|\Delta\mathbf{Y} - \mathbf{F}_M\Delta\tilde{\mathbf{E}}\right\|_{2,2} \le \epsilon, \qquad (5.41)$$

where

$$\epsilon = \|\Delta\mathbf{W}\|_{2,2} = \sqrt{MN_r}\sigma_w. \qquad (5.42)$$

It is verified by theoretical analysis and proofs that, the existence of the solution of the mixed $\ell_{1,2}$-norm minimization problem (5.41) described above and the accuracy of the solution are guaranteed theoretically, this is presented in detail in the performance analysis in Sect. 5.6.

Note that the previously proposed temporal differential measuring approach without exploiting the spatial correlation can be regarded as a special case of the newly proposed structured compressed sensing-based SMDM framework with $N_r = 1$ in (5.38) and (5.39).

Greedy compressed sensing algorithms could be implemented to solve the one-dimensional convex optimization problem (5.34) induced by the temporal differential measuring method, such as the classical SAMP algorithm dealing with sparse recovery with unknown sparsity levels. Using the temporal differential measuring method with the SAMP algorithm in the framework of the classical compressed sensing theory, the NBI $\Delta\tilde{\mathbf{e}}_i^{(r)}$ is recovered and canceled at each receive antenna separately without cooperative reconstruction of NBI from multiple receive antennas that exploits the spatial correlation in MIMO systems. However, since the SAMP algorithm is aimed at the classical compressed sensing based recovery using only one-dimensional measurement, it might become vulnerable and suffer from performance degradation in severe conditions. In order to solve this problem, the spatial correlation of the NBI is fully exploited to improve the stability and accuracy of SAMP for the MIMO system. Under the two-dimensional structured compressed sensing based SMDM framework, we propose the structured sparsity adaptive matching pursuit (S-SAMP) algorithm to effectively solve the multi-dimensional convex optimization problem in (5.39) and reconstruct the spatially jointly sparse matrix $\Delta\tilde{\mathbf{E}}$ accurately.

5.4.3 Structured SAMP Algorithm

In order to solve the structured compressed sensing based NBI recovery problem formulated by the SMDM method, an efficient improved structured compressed sensing greedy algorithm is proposed in this section, i.e. S-SAMP. The pseudo-code of the proposed S-SAMP is summarized in **Algorithm 1**. The inputs of **Algorithm 1** are the measurements matrix $\Delta\mathbf{Y}$, the observation matrix $\mathbf{\Psi} = \mathbf{F}_M$, and the iteration step size δ of the test sparsity level K_t. The iterations are composed of multiple

stages, and K_t is increased by δ when the stage switches. The output of **Algorithm 1** is the final output support $\hat{\Omega}$ and the recovered jointly sparse matrix $\Delta\hat{\mathbf{E}}$ of the NBI s.t. $\Delta\hat{\mathbf{E}}|_{\hat{\Omega}} = \mathbf{\Psi}_{\hat{\Omega}}^{\dagger} \Delta\mathbf{Y}$, $\Delta\hat{\mathbf{E}}|_{\hat{\Omega}^c} = \mathbf{0}$.

It is observed from **Algorithm 1** that the spatial correlation of the NBI is fully exploited in S-SAMP by summing up the values of N_r columns of the measurement matrix $\Delta\mathbf{Y}$ to pick out the maximum K_t entries as the candidate support list in each iteration, instead of picking from only one measurement vector in classical SAMP [36]. Under the two-dimensional structured compressed sensing based SMDM framework, the S-SAMP algorithm takes full advantage of the spatial multiple differential measurements to enhance the robustness of NBI recovery. Especially in severe conditions with insufficient measurement data, large background noise intensity, or higher sparsity levels, S-SAMP ensures better performance than classical compressed sensing algorithms, which is demonstrated by simulations in the following section.

After the recovered spatially jointly sparse NBI matrix $\Delta\hat{\mathbf{E}}$ is obtained by the S-SAMP algorithm, the NBI signals corresponding to the OFDM data blocks at all the receive antennas can be recovered based on this. The r-th column of the recovered jointly sparse matrix $\Delta\hat{\mathbf{E}}$ of the NBI is the recovered NBI differential vector $\Delta\hat{\mathbf{e}}_i^{(r)}$ related to the r-th receive antenna in Eq. (5.34). Hence, according to (5.35) and (5.37), the original frequency-domain NBI vector $\tilde{\mathbf{e}}_i^{(r)}$ associated to the i-th received training sequence $\mathbf{y}_i^{(r)}$ at the r-th receive antenna can be acquired from $\Delta\hat{\mathbf{e}}_i^{(r)}$ by

$$\tilde{e}_{i,k}^{(r)} = \Delta\hat{e}_{i,k}^{(r)} \left/ \left(1 - \exp\left(\frac{j2\pi k\Delta l}{N} \right) \right) \right. , k = 0, 1, \ldots, N - 1. \qquad (5.43)$$

Finally, the frequency domain NBI vector $\tilde{\mathbf{e}}_n^{'(r)} = [\tilde{e}_{n,0}^{'(r)}, \tilde{e}_{n,1}^{'(r)}, \ldots, \tilde{e}_{n,N-1}^{'(r)}]^T$ associated to the received n-th OFDM symbol in the payload at the r-th receive antenna is similarly acquired by

$$\tilde{e}_{n,k}^{'(r)} = \tilde{e}_{i,k}^{(r)} \cdot \exp\left(\frac{j2\pi k\Delta d_{i,n}}{N} \right), k = 0, 1, \ldots, N - 1, \qquad (5.44)$$

where $\{\Delta d_{i,n} = (n - 1)F + (D - i + 1)M\}_{i=2}^{D-1}$ is the distance between the i-th received training sequence $\mathbf{y}_i^{(r)}$ and the n-th OFDM symbol with the frame length of F. Afterwards, the recovered NBI signal is canceled from the received OFDM symbol for each of the N_r receive antennas.

Furthermore, apart from the structured compressed sensing based greedy algorithms, the mixed $\ell_{1,2}$-norm minimization problem (5.41) can be solved by vectorization of the jointly sparse matrix by row, i.e. regarding each row of the unknown jointly sparse matrix as a sub-block of high-dimensional *block sparse* unknown vector. In this way, the original problem can be turned into another structured compressed sensing framework, i.e. the block sparse recovery problem. Specifically, by vectorizing

Algorithm 2 Structured Sparsity Adaptive Matching Pursuit (S-SAMP) for NBI Recovery in the MIMO System

---

Input:
   1) Measurements matrix $\Delta \mathbf{Y}$
   2) Observation matrix $\mathbf{\Psi} = \mathbf{F}_M$
   3) Step size δ.
   Initialization:
1: $\Delta \hat{\mathbf{E}}^{(0)} \leftarrow \mathbf{0}_{N \times N_r}$; $\mathbf{R}^{(0)} \leftarrow \Delta \mathbf{Y}$
2: $\Omega^{(0)} \leftarrow \emptyset$; $K_t \leftarrow \delta$
3: $k \leftarrow 1$; $j \leftarrow 1$
   Iterations:
4: **repeat**
5:   $\mathbf{v} \in \mathbb{C}^N$ s.t. $v_i = \sum\limits_{j=1}^{N_r} \left| \left(\mathbf{\Psi}^H \mathbf{R}^{(k-1)} \right)_{i,j} \right|$
6:   $S_k \leftarrow \text{Max}\{\mathbf{v}, K_t\}$ {Preliminary test}
7:   $C_k \leftarrow \Omega^{(k-1)} \cup S_k$ {Make candidate list}
8:   $\mathbf{u} \in \mathbb{C}^{|C_k|}$ s.t. $u_i = \sum\limits_{j=1}^{N_r} \left| \left(\mathbf{\Psi}_{C_k}^\dagger \Delta \mathbf{Y} \right)_{i,j} \right|$
9:   $\Omega_t \leftarrow \text{Max}\{\mathbf{u}, K_t\}$ {Temporary final list}
10:   $\Delta \hat{\mathbf{E}}^{(k)} \Big|_{\Omega_t} \leftarrow \mathbf{\Psi}_{\Omega_t}^\dagger \Delta \mathbf{Y}$; $\Delta \hat{\mathbf{E}}^{(k)} \Big|_{\Omega_t^c} \leftarrow \mathbf{0}$
11:   $\mathbf{R}_t \leftarrow \Delta \mathbf{Y} - \mathbf{\Psi}_{\Omega_t} \mathbf{\Psi}_{\Omega_t}^\dagger \Delta \mathbf{Y}$ {Compute residue}
12:   **if** $\|\mathbf{R}_t\|_{2,0} \geq \left\| \mathbf{R}^{(k-1)} \right\|_{2,0}$ **then**
13:     $T \leftarrow T + \delta$ {Stage switching}
14:   **else**
15:     $\Omega^{(k)} \leftarrow \Omega_t$; $\hat{\Omega} \leftarrow \Omega_t$; $\mathbf{R}^{(k)} \leftarrow \mathbf{R}_t$
16:     $k \leftarrow k + 1$ {Same stage, next iteration}
17:   **end if**
18: **until** $\|\mathbf{R}_t\|_{2,0} < \epsilon^2$
Output:
   1) Final output support $\hat{\Omega}$
   2) Recovered spatially jointly sparse matrix $\Delta \hat{\mathbf{E}}$, s.t.
   $\Delta \hat{\mathbf{E}} \Big|_{\hat{\Omega}} = \mathbf{\Psi}_{\hat{\Omega}}^\dagger \Delta \mathbf{Y}$, $\Delta \hat{\mathbf{E}} \Big|_{\hat{\Omega}^c} = \mathbf{0}$

---

the Eq. (5.38), we have

$$\text{vec}\left(\Delta \mathbf{Y}^T\right) = \left(\mathbf{F}_M \otimes \mathbf{I}_{N_r}\right) \text{vec}\left(\Delta \tilde{\mathbf{E}}^T\right) + \text{vec}\left(\Delta \mathbf{W}^T\right) \qquad (5.45)$$

where $\text{vec}(\Delta \mathbf{Y}^T)$ and $\text{vec}(\Delta \tilde{\mathbf{E}}^T)$ are the high-dimensional vectors obtained by vectorizing all the row vectors of $\Delta \mathbf{Y}$ and $\Delta \tilde{\mathbf{E}}$, respectively. Let us define the block sparse NBI vector as $\mathbf{x} \overset{\Delta}{=} \text{vec}(\Delta \tilde{\mathbf{E}}^T)$. During vectorization, the original observation matrix $\mathbf{F}_M$ is also turned into $\left(\mathbf{F}_M \otimes \mathbf{I}_{N_r}\right)$ correspondingly, where $\otimes$ denotes the Kronecker product operation. Thus, the mixed $\ell_{1,2}$-norm minimization problem (5.41) has been vectorized and turned into the mixed ℓ_2/ℓ_1-norm minimization problem as given by

$$\hat{\mathbf{x}} = \arg \min_{\mathbf{x} \in \mathbb{N}^{N_r}} \|\mathbf{x}\|_{2,1},$$

$$\mathbf{x} = \mathrm{vec}\left(\Delta \tilde{\mathbf{E}}^T\right), \hat{\mathbf{x}} = \mathrm{vec}(\Delta \hat{\mathbf{E}}^T),$$

(5.46)

$$\Gamma = \{d_1, \ldots, d_{N_\mathrm{B}}\}, \ N_\mathrm{B} = N, \ d_i = N_r \ \forall i,$$ (5.47)

$$\text{s.t.} \ \left\|\mathrm{vec}\left(\Delta \mathbf{Y}^T\right) - \left(\mathbf{F}_M \otimes \mathbf{I}_{N_r}\right)\mathbf{x}\right\|_2 \leq \epsilon,$$ (5.48)

where $\mathbf{x}$ is the block sparse vector obtained by the vectorization of the rows of the matrix $\Delta \tilde{\mathbf{E}}$. It can be known from the principle of vectorization that, the block partition is naturally generated based on the rows, which is denoted by Eq. (5.47), where the number of sub-blocks is $N_\mathrm{B} = N$, and each sub-block $\mathbf{x}[i]$ represents the i-th row of $\Delta \tilde{\mathbf{E}}$. The mixed ℓ_2/ℓ_1-norm $\|\mathbf{x}\|_{2,1}$ is shown by Eq. (2.20). Furthermore, the problem (5.46) can be solved using the block sparse solutions, such as the block orthogonal matching pursuit (B-OMP) greedy algorithm, or the group LASSO convex optimization solution [45]. When the group LASSO convex optimization solution is adopted, the problem model is given by

$$\min \sum_{i=1}^{N_\mathrm{B}} \sqrt{\mathbf{x}[i]^T \mathbf{K}_i \mathbf{x}[i]} \quad \text{s. t.} \quad \|\mathbf{y} - \mathbf{\Psi}\mathbf{x}\|_2 \leq \epsilon,$$ (5.49)

or its equivalent Lagrange relaxation form:

$$\min \left(\frac{1}{2} \|\mathbf{y} - \mathbf{\Psi}\mathbf{x}\|_2^2 + \lambda \sum_{i=1}^{N_\mathrm{B}} \sqrt{\mathbf{x}_i^T \mathbf{K}_i \mathbf{x}[i]}\right),$$ (5.50)

where the observation matrix $\mathbf{\Psi} = \mathbf{F}_M$, and $\mathbf{\Psi}_i^T \mathbf{\Psi}_i$ or the identity matrix $\mathbf{I}_i$ can be adopted as the kernel matrix $\mathbf{K}_i$. $\mathbf{\Psi}_i$ denotes the sub-matrix formulated by the columns of the sub-block $\mathbf{x}[i]$ corresponding to the matrix $\mathbf{\Psi}$. When the kernel matrix in (5.49) is assigned by $\mathbf{\Psi}_i^T \mathbf{\Psi}_i$, the problem model of "kernel block group LASSO" can be formulated as given by

$$\min \sum_{i=1}^{N_\mathrm{B}} \|\mathbf{\Psi}_i \mathbf{x}[i]\|_2 \quad \text{s. t.} \quad \|\mathbf{y} - \mathbf{\Psi}\mathbf{x}\|_2 \leq \epsilon.$$ (5.51)

As a typical model of group LASSO problems, when the identity matrix $\mathbf{I}_i$ is selected as the kernel matrix, the group LASSO problem based on the ℓ_2/ℓ_1-norm minimization, i.e. the "block group LASSO" problem, can be formulated. Thus the block sparse convex optimization algorithms can be utilized to solve it conveniently [45].

5.4.4   Simulation Results and Discussions

The performance of the proposed two-dimensional structured compressed sensing based SMDM method with the proposed S-SAMP algorithm for NBI recovery in the wireless MIMO vehicular transmission systems specified by the IEEE 802.11p WAVE standard [26] is evaluated through simulations. Typically, the simulation setup is configured according to the wireless access in vehicular environments MIMO systems specified by the IEEE 802.11p standard [26], and the typical simulation parameters are listed in Table 5.3. The OFDM sub-carrier number $N = 64$ and length of each training sequence $M = 16$. The number of repeated training sequences sent by each transmit antenna is $D_T = 5$. The 2×2 MIMO or 4×4 MIMO multipath channel model [42] and the ITU-R Vehicular-B multipath channel model [38] in the presence of NBI are adopted. The parameters of the ITU-R Vehicular-B multipath channel are listed in Table 5.2 [38]. The low density parity check (LDPC) code with code length of 1944 bits and code rate of 1/2 as well as the 64QAM modulation are adopted. The compound BLGN interferers model in Sect. 2.3.1 is still adopted as the NBI model.
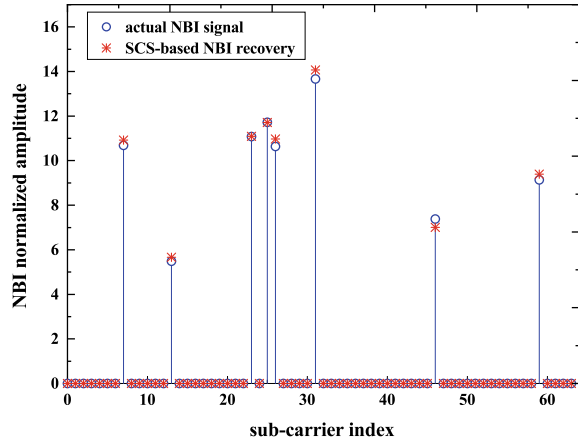
The main evaluation metrics in the simulations contain the NBI recovery process, the MSE of the NBI estimation, the correct recovery probability of the NBI with different sparsity levels or measurement data amount, and the system BER using different schemes, etc. Apart from the proposed SMDM method along with the structured compressed sensing based S-SAMP algorithm in the 2×2 and 4×4 MIMO systems, the NBI recovery performance of the previously proposed classical compressed sensing based TDM method with the SAMP algorithm, which is implemented at each receive antenna separately, is also evaluated using the same MIMO system setup for comparison (as described in Section III.A, it is equivalent to the NBI recovery process in the MISO or SISO system). Besides, the performance of the conventional null space measuring method [4] along with the classical OMP algorithm [46] is also evaluated as a comparison.

The performance of one realization of the NBI recovery using the proposed two-dimensional structured compressed sensing based SMDM scheme with the S-SAMP algorithm for the 2×2 MIMO wireless access in vehicular environments system is illustrated in Fig. 5.12, when the sparsity level $K = 8$ and INR = 30 dB. Without loss of generality, we investigate the actual and estimated NBI signals at one of the receive antennas. The NBI at one certain receive antenna is recovered from the
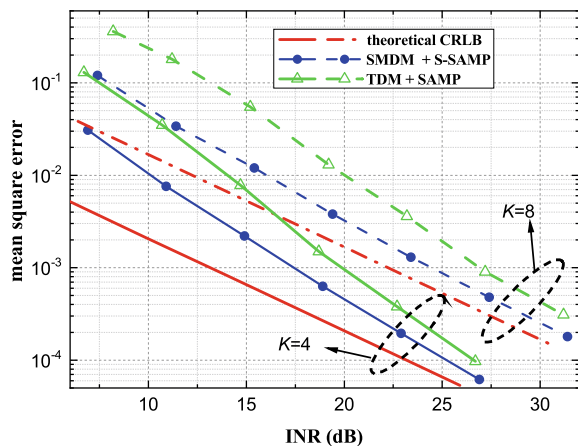
Table 5.3 Simulation parameters of structured compressed sensing based NBI recovery in MIMO system

System	OFDM sub-carrier number	Training sequence length	Constellation mapping	LDPC code length	Code rate
WAVE standard [26]	$N = 64$	$M = 16$	64QAM	1944	0.5

Fig. 5.12 The performance of one realization of NBI recovery using the two-dimensional structured compressed sensing based SMDM scheme with S-SAMP
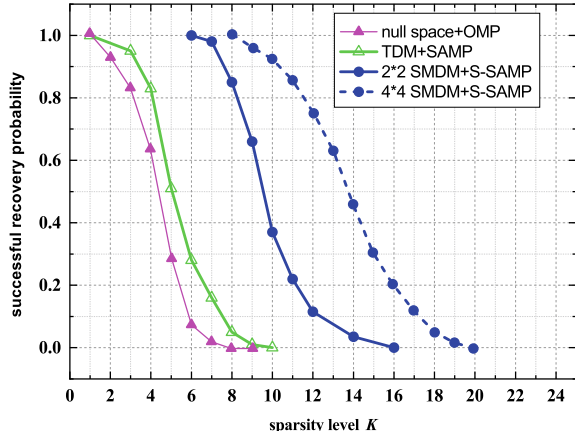
Fig. 5.13 The MSE of NBI recovery versus INR for the two-dimensional structured compressed sensing based SMDM scheme with S-SAMP and the one-dimensional compressed sensing based TDM scheme with SAMP for the 2×2 MIMO system

measurements matrix constituted by the differential measurements at $N_r = 2$ receive antennas. The result in Fig. 5.12 implies that the NBI estimation precisely matches the actual NBI signal.

The MSE performance of NBI recovery is shown in Fig. 5.13. In the 2×2 MIMO wireless access in vehicular environments system, the SMDM scheme with S-SAMP algorithm, and the previous proposed TDM scheme with SAMP algorithm are compared, with the sparsity level $K = 4$ and $K = 8$. The theoretical Cramer-Rao lower bound (CRLB) of $2\sigma_w^2(K/M)$ is depicted as the benchmark. It is shown by the simulation results that, the proposed SMDM scheme with S-SAMP achieves the target MSE of 10^{-3} with the INR of 17.5–24.6 dB at the sparsity level $K = 4$ and $K = 8$, respectively, which has a 2.5 dB gain over the TDM method with SAMP. With the increase of INR, the MSE of the SMDM method asymptotically approaches the CRLB, verifying the recovery accuracy.
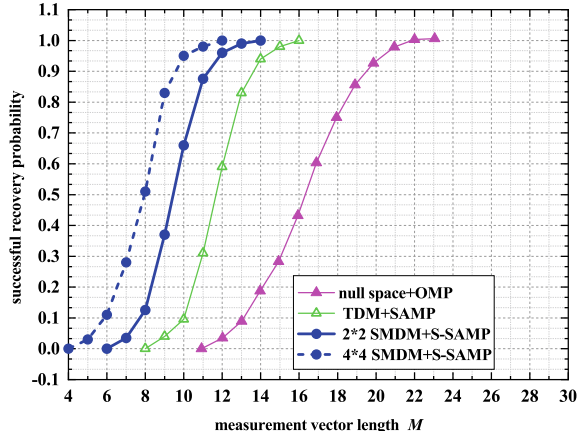
Fig. 5.14 The NBI recovery probability versus sparsity level K for the two-dimensional structured compressed sensing based SMDM S-SAMP and one-dimensional compressed sensing based temporal differential measuring SAMP schemes in the MIMO system

The NBI recovery probability versus the sparsity level K is depicted in Fig. 5.14. Similar to the previous section, the recovery probability is defined as the frequency of successful NBI recovery, i.e. the frequency of MSE$< 10^{-3}$, in a number 10^3 of simulations. It is noted that the SMDM scheme with S-SAMP for 2×2 MIMO and 4×4 MIMO reaches a recovery probability of 0.9 at $K > 7$ and $K > 10$, respectively, while the temporal differential measuring method along with the existing SAMP algorithm and the null space method along with the classical OMP algorithm achieves the successful recovery probability of 0.9 at the sparsity level of $K > 3$ and $K > 2$, respectively. The simulation results indicates that the proposed SMDM method exploiting the spatial correlation can recover the NBI signal at larger sparsity levels and is more robust against the variance of the sparsity level than the previous proposed temporal differential measuring method with the SAMP algorithm in the MIMO system.

To demonstrate the effects of different measurement vector length on the NBI recovery performance, we assume that the length of each training sequence M used as the measurement vector is variant in this case and simulate the corresponding performance. In this way, the recovery probability of both the SMDM method with S-SAMP and the temporal differential measuring method with SAMP versus the measurement vector length M is illustrated in Fig. 5.15. It can be noted from Fig. 5.15 that to reach the successful NBI recovery probability of 0.90, the 4×4 MIMO and 2×2 MIMO SMDM method with the S-SAMP algorithm only require $M = 9$ and $M = 11$ measurement vector length (measurement samples), while longer measurement vector $M = 14$ is required by the MISO/SISO temporal differential measuring method with the conventional SAMP algorithm. The conventional null space measuring method along with the conventional OMP algorithm requires a measurement vector length up to $M = 20$. It can be inferred that the proposed SMDM method takes full advantage of the spatial correlation in MIMO systems based on the structured compressed sensing theory, making the NBI easier to recover and cancel
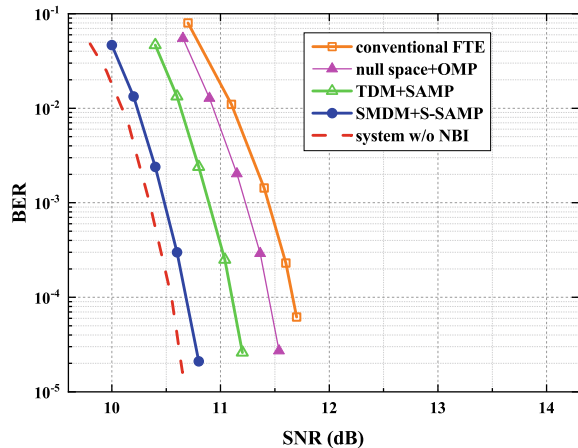
Fig. 5.15 The NBI recovery probability versus measurement vector length *M* for the two-dimensional structured compressed sensing based SMDM S-SAMP and one-dimensional compressed sensing based temporal differential measuring SAMP schemes in the MIMO system

with less measurement data. Hence, using the proposed SMDM method, shorter overhead training sequence in the IEEE 802.11p standard specified preamble is needed for NBI cancelation.

The BER performances of different NBI mitigation schemes over the 2×2 MIMO channel in the presence of NBI are shown in Fig. 5.16, including the proposed SMDM scheme with S-SAMP, as well as the conventional frequency threshold excision method, the conventional null space measuring method along with the conventional OMP algorithm, and the temporal differential measuring method with SAMP for comparison. The ideal case without the NBI is depicted as a benchmark scheme. The sparsity level of the NBI is $K = 8$, and the INR is 30 dB. In the simulations of BER, the vertical Bell Labs layered space-time (V-BLAST) code is adopted, and the data symbols sent by the transmit antennas are independent of each other [47]. The receiver applies the independent demapping max-log-MAP algorithm [40]. The SPA algorithm [48] is applied for LDPC decoding with the maximum iteration number of 50. It is observed from the simulation results in Fig. 5.16 that the proposed SMDM method with S-SAMP outperforms the conventional null space measuring method along with the conventional OMP algorithm and the conventional frequency threshold excision method by approximately 0.7 dB and 0.9 dB, respectively, at the target BER of 10^{-4} in the presence of the NBI with $K = 8$ and INR = 30 dB. With the aid of the spatial correlation under the structured compressed sensing framework, the SMDM method further achieves a 0.4 dB gain over the previous proposed temporal differential measuring method. Moreover, the proposed SMDM method is only about 0.1 dB from the ideal curve without NBI, which demonstrates the accuracy and effectiveness of NBI recovery for MIMO systems.

Fig. 5.16 BER performance comparison of different NBI mitigation schemes for the 2×2 MIMO wireless transmission system

5.5   Sparse Bayesian Learning Based NBI Recovery

For the NBI signal whose interferer frequencies have a frequency offset with respect to the OFDM sub-carriers, considering the block sparse property of the NBI, the sparsity level will significantly increase. The conventional compressed sensing based NBI recovery methods have limited performance, and these methods require to utilize the training sequences for differential measuring. Hence, in this section, a block sparse Bayesian learning based NBI recovery algorithm is proposed. The modeling method of differential block sparse measurement and representation only using the CP-OFDM frame structure without requiring the training sequences is proposed. Making full use of the intra-block correlation of the block sparse NBI signal, the estimation performance of the sparse Bayesian learning method is improved, and the drawbacks of the conventional compressed sensing algorithms in the conditions of large sparsity level and block sparse unknown signals, are overcome. The practical NBI signal in CP-OFDM systems can be recovered accurately and efficiently. The methods and techniques proposed in this section can be applied for the estimation and cancelation of the NBI on the CP-OFDM based LTE/LTE-A signals from the narrowband internet-of-things (NB-IoT), and the NBI recovery and cancelation in smart grid communications, etc.

5.5.1   System Model

(1)*CP-OFDM Signal Model in LTE-A System*
This section takes the NBI generated by the NB-IoT signal on the CP-OFDM signal in LTE-A systems as an instance to investigate and propose the block sparse Bayesian learning based NBI recovery and estimation methods. As adopted in LTE-A stan-

dards [27] as well as many other broadband transmission systems, the CP-OFDM frame structure is composed of the length-V cyclic prefix (CP) and the length-N OFDM block, as illustrated in Fig. 5.17. The parameter N is the number of sub-carriers, and the CP part is the last V samples of its following OFDM block. After being transmitted in the wireless multi-path fading channel with the channel impulse response (CIR) $\mathbf{h}_i = \left[h_{i,0}, h_{i,1}, \ldots, h_{i,L-1} \right]^T$ in the presence of NBI generated by NB-IoT signal, the received i-th CP $\mathbf{p}_i = \left[p_{i,0}, p_{i,1}, \ldots, p_{i,V-1} \right]^T$ before the i-th received OFDM block $\mathbf{x}_i$ in the LTE-A system is given by
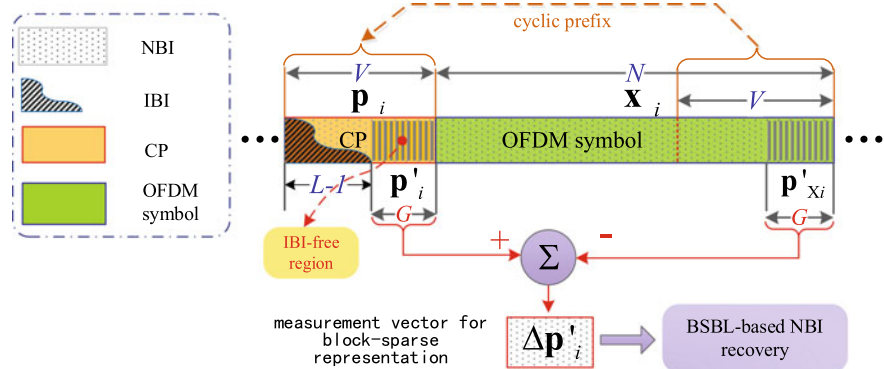
$$\mathbf{p}_i = \Psi_{\text{CP}} \mathbf{h}_i + \mathbf{e}_i + \mathbf{w}_i, \tag{5.52}$$

where $\mathbf{e}_i = \left[e_{i,0}, e_{i,1}, \ldots, e_{i,V-1} \right]^T$ denotes the time-domain NBI vector when we look at the CP part, and $\mathbf{w}_i$ denotes the additive white Gaussian noise (AWGN) vector with zero mean and variance of σ_w^2, while the CP component at the receiver is denoted by $\Psi_{\text{CP}} \mathbf{h}_i$, with the matrix $\Psi_{\text{CP}} \in \mathbb{C}^{V \times L}$ given by

$$\Psi_{\text{CP}} = \begin{bmatrix} x_{i,N-V} & x_{i-1,N-1} & x_{i-1,N-2} & \cdots & x_{i-1,N-L+1} \\ x_{i,N-V+1} & x_{i,N-V} & x_{i-1,N-1} & \cdots & x_{i-1,N-L+2} \\ x_{i,N-V+2} & x_{i,N-V+1} & x_{i,N-V} & \cdots & x_{i-1,N-L+3} \\ \vdots & \vdots & \vdots & \ddots & \vdots \\ x_{i,N-V+L-2} & x_{i,N-V+L-3} & x_{i,N-V+L-4} & \cdots & x_{i-1,N-1} \\ x_{i,N-V+L-1} & x_{i,N-V+L-2} & x_{i,N-V+L-3} & \cdots & x_{i,N-V} \\ x_{i,N-V+L} & x_{i,N-V+L-1} & x_{i,N-V+L-2} & \cdots & x_{i,N-V+1} \\ \vdots & \vdots & \vdots & \ddots & \vdots \\ x_{i,N-1} & x_{i,N-2} & x_{i,N-3} & \cdots & x_{i,N-L} \end{bmatrix} \tag{5.53}$$

whose entries $\{x_{i-1,n}\}_{n=N-L+1}^{N-1}$ represent the last $L-1$ samples of the $(i-1)$-th OFDM block $\mathbf{x}_{i-1}$, which causes inter-block-interference (IBI) on the current i-th CP. Since the $(i-1)$-th OFDM block $\mathbf{x}_{i-1}$ only causes IBI on the first $L-1$ samples of the i-th CP, the last $G = V - L + 1$ samples of $\mathbf{p}_i$ will form the IBI-free region $\mathbf{p}_i' = \left[p_{i,L-1}, p_{i,L}, \ldots, p_{i,V-1} \right]^T$, i.e., $\mathbf{p}_i' = \mathbf{S}_{G,V} \mathbf{p}_i$, where $\mathbf{S}_{G,V}$ denotes the selection matrix composed of the last G rows of the $V \times V$ identity matrix $\mathbf{I}_V$.

The IBI-free region exists in practical broadband transmission systems because a common rule for system design is to configure the guard interval length V to be much larger than the maximum channel delay spread L in the worst case to avoid IBI between OFDM symbols, so L is usually smaller than V in practice, i.e., $L < V$. For instance, all the IEEE 802.11n [25], the ITU-T G.hn [32], IEEE 802.11p [26], and the 3GPP LTE-A [27] standards based on CP-OFDM obey this rule. Even if in certain extreme cases when the channel delay spread is too long so that it exceeds the guard interval length, the guard interval can be extended to a longer mode to ensure the existence of IBI-free region, which is supported by various standards that have extendable CP length modes [25–27]. Hence, the IBI-free region at the end of the i-th CP can be rewritten as

Fig. 5.17 Block sparse representation for block sparse Bayesian learning based NBI recovery through temporal differential measuring method for CP-OFDM symbol in LTE-A systems

$$\mathbf{p}_i^{'} = \mathbf{\Psi}_{\mathrm{CP}}^{'}\mathbf{h}_i + \mathbf{e}_i^{'} + \mathbf{w}_i^{'}, \tag{5.54}$$

where $\mathbf{p}_i^{'}$, $\mathbf{e}_i^{'}$, and $\mathbf{w}_i^{'}$ consist of the last G entries of $\mathbf{p}_i$, $\mathbf{e}_i$, and $\mathbf{w}_i$ in (5.52), respectively, while $\mathbf{\Psi}_{\mathrm{CP}}^{'} \in \mathbb{C}^{G \times L}$ is composed of the last G rows of $\mathbf{\Psi}_{\mathrm{CP}}$ and contains only the entries in $\mathbf{x}_i$, i.e., $\mathbf{\Psi}_{\mathrm{CP}}^{'} = \mathbf{S}_{G,V}\mathbf{\Psi}_{\mathrm{CP}}$. The duplicate of $\mathbf{p}_i^{'}$ at the end of the i-th OFDM block $\mathbf{x}_i$ is given by

$$\mathbf{p}_{Xi}^{'} = \mathbf{\Psi}_{\mathrm{CP}}^{'}\mathbf{h}_i + \mathbf{e}_{Xi}^{'} + \mathbf{w}_{Xi}^{'}, \tag{5.55}$$

where $\mathbf{e}_{Xi}^{'}$ and $\mathbf{w}_{Xi}^{'}$ denote the length-G time-domain NBI and AWGN at the end of the i-th OFDM block, respectively.

(2)*Block Sparse NBI Model*
In this section, we still use the NBI model described in Sect. 2.3.1, i.e. the compound BLGN interferer model [12], and extend it to a more generalized block sparse NBI model with frequency offset. Taking the NB-IoT signal in the LTE-A system as an instance, the block sparse model of the NBI generated by other NBI interferer sources can apply similarly. The NB-IoT signal working in-band in the LTE-A spectrum generates NBI to the receivers of LTE-A systems [21]. Firstly, the frequency offset is not considered, so the classical purely sparse NBI model, i.e. the compound BLGN model, can still be adopted. In the frequency domain at the receiver in LTE-A systems, the generated NBI associated with the i-th received OFDM block or its CP part is commonly modeled by a superposition of tone interferers represented by a purely sparse vector $\tilde{\mathbf{e}}_i = \left[\tilde{e}_{i,0}, \tilde{e}_{i,1}, \ldots, \tilde{e}_{i,N-1}\right]^T$ with length N. Similarly, the time-domain NBI signal corresponding to the CP in (5.52) is denoted by $\mathbf{e}_i = [e_{i,0}, e_{i,1}, \ldots, e_{i,V-1}]^T$, which is related with the frequency-domain NBI vector by the Fourier transform relation given by

$$e_{i,n} = \sum_{k \in \Omega_i} \tilde{e}_{i,k} \cdot \exp(\frac{j2\pi kn}{N}), \quad n = 0, 1, \ldots, V-1, \tag{5.56}$$

where $\Omega_i = \left\{ k \left| \tilde{e}_{i,k} \neq 0 , k = 0, 1, \ldots, N - 1 \right. \right\}$ is the set of the locations of nonzero entries, which is defined as the *support*. The definition of the support and the INR is the same as that in Sect. 2.3.1.

Next, we extend the classical compound BLGN interferer model to the block sparse NBI model with frequency offset [3, 49]. In practice, the spectral tone interferers of the NBI introduced by the NB-IoT signal might not necessarily locate exactly at the OFDM sub-carriers of the LTE-A system, which extends our NBI model to a more general one [3]. In case there is an FO between the OFDM sub-carriers (i.e. the DFT grid of the LTE-A system) and the NBI (i.e. the NB-IoT frequency locations), each nonzero entry of the purely sparse NBI vector will spread out to a few adjacent sub-carriers, making the frequency domain NBI vector $\tilde{\mathbf{e}}_i$ of the i-th CP become a *block sparse* vector $\tilde{\mathbf{e}}_{\mathrm{B}i} = [\tilde{e}_{\mathrm{B}i,0}, \tilde{e}_{\mathrm{B}i,1}, \ldots, \tilde{e}_{\mathrm{B}i,N-1}]^T$ given by

$$\tilde{\mathbf{e}}_{\mathrm{B}i} = \underbrace{\mathbf{F}_N^H \Lambda_{\mathrm{FO}} \mathbf{F}_N}_{\mathbf{C}_{\mathrm{FO}}} \tilde{\mathbf{e}}_i, \tag{5.57}$$

where $\tilde{\mathbf{e}}_i$ is the purely sparse vector with few nonzero entries, and $\Lambda_{\mathrm{FO}} = \mathrm{diag}\{1, \exp(j2\pi\alpha/N), \ldots, \exp(j2\pi\alpha(N-1)/N)\}$ is the FO matrix with the FO modeled by a uniformly distributed variable $\alpha \in (-1/2, 1/2)$ [49]. Thus the time-domain NBI vector associated with the IBI-free region of the i-th CP in (5.54) is

$$\mathbf{e}_i^{'} = \mathbf{S}_{G,N} \mathbf{F}_N \tilde{\mathbf{e}}_{\mathrm{B}i}, \tag{5.58}$$

where $\mathbf{S}_{G,N}$ denotes the selection matrix composed of the last G rows of the $N \times N$ identity matrix $\mathbf{I}_N$, and the last G rows of $\mathbf{F}_N$ is thus denoted by $\mathbf{S}_{G,N}\mathbf{F}_N$. The matrix $\mathbf{C}_{\mathrm{FO}}$ is a *circular* matrix whose first column is the IDFT of the diagonal of Λ_{FO}. Actually, the purely sparse NBI vector $\tilde{\mathbf{e}}_i$ is a special case of (5.57) when there is no FO, and we can derive that $\tilde{\mathbf{e}}_{\mathrm{B}i} = \tilde{\mathbf{e}}_i$ and $\mathbf{C}_{\mathrm{FO}} = \mathbf{I}_N$ when $\alpha = 0$. If $\alpha \neq 0$, $\mathbf{C}_{\mathrm{FO}}$ will have a certain number of nonzero entries with significant magnitude at each column. Its physical mechanism is that each original nonzero entry (tone interferer) generates a certain range of frequency spread around its central frequency. Then, by multiplying $\mathbf{C}_{\mathrm{FO}}$ to the purely sparse vector $\tilde{\mathbf{e}}_i$, the vector $\tilde{\mathbf{e}}_{\mathrm{B}i}$ becomes block sparse. Each tone interferer of the purely sparse NBI signal will become a clustered block around the center tone interferer, so the actual sparsity level of the block sparse NBI signal with FO will turn larger than the original sparsity level K of the purely sparse vector. Thus, the block sparse NBI vector $\tilde{\mathbf{e}}_{\mathrm{B}i}$ can be represented in a block sparse form according to (2.26) as given by

$$\tilde{\mathbf{e}}_{\mathrm{B}i} = [\underbrace{\tilde{e}_{\mathrm{B}i,0}, \ldots \tilde{e}_{\mathrm{B}i,d_1-1}}_{\tilde{\mathbf{e}}_{\mathrm{B}i,1}^T}, \ldots \underbrace{\tilde{e}_{\mathrm{B}i,d_g-1}, \ldots \tilde{e}_{\mathrm{B}i,d_g-1}}_{\tilde{\mathbf{e}}_{\mathrm{B}i,g}^T}]^T \tag{5.59}$$

where the block sparse NBI vector $\tilde{\mathbf{e}}_{\mathrm{B}i}$ is divided into g sub-blocks $\tilde{\mathbf{e}}_{\mathrm{B}i,1} \ldots \tilde{\mathbf{e}}_{\mathrm{B}i,g}$. Since each original NBI interferer will generate a cluster of nonzero entries around the central frequency, the number of the nonzero sub-blocks in the block sparse vector

$\tilde{\mathbf{e}}_{\mathrm{B}i}$, i.e. K_b, is equal to the sparsity level of the original purely sparse NBI vector $\tilde{\mathbf{e}}_i$, i.e. K. Then we have $K_b = K$, and the actual sparsity level of the block sparse NBI signal is larger than that of the original NBI signal, i.e. K.

Without loss of generality, the same FO α is adopted for the tone interferers for simplicity of presentation. In fact, this model can be easily extended to different frequency offsets for different tone interferers by setting a distinct FO matrix $\mathbf{C}_{\mathrm{FO},i}$ for each nonzero tone interferer $\tilde{e}_{i,k}$ in (5.57). The phase offset relation described in the following (5.63) still holds for each tone interferer $\tilde{e}_{i,k}$ with its own FO α_i. By linear superposition of all the tone interferers, the proposed temporal differential measuring method and the formulated sparse Bayesian estimation model, as well as the BSBL algorithm described in the following section, still hold in the same way.

As described previously in Sect. 5.2, it should be noted that there is an important characteristic of NBI, which facilitates the proposed method for block sparse representation: the *temporal correlation*. The temporal correlation claims that, both the support and the amplitude of the NBI keep invariant over the received OFDM symbol of interest. Due to the temporal correlation of the NBI, the support and amplitude of the NBI associated with the CP part and the following OFDM block part are the same, and only their phases are shifted as follows: the time-domain NBI vector associated with the i-th IBI-free region $\mathbf{e}_i'$ should be equal to the time-domain NBI vector $\mathbf{e}_{\mathrm{X}i}'$ associated with the duplicate of the CP in the following OFDM block with only a phase shift, where $\mathbf{e}_{\mathrm{X}i}'$ is given by

$$\mathbf{e}_{\mathrm{X}i}' = \mathbf{S}_{G,N}\mathbf{F}_N\tilde{\mathbf{e}}_{\mathrm{BX}i}. \tag{5.60}$$

So the frequency domain block sparse NBI vector is given by

$$\tilde{\mathbf{e}}_{\mathrm{BX}i} = [\tilde{e}_{\mathrm{BX}i,0}, \tilde{e}_{\mathrm{BX}i,1}, \ldots, \tilde{e}_{\mathrm{BX}i,N-1}]^T \tag{5.61}$$

which is corresponding to the duplicate part in the OFDM block is the phase shifted vector of $\tilde{\mathbf{e}}_{\mathrm{B}i}$ corresponding to the CP part in (5.57), which is given by

$$\tilde{e}_{\mathrm{BX}i,k} = \tilde{e}_{\mathrm{B}i,k} \exp\left(\frac{j2\pi(k+\alpha)\Delta l_{\mathrm{B}}}{N}\right), k = 0, 1, \ldots, N-1, \tag{5.62}$$

where the FO α determines the phase to shift, and Δl_{B} is the distance between the i-th CP and its duplicate at the following OFDM block. Note that $\Delta l_{\mathrm{B}} = N$ in this case and we further have $\tilde{e}_{\mathrm{BX}i,k} = \tilde{e}_{\mathrm{B}i,k} \exp(j2\pi\alpha)$, which yields a simple constant proportional relation only determined by α as follows

$$\tilde{\mathbf{e}}_{\mathrm{BX}i} = \exp(j2\pi\alpha)\,\tilde{\mathbf{e}}_{\mathrm{B}i}. \tag{5.63}$$

5.5.2   BSBL Based NBI Reconstruction for CP-OFDM

(1) *Block Sparse Representation of NBI through Temporal Differential Measuring*
In CP-OFDM frames, the time-domain NBI vector $\mathbf{e}_i^{'}$ associated with the i-th IBI-free region $\mathbf{p}_i^{'}$ is described in (5.58), where its frequency domain form is the block sparse vector $\tilde{\mathbf{e}}_{\mathrm{B}i}$ given in (5.57).

Firstly, we should establish the block sparse representation of the NBI, which can be implemented by the proposed block-sparse temporal differential measuring (BS-TDM) method on the CP-OFDM frame between the CP and the OFDM data block. As illustrated in Fig. 5.17, since the i-th CP is the copy of the last V samples of the i-th OFDM block, the measurement vector can be simply obtained by the differential operation between the received IBI-free region $\mathbf{p}_i^{'}$ in (5.54) and its duplicate $\mathbf{p}_{\mathrm{X}i}^{'}$ in (5.55) at the end of the OFDM block, which eliminates the cyclic data component $\Phi_{\mathrm{CP}}^{'}\mathbf{h}_i$ and yields the block sparse temporal differential measurement vector

$$\Delta\mathbf{p}_i^{'} = \Delta\mathbf{e}_i^{'} + \Delta\mathbf{w}_i^{'}, \tag{5.64}$$

where $\Delta\mathbf{e}_i^{'} = \mathbf{e}_i^{'} - \mathbf{e}_{\mathrm{X}i}^{'}$ and $\Delta\mathbf{w}_i^{'} = \mathbf{w}_i^{'} - \mathbf{w}_{\mathrm{X}i}^{'}$. Thus from (5.58) and (5.60), we have the block sparse representation of the NBI as

$$\Delta\mathbf{p}_i^{'} = \mathbf{S}_{G,N}\mathbf{F}_N\Delta\tilde{\mathbf{e}}_{\mathrm{B}i} + \Delta\mathbf{w}_i^{'}, \tag{5.65}$$

where the length-N block sparse vector to be recovered is

$$\Delta\tilde{\mathbf{e}}_{\mathrm{B}i} = \tilde{\mathbf{e}}_{\mathrm{B}i} - \tilde{\mathbf{e}}_{\mathrm{B}\mathrm{X}i} = (1 - \exp(j2\pi\alpha))\tilde{\mathbf{e}}_{\mathrm{B}i}, \tag{5.66}$$

whose support and block partition are the same with those of $\tilde{\mathbf{e}}_{\mathrm{B}i}$ given by (5.57). Using this block sparse representation in (5.65), $\Delta\tilde{\mathbf{e}}_{\mathrm{B}i}$ can be recovered from the acquired measurement vector $\Delta\mathbf{p}_i^{'}$ in the presence of background AWGN based on the proposed BSBL algorithms. Afterwards, $\tilde{\mathbf{e}}_{\mathrm{B}i}$ can be calculated by (5.66) and the NBI $\tilde{\mathbf{e}}_{\mathrm{B}\mathrm{X}i}$ associated with the i-th OFDM block can be calculated through (5.63). Then, the recovered NBI can be directly canceled out from the information data just by subtracting $\tilde{\mathbf{e}}_{\mathrm{B}\mathrm{X}i}$ from the received frequency-domain OFDM sub-carriers $\mathbf{X}_i$, which is given by

$$\mathbf{X}_i^0 = \mathbf{X}_i - \tilde{\mathbf{e}}_{\mathrm{B}\mathrm{X}i}, \tag{5.67}$$

where $\mathbf{X}_i$ is the DFT of the i-th received OFDM block $\mathbf{x}_i$ as illustrated in Fig. 5.17, while $\mathbf{X}_i^0$ is the frequency-domain OFDM data block free from the NBI generated by the NB-IoT signal. Thus, the NBI-free OFDM data block can be then used for information demapping and decoding.

(2) *Partition Estimated Block Sparse Bayesian Learning (PE-BSBL) for NBI Recovery*
In the typical BSBL framework described in Sect. 2.4.3, the block partition of the block sparse vector to be recovered is known [50]. For initialization, the parameters

including $\{\gamma_t, \mathbf{B}_t\}$ and the covariance matrix Σ_0 are estimated. Afterwards, they are input to the BSBL iterations such as the Expectation Maximization (EM) method, after which the maximum a posterior (MAP) estimation of the block sparse vector can be calculated.

In the proposed PE-BSBL approach, the block partition of the NBI $\tilde{\mathbf{e}}_{Bi}$ will be firstly estimated by power threshold method. The estimated block partition Ω_{Bi} associated with the i-th OFDM block can be acquired by

$$\Omega_{Bi} = \{k \left| |\Delta \tilde{p}'_{i,k}|^2 > \eta_{th}, \ k = 0, 1, \ldots, N-1\}, \tag{5.68}$$

where $\Delta \tilde{\mathbf{p}}'_i = \left[\Delta \tilde{p}'_{i,0}, \Delta \tilde{p}'_{i,1}, \ldots, \Delta \tilde{p}'_{i,N-1} \right]$ is the N-point DFT of $\Delta \mathbf{p}'_i$, and the power threshold η_{th} used to determine the estimated block partition is given by

$$\eta_{th} = \frac{\beta}{N} \sum_{k=0}^{N-1} \left| \Delta \tilde{p}'_{i,k} \right|^2, \tag{5.69}$$

where β is a scaling coefficient that can be configured proportional to the INR in different scenarios, and is empirically given by $\beta = \sqrt{2\sigma_e^2/\sigma_w^2}$ as an appropriate choice. Afterwards, every group of consecutive indices in Ω_{Bi} are marked as one nonzero block. Those indices not included in Ω_{Bi} are labeled as zero blocks. By labeling these blocks, the initial block partition $\Gamma_i = \{S_t\}_{t=1}^{g}$ is estimated, where each block is an index set given by

$$S_t = \{d_{t-1} + 1, d_{t-1} + 2, \ldots, d_t\}, \ \ t = 1, 2, \ldots, g, \tag{5.70}$$

where d_t is the size of the t-th block $\tilde{\mathbf{e}}_{Bi,t}$ given in (5.59) and might be different from each other. Then the initial estimation of the support of the purely sparse vector $\tilde{\mathbf{e}}_i$ in (5.57) can be obtained by picking out the index of the largest entry in each nonzero block, i.e.

$$\Omega_i = \left\{ k \left| k \in \Omega_{Bi}, k = \underset{k \in S_t}{\arg \max} \{|\Delta \tilde{p}'_{i,k}|\}, \ t = 1, 2, \ldots, g \right. \right\}. \tag{5.71}$$

After estimating the block partition, the parameters that need to be learnt can be firstly initialized. Set $\gamma_t^{(0)} = 0$ for zero blocks and $\gamma_t^{(0)} = 1$ for nonzero blocks. According to the BLGN a priori distribution of the NBI as described previously, the variance (auto-covariance) matrix of the purely sparse vector $\tilde{\mathbf{e}}_i$ is a diagonal matrix $\mathbf{V}_{\tilde{\mathbf{e}}_i} \in \mathbb{C}^{N \times N}$ with the diagonal entries being $\{\mathbf{V}_{\tilde{\mathbf{e}}_i}\}_{k,k} = \sigma_e^2$ for $k \in \Omega_i$, and 0 for $k \notin \Omega_i$, because the tone interferers are mutually uncorrelated. According to (5.57), (5.66) and the property of covariance in linear transform, it is derived that

$$\mathbf{V}_{\Delta \tilde{\mathbf{e}}_{Bi}} = |1 - \exp(j2\pi\alpha)|^2 \mathbf{C}_{FO} \mathbf{V}_{\tilde{\mathbf{e}}_i} \mathbf{C}_{FO}^H \stackrel{\Delta}{=} \Sigma_0^{(0)}, \tag{5.72}$$

where $\Sigma_0^{(0)} \in \mathbb{C}^{N \times N}$ is the initialized priori covariance matrix of $\Delta\tilde{\mathbf{e}}_{\mathrm{B}i}$. From (2.28), the intra-block correlation (IBC) matrices $\{\mathbf{B}_t\}_{t=1}^g$ can be initialized by

$$\mathbf{B}_t^{(0)} = \Sigma_0^{(0),t}, t = 1, 2, \ldots, g, \tag{5.73}$$

where $\Sigma_0^{(0),t} \in \mathbb{C}^{d_t \times d_t}$ denotes the corresponding t-th principal diagonal block in $\Sigma_0^{(0)}$. The block sparse NBI signal also has the a priori Gaussian distribution in (5.72), because the purely sparse NBI tone interferers are assumed to be Gaussian distributed, and the spectral leakage due to the frequency offset can be regarded as a linear operation so the generated block sparse NBI signal is still Gaussian distributed based on the random process theory. The background noise follows Gaussian distribution (2.25), and the noise variance $\varepsilon^{(0)}$ can be initialized according to the AWGN distribution or simply set to a value approaching zero [2, 50], where $\varepsilon^{(0)}$ will be adjusted more accurately in the BSBL process.

Then, the BSBL iterations are implemented to recover the block sparse NBI $\Delta\tilde{\mathbf{e}}_{\mathrm{B}i}$ using these initialized parameters. The PE-BSBL algorithm is summarized by the pseudo-code in **Algorithm 3**, where $\bar{\mathbf{x}}^{(k-1),t} \in \mathbb{C}^{d_t}$ is the corresponding t-th block of $\bar{\mathbf{x}}^{(k-1)}$. The output of **Algorithm 3** is the recovered block sparse NBI $\Delta\tilde{\mathbf{e}}_{\mathrm{B}i}$.

In the PE-BSBL algorithm, it is assumed that different blocks might have different sizes, so the IBC matrices $\{\mathbf{B}_t\}_{t=1}^g$ are different from each other and are required to be estimated through the Bayesian learning iterations. The block partition is also required to be estimated before the learning process. In fact, the spectral leakage due to the same frequency offset for different blocks can be regarded as the same. Making use of this observation, we can derive the same IBC matrix for different blocks from the frequency offset matrix $\mathbf{C}_{\mathrm{FO}}$ containing the same pattern of scaling coefficients, before the learning iterations to facilitate the BSBL method, which is described in detail in the next section. Hence, another BSBL based method, Informative BSBL (I-BSBL), is proposed, which is capable of further improving the accuracy of NBI recovery without requiring block partition estimation beforehand.

(3) *Informative Block Sparse Bayesian Learning (I-BSBL) for Block Sparse NBI Reconstruction*

As described previously, for the I-BSBL method, there is no need to estimate the block partition beforehand for initialization. On the other hand, importantly, the IBC within each block caused by the frequency offset can be taken good advantage of as an *informative* aid for the I-BSBL algorithm. The blocks are assumed to have identical size u, and the initial IBC matrices $\{\mathbf{B}_t^{(0)}\}_{t=1}^g$ are initialized to the same matrix $\mathbf{B}^{(0)} \in \mathbb{C}^{u \times u}$, which is more practical since each tone interferer will spread out to the same number of adjacent sub-carriers with the same scaling coefficients due to the same frequency offset. Note that this can also be derived from (5.57) where the t-th column ($t = 1, \ldots, N$) of the circular matrix $\mathbf{C}_{\mathrm{FO}}$ has u significant nonzero entries, i.e. scaling coefficients, around the t-th diagonal entry $(\mathbf{C}_{\mathrm{FO}})_{tt}$, and other entries whose powers are smaller than $\rho|(\mathbf{C}_{\mathrm{FO}})_{tt}|^2$ are neglectable, where ρ is the coefficient used to exclude the insignificant entries.

Algorithm 3 Partition Estimated Block Sparse Bayesian Learning (PE-BSBL)

Input:

    1) Initial IBC parameters $\{\mathbf{B}_t^{(0)}, \gamma_t^{(0)}\}_{t=1}^g$

    2) Initial priori covariance matrix $\Sigma_0^{(0)}$

    3) Initial noise variance $\varepsilon^{(0)}$

    4) Measurement vector $\Delta\mathbf{p}_i'$

    5) Observation matrix $\Phi \overset{\Delta}{=} \mathbf{S}_{G,N}\mathbf{F}_N$

    Initialization:

1:   $\bar{x}^{(0)} \leftarrow \Sigma_0^{(0)}\Phi^T\left(\varepsilon^{(0)}\mathbf{I} + \Phi\Sigma_0^{(0)}\Phi^T\right)^{-1}\Delta\mathbf{p}_i'$

2:   $\Sigma_x^{(0)} \leftarrow \left(\Sigma_0^{(0)-1} + \frac{1}{\varepsilon^{(0)}}\Phi^T\Phi\right)^{-1}$

3:   $\Delta\tilde{\mathbf{e}}_{\mathrm{B}i}^{(0)} \leftarrow \bar{x}^{(0)}, \; \zeta \leftarrow 1 \times 10^{-8}, \; k \leftarrow 0$

    Iterations:

4: **repeat**

5:     $k \leftarrow k+1$ {Next iteration}

6:     $\gamma_t^{(k)} \leftarrow \frac{1}{d_t}\mathrm{Tr}\left[\left(\mathbf{B}_t^{(k-1)}\right)^{-1}\left(\Sigma_x^{(k-1),t} + \bar{x}^{(k-1),t}\left(\bar{x}^{(k-1),t}\right)^T\right)\right]$

7:     $\varepsilon^{(k)} \leftarrow \frac{1}{G}\left[\left\|\Delta\mathbf{p}_i' - \Phi\bar{x}^{(k-1)}\right\|_2^2 + \mathrm{Tr}\left(\Sigma_x^{(k-1)}\Phi^H\Phi\right)\right]$

8:     $\mathbf{B}_t^{(k)} \leftarrow \frac{1}{\gamma_t^{(k)}}\left[\Sigma_x^{(k-1),t} + \bar{x}^{(k-1),t}\left(\bar{x}^{(k-1),t}\right)^T\right]$

9:     $\Sigma_0^{(k)} \leftarrow \mathrm{diag}\left\{\gamma_1^{(k)}\mathbf{B}_1^{(k)}, \gamma_2^{(k)}\mathbf{B}_2^{(k)}, \cdots \gamma_g^{(k)}\mathbf{B}_g^{(k)}\right\}$

10:    $\bar{x}^{(k)} \leftarrow \Sigma_0^{(k)}\Phi^H\left(\varepsilon^{(k)}\mathbf{I} + \Phi\Sigma_0^{(k)}\Phi^H\right)^{-1}\Delta\mathbf{p}_i'$

11:    $\Sigma_x^{(k)} \leftarrow \left(\Sigma_0^{(k)-1} + \frac{1}{\varepsilon^{(k)}}\Phi^T\Phi\right)^{-1}$

12:    $\Delta\tilde{\mathbf{e}}_{\mathrm{B}i}^{(k)} \leftarrow \bar{x}^{(k)}$ {The k-th MAP estimation}

13: **until**

     $\left(\frac{1}{N}\left\|\Delta\tilde{\mathbf{e}}_{\mathrm{B}i}^{(k)} - \Delta\tilde{\mathbf{e}}_{\mathrm{B}i}^{(k-1)}\right\|_1 < \zeta \;\; \& \;\; \left\|\Delta\mathbf{p}_i - \Phi\Delta\tilde{\mathbf{e}}_{\mathrm{B}i}^{(k)}\right\|_2^2 < \varepsilon^{(k)}\right)$ {Halting condition}

Output:

    Recovered block sparse NBI vector $\Delta\tilde{\mathbf{e}}_{\mathrm{B}i} = \Delta\tilde{\mathbf{e}}_{\mathrm{B}i}^{(k)}$

    According to the BSBL theory, the algorithm process towards learning the parameters are not sensitive to the choice of the block size u [50]. If a suitable u is selected by configuring a very small ρ, such as $\rho = 0.01$, the algorithm can avoid excluding significant entries at the cost of a slight increase in computational complexity. Any tone interferer in $\tilde{\mathbf{e}}_i$ will spread out to the same extent to generate a block in $\tilde{\mathbf{e}}_{\mathrm{B}i}$ with the same block size of u located around this tone interferer, and the IBC of different blocks is identical. Exploiting this property, the identical IBC matrix $\mathbf{B}^{(0)}$ can be exactly initialized from the frequency offset matrix $\mathbf{C}_{\mathrm{FO}}$.

Firstly, an artificial *non-overlapping* block-sparse representation of the NBI is built up in order to cope with the unknown block partition. Since the block partition is unknown, the blocks can be located at arbitrary positions and might overlap with each other. There might be in total $N_B \overset{\Delta}{=} N - u + 1$ overlapping blocks in $\Delta\tilde{\mathbf{e}}_{Bi}$, and the t-th block starts and ends at the t-th and $(t + u - 1)$-th entries, respectively. All the nonzero entries of $\Delta\tilde{\mathbf{e}}_{Bi}$ lie within a subset of these N_B blocks. Since the tone interferers of $\tilde{\mathbf{e}}_i$ follow a BLGN distribution and the operation of (5.57) is linear, the t-th block follows a multivariate Gaussian distribution with the covariance matrix of $\gamma_t \mathbf{B}_t$, where $\mathbf{B}_t \in \mathbb{C}^{u \times u}$. As described in Sect. 2.4.3, the prior distribution of the block sparse NBI follows $\Delta\tilde{\mathbf{e}}_{Bi} \sim \mathcal{N}(\mathbf{0}, \Sigma_0)$, but Σ_0 is no longer block diagonal due to the overlapping of blocks. Each $\gamma_t \mathbf{B}_t$ lies along its principal diagonal and might overlap other neighboring $\gamma_j \mathbf{B}_j (t \neq j)$. Hence, the typical BSBL framework described in the PE-BSBL method requires some modifications to be applicable in the I-BSBL method. The covariance matrix Σ_0 can be expanded to a non-overlapping block diagonal matrix $\tilde{\Sigma}_0 \in \mathbb{C}^{N_B u \times N_B u}$ given by

$$\tilde{\Sigma}_0 = \text{diag}\{\gamma_1 \mathbf{B}_1, \ldots, \gamma_{N_B} \mathbf{B}_{N_B}\}, \tag{5.74}$$

where $\{\gamma_t \mathbf{B}_t\}_{t=1}^{N_B}$ no longer overlap with each other. Then the block sparse vector $\Delta\tilde{\mathbf{e}}_{Bi}$ can be decomposed as follows

$$\Delta\tilde{\mathbf{e}}_{Bi} = \sum_{t=1}^{N_B} \mathbf{E}_t \mathbf{z}_t, \tag{5.75}$$

where each non-overlapping block is denoted by $\mathbf{z}_t \in \mathbb{C}^u$, $\mathbb{E}\{\mathbf{z}_t\} = \mathbf{0}$, $\mathbb{E}\{\mathbf{z}_t \mathbf{z}_j^T\} = \delta_{tj} \gamma_t \mathbf{B}_t$ ($\delta_{tj} = 1$ for $t = j$, otherwise $\delta_{tj} = 0$), and the equivalent block sparse vector $\mathbf{z} \overset{\Delta}{=} \left[\mathbf{z}_1^T, \ldots \mathbf{z}_{N_B}^T\right]^T \sim \mathcal{N}_z(\mathbf{0}, \tilde{\Sigma}_0)$. $\mathbf{E}_t \in \mathbb{C}^{N \times u}$ is a zero matrix except that its t-th to $(t + u - 1)$-th rows are replaced by the identity matrix $\mathbf{I}_u$. Obviously, the block partition of the artificial block-sparse vector $\mathbf{z}$ is trivial and known, since $\mathbf{z}$ is simply composed of N_B neighboring blocks with size of u. Now the equivalent I-BSBL framework corresponding to (5.65) can be established as

$$\Delta\mathbf{p}_i' = \sum_{t=1}^{N_B} \mathbf{S}_{G,N} \mathbf{F}_N \mathbf{E}_t \mathbf{z}_t + \Delta\mathbf{w}' \overset{\Delta}{=} \mathbf{A}\mathbf{z} + \Delta\mathbf{w}', \tag{5.76}$$

where $\mathbf{A} \overset{\Delta}{=} \left[\mathbf{A}_1, \ldots \mathbf{A}_{N_B}\right]$ with $\mathbf{A}_t \overset{\Delta}{=} \mathbf{S}_{G,N} \mathbf{F}_N \mathbf{E}_t$. In this way, the block sparse representation for the I-BSBL method is built and is consistent with the typical BSBL framework given in Sect. 2.4.3, since the blocks in $\mathbf{z}$ no longer overlap with each other. It is also derived that $\mathbf{z}$ follows a multivariate distribution. Since the block partition of $\mathbf{z}$ is known, the unknown parameters of the distribution can be learnt through the proposed I-BSBL algorithm whose pseudocode is given in **Algorithm 4**.

Algorithm 4 Informative Block Sparse Bayesian Learning (I-BSBL)

Input:

    1) Informative IBC matrix $\{\mathbf{B}_t^{(0)} = \mathbf{B}^{(0)}, \gamma_t^{(0)} = \gamma^{(0)}\}_{t=1}^{N_B}$

    2) Informative priori covariance matrix $\tilde{\Sigma}_0^{(0)}$

    3) Initial noise variance $\varepsilon^{(0)}$

    4) Block sparse differential measurement vector $\Delta\mathbf{p}_i'$

    5) *Equivalent* observation matrix $\mathbf{A} \overset{\Delta}{=} \left[\mathbf{A}_1, \cdots \mathbf{A}_{N_B}\right]$,

       where $\mathbf{A}_t \overset{\Delta}{=} \mathbf{S}_{G,N}\mathbf{F}_N\mathbf{E}_t$

    Initialization:

1:   $\bar{x}^{(0)} \leftarrow \tilde{\Sigma}_0^{(0)}\mathbf{A}^T\left(\varepsilon^{(0)}\mathbf{I} + \mathbf{A}\tilde{\Sigma}_0^{(0)}\mathbf{A}^T\right)^{-1}\Delta\mathbf{p}_i'$

2:   $\Sigma_x^{(0)} \leftarrow \left((\tilde{\Sigma}_0^{(0)})^{-1} + \frac{1}{\varepsilon^{(0)}}\mathbf{A}^T\mathbf{A}\right)^{-1}$

3:   $\mathbf{z}^{(0)} \leftarrow \bar{x}^{(0)},\ \zeta \leftarrow 1 \times 10^{-8},\ k \leftarrow 0$

    Iterations:

4: **repeat**

5:     $k \leftarrow k + 1$ {Next iteration}

6:     $\gamma_t^{(k)} \leftarrow \frac{1}{u}\mathrm{Tr}\left[\left(\mathbf{B}^{(0)}\right)^{-1}\left(\Sigma_x^{(k-1),t} + \bar{x}^{(k-1),t}\left(\bar{x}^{(k-1),t}\right)^T\right)\right]$

7:     $\varepsilon^{(k)} \leftarrow \frac{1}{G}\left[\left\|\Delta\mathbf{p}_i' - \mathbf{A}\bar{x}^{(k-1)}\right\|_2^2 + \mathrm{Tr}\left(\Sigma_x^{(k-1)}\mathbf{A}^H\mathbf{A}\right)\right]$

8:     $\Sigma_0^{(k)} \leftarrow \mathrm{diag}\left\{\gamma_1^{(k)}\mathbf{B}^{(0)}, \gamma_2^{(k)}\mathbf{B}^{(0)}, \cdots \gamma_{N_B}^{(k)}\mathbf{B}^{(0)}\right\}$

9:     $\bar{x}^{(k)} \leftarrow \Sigma_0^{(k)}\mathbf{A}^H\left(\varepsilon^{(k)}\mathbf{I} + \mathbf{A}\Sigma_0^{(k)}\mathbf{A}^H\right)^{-1}\Delta\mathbf{p}_i'$

10:    $\Sigma_x^{(k)} \leftarrow \left((\Sigma_0^{(k)})^{-1} + \frac{1}{\varepsilon^{(k)}}\mathbf{A}^T\mathbf{A}\right)^{-1}$

11:    $\mathbf{z}^{(k)} \leftarrow \bar{x}^{(k)}$ {The k-th MAP estimation}

12: **until**

     $\left(\frac{1}{uN_B}\left\|\mathbf{z}^{(k)} - \mathbf{z}^{(k-1)}\right\|_1 < \zeta\ \ \&\ \ \left\|\Delta\mathbf{p}_i - \mathbf{A}\mathbf{z}^{(k)}\right\|_2^2 < \varepsilon^{(k)}\right)$

                             {Halting condition}

Output:

    Recovered *equivalent* block sparse vector $\mathbf{z} = \mathbf{z}^{(k)}$

The parameters in (5.74) for the I-BSBL model (5.76) should be initialized to be input into the process of **Algorithm 4**. As has been analyzed, the IBC matrices (covariance matrix of each block) are identical for realistic NBI with frequency offset. The covariance between any pair of entries within a certain block can be calculated by multiplying their corresponding significant entries (scaling coefficients) in the frequency offset matrix $\mathbf{C}_{\mathrm{FO}}$ given by (5.57). Thus, the IBC matrix $\mathbf{B}^{(0)} \in \mathbb{C}^{u \times u}$ can be accurately initialized as

$$\mathbf{B}^{(0)} = \sigma_e^2[b_1, b_2 \ldots, b_u]^H [b_1, b_2 \ldots, b_u], \tag{5.77}$$

where each corresponding significant entry b_j is given by

$$b_j = (\mathbf{C}_{\text{FO}})_{j \lfloor \frac{u+1}{2} \rfloor}, \quad j = 1, 2, \ldots, u, \tag{5.78}$$

where $\lfloor \cdot \rfloor$ is the floor operator. Because any block of the N_B possible blocks might be nonzero or zero blocks with equal probability, it is assumed that $\gamma_t^{(0)} = \gamma^{(0)} = 1/2, t = 1, \ldots, N_\text{B}$ during the initialization phase, and will be updated to asymptotically approaching either 0 or 1 by the I-BSBL algorithm. Thus, it is derived that the non-overlapping covariance matrix (5.74) is initialized by

$$\tilde{\Sigma}_0^{(0)} = \frac{1}{2} \text{diag}\{\underbrace{\mathbf{B}^{(0)}, \ldots, \mathbf{B}^{(0)}}_{N_\text{B} \text{ blocks}}\}. \tag{5.79}$$

After initialization, now the I-BSBL model in (5.76) can be solved by the proposed **Algorithm 4**. By exploiting the prior informative parameters (the IBC matrix $\mathbf{B}^{(0)}$, the covariance matrix $\tilde{\Sigma}_0^{(0)}$, and γ_t) in the extended equivalent framework given by (5.76), the equivalent block sparse vector $\mathbf{z}$ will be accurately recovered by **Algorithm 4** after the learning iterations, and thus the NBI vector $\Delta \tilde{\mathbf{e}}_{\text{B}i}$ is recovered from (5.75).

Till now, we have successfully recovered the block sparse NBI vector, from which the NBI vectors located at the OFDM blocks can be derived due to the temporal correlation of the NBI. The block sparse NBI vector $\tilde{\mathbf{e}}_{\text{BX}i}$ given by (5.63) located at the i-th OFDM block should be calculated for final cancelation. The block sparse differential NBI vector $\Delta \tilde{\mathbf{e}}_{\text{B}i}$ recovered by the proposed PE-BSBL or I-BSBL algorithms can be exploited to derive the block sparse NBI $\tilde{\mathbf{e}}_{\text{B}i}$ located at the i-th CP according to (5.66) as follows,

$$\tilde{\mathbf{e}}_{\text{B}i} = \frac{1}{1 - \exp(j2\pi\alpha)} \Delta \tilde{\mathbf{e}}_{\text{B}i} \tag{5.80}$$

Then $\tilde{\mathbf{e}}_{\text{BX}i}$ can be directly acquired from $\tilde{\mathbf{e}}_{\text{B}i}$ using (5.63). Afterwards, the NBI signal $\tilde{\mathbf{e}}_{\text{BX}i}$ can be completely and accurately canceled from the received i-th frequency-domain OFDM block $\mathbf{X}_i$ to obtain the NBI-free OFDM block $\mathbf{X}_i^0$, as given by (5.67). In this way, the receivers in LTE-A systems are free from the interference generated by the in-band working NB-IoT signals.

5.5.3 Simulation Results and Discussions

The performance of the estimation accuracy and the recovery probability for the proposed BSBL underlying NBI cancelation methods in LTE-A systems is evaluated by extensive simulations in this section. The active data OFDM sub-carrier number is $N = 600$ (when the number of resource block is 50 [27]), and the length of each CP is $V = 144$, as specified in the LTE-A standard [27]. The sub-carrier spacing is 15 kHz, so the occupied active data bandwidth is configured as 9.0 MHz [27], leading to

a CP duration of 4.68 µs. The equivalent baseband multipath six-tap channel, ITU-R Vehicular-A channel model [38] in the presence of NBI with frequency offset, which is widely used to emulate the wireless mobile channel, is applied, where the user equipment (UE) receiver velocity of 20 km/h is used to present the typical low-speed mobile channel. The maximum delay spread of the Vehicular-A channel is 2.51 µs, which is equivalent to the discrete channel length $L = 76$, so the size of the IBI-free region is $G = 68$.[1]
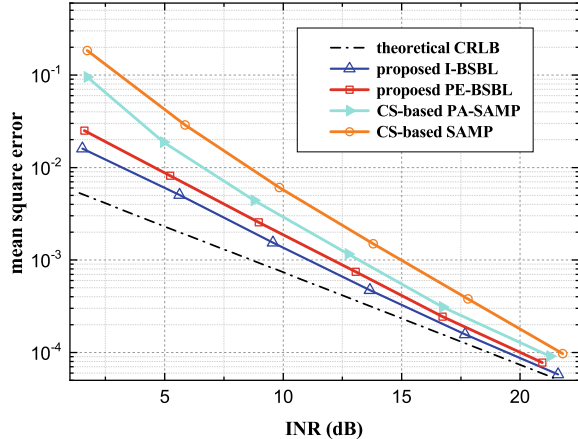
Each tone interferer of the NBI generated by the NB-IoT signal follows a Gaussian distribution. The frequency offset of the NBI is configured a priori known as $\alpha = 0.20$ in the simulations, while it can also be effectively estimated at the receiver through the grid search method [49] in realistic implementation. Since each NB-IoT signal occupies a bandwidth of 200 kHz according to the NB-IoT specifications [21], which is equivalent to 13 sub-carriers in the LTE-A spectrum, the sparsity level of the NBI is assumed to be $K = 13$ in the simulations to emulate one NB-IoT interfering source signal in the LTE-A system. To make the NBI model more general, the support Ω_i of the NBI is assumed to follow a uniform distribution U $[0, N - 1]$ among all the N sub-carriers.[2] Besides, the NBI recovery performance of the previously proposed CS based methods, including sparsity adaptive matching pursuit (SAMP) [36] and the a priori aided SAMP (PA-SAMP), are also evaluated using the same wireless system setup and reported for comparison.

The mean square error (MSE) performance of NBI recovery using the proposed and existing methods are shown in Fig. 5.18. The performances of the proposed BSBL based methods (PE-BSBL and I-BSBL for the recovery of the NBI associated with each CP-OFDM symbol) and the classical CS-based methods (PA-SAMP and SAMP algorithms using the preamble to estimate the NBI) are depicted with the original sparsity level $K = 13$. The theoretical Cramer-Rao lower bound (CRLB) calculated by $2\sigma_w^2(K/V)$ [51] is also included as a benchmark. It is noted from Fig. 5.18 that the I-BSBL and PE-BSBL methods achieve a target MSE of 10^{-3} at the INR of 11.1 and 12.0 dB, respectively, and the I-BSBL approach outperforms the CS-based algorithms, i.e. PA-SAMP and SAMP, by approximately 2.2 and 3.9 dB, respectively. It is also observed that the MSE of the proposed BSBL-based algorithm is asymptotically approaching the theoretical CRLB with the increase of the INR, verifying the validity and accuracy of the proposed methods. The increase of the INR implies that the intensity of the NBI is increased with respect to the background AWGN power, making the NBI signal as measured in the block sparse representation (5.65) easier to reconstruct, and more accurate. Besides, it is indicated

---

[1]In the simulations, the size of IBI-free region can be pre-determined according to the system configuration of frame length and the maximum channel delay spread of the adopted channel. In realistic implementation, the maximum channel delay spread can also be obtained from the prior knowledge of the channel environment and channel statistics, or from the coarse channel estimation at the receiver.

[2]The parameter K represents the sparsity level of the purely sparse NBI vector without frequency offset, and the number of the nonzero blocks in the block sparse NBI signal with frequency offset is $K_g = K$ as described previously.

Fig. 5.18 MSE performance comparison of the proposed BSBL-based and the CS-based methods for NBI recovery in the LTE-A system under the wireless Vehicular-A channel
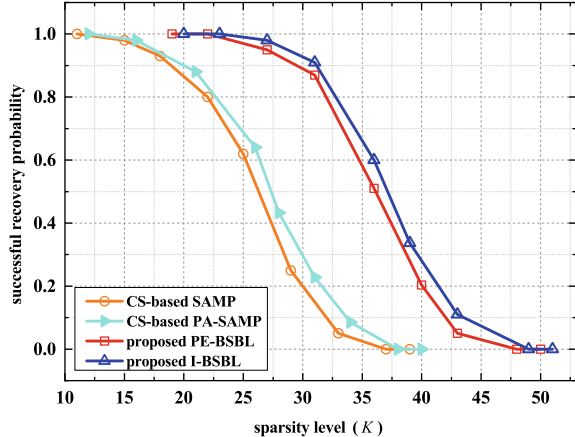
by the simulation results that, the BSBL-based methods outperform the CS-based ones in recovery performance with a low INR.
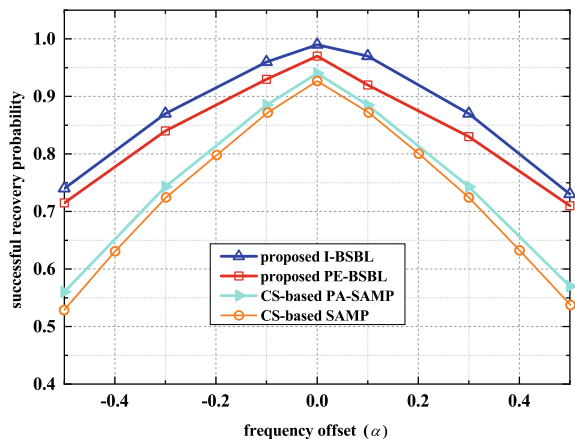
The recovery probability of the proposed NBI recovery method with respect to different sparsity levels is depicted in Fig. 5.19 with the INR = 30 dB. The recovery probability is defined as the rate of the successful NBI estimations (correct support estimation and MSE $< 10^{-3}$) to the total estimations. It is noted that the BSBL based methods and the CS based methods reach a successful recovery probability of 0.90 at the sparsity level of $K = 31$ and $K = 20$, respectively, which indicates that the proposed methods can accurately recover the NBI with large sparsity levels from the acquired measurement data that only has quite a small size. Since each NB-IoT signal occupies 13 sub-carriers in LTE-A spectrum, it is inferred that the proposed BSBL method is capable of effectively recovering and canceling at least 2 in-band NB-IoT interfering signals in the LTE-A system. Moreover, from the gap between the curves of the proposed BSBL and CS based methods, it is implied that the proposed BSBL based methods are more robust to larger sparsity levels, and that the BSBL based methods are particularly effective in recovering the block spare NBI signal that has more nonzero entries due to the spectral spread caused by the frequency offset of the NBI. It can also be noted from Fig. 5.19 that, CS-based methods cannot reach 100% successful recovery in the presence of 1 NB-IoT interfering signal (corresponding to $K = 13$), whereas the proposed BSBL methods have stable 100% successful recovery probability in this case.

To measure the influence of the frequency offset α of the NBI on the proposed methods, the recovery probability with respect to the frequency offset α under the Vehicular-A channel is illustrated in Fig. 5.20, where the frequency offset ranges within $\alpha \in (-1/2, 1/2]$ and $K = 13$ and INR = 30 dB. It is noted from Fig. 5.20 that with the increase of the frequency offset absolute value $|\alpha|$, the recovery successful rate of each method decreases. It is worthwhile to be noted from Fig. 5.20 that, the proposed I-BSBL and PE-BSBL algorithms significantly outperform the conventional CS-based PA-SAMP and SAMP methods that ignore the IBC within

Fig. 5.19 Successful probability of NBI recovery using the proposed BSBL and CS based methods in the LTE-A system under the wireless Vehicular-A channel

Fig. 5.20 NBI recovery probability with respect to different values of frequency offset α in the LTE-A system under the wireless Vehicular-A channel

the blocks. With the increase of the frequency offset, each tone interferer spreads out to a wider block, and it is observed that the gain of the proposed BSBL methods over the CS-based methods grows larger. This implies that the two proposed BSBL based methods can fully exploit the IBC within the blocks of the NBI, whereas the CS-based methods cannot. By initializing in advance and iteratively learning the IBC parameters, a more accurate BSBL process is facilitated to achieve a better recovery performance than the CS-based methods. Note that when $\alpha = 0$ and the block sparse NBI turns to a purely sparse signal, the BSBL methods still outperform the existing CS-based counterparts, because the purely sparse vector is a special case of block sparse vectors where all block sizes are one, and the *a priori* NBI parameter distribution is fully exploited by the BSBL approach and refined more accurate through learning process.

5.6 Performance Analysis of Algorithms

(1) *Computational and Time Complexity Analysis*

First, we analyze the computational complexity of different algorithms, and compare the computational complexity of the CS-based greedy algorithms of SAMP, PA-SAMP, and the structured compressed sensing based greedy algorithm S-SAMP.

For the SAMP algorithm, in each iteration, the computational complexity mainly comes from two parts: one is the complexity needed by the inner product of the measurement matrix and the residue vector, i.e. $\mathcal{O}(MN)$, and the other is the complexity needed by solving the equivalent least squares problem of estimating the temporal sparse vector using the temporal support, i.e. $\mathcal{O}(MK)$. The average iteration number is K. Thus, the total computational complexity of the SAMP algorithm is $\mathcal{O}(M(K + N)K)$.

For the PA-SAMP algorithm, due to the introduction of the prior information, the complexity is different from that of SAMP. To obtain the prior information of the partial support of the sparse vector requires the FFT operation, so the complexity of $\mathcal{O}(N \log_2(N))$ is required. Since the partial support (K_0 in total) is used as the prior information, the average iteration number reduces from K for SAMP downto $K - K_0$ for PA-SAMP. Thus, the total computational complexity of PA-SAMP is $\mathcal{O}(M(K + N)(K - K_0))$.

For the S-SAMP algorithm, the complexity of the spatial multiple differential measuring for the N_r antennas is $\mathcal{O}(MN_r)$. In the iteration process, the complexity of the matrix multiplication between the observation matrix and the residue matrix is $\mathcal{O}(N_r MN)$ for each iteration, and the complexity of the equivalent multi-dimensional least squares problem using the temporal support for the estimation of the temporal jointly sparse matrix is $\mathcal{O}(N_r MK)$. Hence, the total complexity of the S-SAMP algorithm is $\mathcal{O}(N_r M + K N_r M(N + K))$.

Second, to quantitatively measure the runtime of different algorithms, the average number of iterations for the structured compressed sensing based S-SAMP algorithm, the prior aided compressed sensing based PA-SAMP algorithm, the classical compressed sensing based SAMP algorithm, and the OMP algorithm is listed in Table 5.4, where the average number is calculated over 10^3 simulations of NBI recovery. It is indicated by the simulation results that, the average iteration number required by the proposed structured compressed sensing based S-SAMP algorithm is much less than that of the classical compressed sensing based SAMP algorithm. In MIMO systems, the proposed SMDM method along with the S-SAMP algorithm exploiting the temporal-spatial two-dimensional correlation of the NBI for NBI recovery and cancelation has a significant higher convergence rate. Besides, it is shown by the simulation results that, the prior aided information can make the PA-SAMP algorithm have a faster convergence rate and less iteration number compared with the classical SAMP algorithm [36] or the OMP algorithm [46]. Therefore, it is verified that the proposed S-SAMP and PA-SAMP algorithms have a lower time complexity.

Table 5.4 Average number of iterations to reach correct NBI recovery for different algorithms

sparsity level	S-SAMP	PA-SAMP	SAMP [36]	OMP [46]
4	2.42	2.89	3.36	3.93
8	3.79	5.67	7.14	7.72
12	8.63	10.16	12.10	12.23

(2) *Convergence Performance and Solution Existence of the Algorithms*

Now we investigate the solution existence and the accuracy of the solution for the previously described structured compressed sensing multiple measurement vectors problem (5.38), as well as its derivative problem, i.e. the mixed $\ell_{1,2}$-norm minimization problem (5.41). First, we provide Theorem 5.1 to prove that the spatially jointly sparse NBI matrix $\Delta\tilde{\mathbf{E}}$ needed to be recovered in the SCS-MMV model (5.38) can be obtained by solving the mixed $\ell_{1,2}$-norm minimization problem (5.41). Then the existence and accuracy of the solution will be guaranteed. In order to prove Theorem 5.1, we first provide the following lemma:

Lemma 5.1 *Assume that* $\mathbf{y} = \mathbf{\Psi}\mathbf{x}_0 + \mathbf{w}$ *is a noisy measurement of an arbitrary vector* $\mathbf{x}_0 \in \mathbb{C}$, *and let the block-sparse vector* $\mathbf{x}^K$ *denote the optimal* K-block-sparse *approximation of* $\mathbf{x}_0$, *such that*

$$\mathbf{x}^K = \arg\min_{\mathbf{x}^K} \left\| \mathbf{x}^K - \mathbf{x}_0 \right\|_{2,\Gamma}, \quad \forall \text{ block-}K\text{-sparse } \mathbf{x}^K. \tag{5.81}$$

Assume that $\hat{\mathbf{x}}$ *is a solution of the following mixed* l_2/l_1-norm minimization problem:

$$\hat{\mathbf{x}} = \min_{\mathbf{x}} \|\mathbf{x}\|_{2,\Gamma} = \min_{\mathbf{x}} \sum_{i=1}^{N_B} \|\mathbf{x}[i]\|_2 \quad \text{s.t. } \|\mathbf{y} - \mathbf{\Psi}\mathbf{x}\|_2 \leq \epsilon. \tag{5.82}$$

If $\mathbf{\Psi}$ *satisfies the* block-RIP *property with the parameter of* $\delta_{2K}^{(B)} < \sqrt{2} - 1$, *and then we have*

$$
\begin{aligned}
\left\| \hat{\mathbf{x}} - \mathbf{x}_0 \right\|_2 \leq {} & \frac{2(1-\delta_{2K}^{(B)})}{1-(1+\sqrt{2})\delta_{2K}^{(B)}} K^{-1/2} \left\| \mathbf{x}^K - \mathbf{x}_0 \right\|_{2,\Gamma} \\
& + \frac{4\sqrt{1+\delta_{2K}^{(B)}}}{1-(1+\sqrt{2})\delta_{2K}^{(B)}} \epsilon.
\end{aligned}
\tag{5.83}
$$

where the definitions of block sparsity and block-RIP are given in Definition 2.3 and Eq. (2.21). The content of Lemma 5.1 and its proof can be referred to the related content of Theorem 2 in literature [52], so the details of the proof are omitted here. Then, in order to guarantee the existence and accuracy of the solution of the SCS-MMV problem (5.38) and the mixed $\ell_{1,2}$-norm minimization problem (5.41), we provide the following theorem.

Theorem 5.1 *Let K denote the sparsity level of the actual NBI signal. The spatially jointly sparse NBI matrix $\Delta\hat{\mathbf{E}}$ obtained by solving the mixed $\ell_{1,2}$-norm minimization problem (5.41) is the optimal approximation of the actual NBI matrix $\Delta\tilde{\mathbf{E}}$ in the noisy measurement (5.38), which makes the following statement hold, i.e.*

$$\left\| \Delta\hat{\mathbf{E}} - \Delta\tilde{\mathbf{E}} \right\|_{2,2} \leq C_K^{(B)} \cdot \epsilon, \tag{5.84}$$

if the block-sparse observation matrix $\Psi_B = (\mathbf{F}_M \otimes \mathbf{I}_{N_r})$ generated by the observation matrix $\mathbf{F}_M$ given by Eq. (5.38) satisfies the block-RIP condition with the block-RIP parameter of $\delta_{2K}^{(B)} < \sqrt{2} - 1$, where

$$C_K^{(B)} = \frac{4\sqrt{1 + \delta_{2K}^{(B)}}}{1 - (1 + \sqrt{2})\delta_{2K}^{(B)}}. \tag{5.85}$$

The detailed proof of Theorem 5.1 is provided as follows.

Proof Let vec($\mathbf{A}$) denote the vectorization operation of a matrix, which returns a vector composed of all the columns of the matrix $\mathbf{A}$. First, the SCS-MMV measurement model (5.38) is vectorized into:

$$\text{vec}\left(\Delta\mathbf{Y}^T\right) = \left(\mathbf{F}_M \otimes \mathbf{I}_{N_r}\right)\text{vec}\left(\Delta\tilde{\mathbf{E}}^T\right) + \text{vec}\left(\Delta\mathbf{W}^T\right) \tag{5.86}$$

where vec($\Delta\mathbf{Y}^T$) and vec($\Delta\tilde{\mathbf{E}}^T$) are the high-dimensional vectors derived by the vectorization of all the rows of $\Delta\mathbf{Y}$ and $\Delta\tilde{\mathbf{E}}$. Define the block-sparse NBI vector as $\mathbf{x} \triangleq \text{vec}(\Delta\tilde{\mathbf{E}}^T)$. In the vectorization, the original observation matrix $\mathbf{F}_M$ is also turned into $\left(\mathbf{F}_M \otimes \mathbf{I}_{N_r}\right)$, where $\otimes$ denotes the operation of Kronecker product. Then, the mixed $\ell_{1,2}$-norm minimization problem (5.41) is vectorized and turned into a mixed ℓ_2/ℓ_1-norm minimization problem as:

$$\hat{\mathbf{x}} = \arg\min_{\mathbf{x} \in \mathbb{C}^{NN_r}} \|\mathbf{x}\|_{2,\Gamma},$$

$$\mathbf{x} = \text{vec}\left(\Delta\tilde{\mathbf{E}}^T\right), \hat{\mathbf{x}} = \text{vec}(\Delta\hat{\mathbf{E}}^T), \tag{5.87}$$

$$\Gamma = \{d_1, \ldots, d_{N_B}\}, \ N_B = N, \ d_i = N_r \ \forall i, \tag{5.88}$$

$$\text{s.t. } \left\| \text{vec}\left(\Delta\mathbf{Y}^T\right) - \left(\mathbf{F}_M \otimes \mathbf{I}_{N_r}\right)\mathbf{x} \right\|_2 \leq \epsilon, \tag{5.89}$$

where $\mathbf{x}$ is the block-sparse vector composed of the vectorization of all the rows of $\Delta\tilde{\mathbf{E}}$. It can be noted from the principle of vectorization that, the block partition is naturally generated by row as shown by Eq. (5.88), where the number of sub-blocks $N_B = N$, and each sub-block $\mathbf{x}[i]$ represents the i-th row of $\Delta\tilde{\mathbf{E}}$. The mixed ℓ_2/ℓ_1-norm $\|\mathbf{x}\|_{2,\Gamma}$ is given by Eq. (2.20).

Then we can complete the proof of this theorem based on Lemma 5.1. Consider the conditions of Lemma 5.1, the noisy measurement of the block-sparse vector $\mathbf{x} \overset{\Delta}{=} \text{vec}(\Delta \tilde{\mathbf{E}}^T)$ is given by Eq. (5.86), while the solution of the mixed ℓ_2/ℓ_1-norm minimization problem given by (5.87) as described in Eq. (5.82) in Lemma 5.1 is the estimated block-sparse vector $\hat{\mathbf{x}}$.

Thus, consider that the optimal K-block-sparse approximation of the actual NBI vector $\mathbf{x}_0$ to be estimated is given by Eq. (5.81). For this theorem, since the sparsity level of the actual NBI signal is K, the actual NBI vector $\mathbf{x}_0$ to be estimated in Eq. (5.86) is already K-block-sparse (NOT an arbitrary vector) on the block partition Γ given by Eq. (5.88). Hence, $\mathbf{x}^K$ can be calculated as:

$$\mathbf{x}^K = \underset{\forall K\text{-block-sparse } \mathbf{x}^K}{\arg\min} \left\| \mathbf{x}^K - \mathbf{x}_0 \right\|_{2,\Gamma} = \mathbf{x}_0. \tag{5.90}$$

According to the conditions of this theorem, the block observation matrix ($\mathbf{F}_M \otimes \mathbf{I}_{N_r}$) generated by Eq. (5.86) satisfies the block-RIP condition with the block-RIP parameter of $\delta_{2K}^{(\text{B})} < \sqrt{2} - 1$. Thus, according to Lemma 5.1, we have the following conclusion:

$$
\begin{aligned}
\left\| \hat{\mathbf{x}} - \mathbf{x}_0 \right\|_2 &\leq \frac{2(1 - \delta_{2K}^{(\text{B})})}{1 - (1 + \sqrt{2})\delta_{2K}^{(\text{B})}} K^{-1/2} \left\| \mathbf{x}^K - \mathbf{x}_0 \right\|_{2,\Gamma} \\
&\quad + \frac{4\sqrt{1 + \delta_{2K}^{(\text{B})}}}{1 - (1 + \sqrt{2})\delta_{2K}^{(\text{B})}} \epsilon.
\end{aligned}
\tag{5.91}
$$

as described by Eq. (5.90), $\mathbf{x}^K = \mathbf{x}_0$, thus the first term to the right of Eq. (5.91) turns zero. Thus, we have

$$\left\| \hat{\mathbf{x}} - \mathbf{x}_0 \right\|_2 \leq \frac{4\sqrt{1 + \delta_{2K}^{(\text{B})}}}{1 - (1 + \sqrt{2})\delta_{2K}^{(\text{B})}} \epsilon, \tag{5.92}$$

substituting $\hat{\mathbf{x}}$ and $\mathbf{x}_0$ with $\text{vec}(\Delta \hat{\mathbf{E}}^T)$ and $\text{vec}(\Delta \tilde{\mathbf{E}}^T)$, respectively, yields

$$\left\| \text{vec}(\Delta \hat{\mathbf{E}}^T) - \text{vec}(\Delta \tilde{\mathbf{E}}^T) \right\|_2 \leq \frac{4\sqrt{1 + \delta_{2K}^{(\text{B})}}}{1 - (1 + \sqrt{2})\delta_{2K}^{(\text{B})}} \epsilon. \tag{5.93}$$

Note that the mixed $\ell_{1,2}$-norm minimization problem in Eq. (5.87) and the block-sparse measurement model in Eq. (5.86) are the vectorization form of the mixed $\ell_{1,2}$-norm minimization problem in Eq. (5.41) and the SCS-MMV-based multiple measurement model in Eq. (5.38), respectively. Thus, through the inverse operation of turning the vectorized vector back to the original matrix, we have

$$
\begin{aligned}
\left\| \Delta \hat{\mathbf{E}} - \Delta \tilde{\mathbf{E}}_0 \right\|_{2,2} &= \left\| \text{vec}(\Delta \hat{\mathbf{E}}^T) - \text{vec}(\Delta \tilde{\mathbf{E}}_0^T) \right\|_2 \\
&\leq \frac{4\sqrt{1 + \delta_{2K}^{(\text{B})}}}{1 - (1 + \sqrt{2})\delta_{2K}^{(\text{B})}} \varepsilon_S,
\end{aligned}
\tag{5.94}
$$

where it is obvious that the first equality holds: according to the definition in Eq. (5.40), the $\ell_{2,2}$-norm of a matrix calculates the squared power of all the entries of the matrix, while the ℓ_2-norm of the vectorized column vector also calculates the squared power of all the same entries. Consequently, we have finished the proof of this theorem from Eq. (5.94). □

In essence, the proof is derived by turning the mixed $\ell_{1,2}$-norm minimization problem (5.41) into a block-sparse problem in the form of Eq. (5.82) equivalently. Then, by vectorizing the spatially jointly sparse NBI matrix $\Delta\hat{\mathbf{E}}$ by row into the block-sparse framework given by Eq. (5.82), and combined with the constraints of the SCS-MMV problem given by Eq. (5.41), each row of the matrix $\Delta\hat{\mathbf{E}}$ is regarded as a sub-block of the block-sparse model. Then, based on Lemma 5.1 and the equivalent block-sparsity in row of the matrix $\Delta\tilde{\mathbf{E}}$ in Eq. (5.38), the proof of Theorem 5.1 is derived.

Theorem 5.1 has theoretically guaranteed the solution existence of the mixed $\ell_{1,2}$-norm minimization problem (5.41), and verified the solution can accurately approach the NBI signal to be estimated in Eq. (5.38).

(3) *Cramér-Rao Lower Bound of Sparse Recovery*
Next, we will derive the theoretical Cramér-Rao Lower Bound (CRLB) of the MSE of the NBI estimation according to the modern signal processing theory [51]. Assume that the NBI measurement vector as well as the recovery model is given by

$$\mathbf{y}_i = \Phi\tilde{\mathbf{e}}_i + \mathbf{w}. \tag{5.95}$$

Assume that the background noise $\mathbf{w}$ is zero-mean AWGN with the variance of σ_w^2, and then the conditional probability density function of the measurement vector $\mathbf{y}_i$ conditioned on $\tilde{\mathbf{e}}_i$ is given by

$$p_{\mathbf{y}_{i,\Gamma}|\tilde{\mathbf{e}}_{i,\Gamma}}\left(\mathbf{y}_i; \tilde{e}_{i,\Gamma}\right) = \frac{1}{\left(2\pi\sigma_w^2\right)^{M/2}} \exp\left(-\frac{1}{2\sigma_w^2}\left\|y_i - \Phi_\Gamma\tilde{\mathbf{e}}_{i,\Gamma}\right\|^2\right), \tag{5.96}$$

where Γ is the support of the NBI. $\tilde{\mathbf{e}}_{i,\Gamma}$ and Φ_Γ are the components of the NBI vector and the observation matrix corresponding to the support Γ, respectively. Then, the Fisher information matrix $\mathbf{J}(\tilde{\mathbf{e}}_{i,\Gamma})$ [51] corresponding to the NBI can be calculated as

$$[\mathbf{J}(\tilde{\mathbf{e}}_{i,\Gamma})]_{m,n} \overset{\Delta}{=} -E\left\{\frac{\partial^2\ln\left[p_{\mathbf{y}_{i,\Gamma}|\tilde{\mathbf{e}}_{i,\Gamma}}\left(\mathbf{y}_i; \tilde{\mathbf{e}}_{i,\Gamma}\right)\right]}{\partial\tilde{e}_{i,\Gamma,m}\partial\tilde{e}_{i,\Gamma,n}}\right\} = \frac{1}{\sigma_w^2}\left[(\Phi_\Gamma)^H\Phi_\Gamma\right]_{m,n}, \tag{5.97}$$

where $[\mathbf{J}(\tilde{\mathbf{e}}_{i,\Gamma})]_{m,n}$ denotes the entry of row m and column n of the Fisher information matrix $\mathbf{J}(\tilde{\mathbf{e}}_{i,\Gamma})$. $\tilde{e}_{i,\Gamma,m}$ and $\tilde{e}_{i,\Gamma,n}$ denote the m-th and n-th entries of $\tilde{\mathbf{e}}_{i,\Gamma}$, respectively. According to the estimation theory in [51], the CRLB can be derived as

$$\begin{aligned}
\text{(CRLB :)} \quad E\left\{\left\|\hat{\mathbf{e}}_{i,\Gamma} - \tilde{\mathbf{e}}_{i,\Gamma}\right\|^2\right\} &\geq \text{Tr}\left\{\left(\mathbf{J}(\tilde{\mathbf{e}}_{i,\Gamma})\right)^{-1}\right\} \\
&= \sigma_w^2 \text{Tr}\left\{\left((\Phi_\Gamma)^H \Phi_\Gamma\right)^{-1}\right\} \\
&\geq \sigma_w^2 K / \varphi,
\end{aligned} \tag{5.98}$$

where there are two inequalities, so the CRLB is a *lower* bound. The first inequality holds due to the principle of vector CRLB [51]. The second inequality turns to equality if all the columns of the observation matrix Φ_Γ are strictly orthogonal with each other, and in this condition $\Phi_\Gamma{}^H \Phi_\Gamma$ becomes a diagonal matrix (whose diagonal entries are all equal to the self inner product of each column of Φ_Γ, i.e. φ). In fact, the columns of the observation matrix adopted in this chapter, as the partial inverse discrete Fourier transform matrix in Eq. (5.18), i.e. $\Phi_\Gamma = \mathbf{F}_M$, are *not* strictly orthogonal between each other. Hence, the CRLB cannot reach the strict equality. However, since the partial discrete inverse Fourier transform matrix has a good RIP property and semi-orthogonal property [53, 54], it can be adopted as the observation matrix for sparse signal recovery, which is able to asymptotically approach the CRLB. Consequently, the theoretical analysis of the CRLB is consistent with the simulation results of the MSE reported in this chapter.

5.7   Conclusion

In this chapter, the fundamental drawback of the conventional "passive" anti-NBI methods is overcome based on the sparse recovery theory. We cut in the problem from the perspective of "proactive recovery", and propose the NBI recovery methods based on compressed sensing, structured compressed sensing and sparse Bayesian learning, to conduct the accurate and robust recovery and elimination of the NBI signal in severe conditions of different scenarios and broadband transmission systems. Using the proposed methods, the broadband communication system can be free from the impacts of the NBI and the system performance is significantly improved. It is indicated by the theoretical analysis and extensive simulation results that, the NBI recovery and cancelation methods based on sparse recovery theory proposed in this chapter significantly outperform the conventional counterparts, and the estimated NBI can asymptotically approach the theoretical bound. The proposed method of NBI measuring, modeling and reconstruction is promising to provide a new theoretical basis and effective alternative for the accurate recovery and cancelation of the NBI signal in broadband communication systems.

References

1. Candès E, Romberg J, Tao T (2006) Robust uncertainty principles: exact signal reconstruction from highly incomplete frequency information. IEEE Trans Inf Theory 52(2):489–509
2. Donoho D (2006) Compressed sensing. IEEE Trans Inf Theory 52(4):1289–1306
3. Gomaa A, Al-Dhahir N (2010) A compressive sensing approach to NBI cancellation in mobile OFDM systems. In: 2010 IEEE global communications conference (GLOBECOM'10), pp 1–5
4. Gomaa A, Al-Dhahir N (2011) A sparsity-aware approach for NBI estimation in MIMO-OFDM. IEEE Trans Wirel Commun 10(6):1854–1862
5. Alawsh SA, Muqaibel AH (2013) Pilot symbols distribution for compressive sensing based NBI mitigation in UWB systems. In: 2013 IEEE international conference on ultra-wideband (ICUWB'13), pp 148–153
6. Wang Z, Arce GR, Sadler BM, Paredes JL, Hoyos S, Yu Z (2008) Compressed UWB signal detection with narrowband interference mitigation. In: IEEE international conference on ultra-wideband (ICUWB'08), vol 2, pp 157–160
7. Ali A, Masood M, Sohail MS, Al-Ghadhban SN, Al-Naffouri TY (2016) Narrowband interference mitigation in SC-FDMA using bayesian sparse recovery. IEEE Trans Signal Process 64(24):6471–6484
8. Duarte MF, Davenport MA, Wakin MB, Baraniuk RG (2006) Sparse signal detection from incoherent projections. In: 2006 IEEE international conference on acoustics, speech and signal processing (ICASSP'06), vol 3
9. Zhang J, Li Y, Deng B (2012) Parameter estimation with narrowband interference suppression based on compressed sensing. In: 2012 IEEE international geoscience and remote sensing symposium (IGARSS'12), pp 3975–3978
10. Darsena D (2007) Successive narrowband interference cancellation for OFDM systems. IEEE Commun Lett 11(1)
11. Wu Z, Nassar CR (2005) Narrowband interference rejection in OFDM via carrier interferometry spreading codes. IEEE Trans Wirel Commun 4(4):1491–1505
12. Tonello AM, Pecile F (2009) Efficient architectures for multiuser FMT systems and application to power line communications. IEEE Trans Commun 57(5)
13. Umehara D, Nishiyori H, Morihiro Y (2006) Performance evaluation of CMFB transmultiplexer for broadband power line communications under narrowband interference. In: 2006 IEEE international symposium on power line communications and its applications (ISPLC'06), pp 50–55
14. Kang DH, Zhidkov SV, Choi HJ (2010) An adaptive detection and suppression of co-channel interference in DVB-T/H system. IEEE Trans Consum Electron 56(3)
15. Odling P, Borjesson O, Magesacher T, Nordstrom T (2002) An approach to analog mitigation of RFI. IEEE J Sel Areas Commun 20(5):974–986
16. Park J, Kim D, Kang C, Hong D (2003) Effect of bluetooth interference on OFDM-based WLAN. In: 2003 IEEE 58th vehicular technology conference (VTC'03-Fall), vol 2, pp 786–789
17. Ferreira HC, Lampe L, Newbury J, Swart TG (2010) Power line communications—theory and applications for narrowband and broadband communications over power lines. Wiley, UK
18. Zhang J, Meng J (2010) Noise resistant OFDM for power-line communication systems. IEEE Trans Power Deliv 25(2):693–701
19. Matsumoto Y, Shimizu T, Murakami T, Fujii K, Sugiura A (2007) Impact of frequency-modulated harmonic noises from PCs on OFDM-based WLAN systems. IEEE Trans Electromagn Compat 49(2):455–462
20. Matsumoto Y, Takeuchi M, Fujii K, Sugiura A, Yamanaka Y (2005) Performance analysis of interference problems involving DS-SS WLAN systems and microwave ovens. IEEE Trans Electromagn Compat 47(1):45–53
21. Gozalvez J (2016) New 3GPP standard for IoT. IEEE Veh Technol Mag 11(1):14–20
22. Hoymann C, Astely D, Stattin M, Wikstrom G, Cheng JF, Hoglund A, Frenne M, Blasco R, Huschke J, Gunnarsson F (2016) LTE release 14 outlook. IEEE Commun Mag 54(6):44–49

23. Cortes JA, Diez L, Canete FJ, Sanchez-Martinez JJ (2010) Analysis of the indoor broadband power-line noise scenario. IEEE Trans Electromagn Compat 52(4):849–858
24. Bartolini D et al (2005) The italian auction for radio spectrum licences. Universit politecnica delle Marche, Dipartimento di economia
25. IEEE: Wireless LAN medium access control (MAC) and physical layer (PHY) specifications (2009)
26. IEEE: EEE standard for information technology—local and metropolitan area networks—specific requirements—part 11: wireless LAN medium access control (MAC) and physical layer (PHY) specifications amendment 6: wireless access in vehicular environments (2010)
27. 3GPP: 3GPP TS 36.211 v10.3.0—evolved universal terrestrial radio access (E-UTRA); physical channels and modulation (release 8) (2011)
28. 3GPP: 3GPP TS 36.104 v11.4.0—evolved universal terrestrial radio access (E-UTRA); base station (BS) radio transmission and reception (release 11) (2013)
29. Standard CN (2006) Frame structure, channel coding and modulation for digital television terrestrial broadcasting system. GB 20600-2006, Chinese National Standard
30. ETSI: digital video broadcasting (DVB); frame structure, channel coding and modulation for a second generation digital terrestrial television broadcasting system (DVB-T2). ETSI EN 302 755 v1.3.1 (2011)
31. Yan K, Yang F, Pan C, Song J (2012) Reception quality prediction in a single frequency network for the DTMB standard. IEEE Trans Broadcast 58(4):629–636
32. ITU-T: ITU G.9960, unified high-speed wire-line based home networking transceivers—system architecture and physical layer specification (2010)
33. Zimmermann M, Dostert K (2002) Analysis and modeling of impulsive noise in broad-band powerline communications. IEEE Trans Electromagn Compat 44(1):249–258
34. Donoho D, Elad M, Temlyakov V (2006) Stable recovery of sparse overcomplete representations in the presence of noise. IEEE Trans Inf Theory 52(1):6–18
35. Dai W, Milenkovic O (2009) Subspace pursuit for compressive sensing signal reconstruction. IEEE Trans Inf Theory 55(5):2230–2249
36. Do T, Lu G, Nguyen N, Tran T (2008) Sparsity adaptive matching pursuit algorithm for practical compressed sensing. In: Asilomar conference on signals, systems and computers, pp 581–587
37. ITU-R: Error-correction, data framing, modulation and emission methods for digital terrestrial television broadcasting. ITU-R BT. 1306-6. recommendati (2011)
38. Guideline for evaluation of radio transmission technology for IMT-2000 (1997)
39. Dai L, Wang J, Wang Z, Tsiaflakis P, Moonen M (2013) Spectrum- and energy-efficient OFDM based on simultaneous multi-channel reconstruction. IEEE Trans Signal Process 61(23):6047–6059
40. Ten Brink S, Peidel J, Yan RH (1998) Iterative demapping and decoding for multilevel modulation. In: IEEE global communications conference (GLOBECOM'98), vol 1, pp 579–584
41. Shi K, Zhou Y, Kelleci B, Fischer TW, Serpedin E, lker Karsilayan A (2007) Impacts of narrowband interference on OFDM-UWB receivers: analysis and mitigation. IEEE Trans Signal Process 55(3):1118–1128 (2007)
42. Stridh R, Yu K, Ottersten B, Karlsson P (2005) MIMO channel capacity and modeling issues on a measured indoor radio channel at 5.8 GHz. IEEE Trans Wirel Commun 4(3):895–903
43. Berg EVD, Friedlander M (2010) Theoretical and empirical results for recovery from multiple measurements. IEEE Trans Inf Theory 56(5):2516–2527
44. Duarte M, Eldar Y (2011) Structured compressed sensing: from theory to applications. IEEE Trans Signal Process 59(9):4053–4085
45. Garg R, Khandekar R (2011) Block-sparse solutions using kernel block RIP and its application to group LASSO. In: International conference on artificial intelligence and statistics, pp 296–304
46. Tropp J, Gilbert A (2007) Signal recovery from random measurements via orthogonal matching pursuit. IEEE Trans Inf Theory 53(12):4655–4666
47. Wolniansky PW, Foschini GJ, Golden GD, Valenzuela RA (1998) V-BLAST: an architecture for realizing very high data rates over the rich-scattering wireless channel. In: 1998 URSI international symposium on signals, systems, and electronics, pp 295–300

48. MacKay DJC (1999) Good error-correcting codes based on very sparse matrices. IEEE Trans Inf Theory 45(2):399–431
49. Sohail MS, Al-Naffouri TY, Al-Ghadhban SN (2012) Narrow band interference cancelation in OFDM: a structured maximum likelihood approach. In: IEEE 13th international workshop on signal processing advances in wireless communications (SPAWC), pp 45–49. Cesme, Turkey
50. Zhang Z, Rao B (2013) Extension of SBL algorithms for the recovery of block sparse signals with intra-block correlation. IEEE Trans. Signal Process. 61(8):2009–2015
51. Steven MK (1993) Fundamentals of statistical signal processing. PTR Prentice-Hall, Englewood Cliffs, NJ
52. Eldar YC, Mishali M (2009) Robust recovery of signals from a structured union of subspaces. IEEE Trans Inf Theory 55(11):5302–5316
53. Candès J, Plan Y (2011) A probabilistic and RIPless theory of compressed sensing. IEEE Trans Inf Theory 57(11):7235–7254
54. Naffouri T, Quadeer A, Caire G (2014) Impulse noise estimation and removal for OFDM systems. IEEE Trans Commun 62(3):976–989

Chapter 6
Sparse Recovery Based IN Cancelation

Abstract In this chapter, the second key techn ology on the third scientific problem of this book, i.e. the sparse recovery theory based impulsive noise (IN) reconstruction and cancelation, is investigated. The highly efficient new technique of accurate IN recovery and cancelation based on compressed sensing and structured compressed sensing theories is proposed to overcome the limitation of the conventional "passive" anti-IN methods and reach the research target of actively and accurately recover and completely eliminate the IN in broadband communication systems. In this chapter, first, to address the issue of the state-of-the-art methods, the IN recovery and cancelation method based on prior aided compressed sensing is proposed. Second, for the MIMO system, a structured compressed sensing based IN recovery algorithm exploiting spatial correlation is proposed. Finally, the method of combined NBI and IN recovery and cancelation based on the time-frequency combined compressed sensing framework is proposed to overcome the impacts from the NBI and IN on broadband communication systems.

6.1 Introduction

6.1.1 Problem Description and Related Research

The existing methods of IN mitigation mainly include three aspects, i.e. receiver-side nonlinear operation, transmitter-side pre-processing, and receiver-side post-processing. There has been plenty of research on this, which has been described in detail in Chap. 1. The existing conventional methods of IN mitigation have many drawbacks. For example, the mitigation operations introduce nonlinear distortion and cause data loss of the signal of interest. Too much time and frequency resources are occupied, which reduces the efficiency. The estimation is inaccurate, leading to false alarms and errors. The complexity of the design is high. The assumptions of the system and the conditions are not realistic. Most of the conventional methods of IN mitigation is to "passively" mitigate and get rid of the IN, which is not able to completely eliminate it. Hence, we need to investigate highly accurate IN

recovery methods that do not have impacts on the correct demodulation and decoding of the signal of interest, and consume much less time and frequency resources, and much more applicable in practice. The theoretical and technological framework of "actively" and accurately recovering the IN should be established to completely eliminate the impacts of the IN on the system performance, and break the bottleneck that limits the system performance.

In order to address the issues of conventional methods, the compressed sensing and sparse recovery theories can be applied in the problem of IN estimation. According to the definition of the IN, the IN has a bursting property in the time domain and natural sparsity. Thus it satisfies the requirements of the compressed sensing framework. We only need to use a certain approach to obtain the compressed sensing measurement data of the IN in a certain domain. Then the compressed sensing model and the measurement matrix are designed to formulate the compressed sensing measurement and recovery model. The IN can be recovered employing the compressed sensing algorithms.

However, the research on IN mitigation is still mainly focused on the conventional ones. The study on compressed sensing based methods is insufficient. Only a few related works make use of the frequency domain null sub-carriers as the measurement data of the IN and estimate the IN based on compressed sensing algorithms, mainly including the research by Caire [1], Lampe [2], and Naffori [3]. However, the existing compressed sensing based methods have a series of problems. First, in severe conditions such as large sparsity level, insufficient measurement data and low INR, the estimation performance degrades greatly. Second, a large amount of null sub-carriers or pilots are needed to conduct IN estimation, which results in great loss of spectrum efficiency. Besides, the existing methods are only aimed at single antenna systems, not exploiting the spatial correlation of the IN in multiple antennas of the MIMO system. The spatial diversity is not fully utilized to improve the estimation performance. Moreover, the existing methods only consider the sparse estimation of the IN, but have not investigated the severe transmission environment in the presence of both NBI and IN. The time and frequency combined compressed sensing framework is not formulated. The combined NBI and IN recovery and cancelation method is not studied. Hence, the conventional methods have great limitation when the IN is serious.

6.1.2 Research Aims and Problems

In order to address the fundamental limitation of the conventional anti-IN methods in "passively" and incompletely mitigate the IN, and meanwhile solve the problems of a few compressed sensing based IN estimation methods such as unstable performance, inaccurate estimation, low spectrum efficiency, limited performance in MIMO and severe scenarios etc, this chapter cuts in from the perspective of "actively recovering" the IN. The compressed sensing based IN recovery schemes with high spectrum efficiency, accuracy and robustness are studied on. In the frameworks of time-frequency

combined compressed sensing measurement and recovery and the spatially multi-
dimensional structured compressed sensing, the bottleneck of conventional anti-IN
methods is broken. The theoretical bound of IN estimation is approached, and the
system performance of the broadband OFDM system and MIMO system in severe
conditions in the presence of both NBI and IN is significantly improved. Specifically,
the contributions of this chapter are summarized as follows:

- The prior aided compressed sensing based method of IN recovery is proposed,
  which exploits the time domain threshold method to obtain the partial support
  prior information of the IN to reduce the requirement of the frequency domain
  measurement data amount. The compressed sensing recovery model is formulated
  based on partial Fourier transform matrix as the observation matrix, and the PA-
  SAMP algorithm proposed is utilized to accurately recover the IN.
- Based on the spatial correlation of the IN between multiple receive antennas
  in MIMO systems, the spatially multi-dimensional IN measurement method is
  proposed. Combining the measurement data at multiple receive antennas, the IN
  recovery framework based on spatially structured compressed sensing is formu-
  lated. The structured compressed sensing based highly efficient greedy algorithm,
  i.e. Structured Prior Aided SAMP (SPA-SAMP), is proposed. The convergence,
  solution existence and the estimation accuracy of the SPA-SAMP algorithm are
  theoretically guaranteed. It is verified that the proposed method achieves higher
  recovery accuracy and robustness compared with classical compressed sensing
  based algorithms in MIMO systems.
- The NBI and IN combined recovery framework based on time-frequency com-
  bined compressed sensing is formulated. The OFDM frame structure based on
  compressed sensing time-frequency combined measuring is devised. Exploiting
  the differential measuring of the temporal training sequence and the frequency
  domain null sub-carriers, we formulate the NBI and IN combined sparse recovery
  model. With the aid of the prior information of the time and frequency domain
  partial support, the PA-SAMP algorithm is conducted to accurately recover and
  eliminate both NBI and IN.

6.2 System Model

(1) *Time Domain Sparse Impulsive Noise Model*

According to the definition of the IN given in literature, such as described in
Sect. 2.3.1 in Chap. 2, in a quantitative perspective of view, the ratio between the
time duration occupied by the time-domain IN nonzero entries and the time duration
of the OFDM block transmission symbol is no greater than 5% [4, 5]. Specifically in
OFDM systems, the ratio between the number of nonzero entries in the time-domain
IN $\mathbf{z}_i = [z_{i,0}, z_{i,1}, \dots z_{i,N-1}]^T$ corresponding to the i-th OFDM frame and the length
of the OFDM data block N is no greater than 5%. Continuing to use the definitions
and notations of the IN model and parameters given in Sect. 2.3.1, the support is

$\Pi_i = \left\{ j \mid z_{i,j} \neq 0 , \ j = 0, 1, \ldots, N-1 \right\}$. The sparsity level is $K = |\Pi_i|$. Thus we have $K/N \leq 5\%$. The INR between the IN and the background noise is denoted by γ_{IN}, where the IN is regarded as an interference to the system, while the INR is referred to as the power ratio between the power of the IN and the background noise (AWGN), which is shown in Eq. (2.9) for detail.

In the framework of sparse recovery theory, the unknown high-dimensional signal should satisfy the sparse property. The dimension of the time-domain IN corresponding to the OFDM block transmission symbol is N, which belongs to high-dimensional signal. The ratio of the time duration occupied by the nonzero entries, i.e. the bursting impulses, is sufficiently small, so it satisfies the "sparse property" required by the compressed sensing sparse recovery theory. According to the related sparse recovery literature [6], it can be known that we only need to design an observation matrix with good RIP property and formulate the IN sparse measurement model, and then the IN signal in broadband transmission systems can be recovered using sparse recovery methods.

In this chapter, the IN model of Middleton's Class A-Poisson described in Sect. 2.3.1 in Chap. 2 is still used. The definitions of the related parameters are also used, i.e. sparsity level K, support Π_i, and INR γ_{IN}, etc.

(2) *Spatial Correlation of Impulsive Noise*

It is shown by the related literature on IN and realistic channel testing results in MIMO systems that, the IN in MIMO systems has spatial correlation, i.e. spatial domain correlation [7, 8]. Specifically, in MIMO systems, it is assumed that the time-domain IN support (set of nonzero entries locations) of different receive antennas is identical, i.e. the time-domain IN signals at different receive antennas share the same time-domain sparse pattern. The bursting impulses of the IN at different receive antennas occur at the same sampling point, as given by

$$\Pi_{i,(1)} = \Pi_{i,(2)} = \cdots = \Pi_{i,(N_r)} = \Pi_i \tag{6.1}$$

where $\Pi_{i,(r)}, r = 1, \ldots N_r$ denotes the IN support corresponding to the i-th OFDM symbol at the r-th receive antenna. It is indicated by the spatial correlation of the IN that, the time-domain sampling locations of the nonzero entries bursting of the time-domain IN at different receive antennas are the same, while the amplitude might be different [7, 8].

The reason why the IN has spatial correlation is as follows: Usually, the distance between receive antennas of the MIMO system is comparable to the wavelength of the carrier of the signal of interest [9, 10]. Thus, since the IN signal generated by the IN source travels in light speed, the time difference to reach different receive antennas is comparable to the time-domain sampling interval $1/f_c$ of the radio frequency signal of interest in typical broadband communication systems. Because the radio frequency carrier of the signal of interest, i.e. f_c, is much higher than the signal bandwidth B (might be 2–3 orders of magnitude higher), it is commonly reckoned that the baseband bandwidth of the IN is comparable to that of the signal of interest (since the IN is bursting in the time domain, it contaminates the whole signal bandwidth in

the frequency domain). Also, the coherent time of the nonzero entries of the time-domain IN is comparable to the time interval of the time-domain baseband symbols of the signal of interest, i.e. $1/B$.

Hence, f_c is much higher than the baseband bandwidth of the IN signal, and the coherent time of the baseband symbol of the IN signal is much larger than the sampling interval of the radio frequency signal of interest, i.e. $1/B \gg 1/f_c$. Thus, the time difference for the IN signal to reach different receive antennas is much smaller than the coherent time of the IN baseband symbols. We can assume that different receive antennas are suffering from a certain IN burst at the same time, which is equivalent to that the time-domain sampling locations of the IN bursts at different receive antennas are the same. On the other hand, since the channel fading, antenna gain and other parameters might be different for different receive antennas, the amplitude of the IN on the receive antennas might be different from each other.
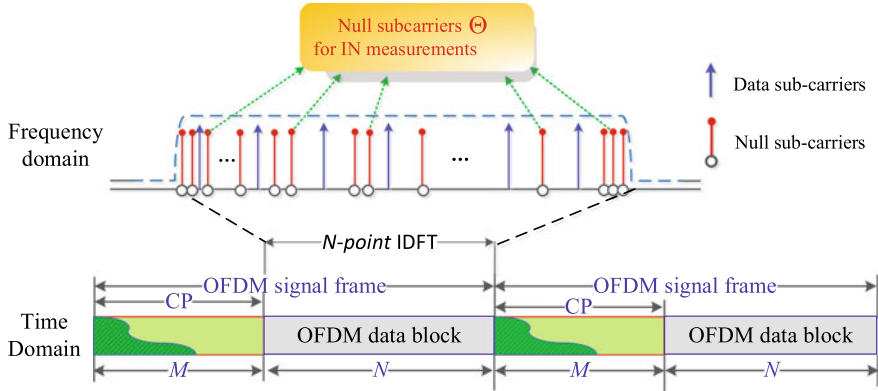
6.3 Prior Aided Compressed Sensing Based IN Cancelation

6.3.1 OFDM System Model with Impulsive Noise

Consider a typical OFDM signal frame as well as the frequency-domain OFDM frame structure is shown in Fig. 6.1, which is commonly specified in OFDM-based communications standards including the 802.11 WLAN [11] and ITU-T G.9960 [12]. In this chapter, the null sub-carriers including the reserved tones and the virtual sub-carrier masks specified in OFDM-based systems, usually for spectrum masks, notching and inter-service interference avoidance, are utilized to acquire the measurement vector for compressed sensing-based IN recovery. In the time domain, the i-th frame $\mathbf{s}_i = \begin{bmatrix} \mathbf{c}^T & \mathbf{x}_i^T \end{bmatrix}^T$ consists of the OFDM data block $\mathbf{x}_i = \begin{bmatrix} x_{i,0}, x_{i,1}, \ldots, x_{i,N-1} \end{bmatrix}^T$ of length N and its cyclic prefix (CP) $\mathbf{c}_i$ of length M. The i-th time-domain OFDM data block is the IDFT of the associated frequency-domain data in the N sub-carriers, which contains a set of reserved null sub-carriers denoted by the set Θ. Then the transmitted signal passes through the multi-path fading channel with the channel impulsive response (CIR) of $\mathbf{h}_i = \begin{bmatrix} h_{i,0}, h_{i,1}, \ldots, h_{i,L-1} \end{bmatrix}^T$ with length L in the presence of the IN $\mathbf{z}_i$. Then, in the frequency domain, the received data in the reserved null sub-carriers set Θ are denoted by

$$\tilde{\mathbf{p}}_i = \mathbf{F}_R \mathbf{z}_i + \tilde{\mathbf{w}}_i, \tag{6.2}$$

where the vector $\tilde{\mathbf{p}}_i = [\tilde{p}_{i,0}, \tilde{p}_{i,1}, \ldots, \tilde{p}_{i,R-1}]^T$ of length $R = |\Theta|$ is the measurement vector of the IN at the null sub-carriers, $\tilde{\mathbf{w}}_i$ denotes the corresponding frequency-domain AWGN vector, while the observation matrix to be used for the compressed sensing-based IN recovery is the partial DFT matrix $\mathbf{F}_R$ given by

Fig. 6.1 Time-frequency OFDM frame structure exploited for compressed sensing-based IN cancelation

$$\mathbf{F}_R = \frac{1}{\sqrt{N}} [\boldsymbol{\chi}_0 \quad \boldsymbol{\chi}_1 \quad \cdots \quad \boldsymbol{\chi}_{N-1}], \qquad (6.3)$$

where the k-th entry of $\boldsymbol{\chi}_m$ is $\exp(-j2\pi mk/N), k \in \Omega, m = 0, \ldots, N-1$. The measurement vector $\tilde{\mathbf{p}}_i$ at the set Θ contains the IN component and the background AWGN, while the OFDM data component is not included since the null sub-carriers are set to zeros.

6.3.2   Priori Aided Compressed Sensing Based IN Recovery

In order to introduce the compressed sensing theory and method, according to the framework of underdetermined linear inverse problem based on compressed sensing theory described in Sect. 2.4.1 in Chap. 2, first we need to obtain the measurement vector of the IN to be recovered, and devise the observation matrix that satisfies the sparse measurement relation. Then the compressed sensing measurement problem model described by Eq. (2.10) can be formulated, and the IN can be recovered using the compressed sensing based algorithm.

As described in the previous section, recall that the measurement vector of IN $\tilde{\mathbf{p}}_i$ as well as the observation matrix $\mathbf{F}_R$ have been acquired from the null sub-carriers in (6.2), which is the formulated compressed sensing IN measurement model. According to the compressed sensing theory [6, 13], the unknown high-dimensional sparse IN vector $\mathbf{z}_i$ can be recovered accurately from the underdetermined measurement data (6.2) containing the power constrained background noise $\tilde{\mathbf{w}}_i$ using the compressed sensing algorithms. As described in Chap. 2, to solve the sparse underdetermined linear inverse problem (6.2) can be equivalent to solving the following convex relaxed ℓ_1-norm minimization problem:

$$\min_{\mathbf{z}_i \in \mathbb{C}^N} \|\mathbf{z}_i\|_1, \quad \text{s.t.} \|\tilde{\mathbf{p}}_i - \mathbf{F}_R \mathbf{z}_i\|_2 \leq \varepsilon_I, \tag{6.4}$$

where ε_I is the power constraint of the AWGN in (6.2). As described previously, the ℓ_1-norm minimization problem (6.4) can be also solved efficiently by classical compressed sensing algorithms. Since the sparsity level of the IN in practical OFDM transmission systems is variable and unknown at the receiver, the classical greedy algorithms of OMP [14] and SP [15] are not suitable. In this chapter, with the aid of the a priori partial support of the IN, the PA-SAMP algorithm can be utilized to recover the IN, which can adapt to varying and unknown sparsity levels. Moreover, the requirement of measurement data amount can be reduced with the help of partial support.

The a priori information of the IN partial support will also improve the performance of compressed sensing-based IN recovery. Since the intensity of IN is normally much higher than that of the time-domain data component or AWGN, it is feasible to obtain a coarse estimation of the IN partial support $\Pi^{(0)}$ at the i-th OFDM data block through thresholding from the received time-domain OFDM data block $\mathbf{x}_i$. The time-domain samples whose powers exceed the given threshold λ_t are included in the partial support $\Pi^{(0)}$, which is given by

$$\Pi^{(0)} = \left\{ n \left| |x_{i,n}|^2 > \lambda_t, n = 0, 1, \ldots, N-1 \right. \right\}, \tag{6.5}$$

where the power threshold λ_t is given by

$$\lambda_t = \alpha \cdot \frac{1}{N} \sum_{n=0}^{N-1} |x_{i,n}|^2, \tag{6.6}$$

where α is a coefficient that can be configured large enough to ensure the accuracy of the time-domain partial support of the IN. The partial support will help improve the performance of the compressed sensing algorithm for IN recovery, especially in severe conditions where the INR is relatively low, the measurement data is insufficient, or the sparsity level is large.

With the aid of the IN partial support $\Pi^{(0)}$, the original IN vector $\mathbf{z}_i$ corresponding to the i-th OFDM data block is able to be efficiently and accurately recovered using the proposed PA-SAMP algorithm of whom the pseudo-code is summarized in Algorithm 1. We only need to replace the input and output with the related values of the IN. Specifically, the input includes the measurement vector $\tilde{\mathbf{p}}_i$, the observation matrix $\Psi = \mathbf{F}_R$, and the a priori partial support $\Pi^{(0)}$, as well as the iteration step size. After the iterations, the output is the estimated final support $\hat{\Pi}_i$ and the recovered IN vector $\hat{\mathbf{z}}_i$, s.t. $\hat{\mathbf{z}}_i|_{\hat{\Pi}_i} = (\mathbf{F}_R)^\dagger_{\hat{\Pi}_i} \tilde{\mathbf{p}}_i$, $\hat{\mathbf{z}}_i|_{\hat{\Pi}_i^c} = \mathbf{0}$.

Finally, the time-domain IN can be both canceled out from the received OFDM data block, and be processed by the successive demapping and decoding modules at the receiver, which is free from the impacts of the IN. Through introducing the aid of the prior information of the partial support, exploiting the prior aided com-

pressed sensing based PA-SAMP algorithm, the requirement of the measurement
data amount is greatly reduced. Thus the spectral efficiency is greatly improved, and
meanwhile the accuracy and stability are improved. Compared with conventional
SAMP algorithm, the PA-SAMP algorithm has a lower complexity, higher accuracy
and applicability, which is analyzed in detail in Sect. 5.3.
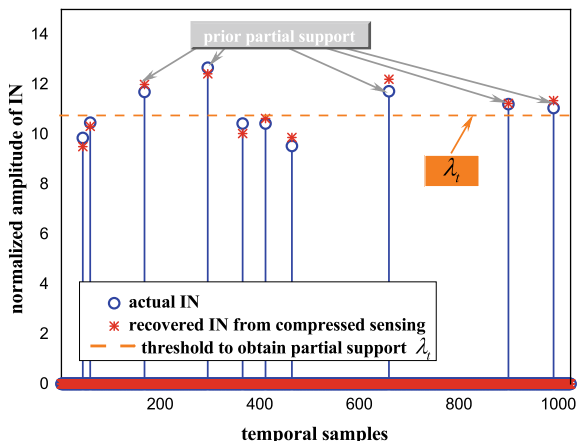
6.3.3   Simulation Results and Discussions

The performance of the proposed CS-based IN cancelation scheme for OFDM-based
systems is investigated and validated through extensive simulations. The simulation
parameters are configured according to the typical wireless communications system.
The OFDM sub-carrier number $N = 1024$, the CP length $M = 128$, and the number
of null sub-carriers $R = 128$. The multi-path fading ITU-R Vehicular-B channel
model [16] in the presence of IN is used. The scaling coefficient for the partial
support acquisition is $\alpha = 5.0$.
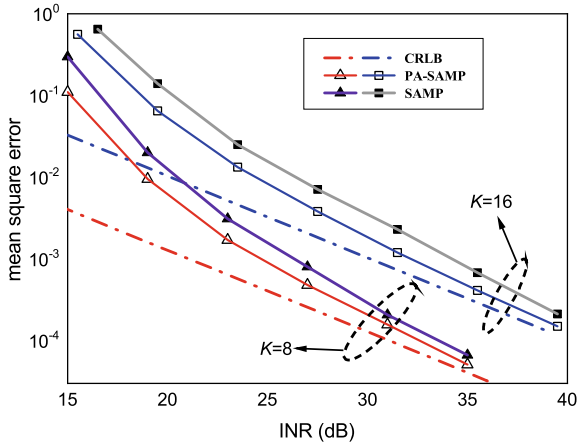
The general process of the proposed approach for compressed sensing-based IN
recovery with the IN parameters of $A = 0.15$, $\omega = 0.02$, $K = 10$, and INR $\gamma_{IN} = 30$
dB is depicted in Fig. 6.2, where the Gaussian mixture model is adopted and the arrival
rate of the IN bursts is described by a Poisson point process with a medium value of
$\lambda = 50$/sec. The IN partial support is firstly obtained using the threshold λ_t in (6.6).
From the null sub-carriers set, we can get the IN measurement vector out of which
the accurate IN is recovered using PA-SAMP. It is observed from Fig. 6.2 that the
final IN estimation based on the PA-SAMP method matches the actual IN very well.

The mean square error (MSE) performance of IN recovery using the proposed
prior aided compressed sensing based method is shown in Fig. 6.3. The classical
compressed sensing based SAMP algorithm is also simulated for comparison. The

Fig. 6.2 IN recovery
process using the proposed
prior aided compressed
sensing based PA-SAMP
method

Fig. 6.3 MSE performance for IN recovery using PA-SAMP and SAMP
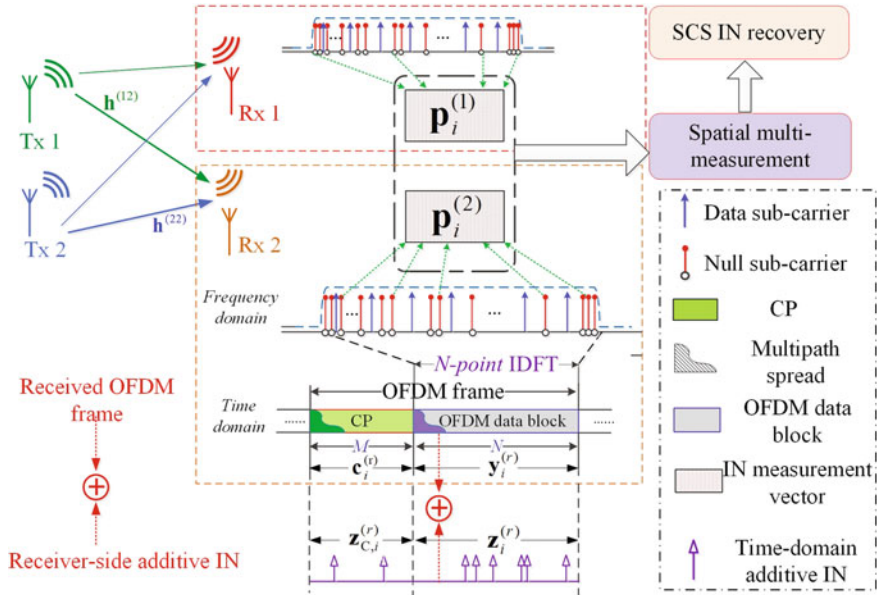
theoretical Cramer-Rao lower bound (CRLB) $2\sigma_w^2 \cdot (K/R)$ is depicted as a benchmark. It can be observed that the PA-SAMP algorithm achieves the target MSE 10^{-3} at the INR of 24.6 and 32.3 dB with $K = 8$ and $K = 16$, respectively, which outperforms SAMP by approximately 1.8 dB. It is noted from the simulation results that the MSE of the proposed method approaches the theoretical CRLB with the increase of the INR, and the high accuracy of the proposed IN cancelation method is verified.

6.4 Structured Compressed Sensing Based IN Cancelation

The classical compressed sensing theory based methods of IN recovery have not fully utilized the spatial correlation of the IN in MIMO systems, so the performance might be degraded in severe conditions such as insufficient measurement data, intensive background noise and large sparsity levels. In this section, we propose the spatially multiple measuring (SMM) method of the IN for MIMO systems, and formulate the framework of IN recovery based on spatially multi-dimensional structured compressed sensing. Furthermore, the improved structured compressed sensing based greedy algorithm, i.e. structured prior aided SAMP (SPA-SAMP), is proposed to achieve a higher recovery accuracy and stability than classical compressed sensing based algorithms.

6.4.1 MIMO System Model with Impulsive Noise

According to the specifications in the IEEE 802.11n/p [11, 17], the signal frame and the frequency-domain structure of a typical wireless MIMO system is illustrated in Fig. 6.4. Without loss of generality, the 2×2 MIMO system is investigated

Fig. 6.4 Time-frequency OFDM frame structure exploited by the SMM method for the structured compressed sensing-based IN recovery and cancelation

in this section, while the proposed scheme is also applicable in arbitrary $N_t \times N_r$ MIMO systems, where N_t and N_r are the number of transmit and receive antennas. The null sub-carriers, including the reserved tones and the virtual sub-carrier masks specified in various communications standards such as the IEEE 802.11p WAVE standard, are utilized by the proposed SMM method to acquire the measurement matrix for structured compressed sensing based IN recovery. In the time domain, the i-th transmitted frame at the t-th transmit antenna consists of the OFDM symbol $\mathbf{x}_i^{(t)} = \left[x_{i,0}^{(t)}, x_{i,1}^{(t)}, \ldots, x_{i,N-1}^{(t)}\right]^T$ of length N and its cyclic prefix (CP) $\mathbf{c}_i^{(t)}$ with length M. The i-th time-domain OFDM symbol $\mathbf{x}_i^{(t)}$ is the inverse discrete Fourier transform (IDFT) of the corresponding frequency-domain data $\tilde{\mathbf{X}}_i^{(t)}$ in the N sub-carriers, which contains some reserved null sub-carriers whose indices are denoted by the set Θ. All the N_t transmit antennas are sending the OFDM symbols simultaneously, then passing through the wireless MIMO channel with the channel impulsive response (CIR) $\mathbf{h}^{(tr)} = \left[h_0^{(tr)}, h_1^{(tr)}, \ldots, h_{L-1}^{(tr)}\right]^T$ between the t-th transmit antenna and the r-th receive antenna. At the receiver, the received i-th OFDM signal frame at the r-th receive antenna is denoted by $[(\mathbf{c}_i^{(r)})^T, (\mathbf{y}_i^{(r)})^T]^T$, which is composed of the received OFDM data block $\mathbf{y}_i^{(r)}$ and its cyclic prefix $\mathbf{c}_i^{(r)}$. The received OFDM data block $\mathbf{y}_i^{(r)}$ is given by

$$\mathbf{y}_i^{(r)} = [y_{i,0}^{(r)}, y_{i,1}^{(r)}, \ldots, y_{i,N-1}^{(r)}]^T = \sum_{t=1}^{N_t} \mathbf{h}^{(tr)} \odot \mathbf{x}_i^{(t)} + \mathbf{z}_i^{(r)} + \mathbf{w}_i^{(r)}, \qquad (6.7)$$

where $\mathbf{z}_i^{(r)}$ and $\mathbf{w}_i^{(r)}$ denote the time-domain additive IN (of length N) at the r-th receive antenna and the time-domain AWGN vector, respectively. The operator $\odot$ denotes cyclic convolution. It is noted that, the length-N time-domain IN signal $\mathbf{z}_i^{(r)}$ is corresponding to the location of the received OFDM data block $\mathbf{y}_i^{(r)}$, which is irrelevant to the CP $\mathbf{c}_i^{(r)}$. Thus, through the DFT operation, the received signal is transferred to the frequency domain as

$$\tilde{\mathbf{Y}}_i^{(r)} = \mathbf{F}_N \mathbf{y}_i^{(r)} = \sum_{t=1}^{N_t} \mathbf{H}^{(tr)} \tilde{\mathbf{X}}_i^{(t)} + \mathbf{F}_N \mathbf{z}_i^{(r)} + \tilde{\mathbf{w}}_i^{(r)}, \qquad (6.8)$$

where $\mathbf{F}_N$ and $\tilde{\mathbf{w}}_i^{(r)}$ denote the N-point DFT matrix and the frequency-domain AWGN vector at the r-th receive antenna, respectively. The $N \times N$ channel frequency response (CFR) matrix between the t-th transmit antenna and the r-th receive antenna is denoted by $\mathbf{H}^{(tr)} = \mathrm{diag}\{\mathbf{F}_N \mathbf{h}^{(tr)}\}$. As has been described previously, the $R = |\Theta|$ null sub-carriers corresponding to the null sub-carrier set Θ out of $\tilde{\mathbf{X}}_i^{(t)}$ at all the transmit antennas are preset to zero. Thus, we can use a selection matrix $\mathbf{S}_R$ to pick out the R sub-carriers corresponding to the set Θ from the received frequency-domain data block $\tilde{\mathbf{Y}}_i^{(r)}$, and obtain a frequency-domain measurement vector of the IN $\tilde{\mathbf{p}}_i^{(r)}$ as given by

$$\begin{aligned} \tilde{\mathbf{p}}_i^{(r)} &= \mathbf{S}_R \tilde{\mathbf{Y}}_i^{(r)} \\ &= \sum_{t=1}^{N_t} \mathbf{S}_R \mathbf{H}^{(tr)} \tilde{\mathbf{X}}_i^{(t)} + \mathbf{F}_R \mathbf{z}_i^{(r)} + \mathbf{S}_R \tilde{\mathbf{w}}_i^{(r)} \\ &= \mathbf{0} + \mathbf{F}_R \mathbf{z}_i^{(r)} + \tilde{\mathbf{w}}_{R,i}^{(r)}, \end{aligned} \qquad (6.9)$$

where the $R \times N$ selection matrix $\mathbf{S}_R$ is composed of the R rows of the $N \times N$ identity matrix $\mathbf{I}_N$ corresponding to the set Θ. The reason why the last equality in Eq. (6.9) holds is that, the entries of $\tilde{\mathbf{X}}_i^{(t)}$ corresponding to the set Θ are zero, so we have $\mathbf{S}_R \mathbf{H}^{(tr)} \tilde{\mathbf{X}}_i^{(t)} = \mathbf{0}$. The $R \times N$ partial Fourier transform matrix $\mathbf{F}_R$ is composed of the R rows of the original N-point DFT matrix $\mathbf{F}_N$ corresponding to the set Θ. Thus, the received data corresponding to the null sub-carrier set Θ at the r-th receive antenna can be simplified and rewritten as

$$\tilde{\mathbf{p}}_i^{(r)} = \mathbf{F}_R \mathbf{z}_i^{(r)} + \tilde{\mathbf{w}}_{R,i}^{(r)}, \qquad (6.10)$$

where the vector $\tilde{\mathbf{p}}_i^{(r)} = [\tilde{p}_{i,0}^{(r)}, \tilde{p}_{i,1}^{(r)}, \ldots, \tilde{p}_{i,R-1}^{(r)}]^T$ of length R is the one-dimensional measurement vector of the IN at the null sub-carriers at the r-th receive antenna. $\tilde{\mathbf{w}}_{R,i}^{(r)}$ denotes the length-R corresponding frequency-domain AWGN vector. Then, it can be derived that the observation matrix for the subsequent structured compressed sensing IN recovery is the partial Fourier transform matrix $\mathbf{F}_R$ as given by

$$\mathbf{F}_{\text{R}} = \frac{1}{\sqrt{N}}[\boldsymbol{\chi}_0 \quad \boldsymbol{\chi}_1 \quad \cdots \quad \boldsymbol{\chi}_{N-1}], \tag{6.11}$$

where the k-th entry of $\boldsymbol{\chi}_m$ is $\exp(-j2\pi mk/N)$, $k \in \Theta$, $m = 0, \ldots, N-1$. Note that the measurement vector $\tilde{\mathbf{p}}_i^{(r)}$ at the set Θ only contains the components of IN and AWGN, while the information data component is not included since the null sub-carriers are set to zeros.

6.4.2 Spatially Multi-dimensional IN Measurement

For the SISO system, the classical compressed sensing based IN measurement model can be formulated. The IN signal $\boldsymbol{\xi}_i$ for the SISO system can be recovered using the one-dimensional measurement vector $\tilde{\mathbf{p}}_i^{(r)}$ given by (6.10). One can apply classical compressed sensing theory and algorithms, including solving the convex relaxed ℓ_1-norm minimization problem, and applying the state-of-art compressed sensing-based greedy algorithms. However, these CS based methods are only aimed at the SISO system and ignores the spatial correlation of the IN in the MIMO system, which might result in performance degradation, particularly when the intensity of the IN is fluctuating and its sparsity is large.

To further improve the immunity to bad conditions, the structure compressed sensing theory is introduced to extend the previous work in SISO systems to MIMO-OFDM systems, leading to the proposed SMM method. The structured compressed sensing based IN recovery model is formulated, and the IN can be efficiently and accurately recovered. In the $N_t \times N_r$ MIMO-OFDM system, the proposed SMM method exploits all the N_r measurement vectors given in (6.10) corresponding to the spatially correlated N_r receive antennas, yielding the structured compressed sensing recovery problem model as given by

$$\tilde{\mathbf{P}} = \left[\tilde{\mathbf{p}}_i^{(1)}, \tilde{\mathbf{p}}_i^{(2)}, \ldots, \tilde{\mathbf{p}}_i^{(N_r)} \right]_{R \times N_r} = \mathbf{F}_{\text{R}} \boldsymbol{\Xi}_0 + \tilde{\mathbf{W}}, \tag{6.12}$$

where $\tilde{\mathbf{P}}$ is the IN multi-dimensional measurement matrix constituted by the N_r measurement vectors in column obtained by Eq. (6.10) at the N_r receive antennas, which is consistent with the structured compressed sensing multi-dimensional measurement vectors (MMV) model introduced in Sect. 2.4.2. $\boldsymbol{\Xi}_0 = [\mathbf{z}_i^{(1)}, \mathbf{z}_i^{(2)}, \ldots, \mathbf{z}_i^{(N_r)}]_{N \times N_r}$ is the spatially jointly sparse IN matrix. Due to the spatial correlation of the IN (6.1) described previously, the columns of the spatially jointly sparse IN matrix share the same support Π_i, while the amplitude of the nonzero entries in the same row of the matrix corresponding to different receive antennas might be different from each other. $\tilde{\mathbf{W}} = [\tilde{\mathbf{w}}_{R,i}^{(1)}, \tilde{\mathbf{w}}_{R,i}^{(2)}, \ldots, \tilde{\mathbf{w}}_{R,i}^{(N_r)}]$ denotes the corresponding frequency-domain AWGN matrix.

The formulated mathematical model in (6.12) complies with the theory of structured compressed sensing MMV model [18, 19]. Each column of the multi-

dimensional measurements matrix $\tilde{\mathbf{P}}$ is one measurement vector of the IN related with one receive antenna, and the spatial correlation is taken good advantage of by the structured compressed sensing measurements model (6.12). Afterwards, according to the structure compressed sensing framework in Sect. 2.4.2, the multiple IN signals within $\mathbf{\Xi}_0$ that are jointly sparse can be simultaneously recovered by solving the mixed $\ell_{0,q}$-norm minimization problem as given by

$$\hat{\mathbf{\Xi}} = \arg \min_{\mathbf{\Xi} \in \mathbb{C}^{N \times N_r}} \|\mathbf{\Xi}\|_{0,q}, \;\; \text{s.t.} \left\|\tilde{\mathbf{P}} - \mathbf{F}_R \mathbf{\Xi}\right\|_{q,q} \le \varepsilon_S, \quad\quad (6.13)$$

where ε_S denotes the error tolerance due to the background AWGN $\tilde{\mathbf{W}}$, and the $\ell_{p,q}$-norm of the matrix $\mathbf{\Xi}$ is defined by

$$\|\mathbf{\Xi}\|_{p,q} = \left(\sum_m \left\|(\mathbf{\Xi}^T)_m\right\|_p^q\right)^{1/q} \quad\quad (6.14)$$

with $(\mathbf{\Xi}^T)_m$ being the m-th row of $\mathbf{\Xi}$. The mixed $\ell_{0,q}$-norm minimization problem in (6.13) is a non-convex and NP-hard one. Fortunately, it can be convex relaxed to a mixed $\ell_{1,2}$-norm minimization problem equivalently according to the structured compressed sensing theory, yielding

$$\hat{\mathbf{\Xi}} = \arg \min_{\mathbf{\Xi} \in \mathbb{C}^{N \times N_r}} \|\mathbf{\Xi}\|_{1,2}, \;\; \text{s.t.} \left\|\tilde{\mathbf{P}} - \mathbf{F}_R \mathbf{\Xi}\right\|_{2,2} \le \varepsilon_S, \quad\quad (6.15)$$

and thus it is derived that the error bound due to AWGN can be calculated by

$$\varepsilon_S = \|\tilde{\mathbf{W}}\|_{2,2} = \sqrt{R N_r}\sigma_w. \quad\quad (6.16)$$

Note that the previously described classical compressed sensing-based approach can be regarded as a special case of the proposed structured compressed sensing-based framework with $N_r = 1$ in (6.12) and (6.13). The structured compressed sensing mixed $\ell_{1,2}$-norm minimization problem (6.15) can be efficiently solved using the structured compressed sensing-based greedy algorithms, such as simultaneous orthogonal matching pursuit (S-OMP) [14], etc. However, S-OMP requires the actual sparsity level to be known to reconstruct the sparse signal, which is impractical for the IN signal in realistic wireless MIMO systems. Moreover, there is no a priori information exploited in state-of-art methods. Hence, we propose the improved structured compressed sensing-based greedy algorithm of SPA-SAMP with the aid of the prior information to solve the mixed $\ell_{1,2}$-norm minimization problem efficiently and accurately, and improve the performance against conventional algorithms in MIMO systems.

6.4.3   Structured Prior Aided SAMP (SPA-SAMP) Algorithm

Unlike our previously proposed classical compressed sensing based greedy algorithm which copes with only one-dimensional measurement vector which is not robust in severe conditions, the proposed structured compressed sensing-based greedy algorithm SPA-SAMP further improves the performance by exploiting the spatial correlation of the IN signals at multiple receive antennas to maximize the accuracy of each iteration in the greedy pursuit process.

Firstly, since the intensity of the IN is normally much higher than that of data component or AWGN in the time domain, it is feasible to obtain a coarse a priori estimation of the partial support $\Pi_i^{(0)}$ of the IN signals at all the N_r receive antennas through power thresholding. The indices of the time-domain samples in the i-th OFDM symbols $\{\mathbf{y}_i^{(r)}\}_{r=1}^{N_r}$ with the average power exceeding the given threshold λ_t are included in the partial support $\Pi_i^{(0)}$, which is given by

$$\Pi_i^{(0)} = \left\{ n \left| \frac{1}{N_r} \sum_{r=1}^{N_r} \left| y_{i,n}^{(r)} \right|^2 \right. > \lambda_t, n = 0, 1, \ldots, N - 1 \right\}, \qquad (6.17)$$

where the power threshold λ_t is given by

$$\lambda_t = \frac{\alpha}{N N_r} \sum_{r=1}^{N_r} \sum_{n=0}^{N-1} \left| y_{i,n}^{(r)} \right|^2, \qquad (6.18)$$

where α is a scaling coefficient that can be configured large enough to ensure the accuracy of the time-domain partial support of the IN. Afterwards, the a priori partial support estimation $\Pi_i^{(0)}$ can be exploited to facilitate the initialization and iterations of SPA-SAMP.

The main principle of the SPA-SAMP algorithm is in the framework of structured compressed sensing and to minimize the mixed $\ell_{1,2}$-norm (6.15) of the spatially jointly sparse IN matrix $\mathbf{\Xi}$. With the aid of the prior information, the support of the IN is solved through iterations. Its pseudo-code is summarized in **Algorithm** 1. Specifically, the input includes the multi-dimensional measurements matrix $\tilde{\mathbf{P}}$, the observation matrix $\Psi = \mathbf{F}_R$, and the a priori partial support $\Pi_i^{(0)}$, as well as the iteration step size Δs, which can be a compromise between the convergence rate and the accuracy. During the multiple iterations, the accuracy of the temporary support estimation $\Pi^{(k)}{}_i$ is improved at each iteration, and the testing sparsity level T is increased by Δs when the stage switches. The halting condition is determined by the $\ell_{2,2}$-norm of the residual matrix $\|\mathbf{R}\|_{2,2} \leq C_\varepsilon \cdot \varepsilon_S$, in which C_ε is a constant controlling the halting condition and its value is given by (6.67) derived in the following proof of Theorem 6.7. The output of the algorithm is the final support $\hat{\Pi}_i$ and the recovered spatially jointly sparse IN matrix $\hat{\mathbf{\Xi}}$, s.t. $\left. \hat{\mathbf{\Xi}} \right|_{\hat{\Pi}_i} = \Psi_{\hat{\Pi}_i}^\dagger \tilde{\mathbf{P}}$, $\quad \left. \hat{\mathbf{\Xi}} \right|_{\hat{\Pi}_i^c} = \mathbf{0}$.

Afterwards, the r-th column of the recovered IN jointly sparse matrix $\hat{\Xi}$ at the output of **Algorithm** 1, namely $\hat{z}_i^{(r)}$, is exactly the estimation of the real time-domain IN signal $z_i^{(r)}$ corresponding to the i-th OFDM symbol at the r-th receive antenna. Then, this recovered IN signal can be canceled out from the received OFDM symbol at the r-th receive antenna before the following demapping and decoding.

The overall structure and explanations of each step of **Algorithm** 1 are described as follows:

Phase 1—Input before the algorithm. The a priori estimated support $\Pi_i^{(0)}$, the initial sparsity level $K^{(0)} = |\Pi_i^{(0)}|$, and the multi-dimensional measurements matrix $\tilde{P}$ are input into the algorithm.

Phase 2—Initialization phase. The initially estimated IN matrix is set by $\hat{\Xi}^{(0)}\big|_{\Pi_i^{(0)}}$ $\leftarrow \Psi_{\Pi_i^{(0)}}^{\dagger}\tilde{P}$, and the initial testing sparsity level is set by $T \leftarrow K^{(0)} + \Delta s$.

Phase 3—Main iterations. The main iterations are composed of the outer and inner loops. The outer loop is a repetition of multiple stages, with each stage being composed of multiple iterations and a different testing sparsity level, and the outer loop terminates until the halting condition of the algorithm is met, i.e. $\|R\|_{2,2} \leq C_\varepsilon \cdot \varepsilon_S$; Within the inner loop of each stage, the iterations process includes: 1) Preliminary test (Line 5–6), where the atoms corresponding to the largest $T - K^{(0)}$ entries generated by the residue matrix projection onto the dictionary $\left(\Psi^H R^{(k-1)}\right)_{l,j}$, are chosen as the preliminary list S_k; (2) Candidate list (Line 7), where the candidate support list L_k for the current iteration is made by aggregating the preliminary test list S_k and the temporary final support of the previous iteration $\Pi_i^{(k-1)}$; (3) Temporary final list (Line 8), where the temporary final support for the current iteration $\Pi_i^{(k)}$ is formed by selecting the largest T entries out of the projection of the measurements matrix $\tilde{P}$ onto the plane spanned by the subset of the dictionary Ψ_{L_k} corresponding to the candidate list L_k; (4) Sparse recovery and residue calculation (Line 10–11), where the estimated IN matrix is calculated based on the least squares principle implemented on the temporary final support $\Pi_i^{(k)}$, and the residue matrix R is calculated using the estimated IN matrix; (5) Stage switching (Line 12–17), where the stage is switched and the testing sparsity level T is increased by Δs when the $\ell_{2,2}$-norm of the residue matrix is greater than that of the previous iteration, otherwise the stage keeps the same and the iteration goes into the next.

Phase 4—Output. The output of the algorithm includes the final support $\hat{\Pi}_i$, and the recovered spatially jointly sparse IN matrix $\hat{\Xi}$ corresponding to the final support.

The solution existence and the convergence of **Algorithm** 5 are theoretically guaranteed, which is described in detail in Sect. 6.6. It should be observed from **Algorithm** 5 that the spatial correlation of the IN signals in the MIMO system is fully exploited in SPA-SAMP by considering the aggregated contributions of all the N_r projections associated with N_r receive antennas when selecting the optimal candidate list in each iteration, instead of making the candidate list from only one measurement vector as in state-of-art algorithms. Hence, the performance of IN recovery is significantly improved, which is reported in the following computer simulations. Furthermore, SPA-SAMP is more applicable in realistic wireless transmission sce-

---

Algorithm 5 Structured a Priori Aided Sparsity Adaptive Matching Pursuit (SPA-SAMP) for IN Recovery in MIMO System.

Input:

  1) *A priori* estimated support $\Pi_i^{(0)}$

  2) Initial sparsity level $K^{(0)} = |\Pi_i^{(0)}|$

  2) Measurements matrix $\tilde{\mathbf{P}}$

  3) Observation matrix $\boldsymbol{\Psi} = \mathbf{F}_\mathrm{R}$

  4) Iteration step size Δs.

  Initialization:

1: $\left.\hat{\boldsymbol{\Xi}}^{(0)}\right|_{\Pi_i^{(0)}} \leftarrow \boldsymbol{\Psi}_{\Pi_i^{(0)}}^{\dagger} \tilde{\mathbf{P}}$ (initially estimated IN matrix)

2: $\mathbf{R}^{(0)} \leftarrow \tilde{\mathbf{P}} - \boldsymbol{\Psi}\hat{\boldsymbol{\Xi}}^{(0)}$ (initial residue matrix)

3: $T \leftarrow K^{(0)} + \Delta s$ (initial testing sparsity level); $k \leftarrow 1$

  Iterations:

4: **repeat**

5:    $\mathbf{v} \in \mathbb{C}^N$ s.t. $v_l = \sum\limits_{j=1}^{N_\mathrm{r}} \left| \left(\boldsymbol{\Psi}^H \mathbf{R}^{(k-1)}\right)_{l,j} \right|$

6:    $S_k \leftarrow \mathrm{Max}\{\mathbf{v}, T - K^{(0)}\}$ {Preliminary test}

7:    $L_k \leftarrow \Pi_i^{(k-1)} \cup S_k$ {Make candidate list}

8:    $\mathbf{u} \in \mathbb{C}^{|L_k|}$ s.t. $u_l = \sum\limits_{j=1}^{N_\mathrm{r}} \left| \left(\boldsymbol{\Psi}_{L_k}^{\dagger} \tilde{\mathbf{P}}\right)_{l,j} \right|$

9:    $\Pi_i^{(k)} \leftarrow \mathrm{Max}\{\mathbf{u}, T\}$ {Temporary final list}

10:   $\left.\hat{\boldsymbol{\Xi}}^{(k)}\right|_{\Pi_i^{(k)}} \leftarrow \boldsymbol{\Psi}_{\Pi_i^{(k)}}^{\dagger}\tilde{\mathbf{P}};$ $\left.\hat{\boldsymbol{\Xi}}^{(k)}\right|_{\Pi_i^{(k)c}} \leftarrow \mathbf{0}$

11:   $\mathbf{R} \leftarrow \tilde{\mathbf{P}} - \boldsymbol{\Psi}_{\Pi_i^{(k)}}\boldsymbol{\Psi}_{\Pi_i^{(k)}}^{\dagger}\tilde{\mathbf{P}}$ {Compute residue}

12:   **if** $\|\mathbf{R}\|_{2,2} \geq \|\mathbf{R}^{(k-1)}\|_{2,2}$ **then**

13:     $T \leftarrow T + \Delta s$ {Stage switching}

14:   **else**

15:     $\hat{\Pi}_i \leftarrow \Pi_i^{(k)};$ $\mathbf{R}^{(k)} \leftarrow \mathbf{R}$

16:     $k \leftarrow k + 1$ {Same stage, next iteration}

17:   **end if**

18: **until** $\|\mathbf{R}\|_{2,2} \leq C_\varepsilon \cdot \varepsilon_S$ {Halting condition}

Output:

  1) Final output support $\hat{\Pi}_i$

  2) Recovered spatially jointly sparse IN matrix $\hat{\boldsymbol{\Xi}}$, s.t. $\left.\hat{\boldsymbol{\Xi}}\right|_{\hat{\Pi}_i} = \boldsymbol{\Psi}_{\hat{\Pi}_i}^{\dagger}\tilde{\mathbf{P}},$ $\left.\hat{\boldsymbol{\Xi}}\right|_{\hat{\Pi}_i^c} = \mathbf{0}$

---

narios than state-of-art structured compressed sensing-based greedy algorithms, such as S-OMP that requires the sparsity level to be known [14].

6.4.4   Simulation Results and Discussions
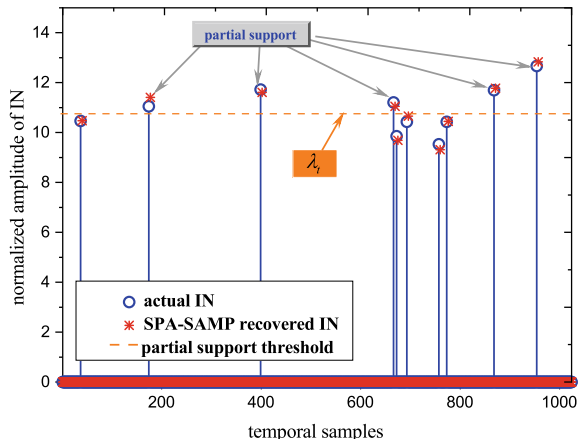
The performance of the proposed structured compressed sensing-based SMM method with the SPA-SAMP algorithm for IN recovery and cancelation in the MIMO wire-

less vehicular systems is evaluated through simulations. The simulation setup is basically configured in a wireless vehicular transmission scenario. The OFDM subcarrier number $N = 1024$ and the number of null sub-carriers $R = 128$. The 16QAM modulation scheme with the low density parity check (LDPC) code with code length of 1944 bits and code rate of 1/2 as specified in wireless local area networks [11] is adopted. The 2×2 MIMO system with spatial correlation at the receive antennas [20] in the presence of IN is adopted, where $N_t = N_r = 2$. The typical 6-tap multipath channel model named by Vehicular B specified by ITU-R is adopted [16], considering the low speed scenario with a receiver velocity of 30 km/h. The scaling coefficient for the partial support acquisition is $\alpha = 5.0$. The parameters of the IN are configured as $A = 0.15$, $\omega = 0.02$, $K = 10$, $\lambda = 50$/s and the INR is $\gamma_{IN} = 30$ dB.
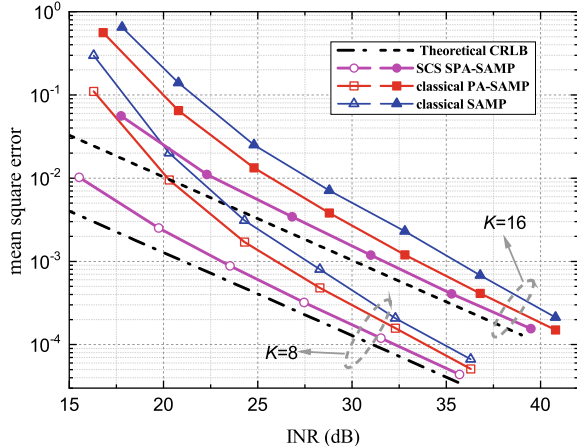
The performance of one realization of the IN recovery using the proposed structured compressed sensing-based SMM method with the SPA-SAMP algorithm for the 2×2 MIMO system is depicted in Fig. 6.5. The partial support is firstly obtained using the threshold λ_t in (6.18). From the null sub-carriers sets at the N_r receive antennas, we can get the joint measurements matrix of the IN from which the accurate IN is recovered using SPA-SAMP. It is observed from Fig. 6.5 that the final IN estimation matches the actual IN very well.

The mean square error (MSE) performances of the proposed SMM method with the structured compressed sensing-based SPA-SAMP algorithm, and the state-of-art compressed sensing-based algorithms (PA-SAMP and SAMP [21]) for IN recovery in the 2×2 MIMO system are shown in Fig. 6.6. The theoretical Cramer-Rao lower bound (CRLB) $\sigma_w^2 \cdot (K/R)$ is illustrated as a benchmark. It can be observed that the proposed structured compressed sensing-based SPA-SAMP algorithm achieves the

Fig. 6.5 General process of IN recovery using the proposed structured compressed sensing-based SMM method with the SPA-SAMP algorithm
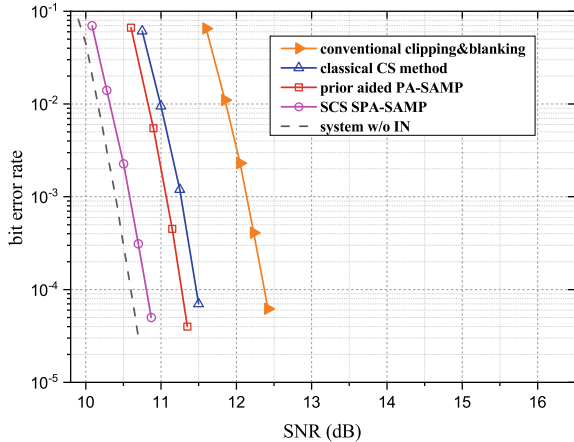
Fig. 6.6 MSE performance of the IN reconstruction using the proposed structured compressed sensing-based SMM method with the SPA-SAMP algorithm compared with state-of-art compressed sensing-based methods in the 2×2 MIMO system

MSE of 10^{-3} at the INR of 23.2 and 32.0 dB with $K = 8$ and $K = 16$, respectively, which outperforms conventional PA-SAMP and SAMP algorithms by approximately 2.2 and 3.8 dB, respectively. It is noted from Fig. 6.6 that the MSE of the proposed SPA-SAMP is asymptotically approaching the theoretical CRLB with the increase of the INR, verifying the high recovery accuracy.

The bit error rate (BER) performance of different IN mitigation and cancelation schemes in the 2×2 MIMO system is illustrated in Fig. 6.7, including the proposed structured compressed sensing-based SMM method with the SPA-SAMP algorithm, as well as the conventional non-compressed-sensing-based method (clipping and blanking [22]), and the classical compressed sensing-based methods (conventional compressed sensing measuring method of SCO [3] along with the SAMP algorithm [21] and our previously proposed PA-SAMP algorithm). The case without the IN is also depicted as a benchmark. In the simulations of BER, the V-BLAST coding is applied for MIMO data, and the transmitted data symbols at each antenna is independent of each other [23]. The receiver employs the independent demapping algorithm of max-log-MAP [24], and the SPA algorithm [25] is applied for LDPC decoding with the maximum iteration number being 50. It can be found that at the target BER of 10^{-4}, the proposed structured compressed sensing-based scheme outperforms the classical compressed sensing-based methods and the conventional clipping and blanking method by approximately 0.7 and 1.5 dB, respectively. Furthermore, the gap between the proposed method and the case without the IN is only about 0.16 dB, validating the accuracy and effectiveness of the proposed IN recovery scheme.

Fig. 6.7 BER performance
of different schemes for IN
mitigation and cancelation
for the 2×2 MIMO system
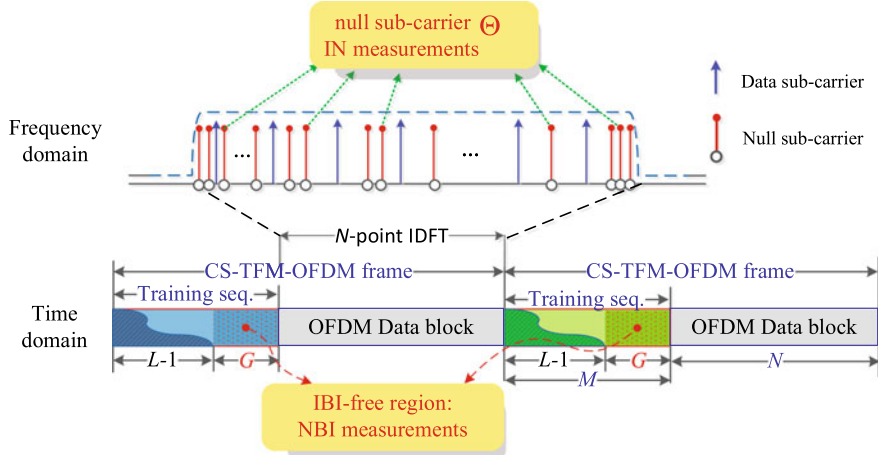
6.5   Compressed Sensing Joint Cancelation of NBI and IN

For the environment in the presence of both NBI and IN, this section formulates
the time-frequency combined compressed sensing framework and devises the time-
frequency training framework and the jointly sparse measurement model. An algo-
rithm of joint recovery and cancelation of the NBI and IN based on time-frequency
combined compressed sensing is proposed.

6.5.1   Time-Frequency Combined Measuring

In conventional wireless or wired vehicular communication systems, there is no
frame design for time and frequency combined training, which is not suitable for
conducting the time-frequency combined sparse measuring of the NBI and IN. Thus,
in this section, we introduce the novel compressed sensing-based time-frequency
measuring OFDM (CS-TFM-OFDM) frame structure to provide technical support
for the time-frequency combined sparse measuring and compressed sensing recov-
ery of the NBI and IN. In the proposed CS-TFM-OFDM frame structure, repeated
training sequences are devised for the temporal differential measuring of the NBI.
Repeated training sequences have already been adopted as guard intervals in the stan-
dards such as digital terrestrial television broadcasting (DTTB) specified in [26] for
channel estimation, synchronization, etc. Meanwhile, the null sub-carriers including
the reserved tones and the virtual mask sub-carriers are widely specified and applied
in state-of-art standards such as IEEE 802.11p and ITU-T G.9960 [11, 12, 17],
which can be utilized to acquire the measurement vector of IN under the proposed
CS-TFM-OFDM framework. Based on this time-frequency training OFDM frame

Fig. 6.8 Time-frequency frame structure of CS-TFM-OFDM exploited for compressed sensing-based joint NBI and IN recovery and cancelation

structure, the NBI and IN combined time-frequency sparse measuring framework can be formulated.

The proposed CS-TFM-OFDM frame structure applied in typical vehicular communication systems is shown in Fig. 6.8. In the time domain, the i-th frame $\mathbf{s}_i = \begin{bmatrix} \mathbf{c}^T & \mathbf{x}_i^T \end{bmatrix}^T$ consists of the constant training sequence $\mathbf{c} = \begin{bmatrix} c_0, c_1, \ldots, c_{M-1} \end{bmatrix}^T$ of length M and the following OFDM data block $\mathbf{x}_i = \begin{bmatrix} x_{i,0}, x_{i,1}, \ldots, x_{i,N-1} \end{bmatrix}^T$ of length N, where the training sequences for different frames are identical. The i-th time-domain OFDM data block is the IDFT of the related frequency-domain data in the N sub-carriers, which contains a set of reserved null sub-carriers denoted by the set Θ^0. Then the transmitted signal passes through the multi-path vehicular channel with the channel impulse response (CIR) of $\mathbf{h}_i = \begin{bmatrix} h_{i,0}, h_{i,1}, \ldots, h_{i,L-1} \end{bmatrix}^T$ with length L in the presence of the NBI $\tilde{\mathbf{e}}_i = \begin{bmatrix} \tilde{e}_{i,0}, \ldots \tilde{e}_{i,N-1} \end{bmatrix}^T$ (with length of N corresponding to N sub-carriers) and the IN $\mathbf{z}_i = \begin{bmatrix} z_{i,0}, \ldots z_{i,N+M-1} \end{bmatrix}^T$ (with length $N + M$ corresponding the the training sequence and OFDM data block), and considering the background AWGN $\mathbf{w}_i$. Then, at the receiver, the time-domain received i-th frame training sequence $\mathbf{y}_i = \begin{bmatrix} y_{i,0}, y_{i,1}, \ldots, y_{i,M-1} \end{bmatrix}^T$ can be presented as

$$\mathbf{y}_i = \mathbf{\Phi}_M \mathbf{h}_i + \mathbf{F}_M \tilde{\mathbf{e}}_i + \mathbf{S}_M \mathbf{z}_i + \mathbf{w}_i, \qquad (6.19)$$

where the $M \times (M + N)$ selection matrix $\mathbf{S}_M = [\mathbf{I}_M \ \mathbf{O}_N]$. The matrices $\mathbf{I}_M$ and $\mathbf{O}_N$ are the $M \times M$ identity matrix and the $N \times N$ zero matrix, respectively. $\mathbf{S}_M \mathbf{z}_i$ is the IN component corresponding to the i-th training sequence (if there exists IN bursting at the location of the training sequence, it is nonzero, otherwise it is zero). The partial inverse Fourier transform matrix $\mathbf{F}_M$ is given by Eq. (5.6). The

training sequence component at the receiver is denoted by $\boldsymbol{\Phi}_M \mathbf{h}_i$, with the matrix $\boldsymbol{\Phi}_M \in \mathbb{C}^{M \times L}$ represented by

$$
\boldsymbol{\Phi}_M = \begin{bmatrix}
c_0 & x_{i-1,N-1} & x_{i-1,N-2} & \cdots & x_{i-1,N-L+1} \\
c_1 & c_0 & x_{i-1,N-1} & \cdots & x_{i-1,N-L+2} \\
c_2 & c_1 & c_0 & \cdots & x_{i-1,N-L+3} \\
\vdots & \vdots & \vdots & \ddots & \vdots \\
c_{L-2} & c_{L-3} & c_{L-4} & \cdots & x_{i-1,N-1} \\
c_{L-1} & c_{L-2} & c_{L-3} & \cdots & c_0 \\
c_L & c_{L-1} & c_{L-2} & \cdots & c_1 \\
\vdots & \vdots & \vdots & \ddots & \vdots \\
c_{M-1} & c_{M-2} & c_{M-3} & \cdots & c_{M-L}
\end{bmatrix}, \tag{6.20}
$$

whose entries $\{x_{i-1,n}\}_{n=N-L+1}^{N-1}$ represent the last $L-1$ samples of the $(i-1)$-th OFDM data block $\mathbf{x}_{i-1}$, which causes inter-block-interference (IBI) on the i-th training sequence. Since the $(i-1)$-th OFDM data block $\mathbf{x}_{i-1}$ only causes IBI on the first $L-1$ samples of the i-th received training sequence $\mathbf{y}_i$, the last $G = M - L + 1$ samples of $\mathbf{y}_i$ will form the *IBI-free* region $\mathbf{q}_i^0 = [y_{i,L-1}, y_{i,L}, \ldots, y_{i,M-1}]^T$ denoted by

$$
\mathbf{q}_i^0 = \boldsymbol{\Phi}_G \mathbf{h}_i + \mathbf{F}_G \tilde{\mathbf{e}}_i + \mathbf{z}_i' + \mathbf{w}_i', \tag{6.21}
$$

where $\mathbf{q}_i^0$ consists of the last G elements of $\mathbf{y}_i$, while $\mathbf{F}_G$ and $\boldsymbol{\Phi}_G$ are the $G \times N$ observation matrix composed of the last G rows of $\mathbf{F}_M$, and the $G \times L$ Toeplitz matrix composed of the last G rows of $\boldsymbol{\Phi}_M$ in (6.20), respectively. The corresponding IN vector $\mathbf{z}_i'$ is composed of the last G entries of $\mathbf{S}_M \mathbf{z}_i$ in (6.19). $\mathbf{w}_i'$ denotes the AWGN vector related to the IBI-free region with zero mean and the variance of σ_w^2. As has been described previously in Sects. 5.5.1 and 5.3.1, the IBI-free region exists in practical wireless communication systems because a common rule for the system design is to configure the guard interval length M to be larger than the maximum channel length L in the worst case to avoid IBI between OFDM data blocks, so L is usually smaller than M, i.e., $L < M$.

In the frequency domain at the receiver as depicted in Fig. 6.8, the received data in the reserved null sub-carriers set Θ^0 are denoted by

$$
\tilde{\mathbf{p}}_i^0 = \mathbf{F}_R \mathbf{z}_i + \mathbf{S}_R \tilde{\mathbf{e}}_i + \tilde{\mathbf{w}}_i, \tag{6.22}
$$

where the vector $\tilde{\mathbf{p}}_i^0 = [\tilde{p}_{i,0}^0, \tilde{p}_{i,1}^0, \ldots, \tilde{p}_{i,R-1}^0]^T$ of length $R = |\Theta^0|$ is the measurement vector of the IN at the null sub-carriers. $\mathbf{S}_R \tilde{\mathbf{e}}_i$ is the frequency-domain NBI component corresponding to the null sub-carriers set Θ^0 (if there exists NBI at the null sub-carriers set Θ^0, its value is nonzero, otherwise it is zero). $\mathbf{S}_R$ is an $R \times N$ selection matrix with $(\mathbf{S}_R)_{i,k_i} = 1$, $k_i \in \Theta^0$, $i = 1, \ldots R$, and other entries being zero. $\tilde{\mathbf{w}}_i$ denotes the corresponding frequency-domain AWGN vector, while

the observation matrix to be used for the compressed sensing-based IN recovery is the partial discrete Fourier transform (DFT) matrix $\mathbf{F}_R$ given by

$$\mathbf{F}_R = \frac{1}{\sqrt{N}}[\boldsymbol{\chi}_0 \quad \boldsymbol{\chi}_1 \quad \cdots \quad \boldsymbol{\chi}_{N+M-1}], \tag{6.23}$$

where the entries $\boldsymbol{\chi}_m$ contains are $\exp(-j2\pi mk/(N+M))$, $k \in \Theta^0$, $m = 0, \ldots,$ $N + M - 1$. The measurement vector $\tilde{\mathbf{p}}_i^0$ at the set Θ^0 contains the IN component and the background AWGN, while the OFDM data component is not included since the null sub-carriers are set to zeros at the transmitter.

6.5.2   Time-Frequency Combined Recovery of NBI and IN

In order to recover the NBI and IN in the framework of CS-TFM-OFDM time-frequency combined compressed sensing, firstly we should obtain the temporal differential measurement vector of the NBI and the frequency-domain sparse measurement vector of the IN. We should guarantee that they are not affecting each other, so that the compressed sensing based time-frequency combined sparse recovery model can be formulated. Thereafter the compressed sensing based algorithms are utilized for NBI and IN recovery.

(1) *NBI temporal differential measurement modeling and compressed sensing recovery*
First, we investigate the acquisition of the NBI measurement vector. The measurement vector is supposed to contain the NBI component. However, the data or training sequence components are mixed up with the NBI in the measurement vector and should be nulled out to improve the performance of compressed sensing-based recovery. Besides, the measurement data impacted by the IN should also be removed so as to avoid the affect of the IN.

Considering conducting temporal differential measuring for the IBI-free region (6.21) of the received training sequence, since the CIR within the adjacent training sequences are the same and can be regarded as invariant ($\mathbf{h}_i \approx \mathbf{h}_{i+1}$), the received training sequence component $\boldsymbol{\Phi}_G \mathbf{h}_i$ can be eliminated by subtracting $\mathbf{q}_{i+1}^0$ from $\mathbf{q}_i^0$, i.e. the temporal differential measuring operation of the IBI-free region in the adjacent training sequences. Thus we have

$$\varDelta \mathbf{q}_i^0 = \mathbf{F}_G \varDelta \tilde{\mathbf{e}}_i + \varDelta \mathbf{w}_i' + \varDelta \mathbf{z}_i', \tag{6.24}$$

where $\varDelta \mathbf{q}_i^0 = \mathbf{q}_i^0 - \mathbf{q}_{i+1}^0 \overset{\varDelta}{=} \left[\varDelta q_{i,0}^0, \ldots \varDelta q_{i,G-1}^0\right]^T$, $\varDelta \mathbf{w}_i' = \mathbf{w}_i' - \mathbf{w}_{i+1}'$, $\varDelta \mathbf{z}_i' = \mathbf{z}_i' - \mathbf{z}_{i+1}'$, while the NBI differential vector $\varDelta \tilde{\mathbf{e}}_i \in \mathbb{C}^N$ is denoted as

$$\varDelta \tilde{\mathbf{e}}_i = \tilde{\mathbf{e}}_i - \tilde{\mathbf{e}}_{i+1} = \left[\varDelta \tilde{e}_{i,0}, \varDelta \tilde{e}_{i,1}, \ldots, \varDelta \tilde{e}_{i,N-1}\right]^T. \tag{6.25}$$

As described in Chap. 5, due to the temporal correlation of the NBI, there is a relation that the frequency-domain NBI vector at the $(i + 1)$-th training sequence $\tilde{\mathbf{e}}_{i+1}$ equals $\tilde{\mathbf{e}}_i$ at the i-th training sequence with a phase shift, i.e., $\tilde{e}_{i+1,k} = \tilde{e}_{i,k} \exp(j2\pi k \Delta l / N), k = 0, 1, \ldots N - 1$. Therefore, the entries of the NBI differential vector in (6.25) are given by

$$\Delta \tilde{e}_{i,k} = \tilde{e}_{i,k} \left(1 - \exp \left(\frac{j2\pi k \Delta l}{N} \right) \right), k = 0, 1, \ldots, N - 1. \qquad (6.26)$$

In order to completely eliminate the possible IN component $\Delta \mathbf{z}'_i$ in the NBI differential vector (6.24), and thus completely avoid any negative impacts of the IN on the effects of NBI temporal differential measuring, we can conduct an operation of refinement on $\Delta \mathbf{q}_i^0$ in the original NBI measurement vector. That is, the power thresholding method can be utilized to exclude the measurement samples possibly contaminated by the IN, i.e. the measurement data samples in $\Delta \mathbf{q}_i^0$ whose power exceeds the following power threshold should be excluded:

$$\eta_t = \alpha \cdot \frac{1}{G} \sum_{m=1}^{G} \left| \Delta q_{i,m}^0 \right|^2, \qquad (6.27)$$

where α is a scaling coefficient given by $\alpha = \sqrt{\sum_{j \in \Pi_i} |z_{i,j}|^2 / (2\sigma_w^2 K)}$ to ensure the accuracy of excluding IN contaminated samples and avoid mislabeled samples impacted by IN. After the refinement operation that excludes the possible IN contamination, the accurate NBI differential vector only containing the NBI and background AWGN components can be obtained given by

$$\Delta \mathbf{q}_i = \mathbf{F}_G \Delta \tilde{\mathbf{e}}_i + \Delta \mathbf{w}'_i, \qquad (6.28)$$

where $\Delta \mathbf{q}_i$ is the refined NBI differential vector after excluding the possible IN contamination. Till now, we have formulated the NBI compressed sensing measurement model (6.28). According to the compressed sensing theory described previously, to solve the compressed sensing underdetermined linear inverse problem can be convex relaxed and turned to solving the following ℓ_1-norm minimization problem:

$$\min_{\Delta \tilde{\mathbf{e}}_i \in \mathbb{C}^N} \| \Delta \tilde{\mathbf{e}}_i \|_1, \quad \text{s.t.} \| \Delta \mathbf{q}_i - \mathbf{F}_G \Delta \tilde{\mathbf{e}}_i \|_2 \leq \varepsilon_N, \qquad (6.29)$$

where ε_N is the noise tolerance generated by the AWGN $\Delta \mathbf{w}'_i$, which can be preset according to the AWGN distribution [6].

Thus, the ℓ_1-norm minimization problem (6.29) can be efficiently solved by compressed sensing greedy algorithms, such as the proposed PA-SAMP algorithm. According the the PA-SAMP algorithm, the partial support of the NBI should be estimated as the prior information. The N-point DFT of the measurement vector $\Delta \tilde{\mathbf{q}}_i = \left[\Delta \tilde{q}_{i,0}, \Delta \tilde{q}_{i,1}, \ldots, \Delta \tilde{q}_{i,N-1} \right]$ contains some partial information of the NBI

support, with some spectral leakage because the measurement vector length G is smaller than N. However, the intensity of the NBI is commonly much higher than that of AWGN, which improves the resolution of the NBI locations in the spectrum of $\Delta \tilde{\mathbf{q}}_i$. Hence, it is feasible to obtain the estimation of the NBI partial support $\Omega^{(0)}$ at the i-th frame through thresholding. The sub-carriers with power exceeding the power threshold λ_f are included in the partial support $\Omega^{(0)}$, which is given by

$$\Omega^{(0)} = \left\{ k \left| \left| \Delta \tilde{q}_{i,k} \right|^2 > \lambda_f, k = 0, 1, \ldots, N-1 \right. \right\}, \tag{6.30}$$

where the power threshold λ_f is

$$\lambda_f = \frac{\beta}{N} \sum_{k=0}^{N-1} \left| \Delta \tilde{q}_{i,k} \right|^2, \tag{6.31}$$

where β is a scaling coefficient that can be configured proportional to the INR in different scenarios, and is empirically given by $\beta = \sqrt{2\sigma_e^2/\sigma_w^2}$ as an appropriate choice that proffers a proper tradeoff between the complexity and accuracy. This is intuitively understandable because when the INR is high, the threshold should become larger to avoid a too aggressive support that might include extra false entries. On the other hand, smaller INR will drive the threshold to become smaller to include more true entries in the partial support, i.e. to make the support less conservative, to avoid complexity increase.

The a priori partial NBI support will help improve the performance of the compressed sensing algorithm for NBI recovery, especially in severe conditions where the INR is relatively lower or the sparsity level is larger.

Thus, we can use the prior aided compressed sensing based greedy algorithm, i.e. PA-SAMP (see Algorithm 1 for detail), to accurately recover the NBI differential vector $\Delta \hat{\mathbf{e}}_i$. According to Eq. (6.26), the frequency-domain NBI differential vector corresponding to the i-th frame training sequence $\tilde{\mathbf{e}}_i$ can be derived from the compressed sensing recovered NBI differential vector $\Delta \hat{\mathbf{e}}_i$ as given by

$$\tilde{e}_{i,k} = \Delta \hat{e}_{i,k} \left/ \left(1 - \exp \left(\frac{j2\pi k \Delta l}{N} \right) \right) \right., k = 0, 1, \ldots, N-1. \tag{6.32}$$

Thus, the frequency-domain NBI vector corresponding to the i-th frame OFDM data block $\tilde{\mathbf{e}}_i^D = \left[\tilde{e}_{i,0}^D, \tilde{e}_{i,1}^D, \ldots, \tilde{e}_{i,N-1}^D \right]^T$ can be similarly obtained as

$$\tilde{e}_{i,k}^D = \tilde{e}_{i,k} \cdot \exp \left(\frac{j2\pi k \Delta d}{N} \right), k = 0, 1, \ldots, N-1, \tag{6.33}$$

where $\Delta d = M$ is the distance between the i-th frame training sequence and the OFDM data block. After obtaining the frequency-domain NBI vector corresponding to the OFDM data block, it can be eliminated. The subsequent demapping and

decoding process of the signal of interest at the receiver can be free from the impact of the NBI.

(2) *Frequency-Domain Sparse Measuring and Compressed Sensing Recovery for IN*
Recall that the measurement vector of IN $\tilde{\mathbf{p}}_i^0$ as well as the observation matrix $\mathbf{F}_R$ have been acquired from the null sub-carriers in (6.22), it is feasible to recover the IN vector in the presence of background AWGN based on the compressed sensing theory.

In order to guarantee the accuracy of compressed sensing based IN recovery, the IN measurement vector should only contain the IN and AWGN components, but not the possibly existing NBI component. Thus, before solving the compressed sensing problem to recover the IN, in order to eliminate the probable influence of the NBI on the compressed sensing-based IN recovery, it is necessary to exclude the NBI contaminated sub-carriers with power exceeding the given threshold η_f from the null sub-carriers set Θ^0, with the threshold given by

$$\eta_f = \frac{\beta^2}{R} \sum_{k=0}^{R-1} \left| \tilde{p}_{i,k} \right|^2, \tag{6.34}$$

where β is given in (6.31). At the null sub-carriers set Θ^0, if there happens to be an NBI contaminated sub-carrier, it will be correctly detected and excluded by this thresholding procedure, because the intensity of the NBI is much higher than that of the frequency-domain component of IN (due to the DFT property) as well as the background AWGN. Therefore, the original null sub-carriers set Θ^0 can be refined to Θ by excluding these possibly NBI contaminated null sub-carriers, and the measurement vector $\tilde{\mathbf{p}}_i^0$ in (6.22) is refined accordingly by excluding the corresponding entries. Then, it can be turned into an NBI-free frequency-domain IN measurement vector $\tilde{\mathbf{p}}_i$ as given by

$$\tilde{\mathbf{p}}_i = \mathbf{F}_R \mathbf{z}_i + \tilde{\mathbf{w}}_i. \tag{6.35}$$

Exploiting the refined measurement vector $\tilde{\mathbf{p}}_i$, the IN recovery problem model can be formulated based on the compressed sensing theory, i.e. the convex relaxed ℓ_1-norm minimization problem as given by

$$\min_{\mathbf{z}_i \in \mathbb{C}^N} \|\mathbf{z}_i\|_1, \quad \text{s.t.} \|\tilde{\mathbf{p}}_i - \mathbf{F}_R \mathbf{z}_i\|_2 \leq \varepsilon_I, \tag{6.36}$$

ε_I is the noise tolerance generated by AWGN $\tilde{\mathbf{w}}_i$.

The ℓ_1-norm minimization problem (6.36) can also be efficiently solved by the compressed sensing based greedy algorithms, such as the PA-SAMP algorithm. The a priori information of the IN partial support will also improve the performance of compressed sensing-based IN recovery. Since the intensity of IN is normally much higher than that of the time-domain data component or AWGN component, it is feasible to obtain the IN partial support $\Pi_i^{(0)}$ at the i-th OFDM data block through the thresholding operation of the received time-domain OFDM data block $\mathbf{x}_i$. The

time-domain samples with power exceeding the given threshold λ_t are included in the partial support $\Pi_i^{(0)}$, which is given by

$$\Pi_i^{(0)} = \left\{ n \left| \left| x_{i,n} \right|^2 > \lambda_t, n = 0, 1, \ldots, N - 1 \right. \right\}, \qquad (6.37)$$

where the power threshold λ_t is given by

$$\lambda_t = \alpha \cdot \frac{1}{N} \sum_{n=0}^{N-1} \left| x_{i,n} \right|^2, \qquad (6.38)$$
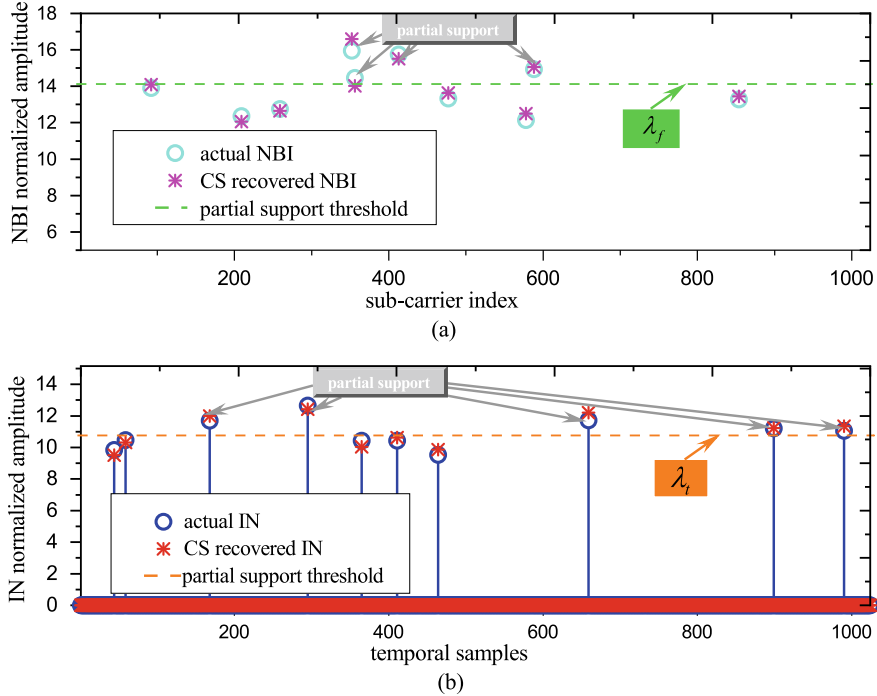
where α is a scaling coefficient given in (6.27). The IN partial support is able to improve the performance of the compressed sensing algorithm for IN recovery, especially in severe conditions where the INR is relatively low or the sparsity level of IN is large.

After obtaining the partial support, the PA-SAMP algorithm (see Algorithm 1 for detail) can be used to recover the IN. After the algorithm is conducted, the recovered time-domain IN vector $\hat{\mathbf{z}}_i$ is output, which is exactly the time-domain IN vector corresponding to the i-th frame OFDM data block. Thus, the IN can be completely removed from the received OFDM data block, and the subsequent demodulation and decoding process can be free from the impact of the IN.

Consequently, the compressed sensing based time-frequency combined recovery method for NBI and IN described in this section, can accurately and efficiently recover the NBI and IN simultaneously, and eliminate the impacts of them from the received signal of interest completely. The proposed method has taken into account the interference between the NBI and IN. The time and frequency domain measurement vectors for the NBI and IN are independent of each other, so the framework of robust and accurate elimination for NBI and IN is formulated.

6.5.3 Simulation Results and Discussions

The performance of the proposed compressed sensing-based simultaneous NBI and IN cancelation schemes for wireless communications scenario is investigated and validated through extensive simulations. The signal bandwidth is configured as 7.56 MHz located at the central frequency of 6 GHz. The ITU-R Vehicular B channel model [16] widely used to emulate the wireless channel with the relative receiver velocity of 30 km/h as low-speed mobility is applied. The OFDM sub-carrier number $N = 1024$, the length of each training sequence $M = 128$, and the number of null sub-carriers $R = 128$ are adopted. The modulation scheme 64QAM and the low density parity check (LDPC) with code length of 64,800 and code rate of 2/3 [27] is adopted. Consider the transmission environment in the presence of both NBI and IN, where the INR of the NBI is INR = 30 dB. The IN arrival rate is described by
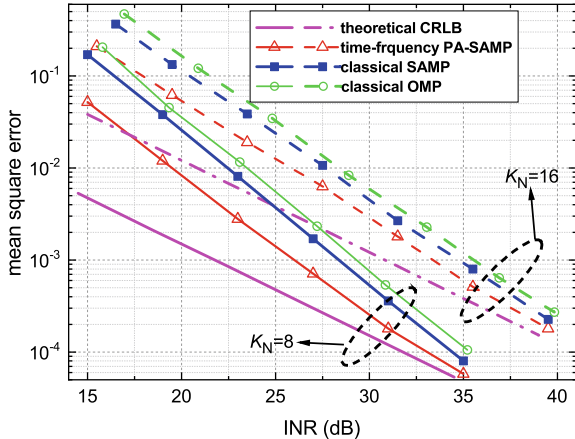
Fig. 6.9 General process of NBI and IN recovery based on time-frequency combined compressed sensing with PA-SAMP algorithm: **a** NBI recover **b** IN recovery

Poisson process with a moderate value of $\lambda = 50/s$, and the instantaneous amplitude of the IN is modeled by the Middleton's Class A distribution with the parameters $A = 0.15$ and $\omega = 0.02$.
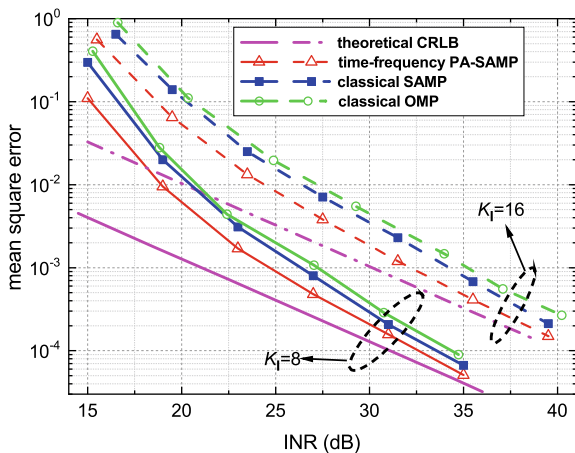
The general process of the proposed approach for compressed sensing based NBI and IN combined recovery is depicted in Fig. 6.9 with the NBI sparsity $K_N = 10$ and IN sparsity $K_I = 10$. It can be noted from the simulation results that the final NBI and IN estimations using the PA-SAMP algorithm accurately match the actual NBI and IN, respectively, in the framework of time-frequency combined compressed sensing framework.

The mean square error (MSE) performance of NBI and IN recovery using the proposed method is shown in Fig. 6.10 and Fig. 6.11, respectively. The theoretical Cramer-Rao lower bounds (CRLB) $2\sigma_w^2 \cdot (K_N/G)$ and $2\sigma_w^2 \cdot (K_I/R)$ for NBI and IN, respectively, are also included as benchmarks. In Fig. 6.10, the performance of the proposed scheme for NBI recovery with the greedy algorithms of PA-SAMP and the classical SAMP [21] and OMP [28] algorithms (assuming that the sparsity level is known for OMP to make the performance of OMP comparable) are depicted for the sparsity level $K_N = 8$ and $K_N = 16$. The PA-SAMP algorithm achieves a target MSE of 10^{-3} at the INR of 26.3 and 33.1 dB with the sparsity level $K_N =$

Fig. 6.10 MSE performance comparison for NBI reconstruction using proposed compressed sensing based scheme with PA-SAMP and SAMP algorithms
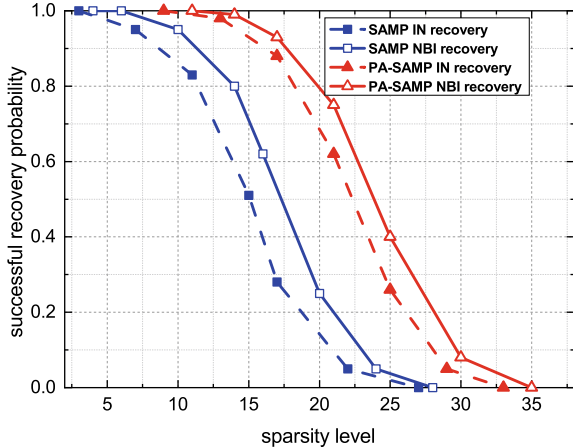

Fig. 6.11 MSE performance comparison for IN reconstruction using proposed compressed sensing based scheme with PA-SAMP and SAMP algorithms

8 and $K_N = 16$, respectively, which outperforms the classical SAMP and OMP algorithms by approximately 1.7 and 2.0 dB, respectively. Figure 6.11 shows the MSE performance of the compressed sensing-based IN recovery scheme. The PA-SAMP algorithm achieves the MSE 10^{-3} at the INR of 24.6 and 32.3 dB with $K_I = 8$ and $K_I = 16$, respectively, which outperforms SAMP and OMP by approximately 1.8 and 2.2 dB, respectively. It is noted from Figs. 6.10 to 6.11 that the MSE of the proposed methods approach the theoretical CRLB with the increase of the INR, so the high accuracy of the proposed simultaneous NBI and IN cancelation method is verified for vehicular communications.

The recovery probability of the proposed simultaneous NBI and IN recovery method versus different sparsity levels under the Vehicular B channel is depicted in Fig. 6.12. The recovery probability is calculated by counting the ratio of successful recovery, i.e. correct support and MSE$< 10^{-3}$, within 10^3 times of simulations. The
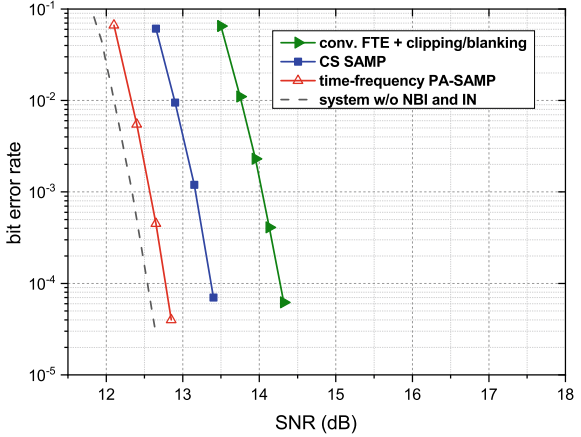
Fig. 6.12 Successful recovery probability of NBI and IN recovery using the proposed time-frequency combined compressed sensing PA-SAMP and SAMP algorithms

proposed simultaneous NBI and IN recovery method based on PA-SAMP reaches a successful recovery probability of 0.9 at the sparsity level of more than 16, which indicates that the proposed method based on PA-SAMP correctly recovers the NBI and IN at large sparsity levels from only a small portion of acquired measurement vector. For the NBI and IN in common wireless communications scenarios, the typical sparsity level of the NBI and IN is between 10 and 20 [3, 29], which indicates the effectiveness of the proposed scheme in practice. It is also noted from the gap between the curves of PA-SAMP and SAMP based methods that the proposed PA-SAMP method can accurately recover NBI and IN with the aid of partial support.

The bit error rate (BER) performance of the proposed simultaneous NBI and IN cancelation scheme under the Vehicular B channel in the presence of both NBI and IN is shown in Fig. 6.13. In the simulations, the receiver employs the independent demapping algorithm of max-log-MAP [24], and the SPA algorithm [25] is adopted for LDPC decoding with the maximum iteration number of 50. The BER performance of the conventional non-compressed sensing-based method, i.e. the traditional frequency threshold excision (FTE) anti-NBI method [30] along with clipping and blanking anti-IN method [31], and the proposed time-frequency combined compressed sensing-based method with the PA-SAMP and SAMP are presented for comparison. The worst case ignoring NBI and IN is also depicted as a benchmark. It can be found that at the target BER of 10^{-4}, the proposed time-frequency combined method with the proposed PA-SAMP algorithm outperforms the proposed method with classical SAMP and the conventional non-compressed sensing-based method by approximately 0.58 and 1.56 dB, respectively. Furthermore, the gap between the proposed method and the ideal case without NBI and IN is only about 0.25 dB, validating the accuracy and effectiveness of the proposed simultaneous NBI and IN recovery method in the severe environment.

Fig. 6.13 BER performance comparison of different mitigation and cancelation schemes in the presence of both NBI and IN

6.6 Algorithm Performance Evaluation

(1) *Computational Complexity Analysis*

The computational complexity of SPA-SAMP is mainly composed of two parts, i.e. the prior information acquisition and the iteration process. The prior information acquisition requires the complexity of $\mathcal{O}(N_\mathrm{r}N)$. The complexity of the iteration process is as follows: Each iteration mainly contains two steps. One is the complexity required by the matrix multiplication between the observation matrix Ψ and the residue matrix $\mathbf{R}$, i.e. $\mathcal{O}(N_\mathrm{r}RN)$. The other is the equivalent least squares problem, i.e. $\hat{\mathbf{\Xi}}^{(k)}\Big|_{\Pi_i^{(k)}} \leftarrow \Psi_{\Pi_i^{(k)}}^\dagger \tilde{\mathbf{P}}$, which requires the complexity of $\mathcal{O}(N_\mathrm{r}RN)$. The total iteration number in average is $K - K^{(0)}$, so the complexity of iteration process is $\mathcal{O}\big((K - K^{(0)})N_\mathrm{r}R(N + K)\big)$. Consequently, the total complexity is also $\mathcal{O}\big((K - K^{(0)})N_\mathrm{r}R(N + K)\big)$. Due to the sparse property of the IN, we have $K \ll N$, so the complexity of SPA-SAMP is moderate in common. Compared with the structured compressed sensing based greedy algorithm, i.e. S-SAMP in **Algorithm** 2 as proposed in Chap. 5 whose complexity is $\mathcal{O}\left(N_r M + K N_r M(N + K)\right)$, it can be noted that the average iteration number is reduced due to the introduction of the prior information of the partial support, which greatly reduces the complexity.

(2) *Solution Existence and Convergence of SPA-SAMP*

Now we analyze the solution existence and the convergence of the proposed SPA-SAMP algorithm, and provide the theoretical proof of the related theorems based on the theory of compressed sensing and structured compressed sensing.

Before providing the theorems to guarantee the solution existence and convergence of the SPA-SAMP algorithm, we first provide Lemma 6.1 to show that the output estimated support of any stage in SPA-SAMP is equivalent to the final output support of the classical subspace pursuit (SP) algorithm [15] with corresponding sparsity level. Then, we provide two theorems to prove the solution existence and

convergence of the proposed SPA-SAMP algorithm based on the Lemma 6.1, with the RIP condition of the observation matrix $\mathbf{F}_R$ and the block-RIP condition of the generated block-sparse observation matrix $\Psi_B = (\mathbf{F}_R \otimes \mathbf{I}_{N_r})$, where $\otimes$ is the Kronecker product operation of matrices.

Lemma 6.1 *The output temporal estimated support of the ℓ-th stage in SPA-SAMP $\forall \ell \in [1, \ldots, \lceil K/\Delta s \rceil]$, is equivalent to the final output support of the SP algorithm [15] with the sparsity level $K_\ell = \ell \cdot \Delta s$.*

The proof of Lemma 6.1 is given as follows.

Proof The key of this proof is to prove the equivalence of the key steps, i.e. the preliminary test (Line 5–6 in Algorithm 1) and making temporary final list (Line 8-9 in Algorithm 1), to those of the SP algorithm in [15], under the condition of the spatial correlation of the IN signals at different receive antennas. We have the following two propositions:

Proposition 6.2 (preliminary test) *The process of the preliminary test (Line 5–6 in Algorithm 5) in SPA-SAMP as given by*

$$S_k \leftarrow \text{Max}\{\mathbf{v} \in \mathbb{C}^N, T - K^{(0)}\} \tag{6.39}$$

$$\text{s.t. } v_l = \sum_{j=1}^{N_r} |(\Psi^H \mathbf{R}^{(k-1)})_{l,j}|, \quad l \in [1, \ldots, N] \tag{6.40}$$

is equivalent to the step 1) of the SP algorithm in [15], i.e.,

$$S_k^{(j)} \leftarrow \text{Max}\{\mathbf{v}^{(j)}, T - K^{(0)}\} \tag{6.41}$$

$$\text{s.t. } v_l^{(j)} = |(\Psi^H \mathbf{r}_j^{(k-1)})_l|, \quad \forall j \in [1, \ldots N_r], \tag{6.42}$$

where $\mathbf{r}_j^{(k-1)} = \mathbf{R}_j^{(k-1)}$ is the j-th column of $\mathbf{R}^{(k-1)}$.

Proposition 6.3 (temporary final list) *The process of making the temporary final list (Line 8–9 in Algorithm 5) in SPA-SAMP as given by*

$$\Pi^{(k)} \leftarrow \text{Max}\{\mathbf{u} \in \mathbb{C}^{|L_k|}, T\} \tag{6.43}$$

$$\text{s.t. } u_l = \sum_{j=1}^{N_r} |(\Psi_{L_k}^\dagger \tilde{\mathbf{P}})_{l,j}|, \quad l \in [1, \ldots, |L_k|] \tag{6.44}$$

is equivalent to the steps (2) and (3) of the SP algorithm in [15], i.e.,

$$\Pi_{(j)}^{(k)} \leftarrow \text{Max}\{\mathbf{u}^{(j)}, T\} \tag{6.45}$$

$$\text{s.t. } u_l^{(j)} = |(\Psi_{L_k^{(j)}}^\dagger \tilde{\mathbf{p}}_i^{(j)})_l|, \quad \forall j \in [1, \ldots N_r]. \tag{6.46}$$

where $\Pi_{(j)}^{(k)}$ is the temporary final list of k-th iteration for j-th receive antenna.

Now we prove the above two propositions. For Proposition 6.2, based on the *orthogonality property* of the least squares principle [32], the process of (6.41) and (6.42) can pick out the best atoms set (columns of Ψ), i.e. $S_k^{(j)}$, which is the most probable to be included in the real support of the corresponding IN vector $\mathbf{z}_i^{(j)}$ out of all the atoms in Ψ, through choosing the largest inner-products between the residue vector $\mathbf{r}_j^{(k-1)}$ and the dictionary matrix Ψ. By doing so, the selected preliminary test of k-th iteration for j-th receive antenna list is given by

$$S_k^{(j)} = \Pi_{(j)} - \Pi_{(j)}^{(k-1)} \bigcap \Pi_{(j)}, \tag{6.47}$$

where $\Pi_{(j)}$ is the real support of the IN signal at j-th receive antenna. Because of the spatial correlation $\Pi_{(j)} = \Pi, \forall j \in [1, \dots N_\mathrm{r}]$, and $\Pi_{(j)}^{(k-1)} = \Pi^{(k-1)}$ due to the Mathematical Induction principle as presented later in this proof, one has

$$S_k^{(j)} = S_k, \quad \forall j \in [1, \dots N_\mathrm{r}]. \tag{6.48}$$

Then, based on (6.48), it can be noted that the preliminary test list calculated from each process of (6.41) associated with the j-th receive antenna yields the same atoms set S_k, hence, the process of (6.39), which picks out the atoms set by accumulating all the N_r residue vector inner-products, is equivalent to (6.41). Thus Proposition 6.2 holds, which guarantees the equivalence of the preliminary test lists of the two algorithms.

For Proposition 6.3, the process of solving the problem (6.45) and (6.46) is picking out the best T atoms set $\Pi_{(j)}^{(k)}$ out of the enlarged candidate list $L_k^{(j)}$, so that the selected set $\Pi_{(j)}^{(k)}$ (temporary final list) is corresponding to the largest T projections (coordinates) of $\tilde{\mathbf{p}}_i^{(j)}$ onto the spanned plane of the atoms (columns) in $\Psi_{L_k^{(j)}}$. Hence, one has

$$\Pi_{(j)}^{(k)} = \Pi_{(j)} \bigcap L_k^{(j)}, \tag{6.49}$$

where $L_k^{(j)} = S_k^{(j)} \bigcup \Pi_j^{(k-1)}$ is the enlarged candidate list with $|L_k^{(j)}| > T$, and from (6.48) along with the spatial correlation, one has

$$L_k^{(j)} = L_k, \quad \forall j \in [1, \dots N_\mathrm{r}] \tag{6.50}$$

$$\Pi_{(j)}^{(k)} = \Pi^{(k)}, \quad \forall j \in [1, \dots N_\mathrm{r}] \tag{6.51}$$

where (6.51) can be further induced in detail using the principle of Mathematical Induction for argument k, based on the margin fact that $\Pi_{(j)}^{(0)} = \Pi^{(0)}, \forall j$, due to the spatial correlation, along with the inductions of (6.47) through (6.49). In fact, for $k = 1$, Eqs. (6.47) through (6.51) hold obviously; for $k \geq 1$, if they hold for $k - 1$, it is obvious that they also hold for k. Based on (6.51), it can be noted that the temporary final list calculated from each process of (6.45) associated with the j-th receive antenna yields the same atoms set $\Pi^{(k)}$, hence, the process of (6.43), which picks out the atoms set by accumulating each of the N_r measurement vector projections, is

equivalent to (6.45). Thus Proposition 6.3 holds, which guarantees the equivalence of making temporary final lists for the two algorithms.

From these two propositions, one can infer that, for the ℓ-th stage of SPA-SAMP (the corresponding sparsity level $K_\ell = \ell \cdot \Delta s$), the preliminary and temporary final lists for each iteration are the same with those of SP with K_ℓ, so the output estimated final supports of them are equal. Consequently, we reach the conclusion that the output estimated final support of the SPA-SAMP at the ℓ-th stage should be the same with that of SP with sparsity level $K_\ell = \ell \cdot \Delta s$.

After this lemma, we derive the following two important theorems concerning about the convergence and performance error bound of the proposed SPA-SAMP algorithm. At the beginning, a lemma concerning about the iteration number within each stage is given as follows:

Lemma 6.4 (iteration number within stage) *Let $n_{\mathrm{it}}(K_\ell)$ denote the number of iterations consumed by the ℓ-th iteration of SPA-SAMP, which has the testing sparsity level K_ℓ. One has*

$$n_{\mathrm{it}}(K_\ell) \leq \frac{1.5 K_\ell}{-\log c_{K_\ell}}, \tag{6.52}$$

where

$$c_{K_\ell} = \frac{2\delta_{3K_\ell}(1 + \delta_{3K_\ell})}{(1 - \delta_{3K_\ell})^3}. \tag{6.53}$$

Proof According to Theorem 8 in [15], the inequality (6.52) holds for the SP algorithm with sparsity level K_ℓ, with the constant (6.53) given by Eq. (6.8) in the SP literature [15]. Then based on the proof of Lemma 6.1, the ℓ-th stage of SPA-SAMP is equivalent to the SP algorithm with the sparsity level of K_ℓ, so the conclusion (6.52) also holds for the ℓ-th iteration stage of the SPA-SAMP algorithm, which completes the proof.

Theorem 6.5 (convergence without noise) *If $\mathbf{F}_R$ satisfies RIP with the RIP constant $\delta_{3K_s} < 0.165$, then SPA-SAMP converges to the exact IN matrix $\mathbf{\Xi}_0$ to be recovered as in $\tilde{\mathbf{P}} = \mathbf{F}_R \mathbf{\Xi}_0$, which is the noiseless case of (6.12), after $\ell_{\max} = \lceil K/\Delta s \rceil$ stages of iterations, and the total number of iterations N_{IT} is bounded by*

$$N_{\mathrm{IT}} \leq \lceil K/\Delta s \rceil \cdot \left(\frac{1.5 K_s}{-\log c_{K_s}} \right) \tag{6.54}$$

where

$$K_s = \lceil K/\Delta s \rceil \cdot \Delta s. \tag{6.55}$$

The proof of Theorem 6.5 is given as follows.

Proof From Theorem 2 in [15], it was proved that the residue norm $\|\mathbf{r}^{(k)}\|_2 < \|\mathbf{r}^{(k-1)}\|_2$, $\forall k$ for any sparsity level K_ℓ if $\mathbf{F}_R$ satisfies RIP with constant $\delta_{3K_s} < 0.165$. Based on Lemma 6.1, the ℓ-th stage of SPA-SAMP is equivalent to SP with sparsity level K_ℓ, so after each iteration of SPA-SAMP in the ℓ-th stage, the residue vector $\|\mathbf{r}_j^{(k)}\|_2 < \|\mathbf{r}_j^{(k-1)}\|_2$, $\forall k$, j. Thus, the $\ell_{2,2}$-norm of the residue matrix satisfies $\|\mathbf{R}^{(k)}\|_{2,2} < \|\mathbf{R}^{(k-1)}\|_{2,2}$ *within each stage* before the stage switching.

Recall that the condition of stage switching for each stage of SPA-SAMP is

$$\|\mathbf{R}^{(k)}\|_{2,2} \geq \|\mathbf{R}^{(k-1)}\|_{2,2}. \tag{6.56}$$

Based on Lemma 6.4, the number of iterations of the ℓ-th stage in SPA-SAMP is bounded by (6.52), so the stage switching condition (6.56) will be met for each stage in SPA-SAMP and each stage will definitely end at that time. Then, concerning about the solution convergence, we have the following proposition

Proposition 6.6 *The global halting condition of SPA-SAMP without noise, which is given by*

$$\left\|\mathbf{R}_{(\ell)}\right\|_{2,2} = \mathbf{0}, \tag{6.57}$$

cannot be met within the stage ℓ, $\ell < \lceil K/\Delta s \rceil$, and thus the stage will finally switch to next one. Until $\ell = \lceil K/\Delta s \rceil$, SPA-SAMP converges to the exact desired solution $\mathbf{\Xi}_0$ and the global halting condition in (6.57) is met.

Here, we denote the residue matrix and the estimated IN matrix at the end of the ℓ-th stage as $\mathbf{R}_{(\ell)}$ and $\hat{\mathbf{\Xi}}_{(\ell)}$, respectively. To prove Proposition 6.6, firstly we use the proof of contradiction to prove the first part of it. Assume that $\exists \ell < \lceil K/\Delta s \rceil$ such that the residue matrix norm of the ℓ-th stage, $\left\|\mathbf{R}_{(\ell)}\right\|_{2,2} = \mathbf{0}$ is met during the ℓ-th stage. Since the sparsity level $K_\ell = \ell \cdot \Delta s < K_s$, ($K_s$ is the real sparsity level), so

$$\exists \mathbf{\Xi}' \neq \mathbf{0}, \text{ s. t. } \mathbf{\Xi}_0 - \hat{\mathbf{\Xi}}_{(\ell)} = \mathbf{\Xi}'. \tag{6.58}$$

Thus,

$$\begin{aligned}
\left\|\mathbf{R}_{(\ell)}\right\|_{2,2} &= \left\|\tilde{\mathbf{P}} - \mathbf{F}_R(\mathbf{\Xi}_0 - \mathbf{\Xi}')\right\|_{2,2} \\
&= \left\|(\tilde{\mathbf{P}} - \mathbf{F}_R\mathbf{\Xi}_0) + \mathbf{F}_R\mathbf{\Xi}'\right\|_{2,2} \\
&= \left\|\mathbf{F}_R\mathbf{\Xi}'\right\|_{2,2} > 0,
\end{aligned}$$

which is contradictory to the assumption. Hence, the global halting condition in (6.57) cannot be met for $\ell < \lceil K/\Delta s \rceil$.

Then, based on the Theorem 1 in [15], the SP algorithm with sparsity level K_s converges to the exact desired solution without noise since $\mathbf{F}_R$ satisfies RIP with constant $\delta_{3K_s} < 0.165$. Thus, based on Lemma 6.1, the $\lceil K/\Delta s \rceil$-th stage with testing sparsity level of K_s is equivalent to SP with sparsity level K_s, and it is guaranteed that SPA-SAMP converges to the exact solution $\mathbf{\Xi}_0$, i.e.

$$\hat{\boldsymbol{\Xi}}_{(\ell_{\max})} = \boldsymbol{\Xi}_0, \tag{6.59}$$

where $\ell_{\max} = \lceil K/\Delta s \rceil$, and $\hat{\boldsymbol{\Xi}}_{(\ell_{\max})}$ denotes the output of the final ($\ell_{\max}$-th) stage. Then, it is evident that

$$\begin{aligned} \left\| \mathbf{R}_{(l_{\max})} \right\|_{2,2} &= \left\| \tilde{\mathbf{P}} - \mathbf{F}_{\mathrm{R}} \hat{\boldsymbol{\Xi}}_{(\ell_{\max})} \right\|_{2,2} \\ &= \left\| \tilde{\mathbf{P}} - \mathbf{F}_{\mathrm{R}} \boldsymbol{\Xi}_0 \right\|_{2,2} = 0, \end{aligned}$$

so Proposition 6.6 holds.

It is evident that the total number of stages of SPA-SAMP is $\lceil K/\Delta s \rceil$ to reach the sparsity level K_s such that $K_s = \lceil K/\Delta s \rceil \cdot \Delta s \geq K$. For each stage $\ell \leq \lceil K/\Delta s \rceil$, due to Lemma 6.4 one has

$$n_{\mathrm{it}}(K_\ell) \leq \frac{1.5K_\ell}{-\log c_{K_\ell}} \leq \frac{1.5K_s}{-\log c_{K_s}}, \ \forall \ell \leq \lceil K/\Delta s \rceil, \tag{6.60}$$

where the second inequality holds because $K_\ell \leq K_s$, $\forall l \leq \lceil K/\Delta s \rceil$, and since the RIP constant δ_{3K_ℓ} in (6.53) is monotonically increasing with K_ℓ (which is easy to verify using a proof of contradiction based on the definition of RIP), we have that c_{K_ℓ} is monotonically increasing with ℓ. Hence, the total number N_{IT} of iterations of SPA-SAMP, including all $\ell_{\max}$ stages, is bounded by

$$N_{\mathrm{IT}} = \sum_{\ell=1}^{\ell_{\max}=\lceil K/\Delta s \rceil} n_{\mathrm{it}}(K_\ell) \leq \lceil K/\Delta s \rceil \cdot \left(\frac{1.5K_s}{-\log c_{K_s}} \right). \tag{6.61}$$

Then (6.54) holds, which completes the proof.

Theorem 6.5 guarantees the convergence of SPA-SAMP to the exact desired solution without background noise. When in the presence of noise, the convergence is guaranteed by the following theorem:

Theorem 6.7 (convergence with noise) *If $\mathbf{F}_{\mathrm{R}}$ satisfies RIP with the constant $\delta_{3K_s} < 0.083$, $K_s = \Delta s \lceil K/\Delta s \rceil$, let the output estimated IN matrix at the end of the final $\ell_{\max} = \lceil K/\Delta s \rceil$-th stage of SPA-SAMP be denoted by $\hat{\boldsymbol{\Xi}}_{(\ell_{\max})}$, then one has that $\hat{\boldsymbol{\Xi}}_{(\ell_{\max})}$ converges to the real IN matrix $\boldsymbol{\Xi}_0$ as in the multiple measurements model $\tilde{\mathbf{P}} = \mathbf{F}_{\mathrm{R}} \boldsymbol{\Xi}_0 + \tilde{\mathbf{W}}$ in (6.12), with the estimation error bounded by*

$$\left\| \boldsymbol{\Xi}_0 - \hat{\boldsymbol{\Xi}}_{(\ell_{\max})} \right\|_{2,2} \leq C'_{K_s} \left\| \tilde{\mathbf{W}} \right\|_{2,2}, \tag{6.62}$$

where

$$C'_{K_s} = \frac{1 + \delta_{3K_s} + \delta_{3K_s}^2}{\delta_{3K_s}(1 - \delta_{3K_s})}, \tag{6.63}$$

and the total number of iterations of SPA-SAMP N_{IT} is upper bounded by (6.54).

The proof of Theorem 6.7 is given as follows.

Proof Similarly to the proof of Theorem 6.5, according to Theorem 10 in [15], it was proved that the residue vector norm $\|\mathbf{r}^{(k)}\|_2 < \|\mathbf{r}^{(k-1)}\|_2$, $\forall k$ for any sparsity level K_ℓ if $\mathbf{F}_{\mathrm{R}}$ satisfies RIP with constant $\delta_{3K_s} < 0.083$ in the presence of background noise. Then similarly, the residue matrix satisfies $\|\mathbf{R}^{(k)}\|_{2,2} < \|\mathbf{R}^{(k-1)}\|_{2,2}$ within each stage. The number of iterations of the ℓ-th stage is still bounded by (6.52) based on Lemma 6.4, so the stage switching condition in (6.56) will be met for each stage in SPA-SAMP.

According to Lemma 6.1, the $\ell_{\max}$-th stage of SPA-SAMP is equivalent to SP with sparsity level of $K_{\ell_{\max}} = K_s$. Then, since $\mathbf{F}_{\mathrm{R}}$ satisfies RIP with the constant $\delta_{3K_s} < 0.083$, based on Theorem 9 in [15], one has

$$\left\| \mathbf{z}_i^{(j)} - \hat{\mathbf{z}}_{(l_{\max})}^{(j)} \right\|_2 \leq C'_{K_s} \left\| \tilde{\mathbf{w}}_i^{(j)} \right\|_2, \forall j \in [1, \dots N_{\mathrm{r}}], \tag{6.64}$$

where $\mathbf{z}_i^{(j)}$ and $\hat{\mathbf{z}}_{(l_{\max})}^{(j)}$ denote the j-th column of matrices $\boldsymbol{\Xi}_0$ and $\hat{\boldsymbol{\Xi}}_{(\ell_{\max})}$, respectively, and the constant C'_{K_s} is given by (6.63), which is derived by Theorem 9 in [15]. Equation (6.64) indicates that the error between any IN vector of the estimated IN matrix and the real one is bounded by the noise power, and it holds for any receive antenna $j \in [1, \dots N_{\mathrm{r}}]$. Then, one has the error of the estimated IN matrix bounded by

$$\left\| \boldsymbol{\Xi}_0 - \hat{\boldsymbol{\Xi}}_{(\ell_{\max})} \right\|_{2,2} \leq C'_{K_s} \left\| \tilde{\mathbf{W}} \right\|_{2,2}, \tag{6.65}$$

since the $\ell_{2,2}$-norm of a matrix calculates the square root of the sum of all entries of the matrix as defined by (6.14), and thus (6.65) is derived from (6.64). Next, we raise a proposition similar to that in Theorem 6.5 as follows:

Proposition 6.8 *The global halting condition of SPA-SAMP with noise, which is given by*

$$\left\| \mathbf{R}_{(\ell)} \right\|_{2,2} \leq C_\varepsilon \cdot \varepsilon_S, \tag{6.66}$$

$$C_\varepsilon = 1 + \sqrt{1 + \delta_{2K_s}^{(\mathrm{B})}} \cdot C'_{K_s}, \tag{6.67}$$

is met at the end of the final stage of $\ell_{\max} = \lceil K/\Delta s \rceil$, and the SPA-SAMP algorithm converges to the exact desired solution $\boldsymbol{\Xi}_0$ with error bounded by (6.65) after the $\ell_{\max}$-th stage ($\delta_{2K_s}^{(\mathrm{B})}$ is the block-RIP constant).

To prove this proposition, we have known that the stage $\ell_{\max} = \lceil K/\Delta s \rceil$ of SPA-SAMP is equivalent to SP with sparsity level K_s based on Lemma 6.1, so after $\ell_{\max}$ stages of SPA-SAMP, the residue matrix $\mathbf{R}_{(\ell_{\max})}$ yields the following

$$\left\| \mathbf{R}_{(\ell_{\max})} \right\|_{2,2} = \left\| \tilde{\mathbf{P}} - \mathbf{F}_R \hat{\mathbf{\Xi}}_{(\ell_{\max})} \right\|_{2,2} \tag{6.68}$$

$$= \left\| \mathbf{F}_R \left(\mathbf{\Xi}_0 - \hat{\mathbf{\Xi}}_{(\ell_{\max})} \right) + \tilde{\mathbf{W}} \right\|_{2,2} \tag{6.69}$$

$$\leq \left\| \tilde{\mathbf{W}} \right\|_{2,2} + \left\| \mathbf{F}_R \left(\mathbf{\Xi}_0 - \hat{\mathbf{\Xi}}_{(\ell_{\max})} \right) \right\|_{2,2} \tag{6.70}$$

$$\leq \left\| \tilde{\mathbf{W}} \right\|_{2,2} + \sqrt{1 + \delta_{2K_s}^{(B)}} \left\| \mathbf{\Xi}_0 - \hat{\mathbf{\Xi}}_{(\ell_{\max})} \right\|_{2,2} \tag{6.71}$$

$$\leq \underbrace{\left[1 + \sqrt{1 + \delta_{2K_s}^{(B)}} \cdot C K_s \right]}_{:=C_\varepsilon} \left\| \tilde{\mathbf{W}} \right\|_{2,2} \tag{6.72}$$

$$= C_\varepsilon \cdot \varepsilon_S, \tag{6.73}$$

where Eq. (6.70) holds due to *Triangle Inequality*, Eq. (6.72) holds because of (6.65), and Eq. (6.73) is derived due to (6.16). The reason why (6.71) holds is as follows:

Let $\mathrm{vec}(\mathbf{A})$ denote the vectorization operation of a matrix, which returns a vector composed of all the columns of the matrix $\mathbf{A}$. Since $\mathbf{\Xi}_0$ and $\hat{\mathbf{\Xi}}_{(\ell_{\max})}$ are block-K_s-sparse after vectorization (the number of rows with nonzero ℓ_2-norm are no more than K_s, with the definition of block sparsity given in Definition 2.3), then $(\mathbf{\Xi}_0 - \hat{\mathbf{\Xi}}_{(\ell_{\max})})$ is block-$2K_s$-sparse after vectorization because there are at most $2K_s$ rows with nonzero ℓ_2-norm (the upper bound is reached when the supports of $\mathbf{\Xi}_0$ and $\hat{\mathbf{\Xi}}_{(\ell_{\max})}$ are completely different). Let $\mathbf{\Xi}' = \mathbf{\Xi}_0 - \hat{\mathbf{\Xi}}_{(\ell_{\max})}$, then

$$\| \mathbf{\Xi} \|_{2,2} = \left\| \mathrm{vec} \left(\mathbf{\Xi}^T \right) \right\|_2, \tag{6.74}$$

since both sides of Eq. (6.74) calculate the square root of the sum of all entries' powers. Assuming that the block observation matrix $\Psi_B = (\mathbf{F}_R \otimes \mathbf{I}_{N_r})$ satisfies the block-RIP with block-RIP constant $\delta_{2K}^{(B)}$, then one has

$$\| \mathbf{F}_R \mathbf{\Xi}' \|_{2,2} = \left\| \mathrm{vec} \left[\left(\mathbf{F}_R \mathbf{\Xi}' \right)^T \right] \right\|_2 \tag{6.75}$$

$$= \left\| (\mathbf{F}_R \otimes \mathbf{I}_{N_r}) \mathrm{vec} \left(\mathbf{\Xi}'^T \right) \right\|_2 \tag{6.76}$$

$$\leq \sqrt{1 + \delta_{2K_s}^{(B)}} \left\| \mathrm{vec} \left(\mathbf{\Xi}'^T \right) \right\|_2 \tag{6.77}$$

$$= \sqrt{1 + \delta_{2K_s}^{(B)}} \| \mathbf{\Xi}' \|_{2,2}, \tag{6.78}$$

where Eq. (6.75) holds since both sides calculate the square root of the summation of the powers of all entries, and the reason is the same with (6.78); Eq. (6.76) holds due to the definitions of the vectorization process and the matrix Kronecker production; Eq. (6.77) holds because of the block-RIP of $(\mathbf{F}_R \otimes \mathbf{I}_{N_r})$.

Till now, we have proved Proposition 6.8. Due to Proposition 6.8, the SPA-SAMP algorithm with noise is guaranteed to reach the global halting condition (6.66) and will end at the ℓ_{max}-th stage, and the estimated IN matrix $\hat{\boldsymbol{\Xi}}_{(\ell_{max})}$ converges to the real IN $\boldsymbol{\Xi}_0$ with error bounded by (6.65). Besides, the total number of iterations N_{IT} is upper bounded by (6.54) with the similar proof to that in Theorem 6.5, thus omitted. Till now, the proof of this Theorem has been completed.

Till this end, the solution existence and the convergence of the proposed SPA-SAMP algorithm in both noiseless and noise cases are theoretically proved and guaranteed. The performance error bound of the estimated IN in the presence of background noise is also derived in closed-form.

6.7 Conclusion

In this chapter, the fundamental drawbacks of the conventional "passive" anti-IN methods are solved with the introduction of sparse recovery and compressed sensing. Cutting in from the "active recovery" perspective of view, the prior aided compressed sensing based method and the spatially correlated multi-dimensional structured compressed sensing based methods of IN recovery and cancelation are proposed. Furthermore, the compressed sensing based NBI and IN joint recovery scheme is proposed in the framework of time-frequency combined sparse measurements. Thus, the NBI and IN can be accurately recovered and eliminated in severe channel conditions, and the transmission performance is free from the NBI and IN. Besides, the theoretical analysis has proved the solution existence and convergence of the proposed algorithm SPA-SAMP, which provides the theoretical basis of the proposed sparse recovery framework. It is shown by theoretical analysis and extensive simulations that, the proposed prior aided multi-dimensional compressed sensing based method for IN recovery and elimination outperforms the state-of-the-art methods significantly, and the accurate recovered IN can be approaching the theoretical bound of estimation. The proposed sparse measuring method and the prior aided compressed sensing modeling theory, as well as the prior aided multi-dimensional compressed sensing based greedy algorithms, can promisingly provide a novel theoretical basis and effective technical solution for the accurate recovery and elimination of IN in broadband communication systems.

References

1. Caire G, Al-Naffouri T, Narayanan A (2008) Impulse noise cancellation in OFDM: an application of compressed sensing. In: 2008 IEEE international symposium on information theory (ISIT'08), pp 1293–1297
2. Lampe L (2011) Bursty impulse noise detection by compressed sensing. In: 2011 IEEE international symposium on power line communications and its applications (ISPLC), pp 29–34
3. Naffouri T, Quadeer A, Caire G (2014) Impulse noise estimation and removal for OFDM systems. IEEE Trans Commun 62(3):976–989
4. Middleton D (1979) Procedures for determining the parameters of the first-order canonical models of class A and class B electromagnetic interference. IEEE Trans Electromagn Compat EMC-21(3):190–208 (1979)
5. Schober R, Lampe L (2004) Sequence detection and adaptive channel estimation for ISI channels under class-A impulsive noise. IEEE Trans Commun 52(9):1523–1531
6. Donoho D, Elad M, Temlyakov V (2006) Stable recovery of sparse overcomplete representations in the presence of noise. IEEE Trans Inf Theory 52(1):6–18
7. Gao P, Tepedelenlioglu C (2007) Space-time coding over fading channels with impulsive noise. IEEE Trans Wirel Commun 6(1):220–229
8. Saaifan KA, Henkel W (2012) A receiver design for MIMO systems over rayleigh fading channels with correlated impulse noise. In: 2012 IEEE global communications conference (GLOBECOM'12), pp 2481–2486
9. Goldsmith A, Jafar SA, Jindal N et al (2003) Capacity limits of MIMO channels. IEEE J Sel Areas Commun 21(5):648–702
10. Zheng L, Tse DNC (2003) Diversity and multiplexing: a fundamental tradeoff in multiple-antenna channels. IEEE Trans Inf Theory 49(5):1073–1096
11. IEEE: Wireless LAN medium access control (MAC) and physical layer (PHY) specifications (2009)
12. ITU-T: ITU G.9960, unified high-speed wire-line based home networking transceivers—system architecture and physical layer specification (2010)
13. Donoho D (2006) Compressed sensing. IEEE Trans Inf Theory 52(4):1289–1306
14. Tropp JA, Gilbert AC, Strauss MJ (2006) Algorithms for simultaneous sparse approximation. part i: Greedy pursuit. Signal Process 86(3):572–588 (2006)
15. Dai W, Milenkovic O (2009) Subspace pursuit for compressive sensing signal reconstruction. IEEE Trans Inf Theory 55(5):2230–2249
16. Guideline for evaluation of radio transmission technology for IMT-2000 (1997)
17. IEEE: IEEE standard for information technology—local and metropolitan area networks—specific requirements–part 11: wireless LAN medium access control (MAC) and physical layer (PHY) specifications amendment 6: wireless access in vehicular environments (2010)
18. Duarte M, Eldar Y (2011) Structured compressed sensing: from theory to applications. IEEE Trans Signal Process 59(9):4053–4085
19. Eldar YC, Mishali M (2009) Robust recovery of signals from a structured union of subspaces. IEEE Trans Inf Theory 55(11):5302–5316
20. Byers GJ, Takawira F (2004) Spatially and temporally correlated MIMO channels: modeling and capacity analysis. IEEE Trans Veh Technol 53(3):634–643
21. Do T, Lu G, Nguyen N, Tran T (2008) Sparsity adaptive matching pursuit algorithm for practical compressed sensing. In: Asilomar conference on signals, systems and computers, pp 581–587
22. Zhidkov SV (2008) Analysis and comparison of several simple impulsive noise mitigation schemes for OFDM receivers. IEEE Trans Commun 56(1):5–9
23. Wolniansky PW, Foschini GJ, Golden GD, Valenzuela RA (1998) V-BLAST: an architecture for realizing very high data rates over the rich-scattering wireless channel. In: 1998 URSI international symposium on signals, systems, and electronics, pp 295–300
24. ten Brink S, Speidel J, Yan RH (1998) Iterative demapping and decoding for multilevel modulation. In: IEEE global communications conference (GLOBECOM'98), vol 1, pp 579–584

25. MacKay DJC (1999) Good error-correcting codes based on very sparse matrices. IEEE Trans Inf Theory 45(2):399–431
26. Standard CN (2006) Frame structure, channel coding and modulation for digital television terrestrial broadcasting system. GB 20600-2006, Chinese National Standard
27. ETSI: Digital video broadcasting (DVB); frame structure, channel coding and modulation for a second generation digital terrestrial television broadcasting system (DVB-T2). ETSI EN 302 755 v1.3.1 (2011)
28. Tropp J, Gilbert A (2007) Signal recovery from random measurements via orthogonal matching pursuit. IEEE Trans Inf Theory 53(12):4655–4666
29. Hasan SF, Ding X, Siddique NH, Chakraborty S (2011) Measuring disruption in vehicular communications. IEEE Trans Veh Technol 60(1):148–159
30. Shi K, Zhou Y, Kelleci B, Fischer TW, Serpedin E, lker Karsilayan A (2007) Impacts of narrowband interference on OFDM-UWB receivers: analysis and mitigation. IEEE Trans Signal Process 55(3):1118–1128
31. Zhidkov SV (2003) Impulsive noise suppression in OFDM-based communication systems. IEEE Trans Consum Electron 49(4):944–948
32. Steven MK (1993) Fundamentals of statistical signal processing. PTR Prentice-Hall, Englewood Cliffs, NJ

Chapter 7
Conclusions

Abstract This monograph is aimed at the urgent needs of the ever-increasing transmission performance of the next-generation broadband communications systems. It is focused on the key bottleneck that limits the current broadband transmission performance seriously, i.e. the non-conventional interference and noise, NBI and IN. The drawbacks of the conventional methods such as high implementation complexity, low applicability, low estimation accuracy and unstable performance, etc., should be overcome by breaking the fundamental limitation of the conventional "passive" anti-NBI and anti-IN approaches. In this chapter, we draw the conclusions of this book.

7.1 Contributions

This monograph cuts in from the views of "scrambling", "diversifying", and "recovering", to expand the research on the key technologies on NBI and IN mitigation and cancelation. Through the optimized synchronization frame structure design, the synchronization algorithm, which is robust to NBI, is achieved. Through the maximized time-frequency diversity interleaving scheme, the optimal time-frequency combined interleaver design is implemented in the environment with both NBI and IN.

By introducing the recently emerging sparse recovery theory, the time-frequency-space multi-dimensional structured compressed sensing measurement and recovery model is formulated. The classical compressed sensing algorithms are effectively improved concerning the characteristics of NBI and IN. The prior aided compressed sensing and structured compressed sensing based sparse recovery algorithms are proposed, which is able to recover and cancel the NBI and IN accurately and stably in severe conditions, such as insufficient measurement data and large sparsity level. The presentation idea of this monograph is as follows: raising the scientific problems, setting the research targets, searching for the ideas, making the research regimes, conducting theoretical analysis and simulations, and deploying system applications and standardizations.

   We focus on solving the three major scientific problems on NBI and IN mitiga-
tion and cancellation, and have set explicit research targets. Accordingly, we have
proposed the main contributions, and validated the reliability and effectiveness of
the proposed schemes by theoretical analysis and simulations. We have also pushed
forward the applications in practice and the standardization process of the proposed
techniques. The proposed theory and technology have theoretical and application
value, and provide theoretical basis and effective technical solution for relieving the
impacts of special noises in the new generation broadband transmission systems.

   Towards the three scientific problems and the corresponding research targets
raised in this book, the key technical routine is as follows: mitigating the noise and
interference by "scrambling" $\rightarrow$ avoiding the noise and interference by "diversity"
$\rightarrow$ eliminate the noise and interference by "recovery". In this way, three major con-
tributions are formulated, and we have investigated four research issues accordingly.
The key theoretical framework and technical system of NBI and IN mitigation and
cancelation for the new generation broadband communications system is formulated,
which breaks the fundamental performance limitation of the conventional methods.
The contents in this book might provide positive contributions to the academia and
industry in this area. The contributions are concluded in detail as follows.

7.1.1   Anti-NBI Frame Design and Synchronization Method

- Main contribution:
  Synchronization is crucial to the performance of broadband communication sys-
  tems, especially for OFDM systems. In the presence of NBI, the frame synchro-
  nization and carrier recovery are seriously affected. The conventional synchro-
  nization frame design and synchronization algorithms were not designed for anti-
  NBI, which resulted in low synchronization accuracy, high error rate and severe
  performance degradation in the presence of NBI. Therefore, the problem of accu-
  rate and efficient synchronization in the presence of NBI has become the utmost
  important problem for the system performance. In this book, we have investigated
  the OFDM preamble design that effectively mitigates the NBI, and designed the
  efficient and robust algorithms of receiver-side frame synchronization and carrier
  recovery. Besides, the signalling transmission method, which is robust to NBI,
  is also investigated. The proposed methods can solve the problems of conven-
  tional synchronization methods and guarantee the synchronization performance
  of OFDM systems in the presence of NBI, which provides a basic technical guar-
  antee for the system performance.
- Technical content and routine:
  We follow the idea of designing a "scrambled" synchronization frame structure
  to mitigate the NBI. To address the scientific problem of overcoming the severe
  impacts of the NBI on the receiver synchronization performance, we have proposed
  the optimized synchronization frame structure design as well as the receiver-side
  efficient and robust synchronization algorithm. An OFDM-based preamble with

improved temporal structure has been designed, which enjoys the advantages of both Schmidl's and Minn's methods. More importantly, a novel scrambling operation is proposed, which is applied in the temporal preamble of the OFDM symbol to mitigate the impact of the NBI on synchronization. Two groups of identical training sequences distributed in turn over the active sub-carriers are devised, which is used to achieve diversity gain in frequency-selective fading channels. The relative distance between the two groups of training sequences can be changed, so that several bits of signalling information can be conveyed. Using this scheme, the receiver can rapidly and accurately obtain the basic transmission parameters.

- Application prospects:
The OFDM-based preamble designed in this book can significantly improve the timing and carrier synchronization performance in the presence of NBI, and guarantee the robust transmission of the signalling information of the OFDM system. The NBI existing widely in wired or wireless channels can be mitigated effectively. The proposed preamble and frame structure design has been adopted as the broadband power line communications specifications in physical layer, which is promising to be further applied in many other different communication systems impacted by NBI.

7.1.2 Optimal Time-Frequency Combined Interleaving

- Main contribution:
Conventional interleaving schemes have many drawbacks, such as complicated design, redesign for each different coded modulation scheme, low flexibility and universally applicability, etc. Time and frequency interleaving is not considered at the same time, so the frequency and time domain bursting errors cannot be avoided. There is no optimal guarantee for conventional bit or symbol interleaving patterns, so they cannot be sure to achieve the optimal and maximum time and frequency diversity gains. To this end, this book has proposed the optimal time-frequency combined interleaving scheme in the presence of NBI and IN, including the interleaving parameter optimization scheme with the maximum time diversity gain, and the symbol interleaving block cyclic shifting technique with maximum frequency diversity gain. In this way, the time-frequency diversity gains are maximized, and the time and frequency domain bursting errors are avoided effectively. The interleaving and decoding performance in the presence of both NBI and IN can be significantly improved.
- Technical content and routine:
We follow the idea of providing the maximum time-frequency diversity gains to avoid the NBI and IN. To address the scientific problem of improving the time-frequency interleaving performance in the presence of both NBI and IN, we have proposed the optimal time-frequency combined interleaving scheme. Based on the proposed two theoretical criteria, the optimal time-frequency interleaving scheme is proposed to avoid the NBI and IN in broadband communication systems. Based

on these criteria, we can guide the optimization of interleavers and significantly improve the time and frequency diversity gains. Specifically, one criterion is satisfied by optimizing the distribution of OFDM data blocks in the forward error checking codewords. The other criterion is satisfied by optimizing the distribution of OFDM sub-carriers in the forward error checking codewords. Based on the theoretical optimization criteria, we have investigated and proposed the block interleaver with the optimal interleaving size as the time interleaving scheme, and proposed the sub-matrix row cyclic shifting technique as the novel frequency interleaving scheme. The proposed interleaving schemes are at the symbol level instead of bit level, which is able to achieve better effectiveness with lower implementation complexity.

- Application prospects:
  The proposed optimal time-frequency combined interleaving scheme is able to achieve a better anti-NBI and anti-IN capability with shorter interleaving delay and lower complexity compared with conventional schemes. It is likely to provide a simple, efficient and robust anti-NBI and anti-IN interleaving scheme for the coded OFDM block transmission system. It can also be widely applied in other channel conditions impacted by NBI and/or IN. The optimal time-frequency combined interleaving scheme investigated in this book has been adopted by the advanced digital terrestrial multimedia broadcasting standards, and it is promising to provide technical support for the new generation digital communication and multimedia transmission systems.

7.1.3 Sparse Recovery Based NBI and IN Cancelation

- Main contribution:
  Most of the state-of-the-art NBI and IN mitigation methods are limited in the conventional signal processing regime, which is stuck in the bottleneck of "passively" combatting against noise and interference. The research on the sparse recovery based NBI and IN estimation is insufficient. In this book, based on the recently emerging advanced sparse recovery theory, the NBI and IN measurement and recovery models are formulated. Moreover, the time-frequency-space multi-dimensional structured compressed sensing based efficient and accurate recovery method is proposed, which greatly outperforms classical compressed sensing algorithms and solves the problem of conventional methods. Thus, the combined "active" recovery and cancelation of NBI and IN is implemented.
- Technical content and routine:
  We follow the idea of accurate sparse recovery for completely canceling the NBI and IN, and have mainly conducted the following two aspects of research:
  First, to address the third scientific problem of breaking the bottleneck of conventional passive NBI and IN mitigation methods for accurate recovery and complete cancelation, we have proposed the sparse recovery based NBI reconstruction method as well as efficient optimized sparse recovery algorithms. The

NBI temporal differential measuring method independent of the channel estimation is proposed, which exploits the training sequences between signal frames or the preamble repeated training sequences to conduct the low-complexity differential operation to obtain the NBI measurement vector. The partial Fourier transform matrix is utilized as the observation matrix to formulate the compressed sensing based NBI reconstruction problem model. The prior aided sparsity adaptive matching pursuit (PA-SAMP) algorithm is proposed, which effectively improves the NBI recovery efficiency and accuracy in severe conditions.

Based on the temporal and spatial correlation of the NBI, we have proposed the spatially multi-dimensional differential measuring method, which combines the measurement data at multiple receive antennas to formulate the time-space two-dimensional structured compressed sensing NBI reconstruction model in MIMO systems. The structured compressed sensing based efficient greedy algorithm, i.e. structured SAMP (S-SAMP), is proposed to achieve higher recovery efficiency and robustness than classical compressed sensing algorithms. The block sparse Bayesian learning (BSBL) theory is introduced to the problem of NBI estimation. To address the extended case of the block-sparse NBI with frequency offset, the CP-OFDM frame structure is utilized to obtain the NBI differential measurement data and formulate the sparse Bayesian learning based framework. Based on the block partition estimation, the partition estimated BSBL algorithm is proposed. Furthermore, the intra-block correlation is fully utilized to propose the informative BSBL (I-BSBL) algorithm, which further improves the sparse recovery accuracy.

Second, to address the other key issue of the third scientific problem, we have proposed the sparse recovery based IN reconstruction and cancelation method as well as the corresponding efficient sparse recovery algorithms. We have proposed the prior information aided compressed sensing based IN recovery method, which employs the temporal thresholding method to obtain the partial support of the IN to reduce the requirement of measurement data. The compressed sensing recovery model is formulated using partial Fourier transform observation matrix, and the proposed compressed sensing greedy algorithm PA-SAMP is utilized to accurately recover the IN.

According to the spatial correlation of the IN between multiple receive antennas in MIMO systems, we have proposed the spatially multi-dimensional measurement method, which combines the measurement data at multiple receive antennas to formulate the spatially structured compressed sensing based IN recovery framework. The structured compressed sensing based efficient greedy algorithm, i.e. structured prior aided SAMP (SPA-SAMP), is proposed. The solution existence and the convergence of SPA-SAMP are theoretically proved. It is shown that the proposed method is able to achieve higher recovery accuracy and robustness than classical compressed sensing algorithms.

Furthermore, we have proposed the time-frequency combined compressed sensing based NBI and IN recovery framework, and designed the compressed sensing time-frequency combined measuring frame structure, i.e. CS-TFM-OFDM, which exploits the differential measurement of the temporal training sequences and the null sub-carriers to formulate the NBI and IN combined sparse recovery model.

With the aid of the partial support as prior information, PA-SAMP is utilized to achieve simultaneous accurate recovery and cancelation of NBI and IN.

- Academic and application prospects:
  The proposed theoretical framework and core techniques can significantly improve the NBI and IN estimation performance in complicated conditions such as different sparsity level, wide range of INR and insufficient measurement data, etc. The recovery accuracy of the proposed methods are approaching the theoretical CRLB. The system bit error rate is approaching the system performance without NBI and IN, which significantly outperforms the conventional methods. The related research outcomes have laid the academic basis and provided effective technical solutions for NBI and IN combined sparse recovery and cancelation. They are also promising to be widely applied in many practical broadband transmission systems, such as power line communications, wireless communications, etc., where the NBI and IN in realistic channels can be accurately recovered and eliminated.

7.2   Further Research

Due to the limitation of time and ability of the author, the research in this book cannot be perfect, and there are inevitably some constraints and aspects to be further studied on. Upon accomplishing the research works in this book, we have tried to raise some possible further research possibilities to extend and deepen this work, listed as follows:

1. The synchronization frame structure and algorithm are mainly aimed at mitigating the NBI, while the frame design for IN mitigation remains unrevealed. Furthermore, one can study the duality optimal design of the synchronization frame structure for simultaneous mitigation of NBI and IN to improve the spectrum efficiency and reduce the time and frequency resource consumption. Thus, the frame structure can be applicable for severe channel conditions with both NBI and IN. Besides, the frame header with flexibly switching modes suitable for the channels with NBI and IN is also designed.

2. The current time-frequency combined interleaving scheme in this book is aimed at the channel condition with both NBI and IN, and it is optimized and designed according to the criterion of maximizing the time and frequency diversity gains. In the future, we can utilize the theoretical tools such as information theory, the extrinsic information transfer curve [3, 9], and the statistical model of NBI and IN, to analyze the theoretical channel capacity. The theoretically achievable channel capacity and the bound of the time-frequency diversity gain can be achieved through the bit or symbol interleaving schemes in the presence of NBI and IN. The capacity approaching method of the combined interleaving with maximum time-frequency diversity gain can be designed to further improve the interleaving performance and adapt to different scenarios and system requirements.

3. The spatially multi-dimensional structured compressed sensing based NBI recovery algorithm proposed in this book is mainly utilizing the spatial correlation of the NBI at multiple receive antennas to obtain the multi-dimensional differential measurement vectors, and thus to formulate the structured compressed sensing sparse recovery model for NBI reconstruction. Furthermore, we can exploit the temporal correlation of the NBI to conduct the differential measuring for a number of consecutive adjacent OFDM symbols to obtain the temporal multi-dimensional differential measurement matrix. In this way, we can formulate the temporal multi-dimensional structured compressed sensing based NBI recovery framework, which is promising to further improve the NBI recovery performance in SISO systems.

4. We have investigated the block sparse Bayesian learning based NBI recovery algorithm in CP-OFDM systems with frequency offset in this book. As far as IN is concerned, we have been mainly focused on prior aided compressed sensing and structured compressed sensing based IN recovery methods. Thus, we can further study on the IN recovery algorithms in the framework of sparse Bayesian learning [7, 8]. In this way, the IN recovery accuracy can be further improved in severe conditions such as large sparsity level, low INR and insufficient measurement data.

5. The IN model investigated in this book is mainly the classical sparse signal model. In practical systems, there exist block-sparse IN models, such as the block-sparse IN caused by the timing offset or the clustering of the IN source [4]. Hence, we need to further study the enhanced algorithms for block-sparse models and structured compressed sensing or block-sparse recovery based theories. In this way, the IN recovery performance in the condition of block-sparsity can be guaranteed.

6. Currently, the NBI and IN mitigation and cancelation schemes have been focused on the physical layer and point to point transmission. The proposed techniques, including the frame structure design and synchronization algorithms, the time-frequency combined interleaving scheme for baseband complex symbols, the equivalent baseband NBI and IN recovery, are all cutting in from the physical-layer perspective of view and aimed at the performance optimization for point to point transmission. If we consider the multi-point transmission scenarios such as multi-cast and self-organizing networks, the cooperative IN estimation and cancelation algorithms based on multi-user cooperative communications can be further investigated. The upper-layer communication and interference cancelation protocols for NBI and IN remain to be further studied.

7. Considering the popular 5G and B5G technologies, we can further study the influence of NBI and IN on the novel coded modulation techniques in the next-generation wireless communication, such as the new channel coding (e.g.. LDPC code [1] and polar code [2] adopted by 5G eMBB standards), new non-orthogonal multiple access (e.g.. sparse code multiple access [6]), multi-user massive MIMO [5], etc. In the complicated scenarios and requirements including multi-node, multi-user, low power consumption, wide coverage, enormous

capacity, high rate, ultra-reliable low latency, etc., the flexible, efficient and accurate NBI and IN recovery and cancelation algorithms can be designed. Moreover, the new coded modulation techniques can be optimized and designed for better anti-NBI and anti-IN capability.

References

1. 3GPP: Future mobile communication forum, 5G white paper (2015)
2. Arikan E (2009) Channel polarization: a method for constructing capacity-achieving codes for symmetric binary-input memoryless channels. IEEE Trans Inform Theory 55(7):3051–3073
3. Ashikhmin A, Kramer G, ten Brink S (2004) Extrinsic information transfer functions: model and erasure channel properties. IEEE Trans Inform Theory 50(11):2657–2673
4. Lampe L (2011) Bursty impulse noise detection by compressed sensing. In: 2011 IEEE international symposium on power line communications and its applications (ISPLC), pp 29–34
5. Larsson EG, Edfors O, Tufvesson F, Marzetta TL (2014) Massive MIMO for next generation wireless systems. IEEE Commun Mag 52(2):186–195
6. Nikopour H, Yi E, Bayesteh A, Au K, Hawryluck M, Baligh H, Ma J (2014) SCMA for downlink multiple access of 5G wireless networks. In: 2014 IEEE global communications conference, pp 3940–3945
7. Tipping ME (2001) Sparse bayesian learning and the relevance vector machine. J Mach Learn Res 1:211–244
8. Wipf DP (2011) Sparse estimation with structured dictionaries. In: Advances in neural information processing systems, pp 2016–2024
9. Zhu X (2001) Fundamentals of applied information theory. Tsinghua University Press, Beijing